DEVELOPMENT AND IMPLEMENTATION OF A FT-ICR MASS SPECTROMETER FOR THE INVESTIGATION OF ION CONFORMATIONS OF PEPTIDE SEQUENCE ISOMERS CONTAINING BASIC AMINO ACID RESIDUES BY GAS-PHASE HYDROGEN/DEUTERIUM EXCHANGE

A Dissertation

by

JOSEPH THOMAS MARINI

Submitted to the Office of Graduate Studies of
Texas A&M University
in partial fulfillment of the requirements for the degree of

DOCTOR OF PHILOSOPHY

December 2003

Major Subject: Chemistry

DEVELOPMENT AND IMPLEMENTATION OF A FT-ICR MASS SPECTROMETER FOR THE INVESTIGATION OF ION CONFORMATIONS OF PEPTIDE SEQUENCE ISOMERS CONTAINING BASIC AMINO ACID RESIDUES BY GAS-PHASE HYDROGEN/DEUTERIUM EXCHANGE

A Dissertation

by

JOSEPH THOMAS MARINI

Submitted to Texas A&M University
in partial fulfillment of the requirements
for the degree of

DOCTOR OF PHILOSOPHY

Approved as to style and content by:

David H. Russell
(Chair of Committee)

Daniel A. Singleton
(Member)

Simon W. North
(Member)

Andy C. LiWang
(Member)

Emile A. Schweikert
(Head of Department)

December 2003

Major Subject: Chemistry

ABSTRACT

Development and Implementation of a FT-ICR Mass Spectrometer for the Investigation

of Ion Conformations of Peptide Sequence Isomers Containing Basic Amino Acid

Residues by Gas-Phase Hydrogen/Deuterium Exchange. (December 2003)

Joseph Thomas Marini, B.A., La Salle University

Chair of Advisory Committee: Dr. David H. Russell

The gas-phase hydrogen/deuterium (H/D) exchange of protonated di- and tripeptides containing a basic amino acid residue has been studied with a Fourier transform ion cyclotron resonance (FT-ICR) mass spectrometer. Bimolecular reactions are monitored as a function of time providing exchange efficiencies and temporal distributions for the peptide ions. Results from these experiments indicated that position of the basic residue within the peptide (*i.e.* *N*-terminal, internal, or *C*-terminal) influences gas-phase H/D exchange, suggesting unique peptide ion conformations.

The FT-ICR mass spectrometer employed for these gas-phase H/D exchange studies was modified from its original design. Instrument modifications include development of an internal matrix assisted laser desorption ionization (MALDI) source for peptide protonation. In addition, a two-section cell was utilized, allowing control of ion motion and factors affecting gas-phase ion molecule reactions.

Systems investigated in these gas-phase H/D exchange studies are peptides containing the same amino acid residues but different sequences. These sequence

isomers display dissimilar reaction efficiencies and temporal distributions for deuterium incorporation depending on the primary structure of the peptide ion. Specifically, $[M+H]^+$ peptide ions containing a *N*-terminal basic residue demonstrate unique H/D exchange behavior when compared to their internal and *C*-terminal counterparts. These differences are attributed to dissimilar intramolecular bridging interactions involved with inductive stabilization of the charge site.

Gas-phase H/D exchange of peptide sequence isomers was also probed with various deuterium reagents. Findings suggest that different reagents also influence H/D exchange reaction rate efficiencies and temporal distributions. These dissimilarities are ascribed to relative gas-phase basicity and proposed mechanistic exchange differences for the deuterium reagents.

DEDICATION

This dissertation is dedicated to my parents, Joseph Attilio Marini, Jr. and Barbara Ann Marini. Their love, support and encouragement have inspired me in the pursuit of my education. Thank you for everything.

ACKNOWLEDGEMENTS

TABLE OF CONTENTS

Page

LIST OF FIGURES

FIGURE   Page

LIST OF TABLES

CHAPTER I

INTRODUCTION

Background

Investigation of peptide and protein structure is an active area of research in the life sciences. The emphasis placed on conformational determination of biological molecules is based upon the influence that protein structure has on bioactivity. Often, loss of a protein's native structure causes a consequential loss in activity. Therefore, the secondary and tertiary structure of peptides and proteins has received considerable attention and has been investigated by various instrumental techniques, in an attempt to understand factors affecting reactivity of biomolecules.

Many structural studies of peptides and proteins have been carried out using spectroscopic methods under solution phase conditions. These include but are not limited to, nuclear magnetic resonance (NMR), circular dichroism (CD) and fluorescence spectroscopy. Investigating biological molecules under solution phase conditions is attractive since most proteins exist under aqueous physiological conditions. Despite the utility of studying protein structure by spectroscopic means, there are inherent limitations. First, these approaches measure average properties of the sample. Hence, investigation by these methods yields information about an ensemble of closely related structures. Second, probing biological conformations by NMR is time

---

This dissertation follows the style and format of the *Journal of the American Chemical Society.*

consuming and relatively complicated while CD and fluorescence spectroscopy reveal limited information about the molecule.

With the introduction of new ionization sources, such as electrospray ionization (ESI)[1,2] and matrix-assisted laser desorption ionization (MALDI),[3] it is now possible to introduce large, non-volatile compounds into the gas-phase. Development of these ion sources has contributed to the expansion of mass spectrometry as a tool for biological structural analysis,[4,5] aiding solution phase studies. Of the mass spectrometry sources used for ionization of biomolecules, MALDI is arguably the easiest ionization method to implement. Introduced by Karas and Hillenkamp in 1987, MALDI is based upon photoexcited proton transfer. Samples are typically prepared by mixing the analyte in a volatile solvent with excess matrix (mole ratio 1:100-50,000). Matrices are usually chromophore containing organic acids such as 2,5-dihydroxybezoic acid, 4-hydroxy-3-methoxycinnamic acid, and α-cyano-4-hydroxycinnamic acid. Following mixing of matrix and analyte, aliquots of the solution are placed upon a metallic probe and the solvent is allowed to evaporate. Solvent evaporation creates a crystal with the analyte entrained within the matrix lattice. After crystal formation, MALDI samples are placed in the source region of a mass spectrometer and irradiated with a laser pulse. Irradiation, typically at 337 nm, results in resonant absorption of the matrix molecule. The rapid heating of the MALDI sample causes prompt desorption of matrix and analyte into the gas-phase, as well as ionization of the analyte molecule by the matrix[6] (Figure 1). This relatively gentle ionization technique has extended the capabilities of mass spectrometry, allowing the analysis of large, non-volatile biomolecules.
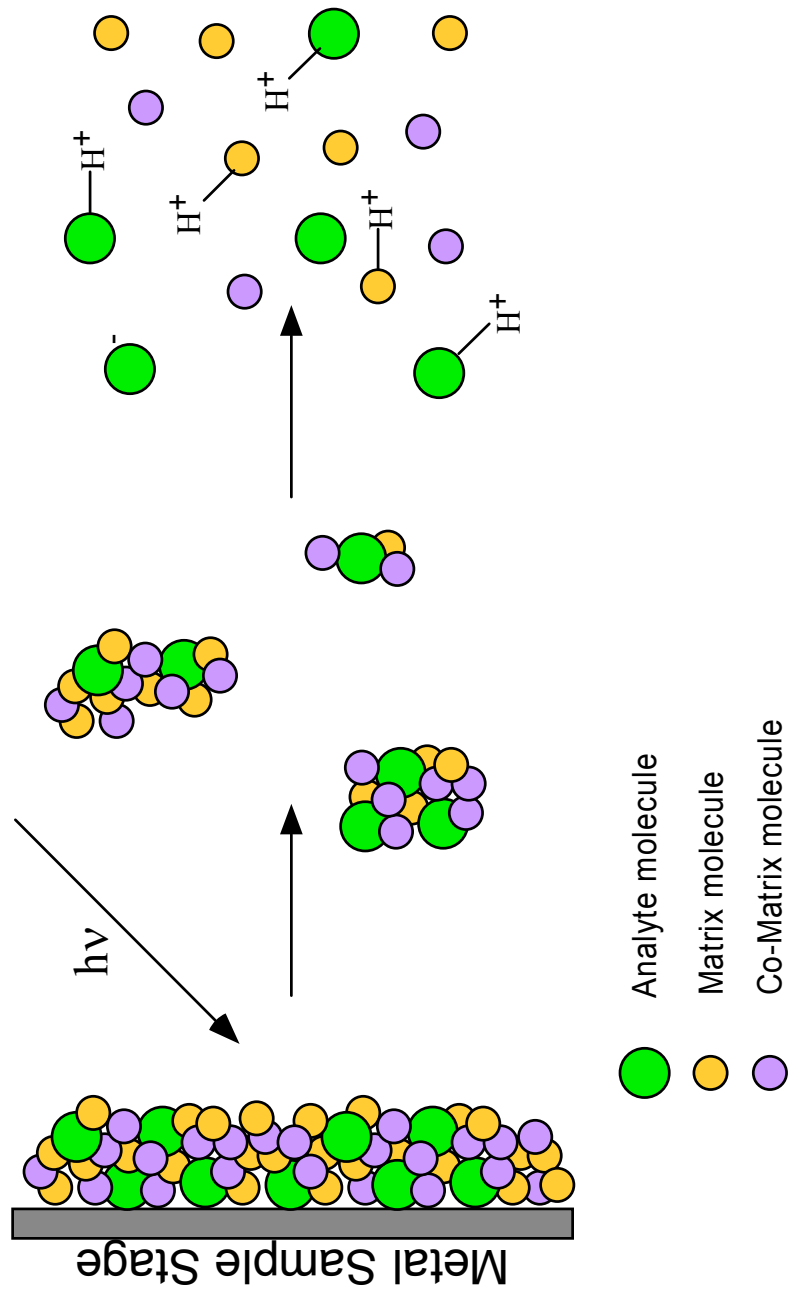
Figure 1. Pictorial representation of the MALDI ionization process. Protonated analye and matrix ions.

Methods for Investigating Gas-Phase Biomolecules

The ability to produce intact biomolecules in the gas-phase has assisted understanding of factors influencing protein structure.[7,8] Investigating peptides and proteins in the absence of solvent reveals intrinsic intermolecular interactions within the molecule as hydration effects are eliminated. By independently studying the effects of intramolecular interactions on secondary and tertiary structure of peptides and proteins, the influence of hydration can be better understood. Hence, investigation of these factors independently aids results obtained by solution phase investigations.

Despite the influence that novel ionization sources have on mass spectrometry, relatively few methods are available for structural determination of biological molecules in the gas-phase. These methods include ion dissociation,[9,10] ion mobility,[11] and gas-phase ion molecule reactions.[12] Investigating peptide and protein structure by dissociation methods typically involves vibrational excitation of the analyte ion to facilitate unimolecular dissociation. Activation generates fragment ions that represent connectivity of the precursor ion structure. Although numerous dissociation techniques have been utilized in mass spectrometry,[13,14,15,16,17,18,19] limited information is gained about certain (*i.e.* hydrogen bonding) intermolecular forces within peptide ions through dissociation. Despite this limitation, dissociation methods are of paramount importance for sequencing, revealing the primary structure of the peptide ion.

The implementation of ion mobility for investigation of peptide ion conformations is a relatively novel application.[20,21] Ion mobility utilizes physical methods to deduce structural information about ions by making drift time measurements.

The drift time collision cross-section of a peptide ion is related to its three-dimensional shape from which secondary structural information can be inferred. Ion mobility measurements are based upon how rapidly an ion moves through a buffer gas under the influence of a weak electric field. Conformational differences between ions result in gas-phase separation, as molecular size and collision cross section are proportional. Hence, gas-phase ions can be separated based upon dissimilarities in collision frequency, allowing for conformational differentiation.[22]

Ion mobility measurements are typically performed in a drift tube, of a predefined length, at several torr of helium. The drift tube consists of a linear arrangement of ring electrodes connected in series by resistors, producing a uniform electric field. Initiated by injecting an ion packet into the drift tube, separation is achieved by ion collisions with the neutral buffer gas. After transversing the drift region, ions are introduced into the source of a mass spectrometer where they are mass to charge analyzed and detected (Figure 2). Mobility of the ion is obtained by measuring the time required to reach the detector, providing an experimentally determined cross section value. Deducing conformational information from ion-mobility is achieved by comparing experimentally determined collision cross sections to theoretical values, obtained from structures generated with molecular dynamic calculations. For example, a series of experiments performed by Jarrold revealed that cytochrome *c* and selected biomolecules, assume dissimilar gas-phase conformations based upon charge state.[23] These charge state conformational differences were attributed to opposing inductive and Coulombic interactions. In an unrelated study, Jarrold utilized mobility measurements to

N₂ Laser

TOF Detector

TOF Region

Mobility Detector

Direct Insertion Probe

Ion Mobility Cell

Orthogonal Extraction

Concentric Ring System
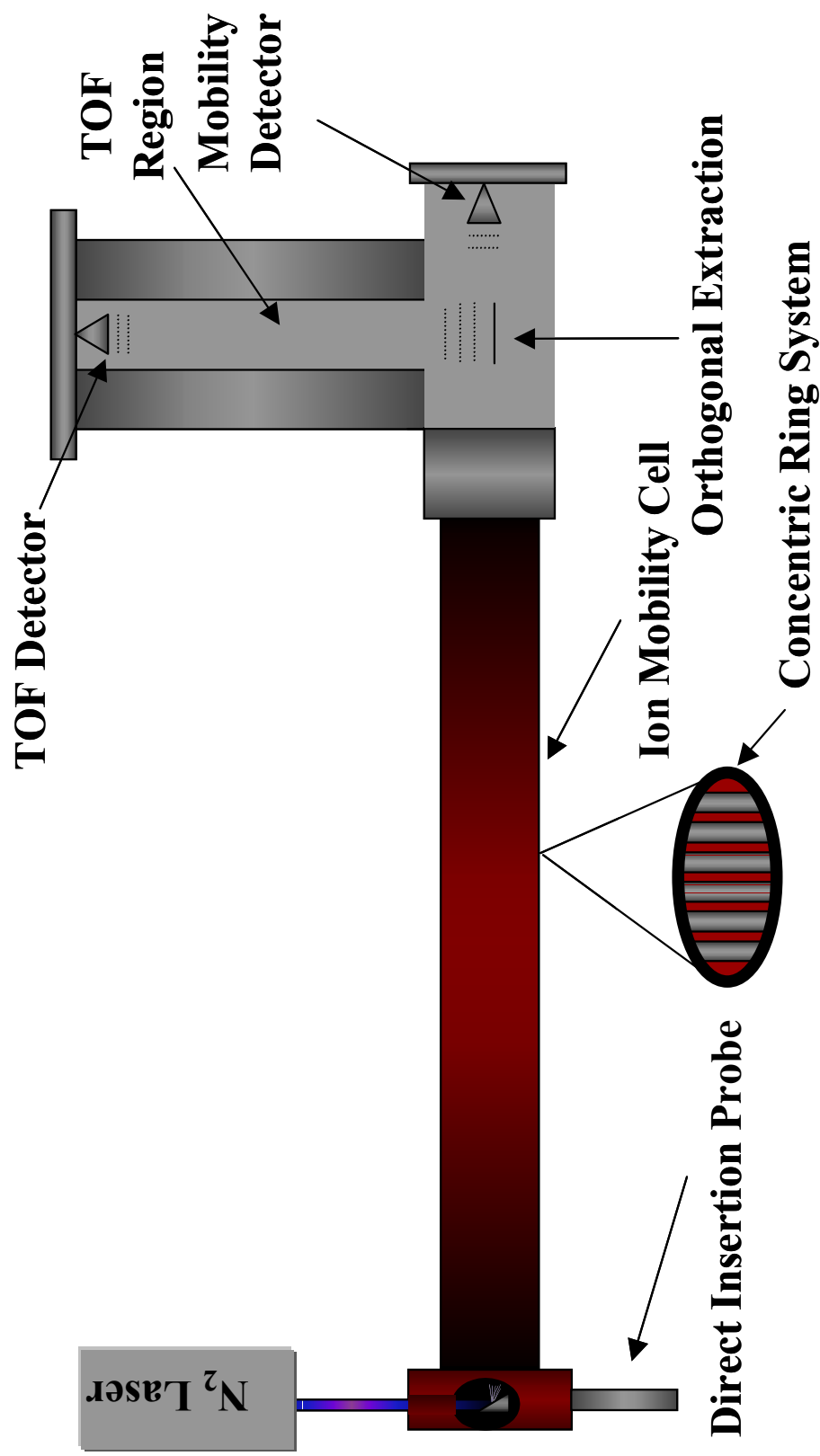
Figure 2. Schematic representation of a Ion Mobility-o-TOF MS.

study polyglycine and polyalanine peptides.[20] Results suggested that these peptide ions,

self-solvate resulting in globule conformations. Hence, ion mobility measurements have

been used in conjunction with molecular dynamic calculations to deduce ion

conformations, revealing secondary structure information for peptides and proteins.

The implementation of mass spectrometry for studying gas-phase ion-molecule

reactions is a long-standing and well-established field. Investigation of ion molecule

reactions by mass spectrometry has provided information about ion structure and been

used to infer structural information for peptide ions.[24] Of the ion-molecule probes

employed for structural determination, none have been as successful as

hydrogen/deuterium (H/D) exchange. This isotope-labeling technique is based upon the

exchange of labile hydrogens (*i.e.* amine, amide, and –OH) with a deuterium reagent.

Deuterium incorporation is proposed to occur at exchange positions that are exposed to

the reagent gas, providing information on molecular structure.[25] Thus, utilization of

mass spectrometry with gentle molecular probes such as gas-phase H/D exchange can

provide key insight into the intrinsic factors that determine gas-phase ion structure.

Many different mass spectrometers have been utilized for investigation of

peptide conformations by gas-phase H/D exchange. For example, Dokkeran and

Harrison implemented a hybrid magnetic sector/quadrupole mass spectrometer for

investigation of the twenty common amino acids and selected di- and tripeptides.[26]

Results from reaction with ND_3 revealed that basic amino acid residues were less

efficient at H/D exchange when compared to their alkyl side chain counterparts. In

addition, it was concluded that the reaction time within the collision cell was insufficient

for desired measurements. In a separate experiment, McLuckey utilized a quadrupole ion trap mass spectrometer to monitor the gas-phase H/D exchange of bradykinin ions.[27] These studies suggest the existence of two gas-phase ion conformations for bradykinin.

Of the mass spectrometers employed for investigation of peptide ion conformations by gas-phase H/D exchange, Fourier-transform ion cyclotron mass spectrometry (FT-ICR MS) has been used for the majority of these studies. The advantages of FT-ICR MS over other mass spectrometers include, ultra high mass resolution,[28,29] multichannel detection (Fellget advantage),[30,31] adaptability of numerous ionization sources,[32,33] non-destructive detection,[34,35] and the ability to isolate and store ions.[36,37] These attributes have been utilized by various groups to infer structural features of biomolecules. For example, Freitas and Marshall utilized a FT-ICR MS for the investigation of bradykinin ions.[38] These gas-phase H/D exchange studies were interpreted as evidence that bradykinin exists as a zwittterion in the gas-phase. Experiments performed by Beachamp implemented a FT-ICR MS to examine the H/D exchange reactions of protonated glycine oligomers with different deuterium reagents.[39] Findings from these studies showed that reaction kinetics were highly dependent on peptide structure and the gas-phase basicity of the exchange reagents. Hence, the advantages afforded by FT-ICR MS, with delicate ionization sources such as MALDI, have provided a powerful and convenient means for investigation of peptide ion secondary structure.

Gas-phase H/D exchange experiments utilizing a FT-ICR MS are typically performed in a cell. The cell, usually consisting of three pairs of parallel plates, is

assembled to make a cube and oriented within a uniform magnetic field under ultra high vacuum conditions ($<10^{-9}$ torr). A combination of magnetic and electric fields creates a three-dimension trap, allowing for ion storage. While trapped, the peptide ions are exposed to low pressures (5×10^{-8} to 1×10^{-7} torr) of deuterium reagent gas, such as D_2O or ND_3, for various time intervals. This variable ion-molecule reaction delay is followed by mass analysis and detection. The relative intensities of the mass spectral peaks (Figure 3) reveal the amount of deuterium incorporated during the reaction period. These intensities are recorded as a function of reaction time, producing temporal plots (Figure 4) from which kinetic rates and extent of deuterium incorporation can be obtained. It has been suggested that these measurements can be used to infer structural features of complex peptide ions and may reveal sites of ionization.[40,41]

Factors Affecting Gas-Phase H/D Exchange

Despite the utilization of FT-ICR MS for investigation of peptide and protein conformations by gas-phase H/D exchange, relatively few studies have been performed to determine structural and mechanistic features influencing reaction. Issues affecting the rate and extent of deuterium incorporation have been quite controversial and are a continuing source of question. For example, Wyttenback and Bowers have suggested that a molecule's protonation site is the most influential factor affecting gas-phase H/D exchange.[25] They proposed that the mechanism for H/D exchange involves the protonated charge site and a nearby basic site. The proximity of these sites, as well as the accessibility of the reagent gas, dramatically affects rates and extent of deuterium
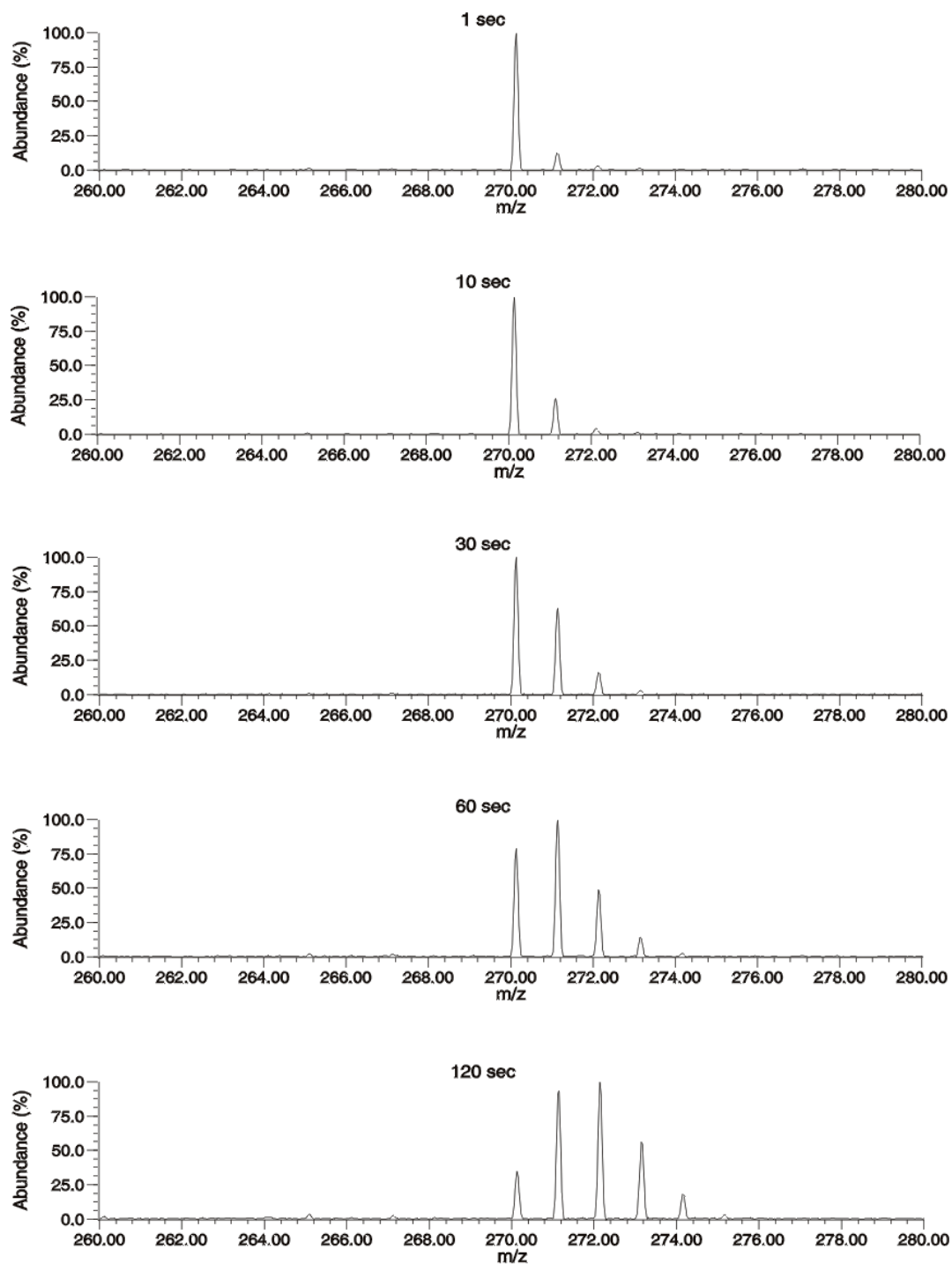
Figure 3. Partial mass spectra of protonated GlyGlyHis reacted with
deuterated methanol. Reaction times ranging from 1 - 120 seconds.
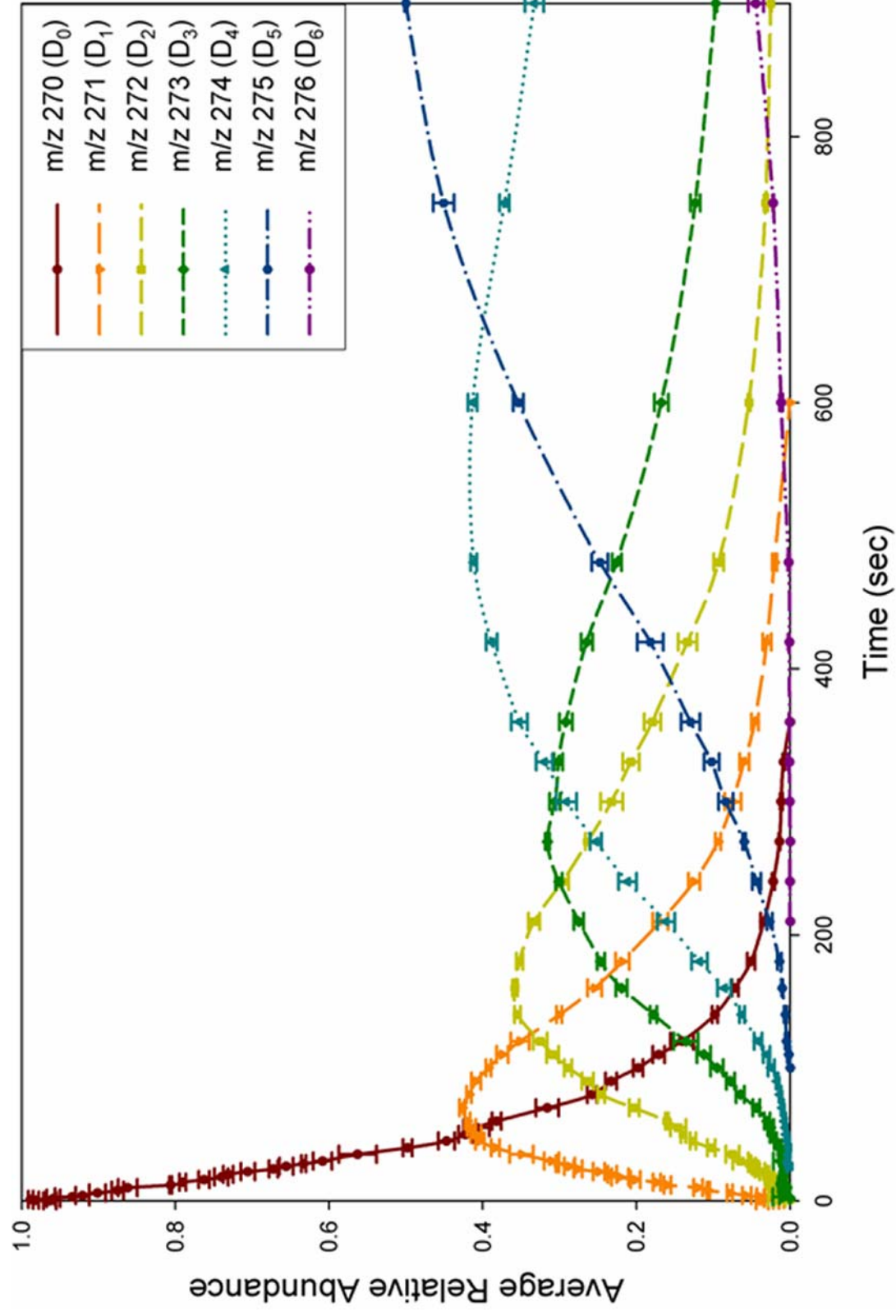
Figure 4. Temporal plot for gas-phase H/D exchange of protonated GlyGlyHis with deuterated methanol at ~1.4 E -7 torr.

uptake. Charge site initiated H/D exchange has also been investigated by Beauchamp.[42] Beauchamp suggests that crown ether complexation inhibits H/D exchange of protons located at the charge site, while protons involved with inductive stabilization by remote hydrogen bonding are unaffected. Conversely, experiments performed by Gard and Lebrilla were interpreted as evidence that the site of protonation is not necessarily the sole or even primary site of exchange.[43] This conclusion was based upon investigation of selected amino acids and their methyl ester derivatives, revealing that carboxylic acid functional groups undergo H/D exchange three to ten times faster than amines. Hence, it appears that the factors affecting H/D exchange remain a source of debate. Studying these factors is important for better understanding of the conformational information obtained by gas-phase H/D exchange.

Many of the experiments performed to elucidate factors influencing gas-phase H/D exchange have been carried out on non-polar, aliphatic amino acids and peptides.[39,43,44,45,46] In these systems, the most likely site for protonation is the *N*-terminal amine, with possible charge site solvation by amide carbonyl groups.[47] Although understanding of gas-phase H/D exchange has been gained by studying these systems, the effect that basic amino acid residues have on deuterium incorporation has received little attention. Unlike the other commonly occurring amino acids, histidine, lysine, and arginine are most likely protonated on their respective side chains.[48,49,50] Therefore, peptides containing these amino acids are presumably protonated on the side chain of the basic residue, with intramolecular charge solvation by neighboring functional groups. Given that charge site location appears to influence deuterium

incorporation, elucidation of effects that basic residues have on H/D exchange is essential to better understand information gained from such experiments. The objective of the research described herein is to investigate the influence that basic residues have on deuterium incorporation for peptide ions. Specifically, these experiments attempt to unravel the effect that position (*i.e.* *N*-terminal, internal, or *C*-terminal) of the basic amino acid has on H/D exchange. To perform the desired gas-phase H/D exchange experiments a FT-ICR MS, employing a MALDI source was, designed, fabricated, and tested.

CHAPTER II

EXPERIMENTAL

Instrument Apparatus

Fourier transform-ion cyclotron resonance mass spectrometry (FT-ICR MS) is an instrument technique that effectively converts ionic mass-to-charge ratio (m/z) to an experimentally observable frequency. Since its introduction by Comisarow and Marshall[51] in 1973, FT-ICR MS has experienced explosive growth. Of the numerous advantages afforded by FT-ICR MS, the two most utilized attributes are the ultra high m/z resolution and ion storage capabilities. These characteristics have been utilized for the accurate m/z determination of complex petroleum products[52] and peptide isobars[53] as well as ion structural characterization by dissociation[54,55] and ion-molecule reaction chemistry.[56,57] In addition, the versatility of FT-ICR MS has spawned numerous instrument alterations,[58,59,60,61] allowing investigation of different chemical systems. For example, Marshall[62] employed a dual octupole ion guide to externally accumulate ions for subsequent ejection into a FT-ICR MS instrument, resulting in increased sensitivity and resolution of electrosprayed peptide ions. Despite the many modifications employed for FT-ICR MS optimization, the instrument consists of four basic components. The first element, characteristic of all FT-ICR MS, is the magnet. Although many of the first FT-ICR MS utilized electromagnets, the high field strengths afforded by super-conducting solenoid magnets dramatically increased the performance of the technique.

Some of the advantages provided by high magnetic fields include, improved m/z resolving power, increased data acquisition speed, enhanced upper m/z limits, improvement in stored ion densities, and prolonged ion trapping duration.[63] Due to the benefits of conducting FT-ICR MS at elevated magnetic field strengths, superconducting magnet technology remains an expanding area of development.

The second instrument component is the FT-ICR MS cell. Although various designs have been developed and implemented, all cells consist of at least three pair of parallel electrodes oriented to make a geometric shape of finite volume. One of the first cells utilized for FT-ICR MS was a cubic design[64] (Figure 5). This cell is oriented in the homogeneous magnetic field region with two pair of electrodes aligned parallel and the other pair orthogonal to the field axis. The plates orthogonal to the magnetic field are referred to as trapping electrodes, while one pair of plates oriented parallel to the field are called transmitter electrodes and the other pair receiver electrodes. Described in the following sections, combination of magnetic and electric fields allows m/z analysis and detection, as well as, ion confinement.

The third instrument component of a FT-ICR MS is the high vacuum chamber. Oriented through the bore of a superconducting magnet, the vacuum chamber maintains the FT-ICR MS cell at low pressures ($<10^{-9}$ torr). High pressures influence FT-ICR MS performance during mass analysis and detection, because ion-neutral collisions degrade m/z resolution and sensitivity.[65] Therefore, most FT-ICR MS instruments utilize the high pumping speeds obtainable by cryogenic or turbomolecular pumps.

The fourth part of a FT-ICR MS is the data acquisition system. This consists of a
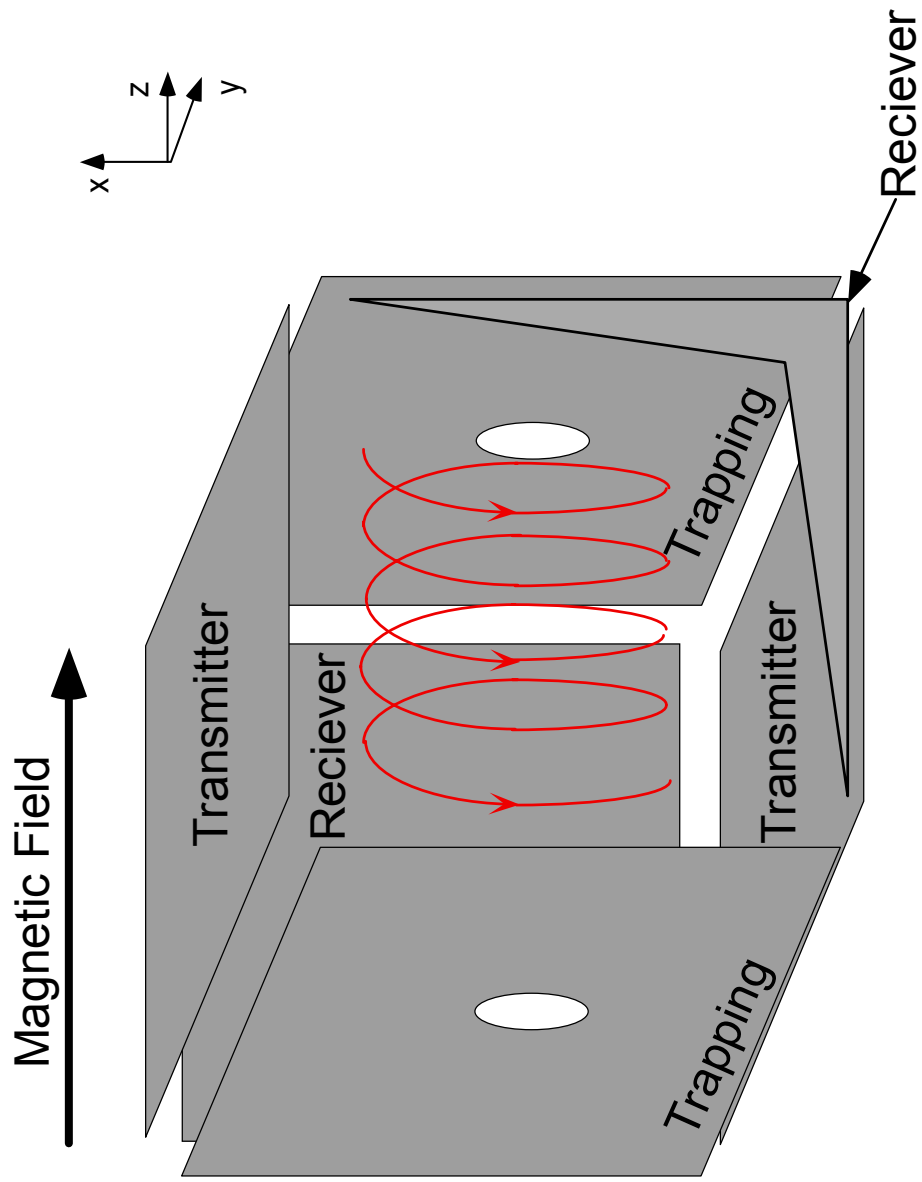
Figure 5. Schematic representation of a typical cubic cell.

computer, frequency synthesizer, pulsed delay generator, broadband radio frequency synthesizer, preamplifier, and a fast transient digitizer. These components control the cell electrodes allowing for m/z analysis and detection.

Principles of Ion Motion in FT-ICR MS

FT-ICR MS is based upon the motion of a gas-phase ion in a spatially uniform magnetic field. An ion in a magnetic field experiences an inward directional Lorentz force, F_L, perpendicular to the magnetic field direction (axis z).

$$F_L = qv_{xy}B \tag{1}$$

$$F_C = mv_{xy}^2/r \tag{2}$$

$$\omega_c = qB/m \tag{3}$$

Given by equation 1, the Lorentz force is the product of q (or z), the charge of the ion (in Coulombs), v_{xy}, the velocity of the ion (in meters/second) and, B, the magnetic field strength (in Tesla). This force, imposed by the magnetic field, causes the ion to proceed in a circular "cyclotron" orbit about the x-y plane, confining the ion in that dimension (Figure 6). Procession of an ion in a circular orbit produces an outward directional centrifugal force, F_C, (equation 2; m is the ion mass in kilograms, and r is the radius of the ion orbit in meters) balancing the force from the magnetic field. By setting equations 1 and 2 equal to each other one can derive equation 3, the celebrated cyclotron equation. The cyclotron equation predicts that an ion in a magnetic field, at some value B, will
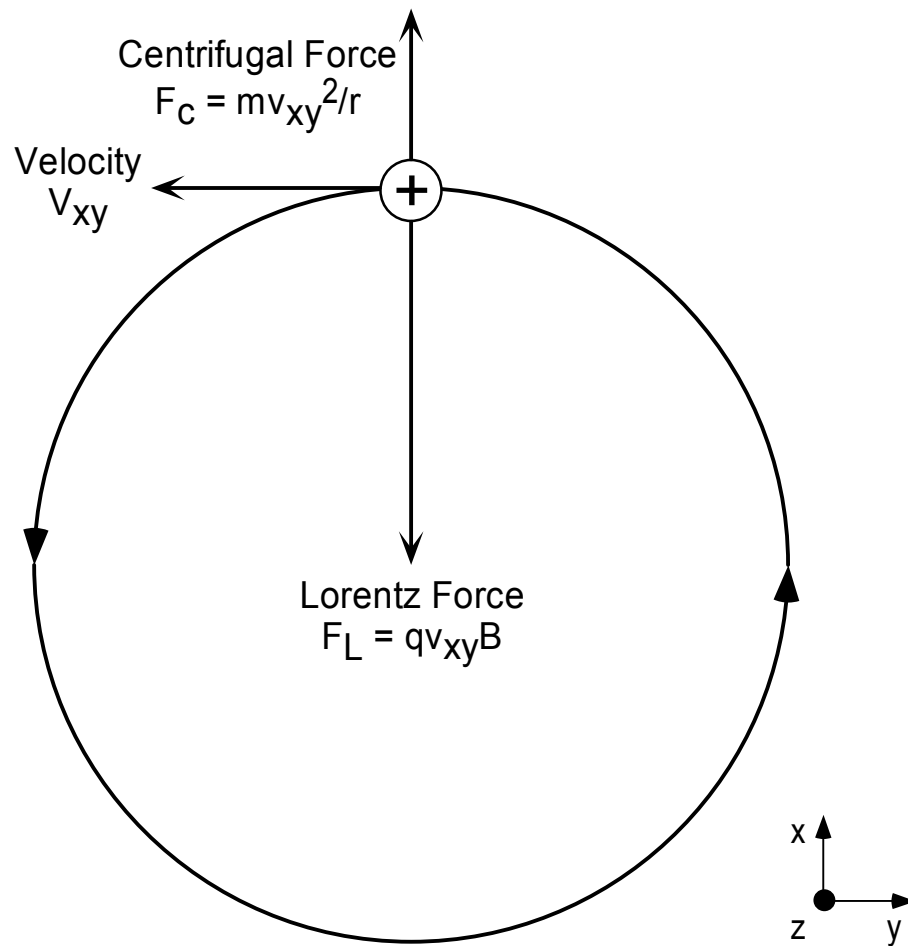
Figure 6. Schematic diagram of cyclotron motion and the forces acting upon an ion in a magnetic field.

proceed in circular orbit at a frequency, ω_c, inversely proportional to the m/z of the ion. Hence, cyclotron motion of an ion in a magnetic field is frequency dependent, and the basis of mass to charge measurements in FT-ICR MS. Although ion motion perpendicular to the magnetic field is confined, motion parallel to the field is unobstructed. This unrestricted motion allows ions to escape the magnetic field along the z-axis. To confine ions within the magnet, McIver implemented an electrostatic potential, orthogonal to the magnetic field axis.[66] Axial confinement is typically achieved by placing two low voltage (~1 V) parallel, "trapping plate," electrodes within the magnetic field. Application of an electrostatic potential, perpendicular to the magnetic field dimension, confines ions to simple harmonic motion along the z-axis (Figure 7). Implementation of a trapping potential within a magnetic field confines ion motion in three dimensions, allowing for prolonged gas-phase ion storage.

In addition to an axial confining field, generated by the trapping plates, electrostatic potentials also create radial repulsive forces in the x-y plane (Figure 8). This force opposes the magnetic field (Figure 9), thereby decreasing the effective magnetic field strength. Reducing the magnetic field strength has a proportional effect on ion cyclotron frequency, causing increases in measured m/z values. Therefore, radial components of the electric field must be taken into consideration for accurate m/z measurements in FT-ICR MS. In addition to affecting ion cyclotron frequency, application of an electrostatic potential within a magnetic field generates a third fundamental motion in FT-ICR MS, magnetron motion. Magnetron motion is the procession of and ion's cyclotron orbit center about the electrostatic potential surface
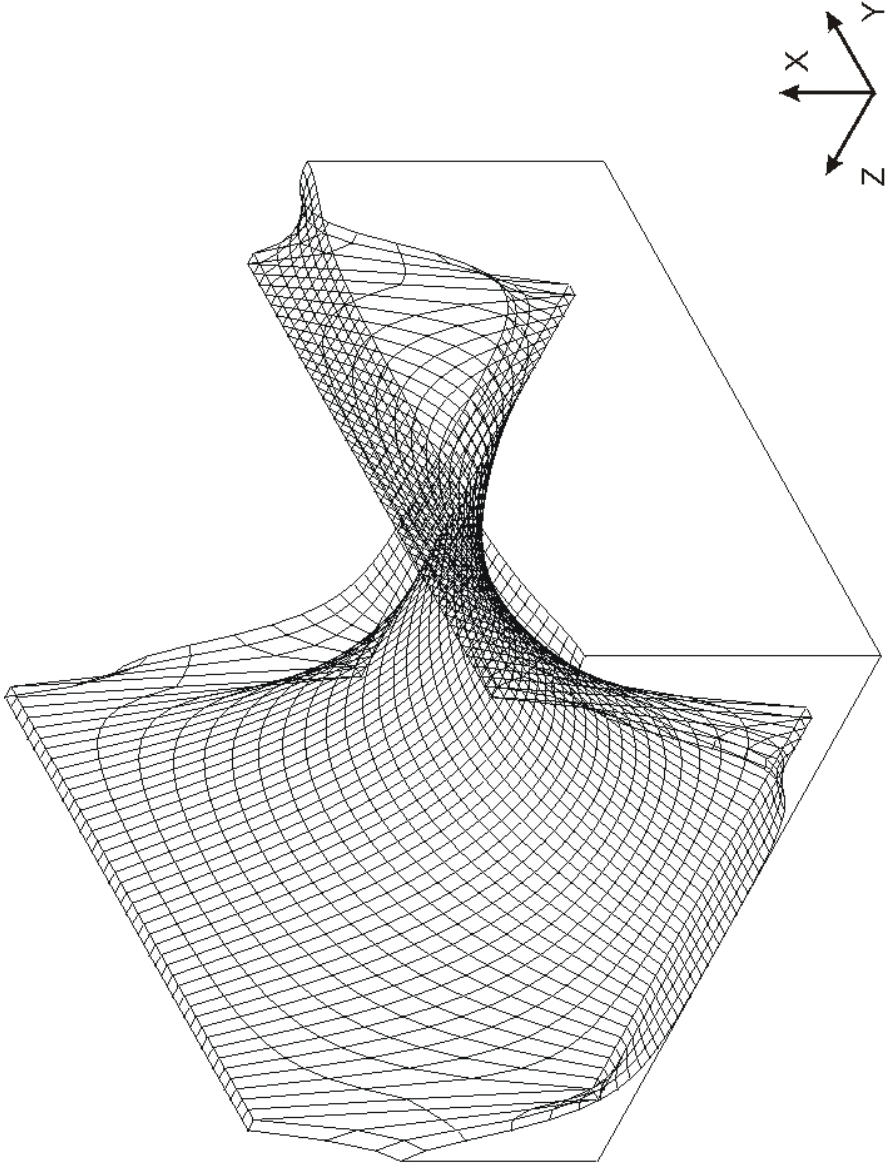
Figure 7. Plot of the axial component for the electrostatic trapping potential of a cylindrical cell with dimensions 4.0 cm x 4.0 cm.
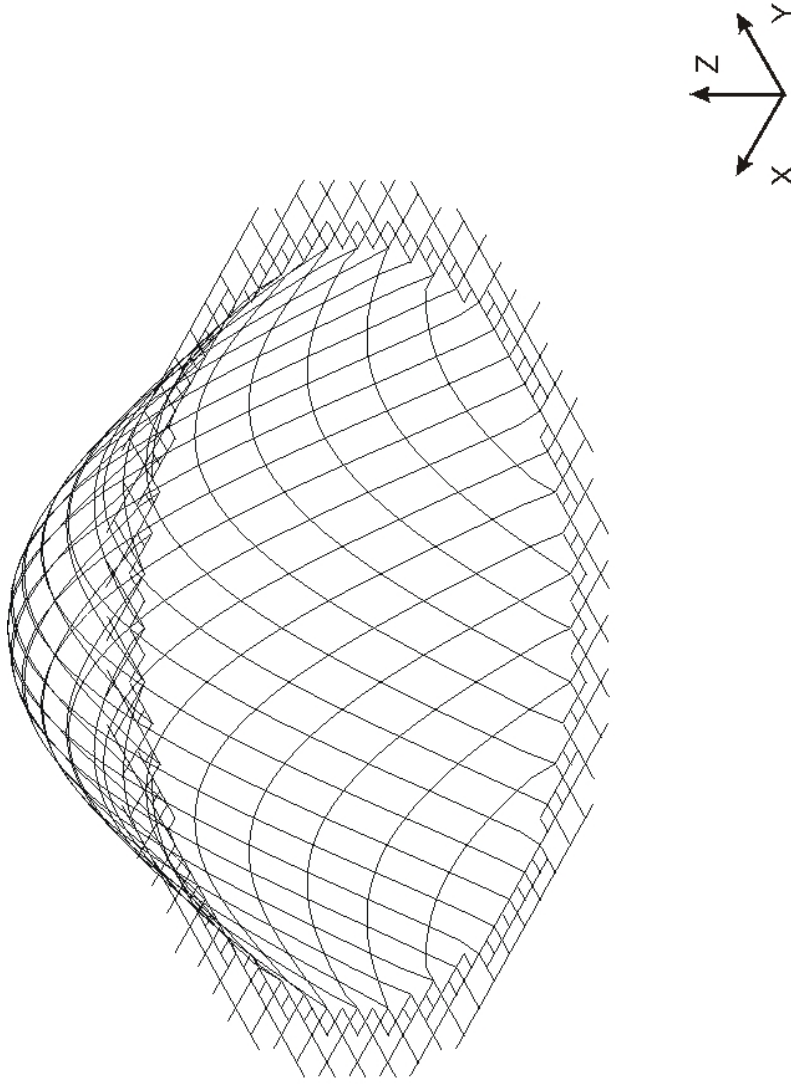
Figure 8. Plot of the radial component for the electrostatic trapping potential of a cylindrical cell with dimensions 4.0 cm x 4.0 cm.

Radial Electric Field

Centrifugal Force
$F_C = mv_{xy}{}^2/r$

Axial Electric Field

Velocity
V_{xy}

Lorentz Force
$F_L = qv_{xy}B$

x

y

z
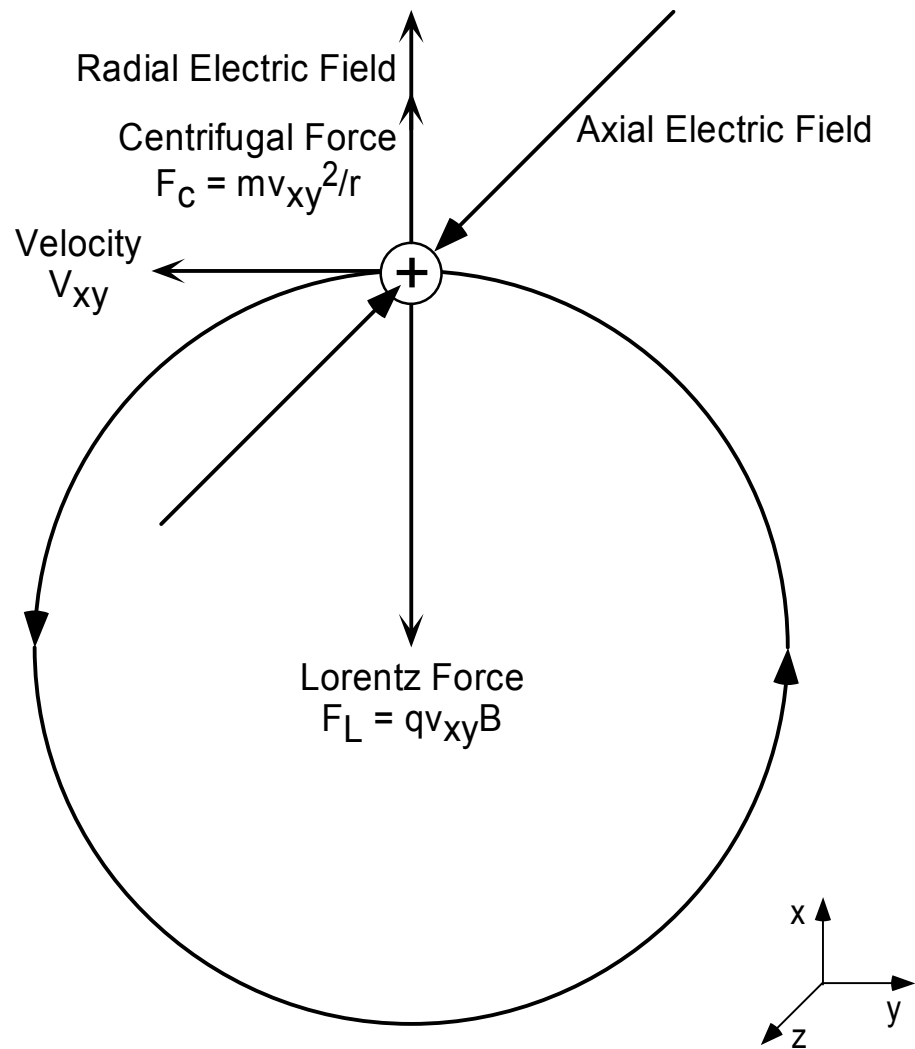
Figure 9. Schematic diagram of cyclotron motion and the forces acting upon an ion by crossing magnetic and electric fields.

(Figure 10) generated by the trapping field. Magnetron amplitude is dependent upon displacement of the cyclotron orbit from the radial electric field center. This ion motion serves no useful purpose, but rather is a byproduct of crossing magnetic and electric fields.

Mass-to-Charge (m/z) Measurements in FT-ICR MS

Mass to charge measurements in FT-ICR MS is based upon observation of an ion's cyclotron frequency in a spatially uniform magnetic field. Detection is preceded by radial expansion of the cyclotron orbit by two "transmitter" electrodes oriented parallel to the magnetic field. Excitation is achieved by applying a dipolar, sinusoidal electric field on the transmitter plates, resonant with the cyclotron frequency of the ion.[51] This dipolar electric field results in energy absorption by the ion, increasing its cyclotron orbit. Cyclotron orbit expansion creates a phase coherent packet of ions with the same m/z for subsequent detection (Figure 11). Dipolar excitation may also be employed for m/z selective ejection of unwanted ions by increasing cyclotron orbits to dimensions greater than the cell geometry.[63] Excitation may also be used to increase the internal energy of an ion by ion-neutral collisions, facilitating unimolecular dissociation.[63] In typical FT-ICR MS experiments, it is desirable to detect series of ions over a defined m/z range. Excitation of ions with different m/z values is accomplished by applying multiple frequencies to the transmitter plates[67]. Referred to as, "broadband excitation," this is typically achieved by a rapid frequency sweep, or radio frequency "chirp." An alternative mode for broadband excitation in FT-ICR MS is, Stored Waveform Inverse

.

.

Cyclotron
Orbit

Center of the radial
electrostatic potential

Magnetron
Orbit

x
z y
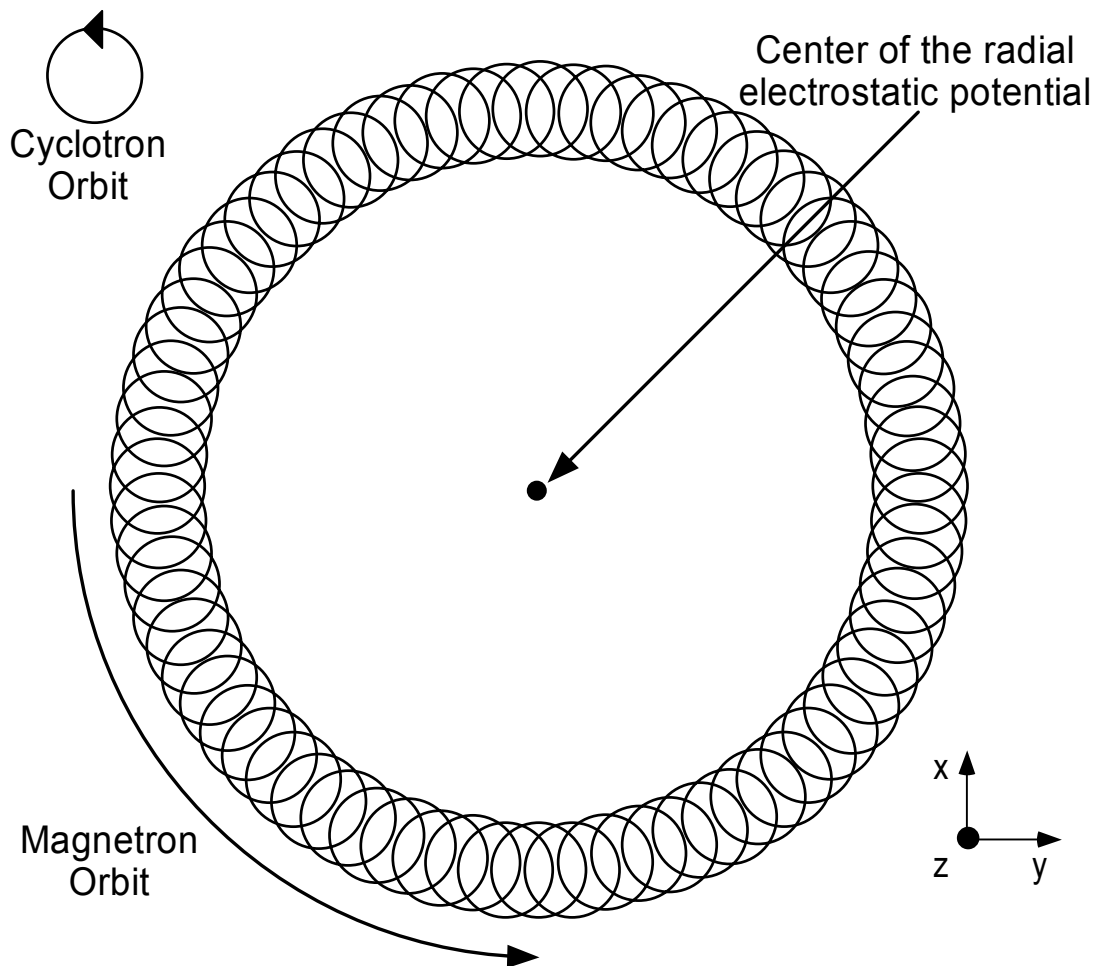
Figure 10. Schematic diagram of cyclotron and magnetron motions for
an ion, caused by crossing magnetic and electric fields.
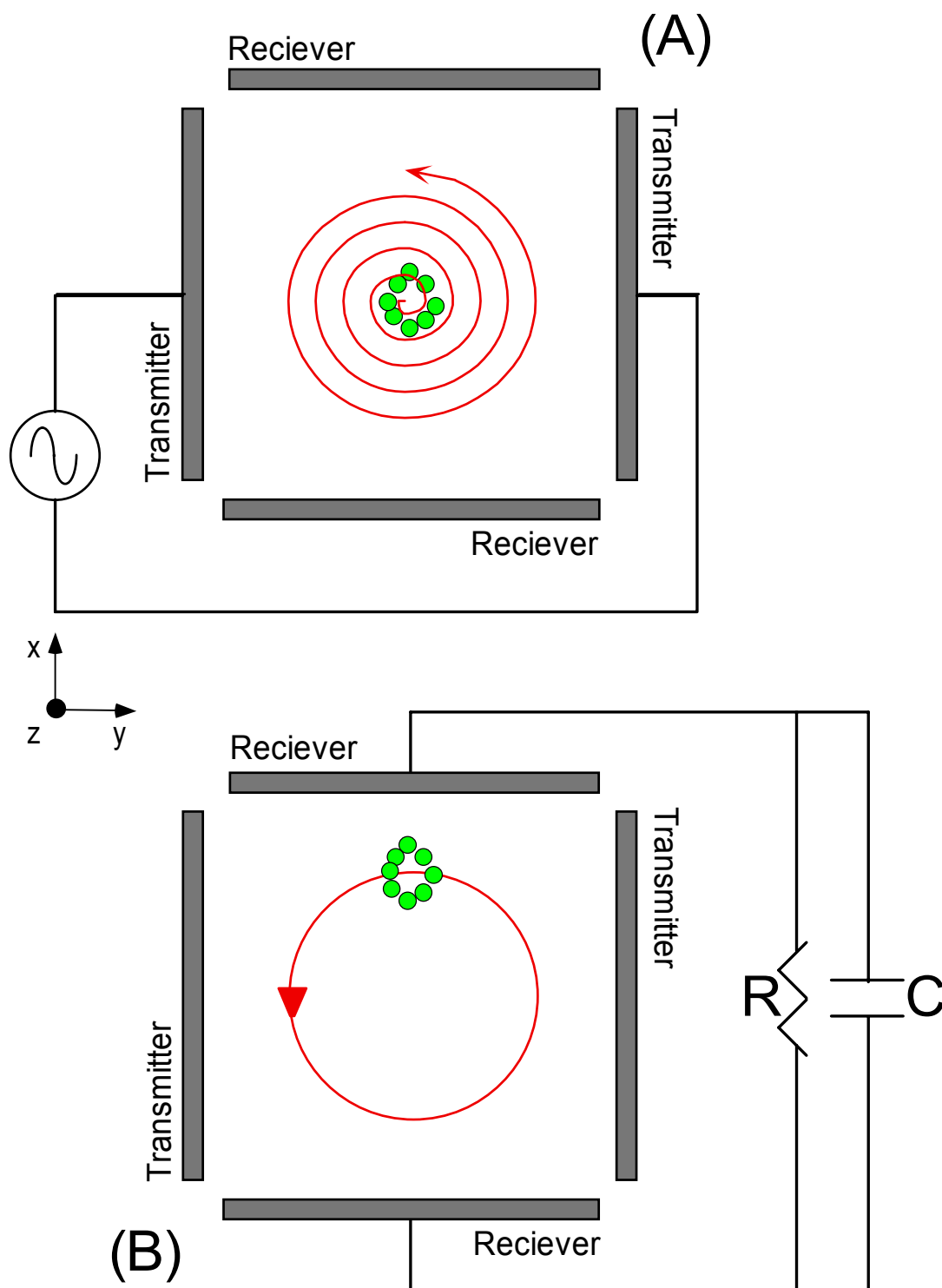
Figure 11. Pictorial representation of (a) excitation and (b) detection events
for m/z measurements in FT-ICR MS.

Fourier Transform (SWIFT).[68,69]

Following dipolar excitation, the ion packet's cyclotron orbit is detected as an oscillating point charge between a pair of "receiver" electrodes, oriented parallel to the magnetic field axis.[70] The periodic ion motion induces an alternating image current between the receiver plates. This induced radio frequency signal corresponds to the time domain oscillation of the excited ion. The convoluted transient signal is Fourier transformed, resulting in a cyclotron frequency spectrum that is mass to charge dependent (Figure 12).

Basic FT-ICR MS Experimental Sequence

Unlike other mass spectrometers, FT-ICR MS is considered a tandem in time technique. This means that ion manipulation occurs temporally rather than spatially. The separation of events in time allows for design of sophisticated experiments with minimal instrument modifications. Despite the complexity associated with time-separated processes, all FT-ICR MS experiments consist of four basic events (Figure 13). The initial step in the experimental sequence is the removal of all ions from the FT-ICR MS cell. Referred to as the "quench" event, this process ejects ions from the cell by applying antisymmetric voltages to the trapping electrodes. Under these conditions, ions are ejected axially in approximately one millisecond. Following ion removal, new ions are formed in or transported into the cell. Since FT-ICR MS is a tandem in time technique, pulsed ionization sources such as MALDI are compatible. Ionization and trapping are followed by broadband excitation. As described in the preceding section,

Time Domain Signal

Fourier Transform
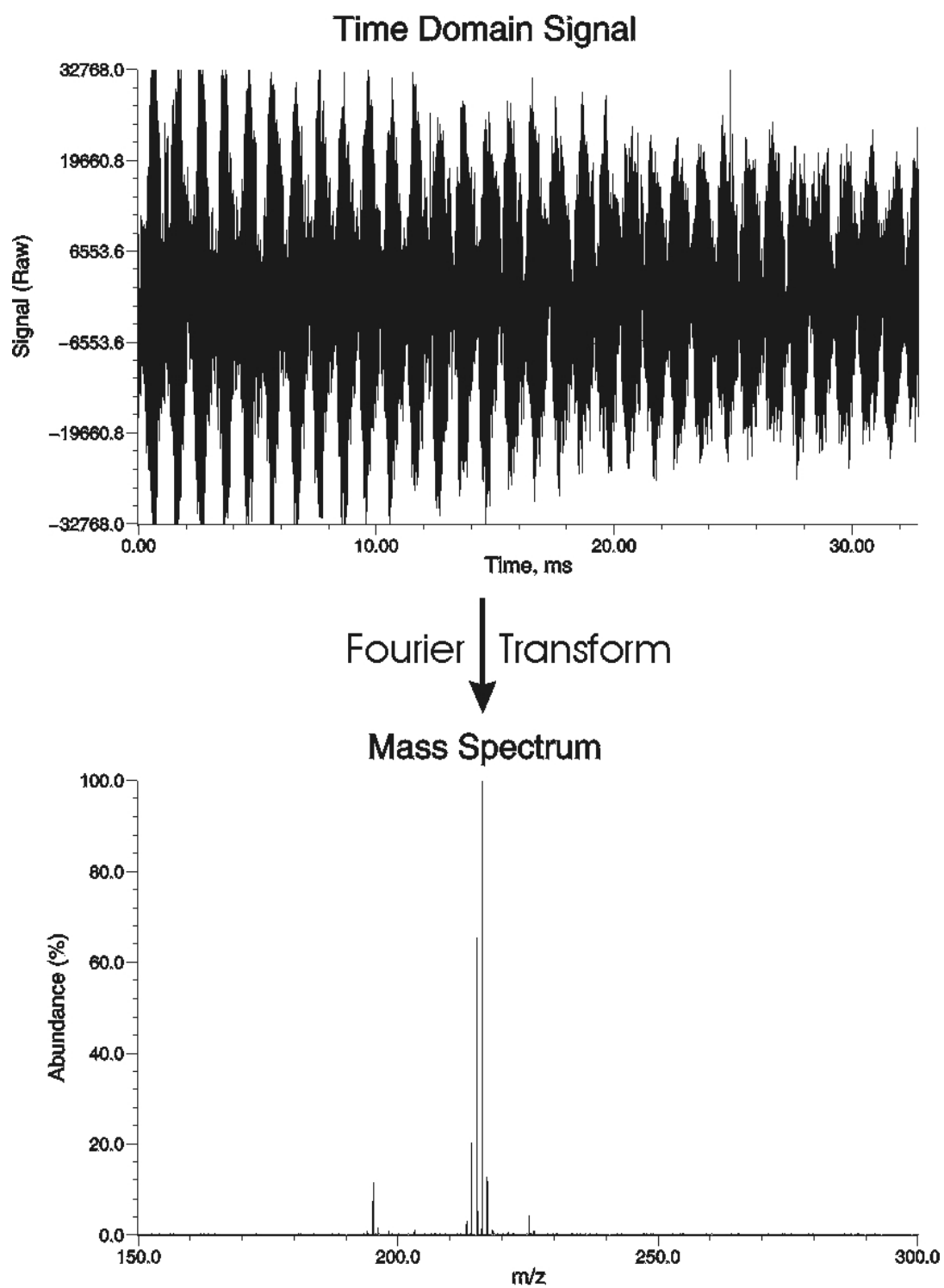
Mass Spectrum

Figure 12. Time domain transient signal and its corresponding mass spectrum produced by Fourier transform.
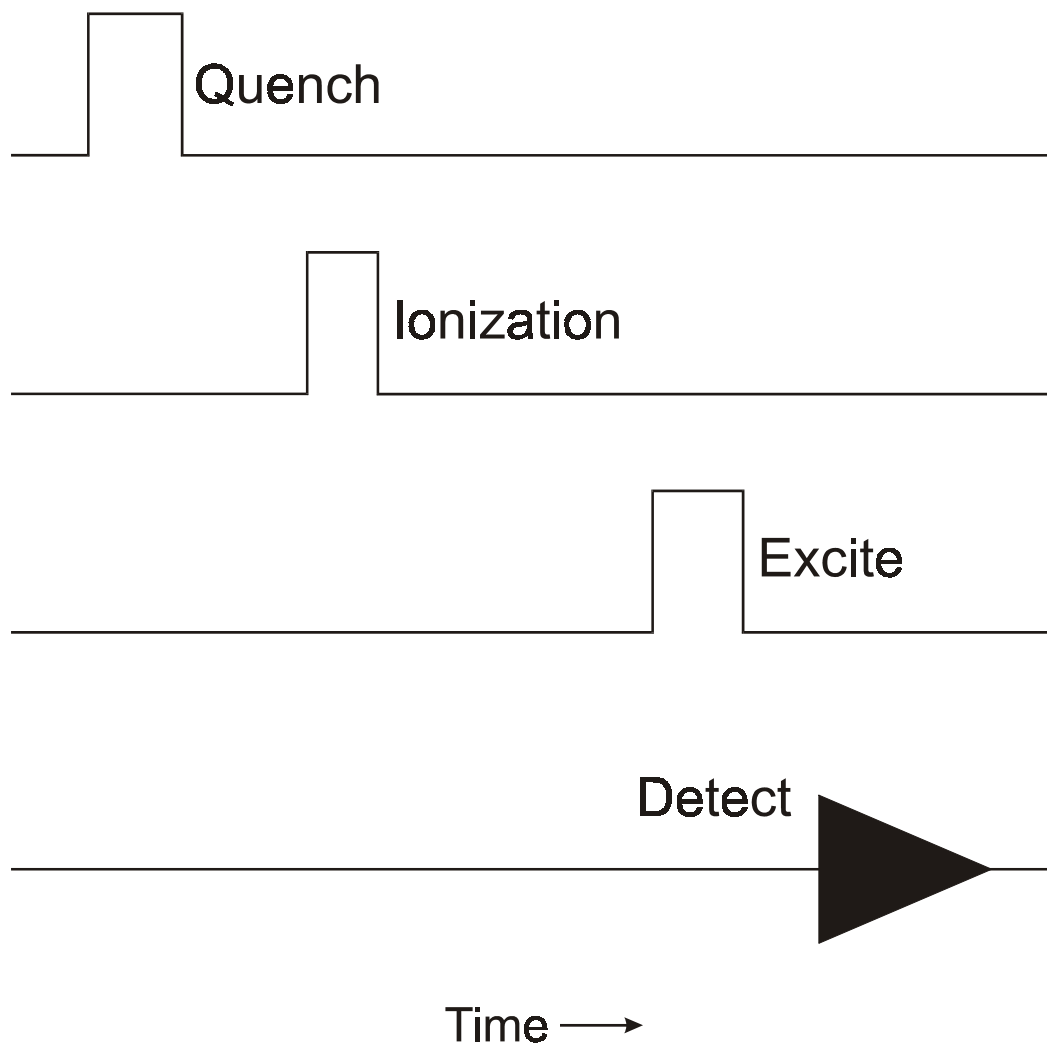
Figure 13. Experimental sequence illustrating the basic steps necessary for acquiring a mass spectrum by FT-ICR MS.

excitation causes expansion of cyclotron orbits, resulting in phase coherent ion packets with the same m/z values. FT-ICR MS experimental sequences conclude with the detection event. This is achieved by observing the m/z dependent frequency of ions, recorded as oscillating image currents on the receiver electrodes.

The tandem in time capabilities afforded by FT-ICR MS allows experimental modifications with minimal instrument alterations. Achieved by inserting additional time events between ion formation and excitation, experimental sequences can be modified for ion structural studies by dissociation or ion-molecule reactions. The ease of sequence alterations, coupled with ion storage capabilities, make FT-ICR MS an ideal mass spectrometer for fundamental gas-phase ion-molecule studies.

MALDI in a FT-ICR MS

The development of soft ionization techniques, such as MALDI, has extended the capabilities of mass spectrometry for investigation of high molecular weight, nonvolatile compounds. Although MALDI has been extensively used in time-of-flight mass spectrometry (TOF MS), the high resolution and ion storage capabilities afforded by FT-ICR MS make it an attractive alternative to TOF MS. The ability to analyze MALDI formed ions by FT-ICR MS was first demonstrated in 1992 by Wilkins.[71] Referred to as internal source MALDI, ions were produced by situating the matrix sample in close proximity (< 2 cm) to one of the trapping electrodes and irradiating it with a pulsed dye laser. Desorbed ions were translationally cooled by applying an antisymmetric, electrostatic potential on the trapping electrodes, resulting in ion deceleration.

Following a fixed deceleration time, potentials on the trapping electrodes were changed to maintain a symmetric field for axial ion confinement. Termed, "gated trapping," this electrostatic deceleration technique traps MALDI formed ions for subsequent analysis by FT-ICR MS.

Despite advantages afforded by coupling MALDI with FT-ICR MS, the internal ion source suffers for inherent limitations. According to Beavis and Chait,[72] MALDI formed ions travel at an average velocity of 750 meters/second (m/s). From their experimental results, they suggest that the mean velocity is independent of molecular weight, indicating a proportional relationship between translational energy and ion mass. Hence, deceleration of MALDI formed ions by gated trapping is relatively inefficient for high molecular weight compounds, and an obstacle for coupling internal source MALDI with FT-ICR MS. To circumvent these limitations, various instrument alterations[73,74] have been utilized to increase the gated trapping efficiency of ions formed by internal source MALDI. For example, Russell and coworkers have employed a metal chamber (referred to as a "waiting room") that seals around the sample of a direct-insertion probe to translationally cool MALDI formed ions.[73,75,76] Although these modifications have increased upper m/z limits and trapping efficiency, modifying the MALDI sample preparation method by adding fructose or sucrose co-matrices have shown to significantly increase gated trapping efficiency of MALDI formed ions.[76,77] Wilkins has speculated[71] that advantages associated with co-matrix addition are attributed to decomposition of the relatively volatile sugar during laser desorption, producing transient water and carbon dioxide molecules. This momentary high pressure region in

the MALDI desorption plume may serve to collisionally cool the analyte ions, allowing increased trapping efficiency.

In addition to an axial velocity component, MALDI formed ions also possess a radial element due to the desorption event.[78] In FT-ICR MS, radial dispersion produces spatially diffuse ions with multiple cyclotron and magnetron components. Upon excitation, the ions are observed to have various cyclotron frequencies due to their initial radial displacement. Unfortunately, cyclotron orbits with multiple amplitudes yield phase incoherent ion motion, causing poor detection performance in FT-ICR MS. Therefore, radial displacement must be corrected to fully utilize the attributes afforded by FT-ICR MS. The adverse effects of radial dispersion can be corrected by axially compressing the ions to a common point in space prior to excitation. One way to produce a well-defined ion packet for subsequent excitation is by quadrupolar axialization (QA).[79,80] Adapted for FT-ICR MS by Marshall,[81] QA is based upon coupling cyclotron and magnetron ion motions. In the presence of a collision gas, cyclotron and trapping motions contract while magnetron motion expands. Under ion-neutral collision conditions, application of an azimuthal quadrupolar field, at the ion's unperturbed cyclotron frequency, efficiently converts magnetron to cyclotron motion causing radial ion collapse to the cell center. QA has been shown to increase FT-ICR MS performance[82,83,84,85,86] and is accepted as a common radial ion cooling technique.

Besides enhancing detection performance, QA can also be used to increase axial ion transfer efficiency to other regions of the FT-ICR MS instrument.[87,88] Experiments described herein, utilize this feature to increase the transmission of MALDI formed ions

in a two-section FT-ICR MS cell. The two-section cell design was employed for spatial separation of ion cooling and ion-molecule reaction events. This cell allows control of factors influencing gas-phase ion-molecule reactions, by dividing the vacuum system with a conductance limit.[59,89] Despite issues and limitations associated with coupling internal source MALDI with FT-ICR MS, the relative ease and affordability of instrument modification make it a technique that is still implemented.[90,91]

TAMU FT-ICR Mass Spectrometer

The FT-ICR MS instrument used in these gas-phase H/D exchange studies is illustrated in Figure 14. It consists of an Oxford superconducting magnet, a Finnigan Odyssey data system and Nd:YAG laser, a high vacuum chamber, and a home built differentially pumped two-section cell. The instrument was modified from its original design to incorporate a solid-state insertion probe for internal source MALDI and a quartz view port for ultra-violet (UV), laser light transmission.

Magnet

The FT-ICR MS described herein utilizes a 3 Tesla (T) (127.7 MHz proton) field generated by an Oxford, model 125/150, horizontal bore (15 cm), superconducting magnet. The magnet consists of a leak-tight insulated assembly that incorporates a superconducting solenoid and a cryostat assembly. The cryostat assembly consists of two cambers. The inner chamber contains a solenoid and maintains the temperature at 4 Kelvin with liquid helium. This inner chamber is surrounded by a gas cooled shield and

an outer liquid nitrogen vessel. The cryostat assembly is enclosed by an outer vacuum case to thermally isolate the cryogens from ambient atmospheric temperatures.

Data System

All aspects controlling the FT-ICR MS electronics are operated by a Finnigan Odyssey data system. The system consists of a Sun Sparc station 5, an Odyssey FT/MS tower interface, a Finnigan SWIFT Cell Controller, an Extrel high voltage excite amplifier, a Nicolet dual pre-amplifier, and a Finnigan QuadAX switch unit. The cell controller externally triggers a New Wave Research, (model #MiniLase-20, Fremont, California, USA) Nd:YAG laser operated at 355 nm for MALDI ionization.

Vacuum System

The vacuum chamber consists of a 70 inch long, 4 inch inner diameter, stainless steel, main vacuum tube, oriented through the bore of the 3 T superconducting magnet. The camber is pumped by two 300 letter/second (l/s) diffusion pumps (Alcatel, Fremont, California, USA) situated on either side of the superconducting magnet. Each diffusion pump is separated from the main vacuum chamber with pneumatic gate valves, controlled by an external circuit. The diffusion pumps are backed with individual mechanical pumps, separated by molecular sieve filters. Ion gauges are situated above each diffusion stack and measure chamber pressures with vacuum gauge controllers (model #270 and #307, Gravill-Phillips, Bolder, Colorado, USA). The ion gauges were pressure calibrated by using parameterized ion gauge response factors[92]. Baseline pressures of less than 5×10^{-9} torr are routinely achieved following bake-out. The bake-out assembly consists of two, General Electric, quartz infrared lamps positioned in each
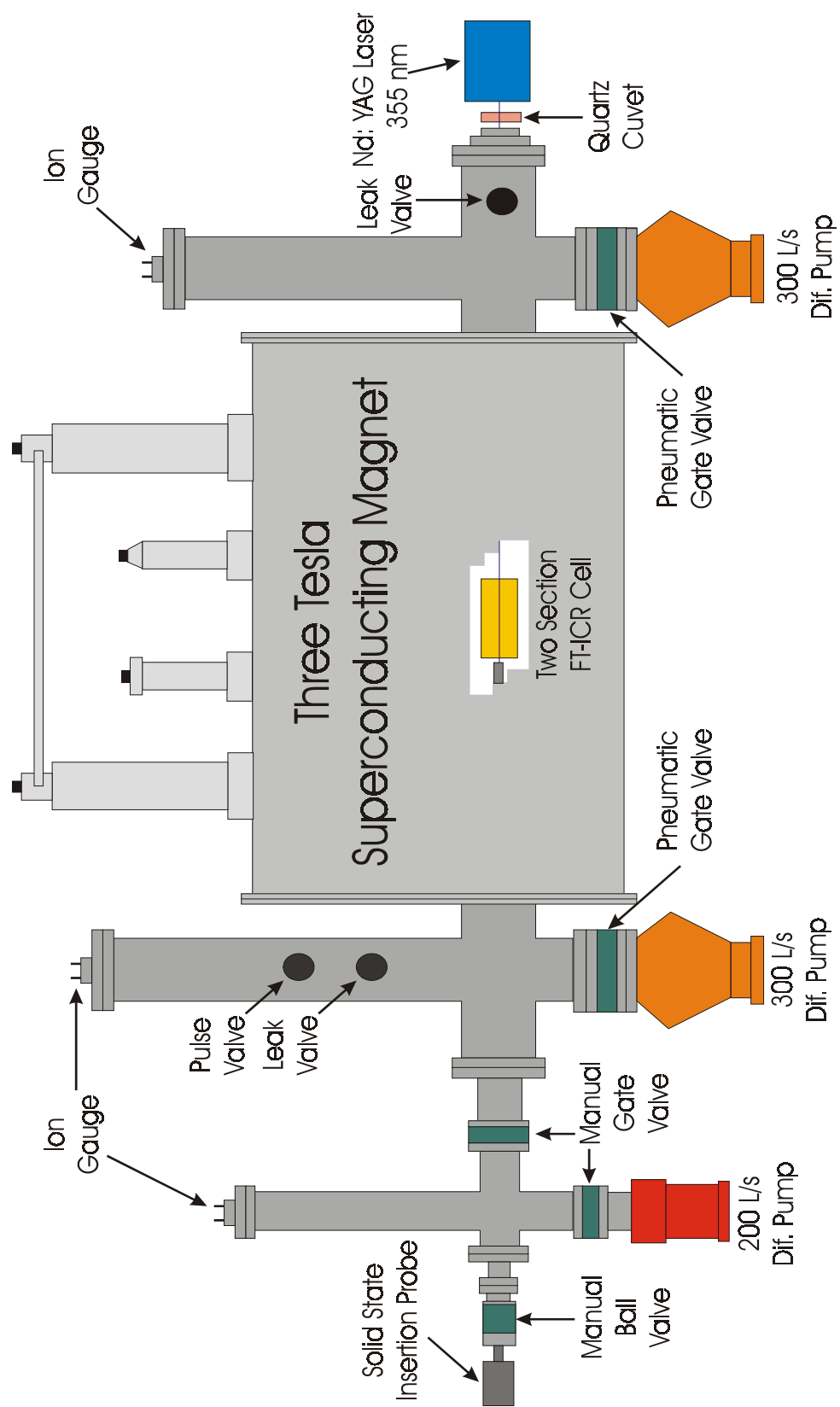
Figure 14. Schematic of the TAMU FT-ICR mass spectrometer employed for gas-phase H/D exchange.

diffusion stack and a, Brisk Heat, resistively heated blanket, wrapped around the main vacuum tube.

To accommodate a solid-state insertion probe for internal source MALDI, the vacuum chamber, described in the preceding paragraph, was modified from its original design. Teflon seals were incorporated to generate a vacuum tight fit around the rod of the direct insertion probe. Due to the inefficiency of these seals for maintaining pressure differences greater than four orders of magnitude, a differentially pumped insertion lock was incorporated, preserving the main chamber's vacuum integrity. The differential region, kept at ~5 × 10^{-6} torr by a Varian 200 l/s diffusion pump, is isolated from the main vacuum chamber by a manual gate valve. A low pressure region (~4 × 10^{-2} torr), sustained by a mechanical pump, is separated from the insertion lock by a manual ball valve. In addition to these changes, a quartz view port was mounted on the opposite side of the vacuum system, allowing transmission of UV laser light into the chamber.

Located on each end of the vacuum system are variable leak valves (model #951-5106, Varian, Inst., Walnut Creek, California, USA), used for reactant gas introduction. These valves admit gas into the chamber at a constant rate, resulting in stable reagent pressures. The static operating pressures ranged from 1 × 10^{-8} to 2 × 10^{-7} torr, allowing determination of ion-molecule reaction rate efficiencies. In addition, a double pulse valve unit was also mounted to the main vacuum chamber. This unit consists of a toggle valve, a gas manifold, and two pulse valves (model #9-199-900 and #009-0143-900, General Valve Corp., Fairfield, New Jersey, USA) connected in series by a 0.25 inch stainless steel tube. The pulse valves fire in succession to admit collision gas into the

vacuum chamber for QA, resulting in a maximum pressure increase of 1×10^{-6} torr. Vacuum baseline pressures are typically restored in approximately two seconds by the diffusion pumps. All valve systems are connected to a roughing line maintained by a separate mechanical pump. The normal pressure of the backing line is 4×10^{-2} torr and is connected to each valve by individual toggle valves.

Differentially Pumped Two Section Cell

A schematic of the differentially pumped two-section FT-ICR MS cell, used in these gas-phase H/D exchange studies, is illustrated in Figure 15. The cell components are machined from 101 oxygen free copper, and assembled by press fitting 0.0625" ruby spheres (Alceram Technologies Inc.) between the electrodes that comprise the cell. The two-section cell consists of two collinear (4.0 cm × 4.0 cm), cylindrical cells, which share a common trapping electrode. Conventionally referred to as the "conductance limit," this common trapping electrode has a 0.079" (2 mm) aperture allowing ion partitioning between cells by applying an antisymmetric electric field to the trapping electrodes. The conductance limit also separates the vacuum chamber allowing for pressure differentials of approximately two orders of magnitude. The trapping electrode on the source cell consists of a 20 line per inch copper grid that is stretch over an oxygen free copper frame. This wire mesh (Buckbee-Mears, St. Paul, Minnesota, USA) electrode defines the electric field and facilitates high ion transmissions into the source cell upon MALDI desorption. The trapping electrode on the analyzer cell consists of a solid copper plate with a 0.079" (2 mm) aperture. This electrode supports a 1 inch (25.4 mm) diameter, 3.94" (100 mm) focal length, fused silica, plano convex lens (part #014-
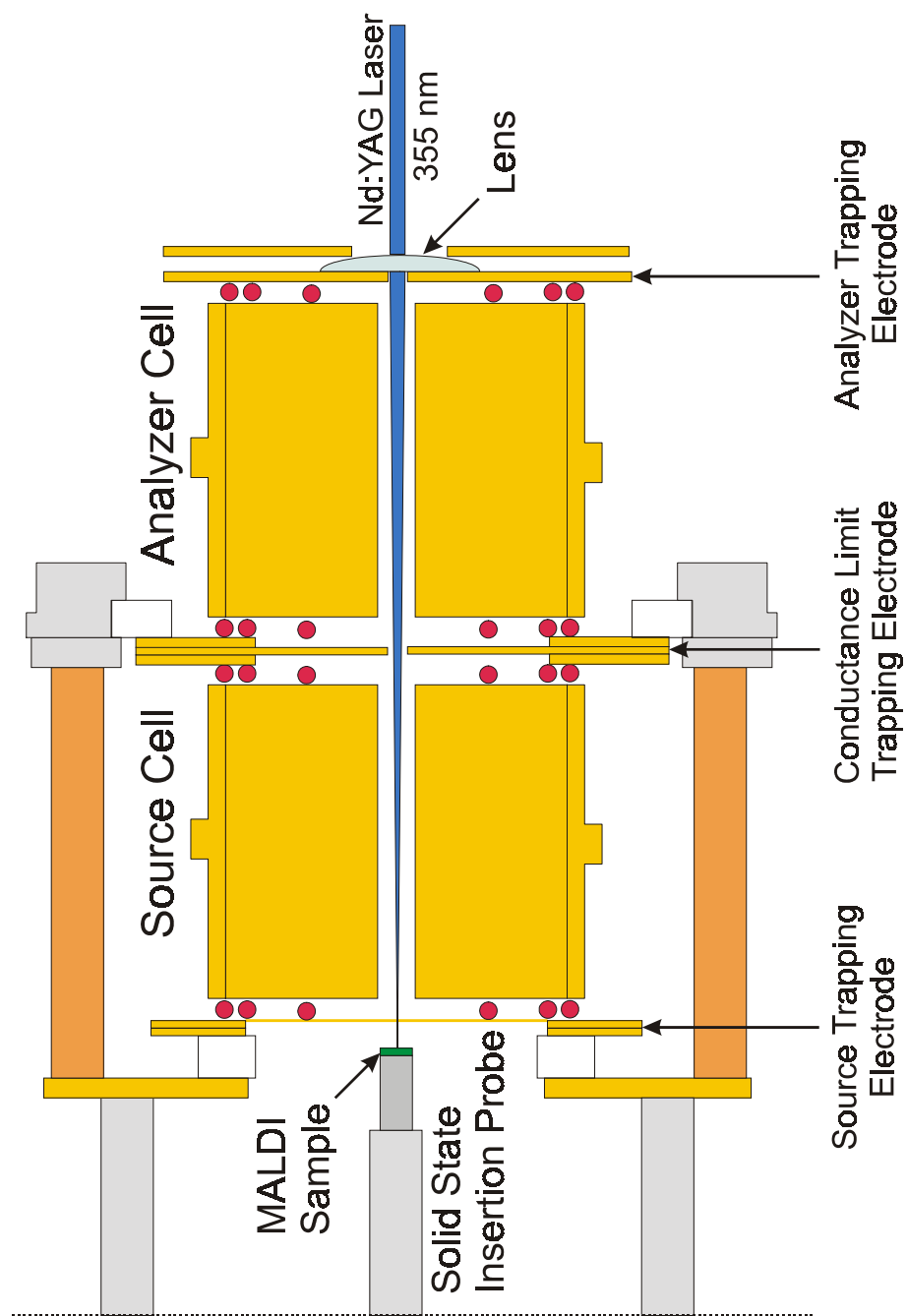
Figure 15. Schematic of the differentially pumped two-section FT-ICR MS cell employed for gas-phase H/D exchange.

0570, OptoSigma, Santa Ana, California, USA), utilized to focus the output from a Nd:YAG laser for MALDI. In addition, the mounted lens can be replaced by an electron impact source for ionization of volatile gas samples.

The assembled two-section FT-ICR MS cell is oriented in the homogeneous region of the magnetic field and maintained at baseline pressures, provided by the main vacuum chamber. Positioning is achieved by mounting the cell to a chassis that is connected to the main vacuum tube. The chassis consists of four, three foot long, radio frequency (RF) and four short Bayonet Navel Connector (BMC) feedthroughs that are welded to a six inch conflat flange (CF). The four RF feedthroughs are electrically connected to the transmitter and receiver electrodes of the source cell. The four BMC feedthroughs are electrically connected to the transmitter and receiver electrodes of the analyzer cell through fabricated RF wires. These RF lines consist of single stranded Kapton coated wires (Insulator Seal Inc., KAP 2), oriented through Teflon tubes having 0.050" inner and 0.250" outer diameters. These Teflon tubes act as a dielectric constant and are covered by stainless steel braided shielding (Insulator Seal Inc.), which is connected to electrical common. In addition to constructing these coaxial wires, single stranded Kapton coated wires were also used to electrically connect the trapping plate electrodes to a 2.75" CF feedthrough.

MALDI Sample Preparation and Vacuum Introduction

The "dried droplet" MALDI sample preparation method[93,94] was employed for analysis of peptide samples by internal source MALDI FT-ICR MS. This method entails

premixing analyte and matrix solutions and co-depositing them upon a metal sample stage. For the experiments described herein, relatively cool MALDI matrices were chosen to reduce metastable ion decay. The specific matrices used in these studies were, 4-hydroxy-3-methoxycinnamic acid (ferulic acid) for analysis of histidine containing di- and tripeptides, and 2',4',6'-trihydroxyacetophenone monohydrate (THAP) for MALDI of peptides containing lysine or arginine residues. These matrixes were purchased from Sigma-Aldrich Corporation and used without further purification. To increase gated trapping efficiency and minimize metastable ion dissociation a co-matrix, D-fructose (Sigma Chemical, St. Louis, Missouri, USA), was added to the MALDI matrix solution prior to addition with the analyte. A 10 mM solution of each peptide (Bachem, King of Prussia, Pennsylvania, USA) was prepared by dissolving the sample in deionized water containing 0.1% acetic acid by volume. The peptide solution was mixed with an appropriate volume of 500 mM D-fructose and 250 mM MALDI matrix solutions to obtain a D-fructose/matrix/peptide mole ratio of 40:20:1. Successive 30μl applications of the mixture were added to the MALDI sample stage until the metal surface was covered. Following solvent evaporation, the MALDI sample stage is mounted on the end of a solid-state insertion probe for subsequent introduction into the FT-ICR MS. The 36 inch long, 0.5 inch wide solid-state insertion probe is manually introduced into each vacuum region of the FT-ICR MS, allowing for pressure stabilization prior to insertion into subsequent vacuum regions. The sample stage, is situated approximately 2 cm from the source trap plate of the FT-ICR MS cell for subsequent laser irradiation by a frequency tripled (355 nm) Nd:YAG laser.

Deuterium Reagent Gas Introduction

Deuterium reagents, for gas-phase H/D exchange studies, are introduced into the system by variable, Varian, leak valves (model #951-5106) oriented on each end of the vacuum chamber. Reagents used in these studies include, ammonia-d_3, methanol-d_4, and acetic acid-d_4. Ammonia-d_4 was purchased from Cambridge Isotope Laboratories, Inc. and is introduced into to vacuum system with the aid of a Matheson (model# 3320) lecture bottle regulator. Methanol-d_4 and acetic acid-d_4 were purchased from Aldrich Chemical Company and degassed by multiple freeze-pump-thaw cycles prior to vacuum system introduction. The static operating pressures for reagent gasses ranged from 1.0×10^{-8} to 2.0×10^{-7} torr. The vacuum chamber was primed with the deuterium reagent for at least two hours prior to data collection allowing the complete exchange of all surfaces.

FT-ICR MS Experimental Sequence for Gas-Phase H/D Exchange

The experimental sequence used for the gas-phase H/D exchange studies described herein, is shown in Figure 16 (pictorial representation shown in Figure 17). The sequence is initiated by a 50 ms quench pulse, resulting in removal of all ions from the FT-ICR MS cells. This is achieved by applying a +9 volt potential to the conductance electrode while maintaining the source and analyzer electrodes at electrical common. The application of this antisymmetric field results in axial ion ejection. Following the quench event, the Nd:YAG laser, operating at 355 nm, is triggered by a Finnigan SWIFT cell controller. The laser output is focused by a fused silica lens, mounted to the analyzer cell trapping electrode, through the 0.079" (2 mm) conductance

Experimental Sequence for MALDI FT-ICR MS

Quench
(0.100s)

Ionization

Gated Deceleration
(0.000240s)

Fixed Delay
(0.050s)

SWIFT Ejection

Pulse Valve 1
(0.005s)

Pulse Valve 2
(0.005s)

QA
(1-2 s)

Transfer Delay
(0.250ms)

Ion Transfer
(0.000250s)

Variable Reaction
(5ms – 15min)

Excite

Detect
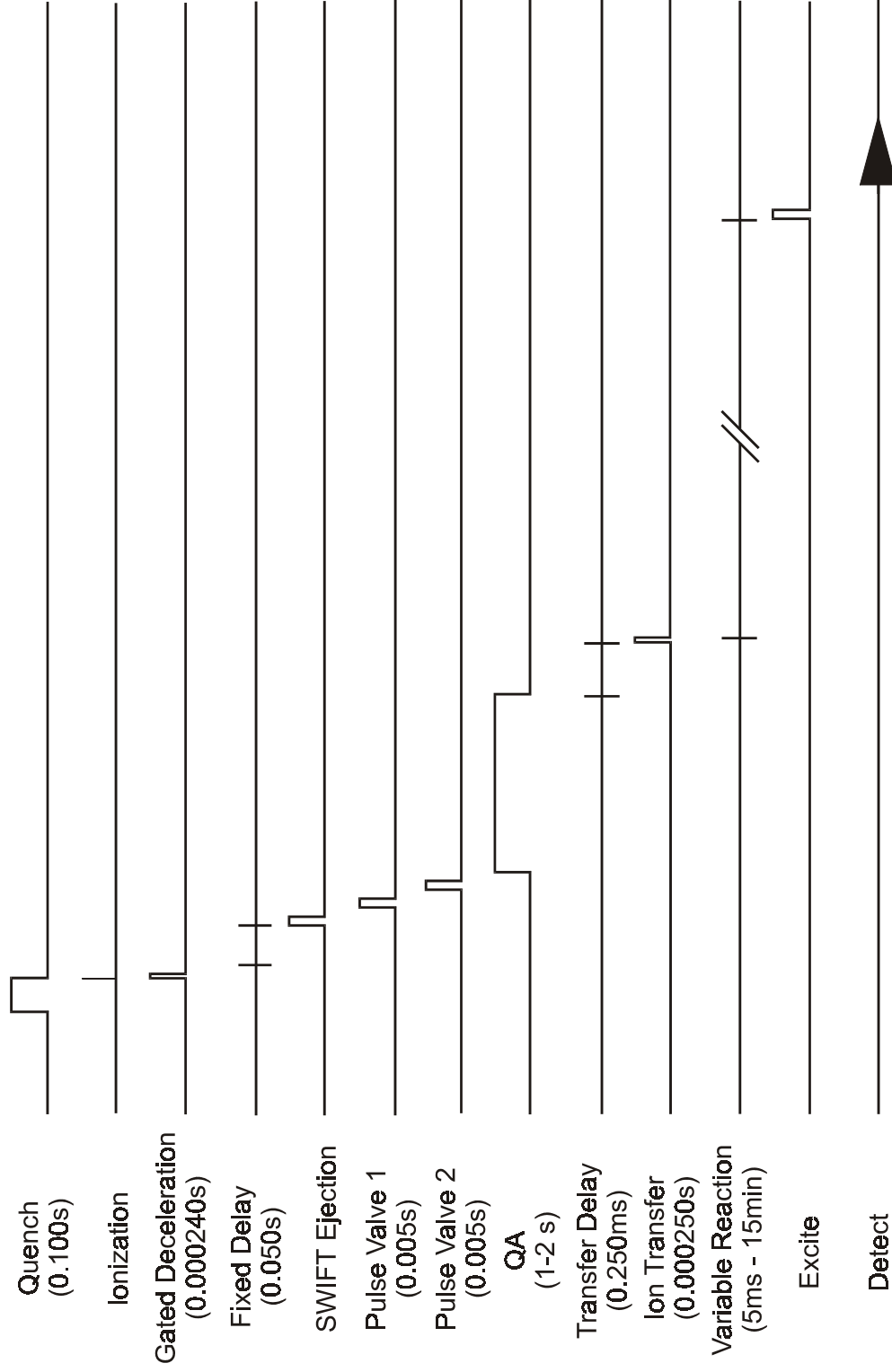
Figure 16. Experimental sequence used for gas-phase H/D exchange of protonated peptides.
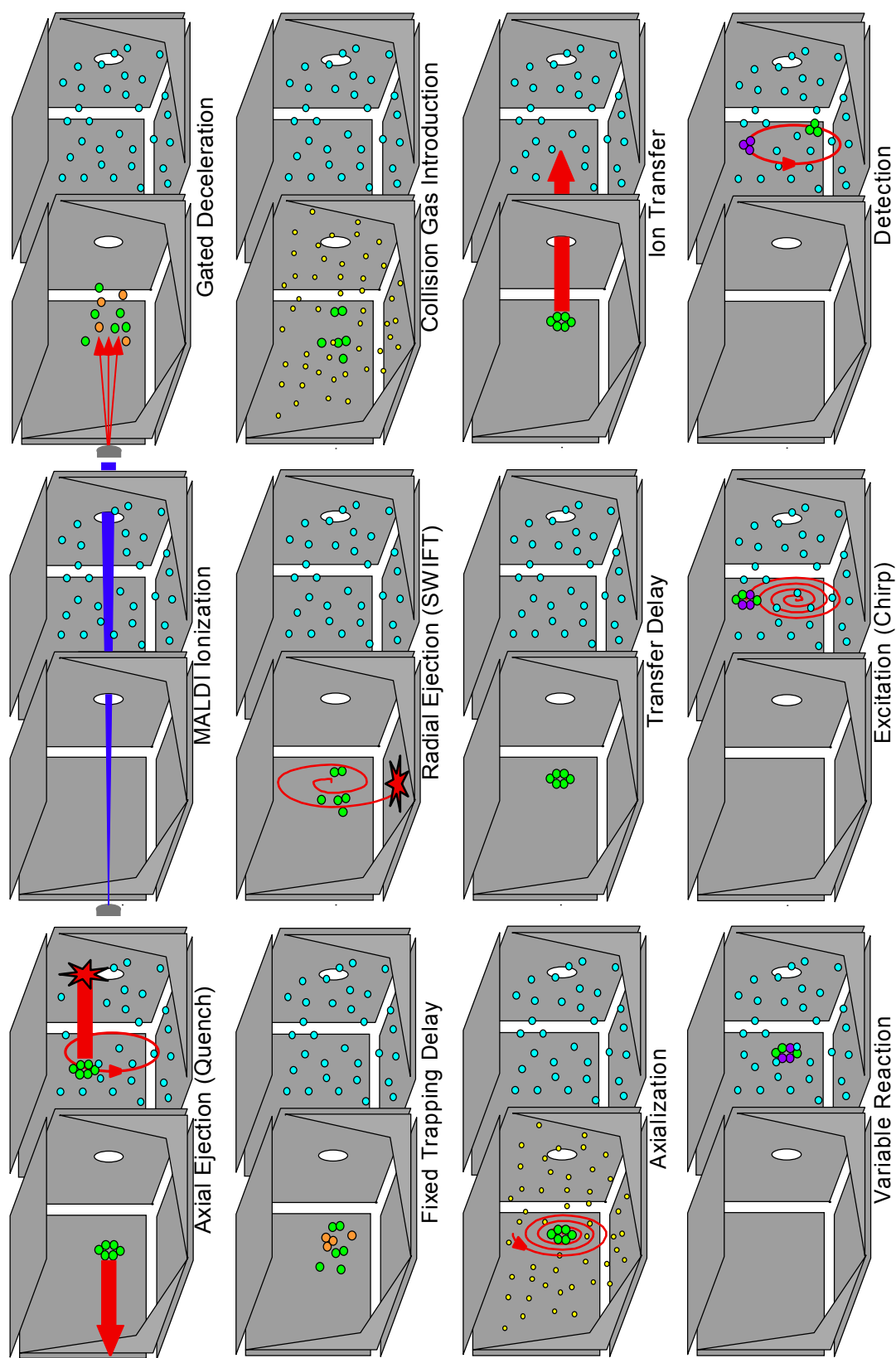
Figure 17. Pictorial representation of experimetal sequence used for gas-phase H/D exchange of protonated peptides.

limit aperture to the MALDI sample. Laser attenuation is achieved by orienting a 1 cm quartz cuvet, containing a 75-120 μM solution of Vitamin B_{12} in the laser beam path. A gated trapping time of 240 μs follows MALDI ionization of the reactant peptide ion, after which, a symmetric +1 volt potential is applied to the trapping electrodes for axial ion confinement. Selective ejection of matrix ions is achieved by application of SWIFT pulses. Radial ion ejection is followed by pulse valve introduction of helium collision gas for QA. After a fixed time delay, an azimuthal quadrupolar field is applied to the cell at the protonated peptide's cyclotron frequency, causing radial compression of the ion packet. The QA event lasts for 1-2 s, after which, peptide ions are transferred to the analyzer cell by decreasing the conductance limit voltage to electrical common. Transferred ions are subsequently stored in the analyzer cell by restoring the conductance limit electrode potential to +1 volt. Ions trapped in the analyzer cell are exposed to a background pressure of deuterium gas for various time intervals ranging from 5 ms – 15 min at 1×10^{-8} to 2×10^{-7} torr. This variable reaction delay is followed by broadband dipolar excitation and detection. The experimentally determined pseudo first order rate constant, obtained by measuring the product ion distribution as a function of time, is compared to theoretical ADO (Average Dipole Orientation Theory) collision rate constant, revealing the peptide ion's H/D exchange efficiency for reaction with a selected deuterium reagent.

Determination of Gas-Phase H/D Exchange Reaction Efficiencies

The gas-phase H/D exchange efficiencies reported in these studies assume that the bimolecular ion-molecule reactions follow pseudo-first order kinetics, as the reagent gas concentration ([D]) is much higher than the ion densities ($[M+H]^+$) stored in the FT-ICR MS cell (Equation 4). Pseudo-first order rate constants, k_{obs}, are determined by monitoring the abundance of the reactant ion, $[M+H]^+$, as a function of time. Ions exhibiting multiple decay rates were fit to a double exponential decay (Equation 5), revealing the individual rate constants, k_{obs}, for the multi-component system.

$$[M+H]^+_t = [M+H]^+_0 \exp(-[D]k_{obs}t) \qquad (4)$$

$$[M+H]^+_t = [M+H]^{+'}_0 \exp(-[D]k_{obs}'t) + [M+H]^{+''}_0 \exp(-[D]k_{obs}''t) \quad (5)$$

$$k_{exp} = k_{obs} \times S/(P_{neu} \times C \times g) \qquad (6)$$

The experimental rate constant, k_{exp}, is obtained by using Equation 6, where S is a correction factor reflecting ion gauge sensitivity to a specific neutral reagent, P_{neu} is the pressure of the reagent gas recorded by the ion gauge, g is a geometry correction factor representing the distance between the ion gauge and FT-ICR MS cell, and C is a constant (3.239×10^{16}) allowing for conversion of units to molecules/cm^3. Geometry correction factors, g, can be obtained by measuring reactions with known rate constants employing the reagent gas of interest.

The theoretical or collision rate constant, k_{col}, is determined from the capture collision model developed by Su and Chesnavich[95] as illustrated in Equations 7 and 8.

$$k_{col} = k_L \ (0.509)^2/10.526 + 09754 \ ; \ p<2 \qquad\qquad (7)$$

$$k_{col} = k_L(0.4767p + 0.6200); \ p>2 \qquad\qquad (8)$$

$$\text{where} \quad p = \mu_D/(2 \times k_B T)^{\frac{1}{2}}$$

$$K_L = 2\pi(\alpha/\mu)^{\frac{1}{2}}$$

Derived from parameterized trajectory calculations, k_L is the Langevin collision rate, T is the temperature, k_B is the Boltzmann constant, μ_D is the dipole moment of the neutral molecule, α is the polarizability of the neutral reagent, and μ is the reduced mass. The gas-phase H/D exchange efficiency is given by k_{exp}/k_{coll}.

CHAPTER III

THE GAS-PHASE HYDROGEN/DEUTERIUM EXCHANGE OF SELECTED DI-

AND TRIPEPTIDES CONTAINING A HISTIDINE AMINO ACID RESIDUE

Introduction

Gas-phase hydrogen/deuterium (H/D) exchange is widely used to investigate protein and peptide ion conformations.[96,97] Since its introduction as a structural probe for gas-phase ions in 1972 by Hunt and coworkers,[98] gas-phase H/D exchange has been utilized to distinguish isomeric species[99] and to probe conformational changes in large molecules by mass spectrometry.[100] Several experiments aimed at understanding the mechanism(s) of H/D exchange in biological molecules have been reported, but the majority of these studies were carried out on non-polar, aliphatic amino acids and peptides.[39,43,44,45,46] In these systems, the most likely site for protonation is the *N*-terminal amine, with charge site solvation by amide carbonyl groups.[47,101,102,103,104] Consequently, these studies ignored the effects that basic amino acid residues have on the rate and extent of deuterium incorporation for peptide ions. Peptides containing histidine, lysine or arginine amino acids can also be protonated on the basic side chain nitrogen, and stabilized by intramolecular charge site solvation.[50,105,106,107] Since charge site location has been proposed as a factor influencing gas-phase H/D exchange,[25,39] understanding the effects of basic residues on deuterium incorporation is important.

In this study, gas-phase H/D exchange reactions of protonated peptides containing a basic residue were performed to elucidate effects that the amino acid's sequence position (*i.e. N*-terminal, internal, or *C*-terminal) has on reaction efficiency and extent of deuterium incorporation. The sequence isomers employed for these studies are di- and tripeptides containing histidine and glycine amino acid(s). Several independent studies have suggested that the imidazole ring of histidine is protonated with intramolecular charge solvation by neighboring functional groups.[44,50,105,108] Consequently, sequence position of the histidine residue could strongly influence intramolecular bridging interactions within the protonated peptide. For example, bridging the ionizing proton by functional groups with similar GBs have been attributed to enhanced H/D exchange efficiencies despite unfavorable GB between the analyte ion and deuterium reagent.[39,45,46,107] Therefore, sequence isomers demonstrating different H/D exchange temporal distributions and reaction efficiencies may be ascribed to dissimilar bridging interactions within the protonated peptide, suggesting unique ion conformations.

From the gas-phase H/D exchange results presented herein, we suggest that sequence position of the histidine residue dramatically influences the reaction efficiency and extent of deuterium incorporation. The dissimilar H/D exchange temporal distributions and reaction efficiencies are rationalized by different intramolecular interactions involved with inductive stabilization of the charge site.

Results

Gas-Phase H/D Exchange with Methanol-d4

The oligopeptides investigated in these gas-phase H/D exchange studies are sequence isomers containing histidine and glycine amino acid residues (see Table 1).

Table 1. Hydrogen/deuterium exchange efficiency (k_{exp}/k_{coll}) for incorporation of the first deuterium in histidine containing oligopeptide $[M+H]^+$ ions when reacted with methanol-d4 or ammonia-d3.

$[M+H]^+$	Methanol-d4	Ammonia-d3
HisGly	0.058	0.63
GlyHis	0.016	0.64
HisGlyGly	0.042	0.58
GlyHisGly	0.0080	0.39
GlyGlyHis	0.0023	0.56

These peptides were selected to access the affect that position (*i.e.* *N*-terminal, internal or *C*-terminal) of the basic imidazole ring on reaction efficiency and extent of deuterium incorporation. Temporal plots illustrating H/D exchange for the $[M+H]^+$ ions of HisGly and GlyHis with methanol-d4, are contained in Figures 18 and 19, respectively. These sequence isomers illustrate the dissimilar H/D exchange chemistry of dipeptides containing the same amino acids but different sequences. For HisGlyH$^+$, the first three exchanges proceed relatively fast, whereas the remaining exchanges are much more gradual. Comparatively, GlyHisH$^+$ incorporates deuterium slower than HisGlyH$^+$, exchanging four hydrogen atoms for deuterium at comparable rates while the remaining exchanges are relatively hindered. A series of partial mass spectra for these histidine

Figure 18. Temporal plot for gas-phase H/D exchage of protonated HisGly with deuterated methanol at ~1.4 E-7 torr.
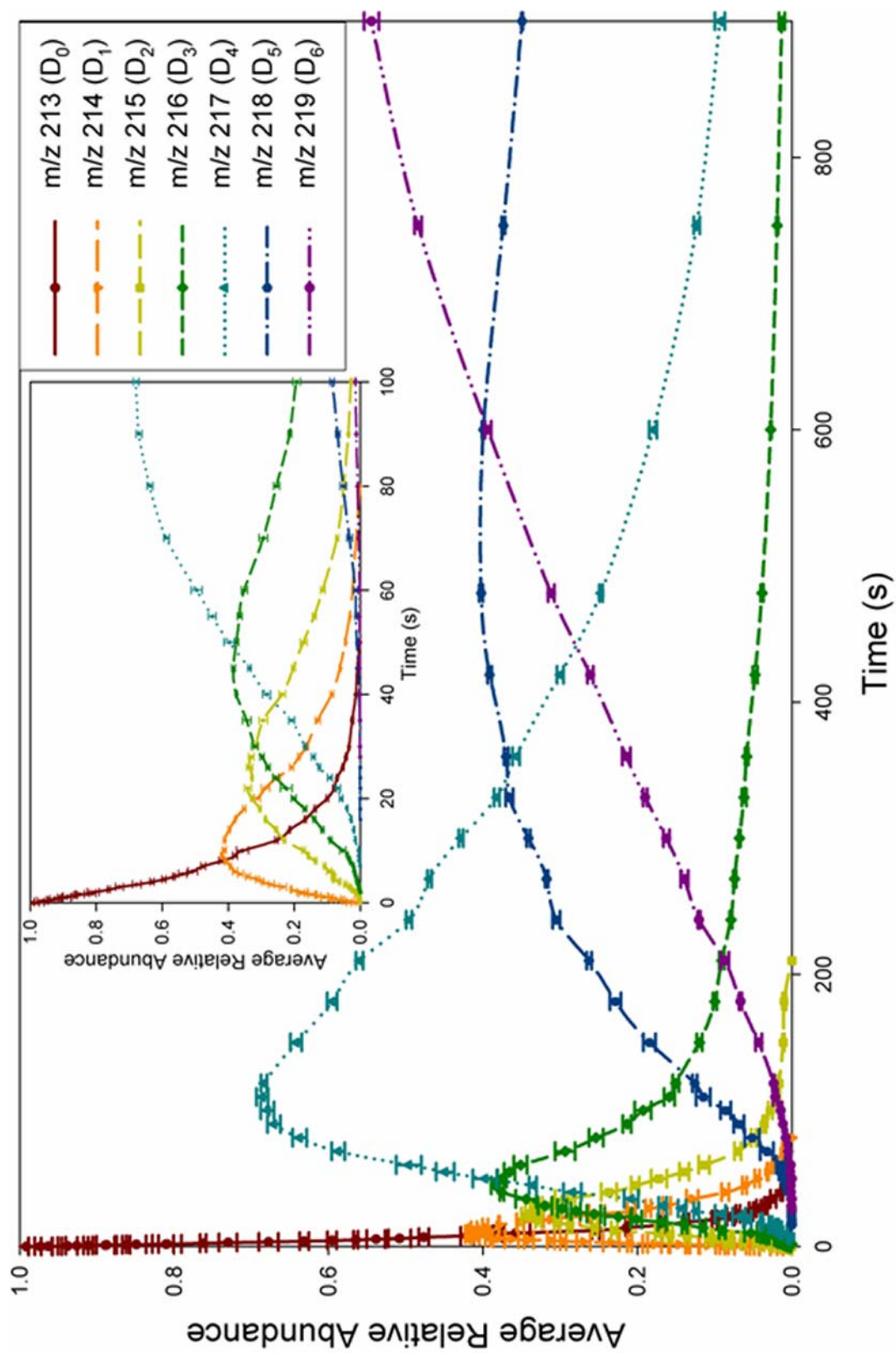
Figure 19. Temporal plot for gas-phase H/D exchange of protonated GlyHis with deuterated methanol at ~1.4 E-7 torr.

containing dipeptide ions, reacted with methanol-d_4, is illustrated in Figures 20 and 21.

The gas-phase H/D exchange of tripeptides containing one histidine and two glycine amino acid residues were also investigated. The $[M+H]^+$ ions of HisGlyGly, GlyHisGly, and GlyGlyHis also react very differently with methanol-d_4 (see Figures 22, 23, and 24, respectively). For example, HisGlyGlyH$^+$ undergoes three facile exchanges, whereas three of the remaining four hydrogens exchange at significantly reduced efficiencies. Comparatively, gas-phase H/D exchange of GlyHisGlyH$^+$, performed under similar experimental conditions, displays reduced reaction efficiency for incorporation of the first deuterium, but exchanges all labile hydrogens at comparable reaction efficiencies during the time course of the experiment. Finally, the H/D exchange for GlyGlyHisH$^+$ is the least efficient of all the sequence isomers, incorporating five deuteriums at comparable rates while the sixth exchange is comparatively slower.

Gas-Phase H/D exchange with Ammonia-d_3

Reactions of the same histidine di- and tripeptides with ammonia-d_3 were performed under similar conditions used for methanol-d_4. Decreasing the gas-phase basicity difference between the peptide ion and deuterium reagent, exchange is more efficient with ammonia-d_3 and demonstrates deviations in H/D exchange temporal distributions when compared to results obtained with methanol-d_4. As seen in Figures 25 and 26, HisGlyH$^+$ and GlyHisH$^+$ appear to have similar temporal plots for deuterium incorporation and identical reaction efficiencies for the first exchange (Table 1). Closer inspection of each peptide ion's respective temporal plot indicates that subsequent
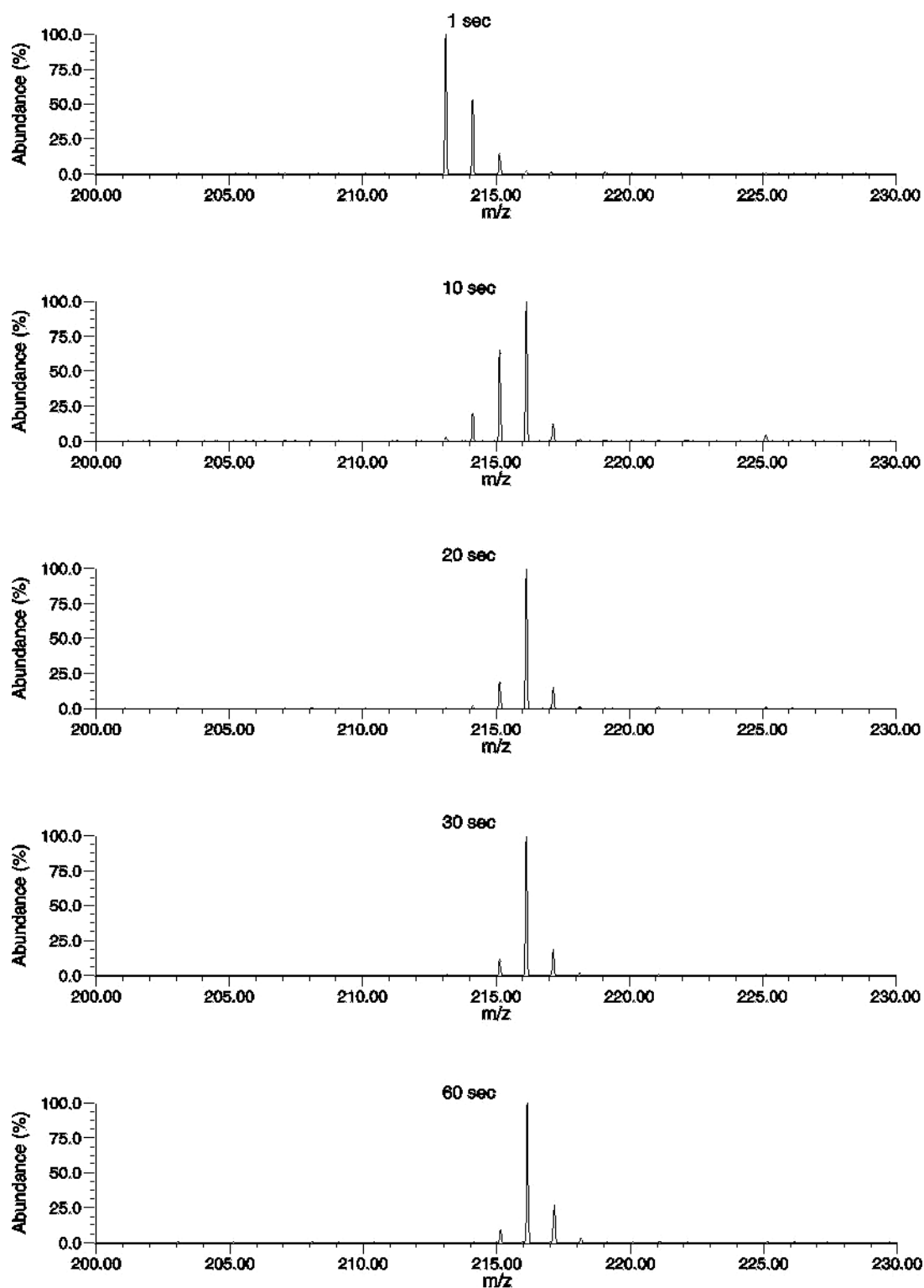
Figure 20. Partial mass spectra of protonated HisGly reacted with deuterated methanol. Reaction times ranging from 1 - 60 seconds.
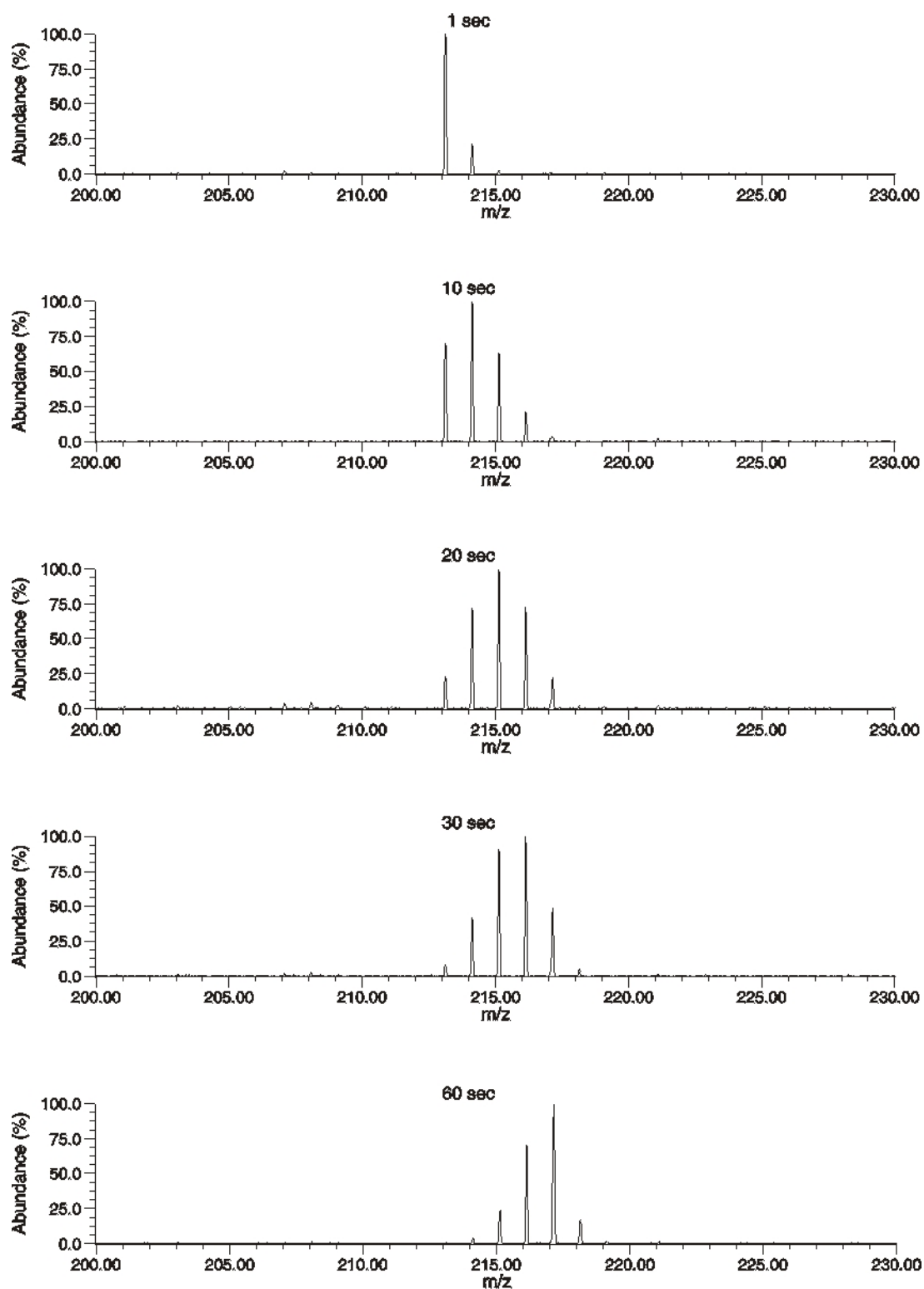
Figure 21. Partial mass spectra of protonated GlyHis reacted with deuterated methanol. Reaction times ranging from 1 - 60 seconds.
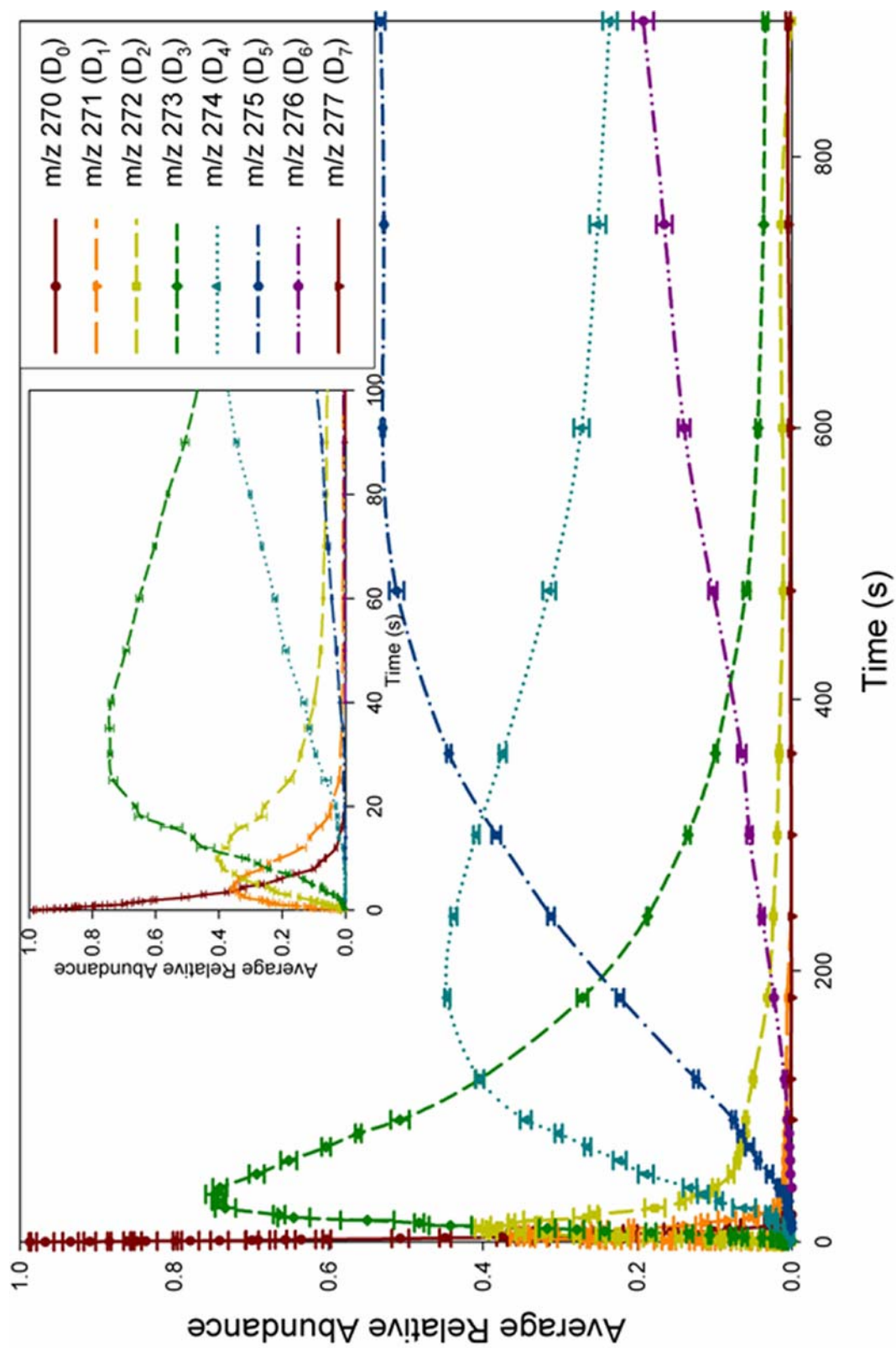
Figure 22. Temporal plot for gas-phase H/D exchange of protonated HisGlyGly with deuterated methanol at ~1.4 E-7 torr.
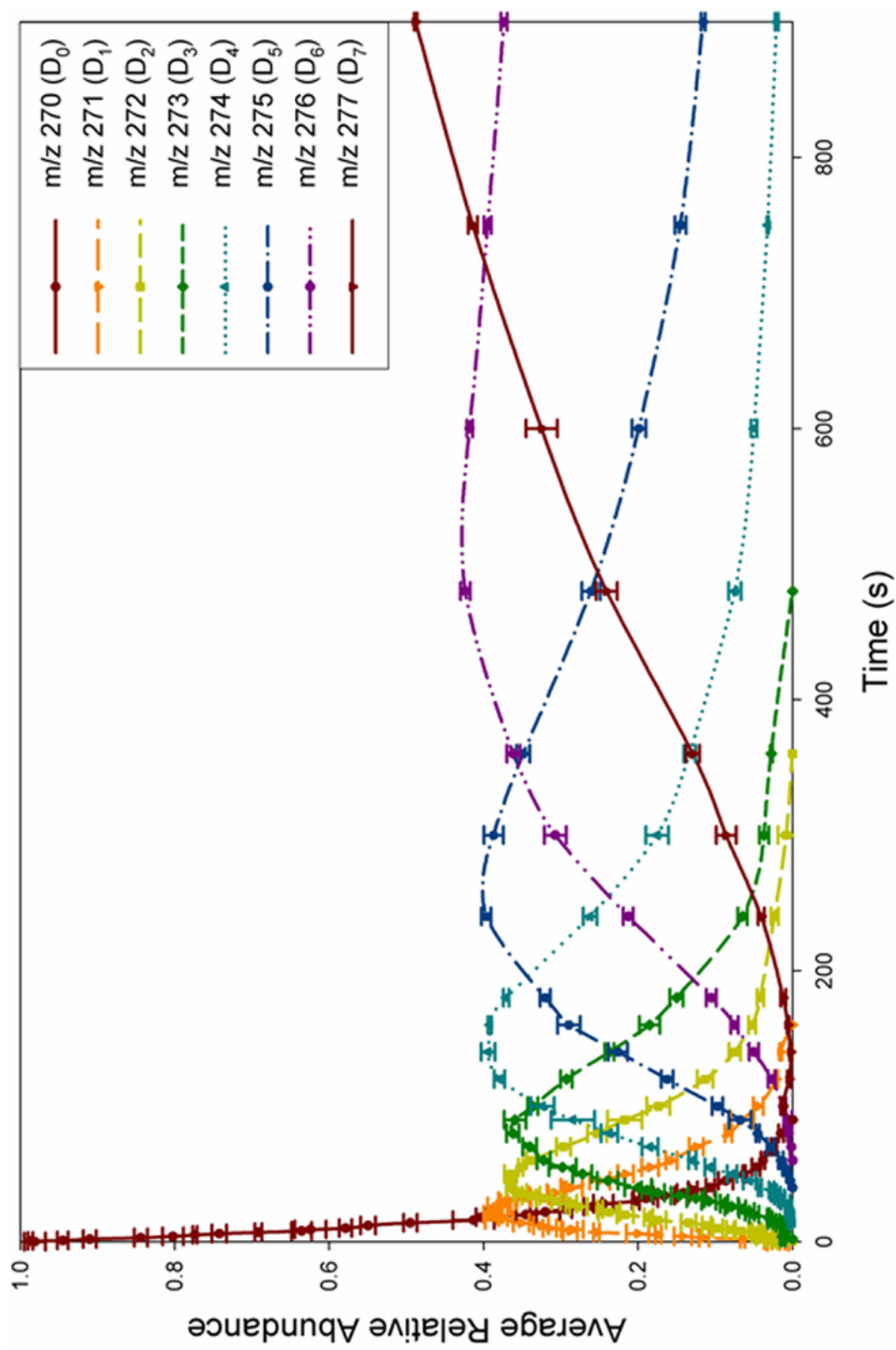
Figure 23. Temporal plot for gas-phase H/D exchange of protonated GlyHisGly with deuterated methanol at ~1.4 E-7 torr.
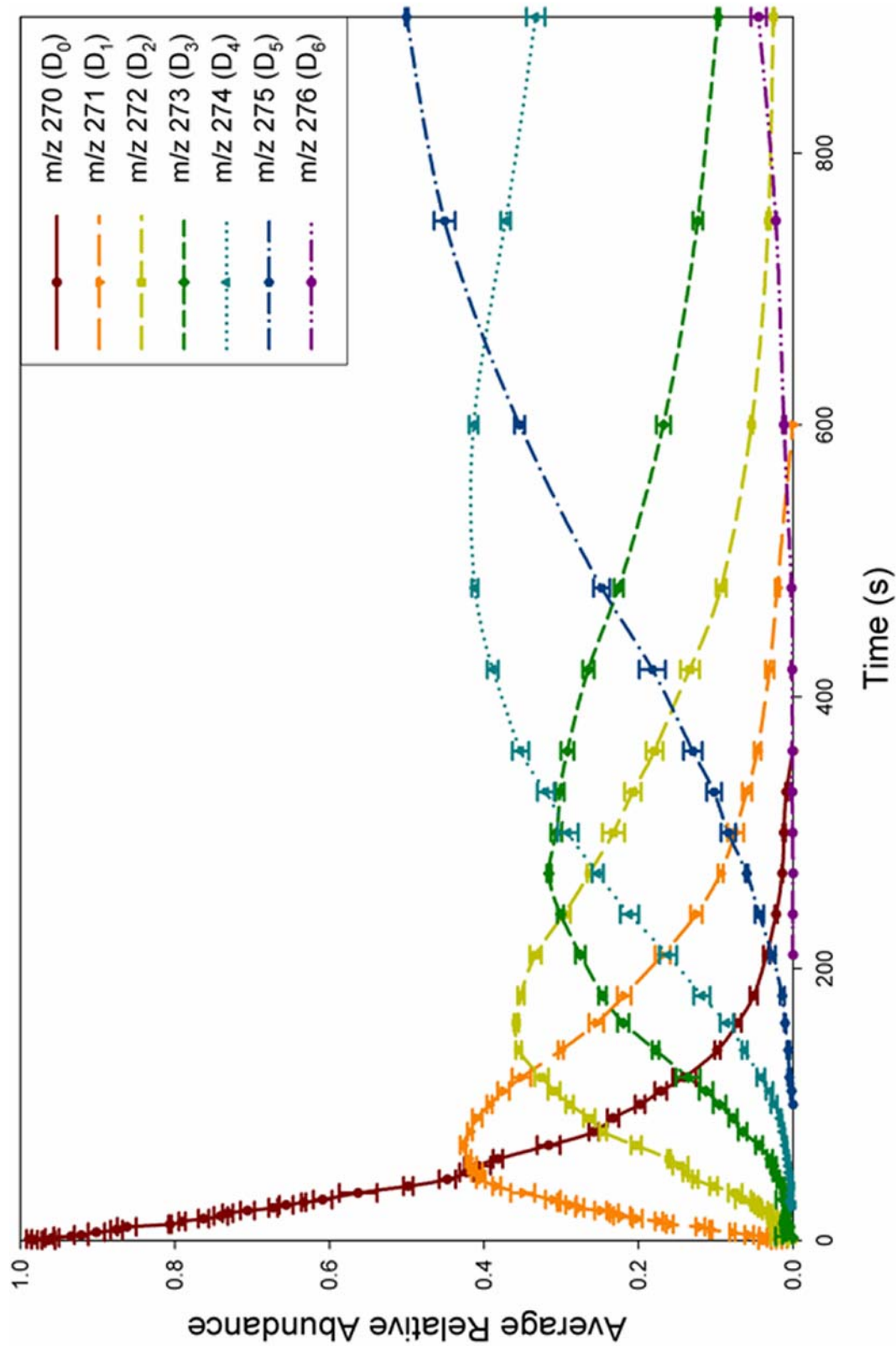
Figure 24. Temporal plot for the gas-phase H/D exchange of protonated GlyGlyHis with deuterated methanol at ~1.4 E-7 torr.
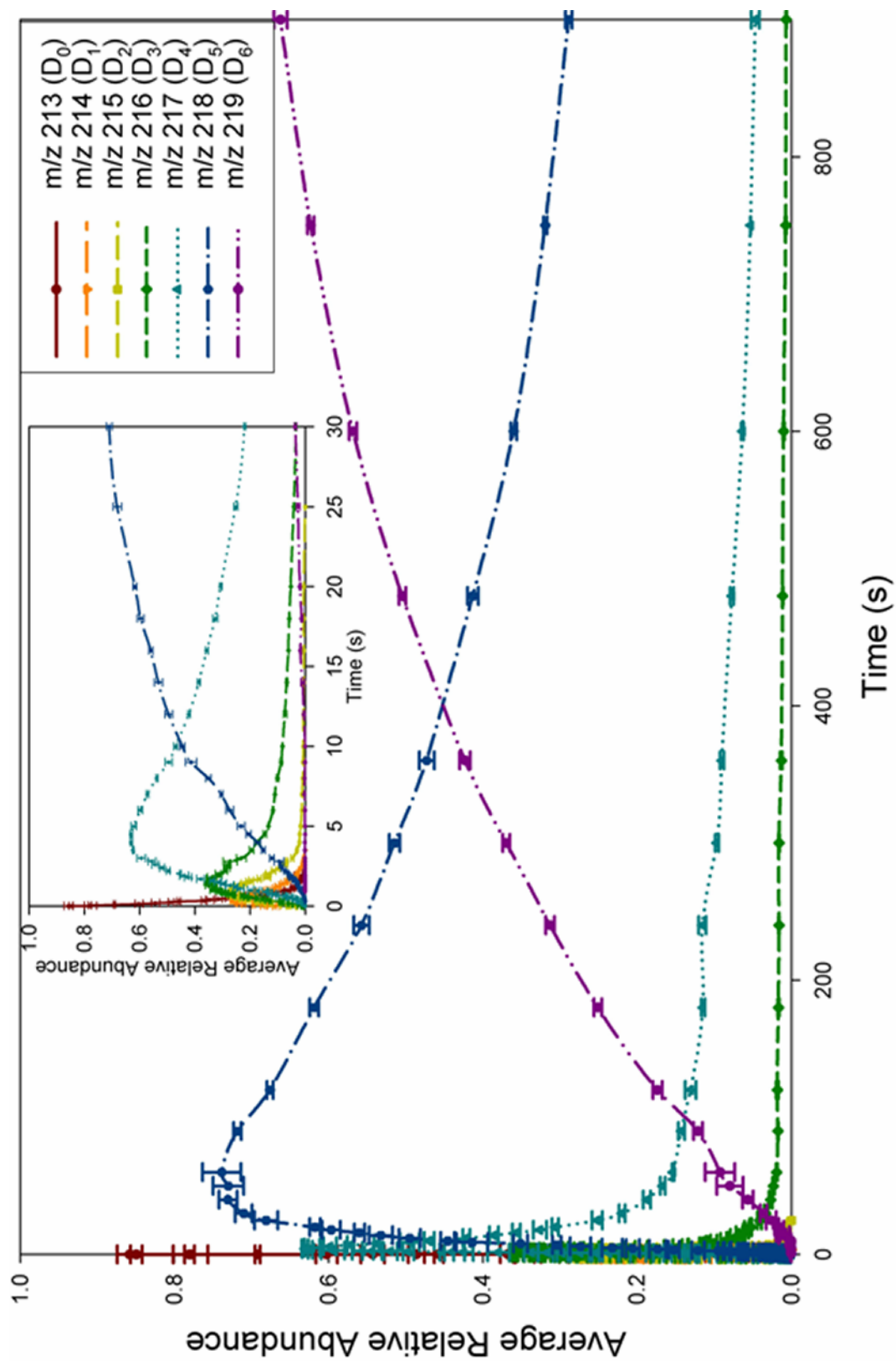
Figure 25. Temporal plot for gas-phase H/D exchange of protonated HisGly with deuterated ammonia at ~6.6 E-8 torr.
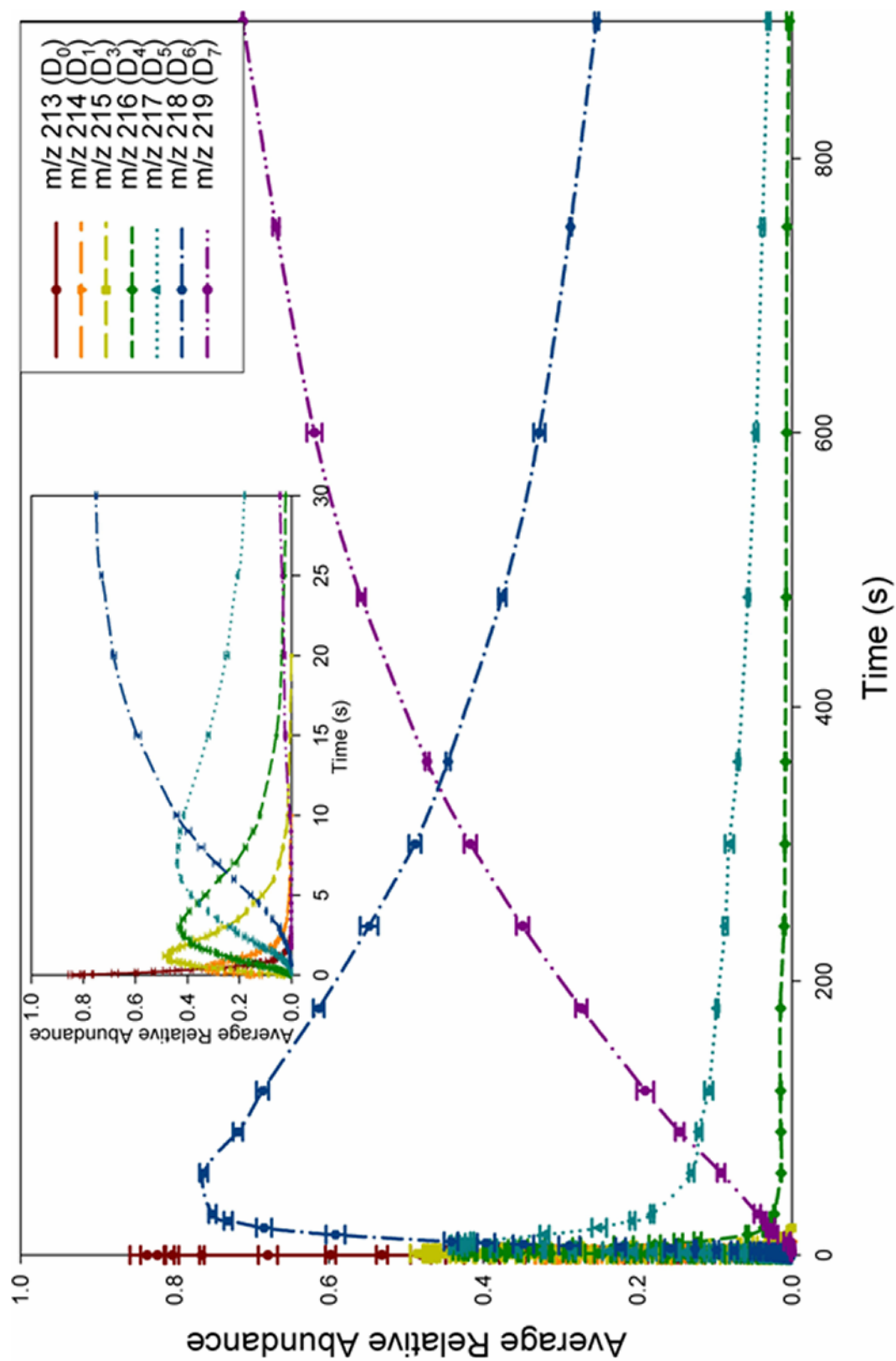
Figure 26. Temporal plot for gas-phase H/D exchange of protonated GlyHis with deuterated ammonia at ~6.6 E-8 torr.

incorporation of deuterium is more efficient for HisGlyH$^+$ than for GlyHisH$^+$. Both of these histidine containing dipeptides rapidly exchange five of six labile hydrogens, with the sixth exchanging occurring relatively inefficiently.

Reaction of the [M+H]$^+$ ions of HisGlyGly, GlyHisGly, and GlyGlyHis with ammonia-d$_3$ also demonstrates differences in H/D exchange when compared to results obtained with methanol-d$_4$, illustrated in Figures 27, 28 and 29 respectively. The time dependent incorporation of deuterium for HisGlyGlyH$^+$ and GlyGlyHisH$^+$ appear similar, exchanging five labile hydrogens at comparable reaction efficiencies while the remaining hydrogens are inefficient or not observed during the time course of the experiment. Although HisGlyGlyH$^+$ and GlyGlyHisH$^+$ display nearly identical reaction efficiencies (Table 1) for the first exchange, closer inspection of the respective temporal plots suggest that subsequent deuterium incorporation is more rapid for HisGlyGlyH$^+$ than GlyGlyHisH$^+$. Finally, incorporation of the first deuterium for reaction of GlyHisGlyH$^+$ with ammonia-d$_3$ is comparatively less efficient than its sequence isomers, exchanging all labile hydrogens during the time course of the experiment.

Discussion

Gas-phase H/D exchange studies of model peptides and polyfunctional molecules, independently investigated by Beauchamp,[39,109] Lebrilla,[12,43,44,46,107,110] and Nibbering[45] have suggested that deuterium incorporation is influenced by three factors. These include: (i) the gas-phase basicity (GB) difference between the analyte ion and the deuterium reagent, (ii) the intramolecular interactions involved with solvation of the

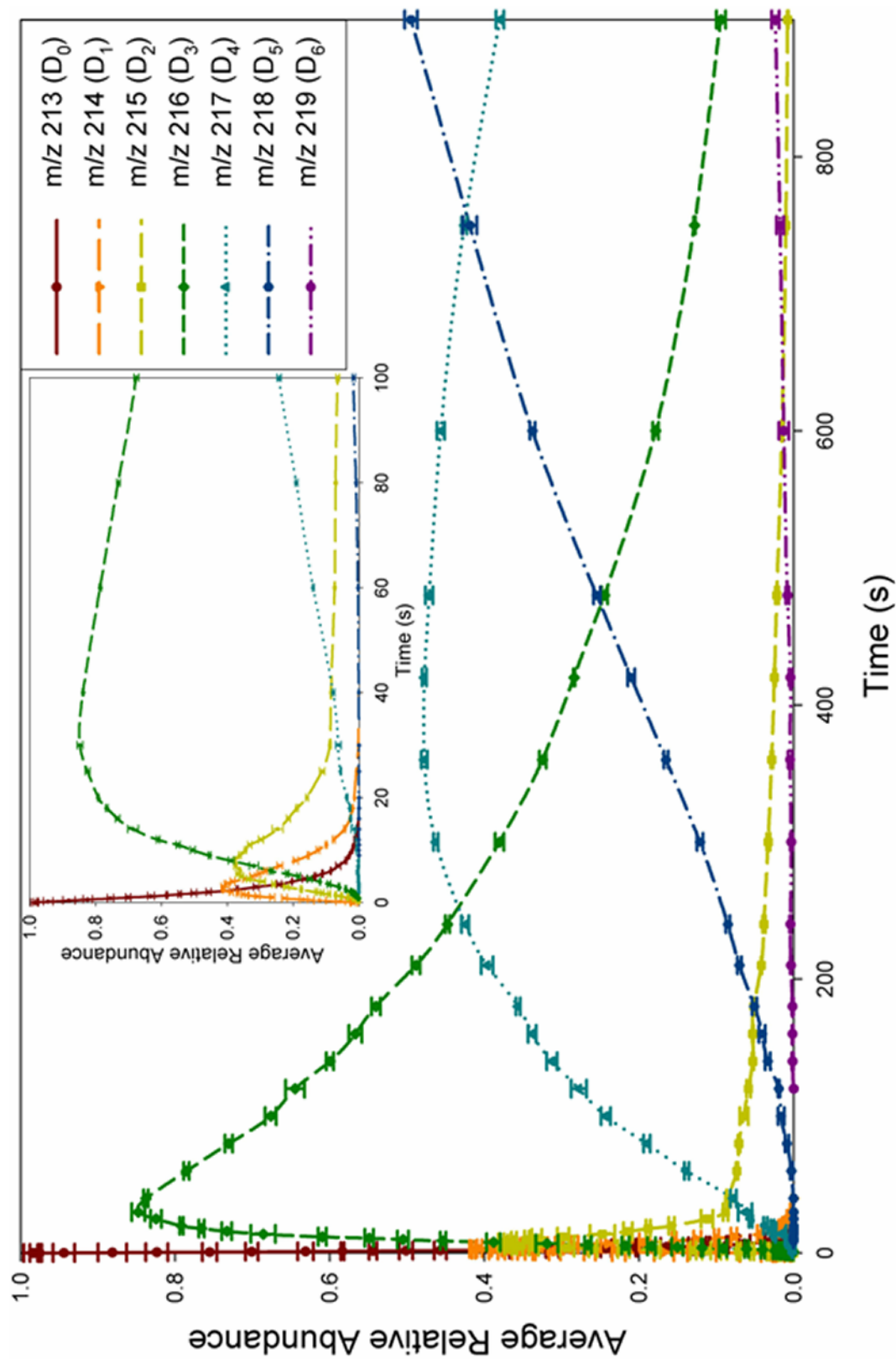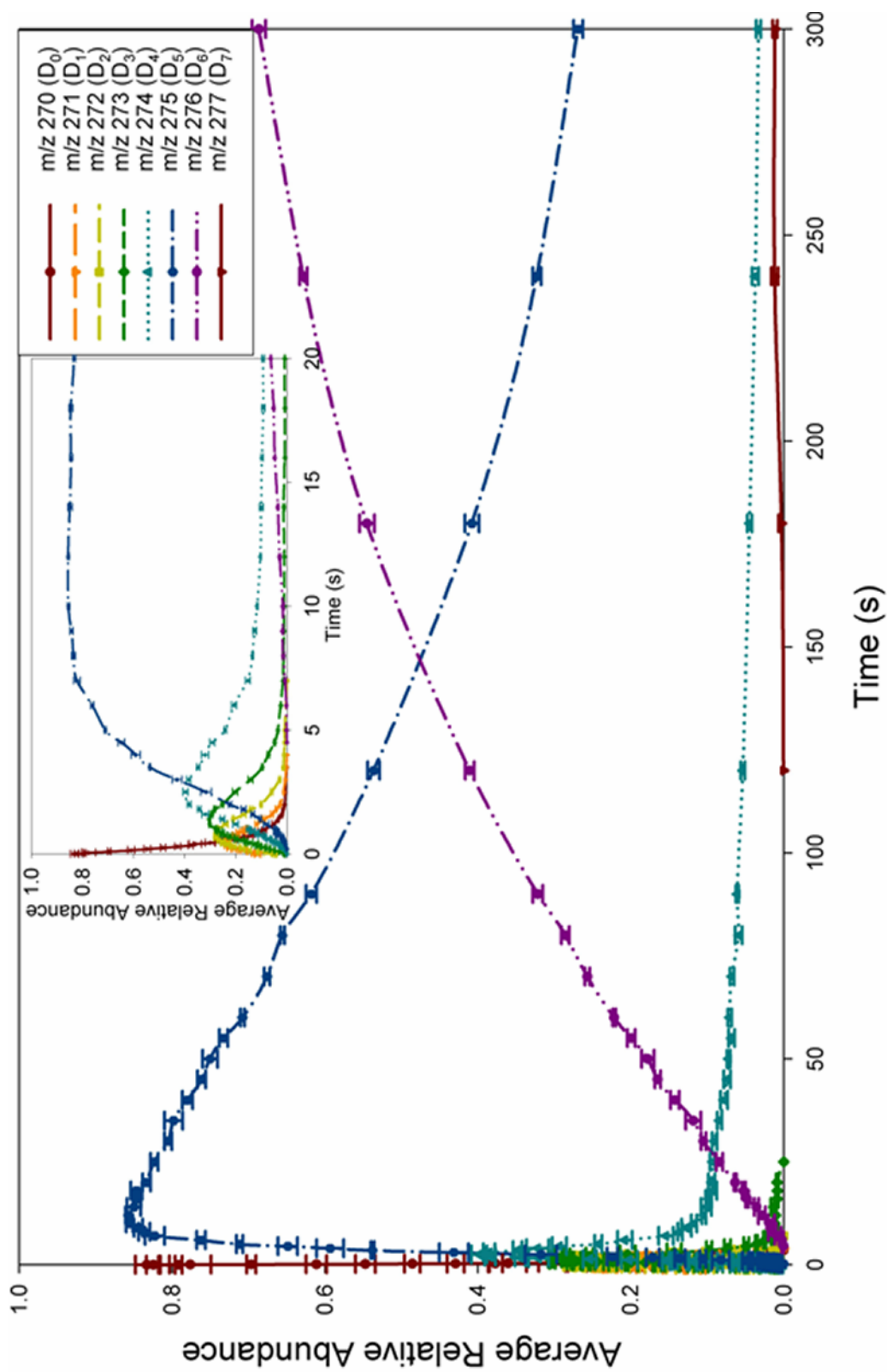Figure 27. Temporal plot for gas-phase H/D exchange of protonated HisGlyGly with deuterated ammonia at ~6.6 E-8 torr.
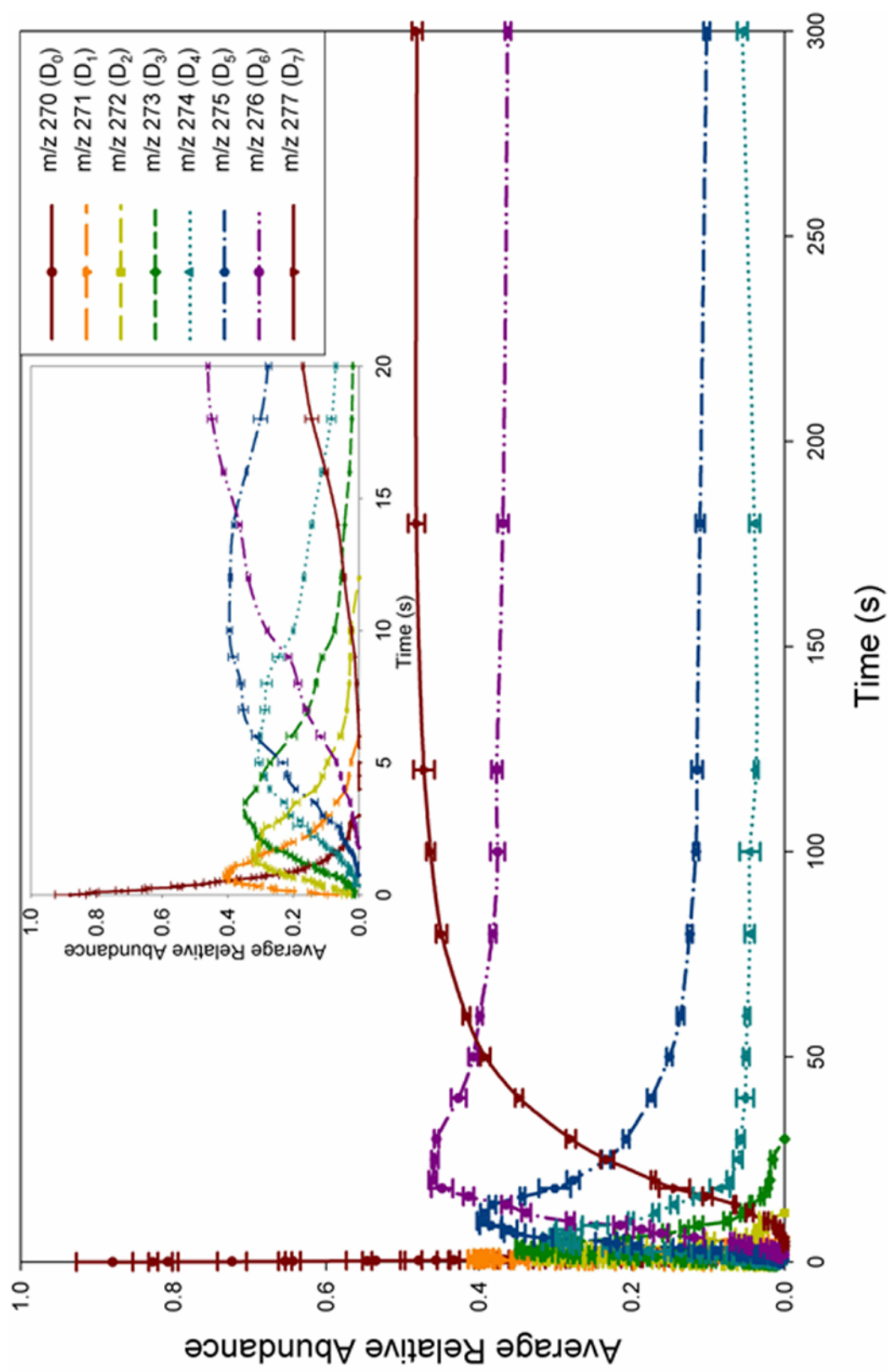
Figure 28. Temporal plot for gas-phase H/D exchange of protonated GlyHisGly with deuterated ammonia at ~6.6 E-8 torr.
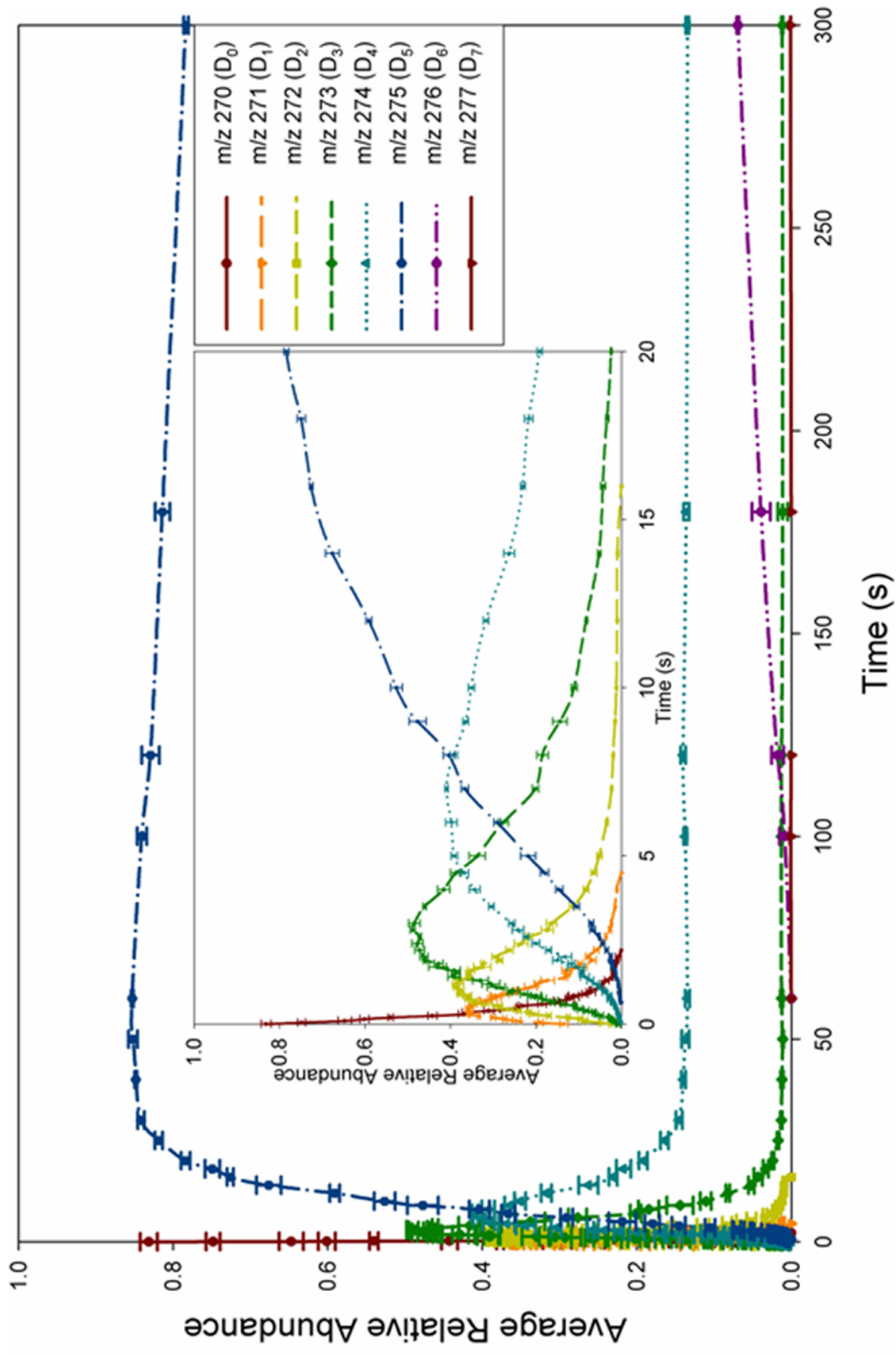
Figure 29. Temporal plot for gas-phase H/D exchange of protonated GlyGlyHis with deuterated ammonia at ~6.6 E-8 torr.

proton, and (iii) the accessibility of the charge site by the deuterium reagent. Due to the relatively small size of the oligopeptides investigated in these gas-phase H/D exchange studies, accessibility contributions should have minimal affects on deuterium incorporation. Hence, the temporal variations observed for gas-phase H/D exchange experiments are likely attributed to GB differences between the protonated peptide ion and deuterium reagent, and the intramolecular interactions involved with charge solvation.

Gas-Phase H/D Exchange of the Dipeptides with Methanol-d₄

As discussed in the preceding section, protonated di- and tripeptide sequence isomers, containing a histidine amino acid residue, demonstrate different temporal plots for deuterium incorporation when reacted with methanol-d_4. The contrasting gas-phase H/D chemistry between dipeptide ions containing the same amino acid residues but different sequences may be attributed to involvement of different functional groups for charge site stabilization. Dissimilar intramolecular interactions most likely produce unique GB values for the peptide sequence isomer. Proposed as an influential factor in gas-phase H/D exchange,[39,45,46] GB differences between the peptide ion and deuterium reagent has an inversely proportional effect on deuterium incorporation, possibly contributing to the dissimilar reaction rate efficiencies observed for HisGlyH$^+$ and GlyHisH$^+$.

Proposed gas-phase ion conformations for HisGly and GlyHis [M+H]$^+$ ions are based upon the relative GB differences between functional groups within the peptide and their general proximity to the charge site. Several independent studies and

semiempirical calculations have suggested that histidine,[44,111] and related molecules,[105] are protonated on the imidazole ring with intramolecular charge solvation by the amino group. Bridging the ionizing proton between the imidazole ring and amine is a possible stabilizing interaction for *N*-terminal histidine containing peptides due to their general proximity and similar GB. This peptide ion conformation may explain the three rapid exchanges observed for gas-phase H/D exchange of HisGlyH$^+$ with methanol-d$_4$, as rationalized by the proposed mechanism illustrated in Scheme 1.

Scheme 1
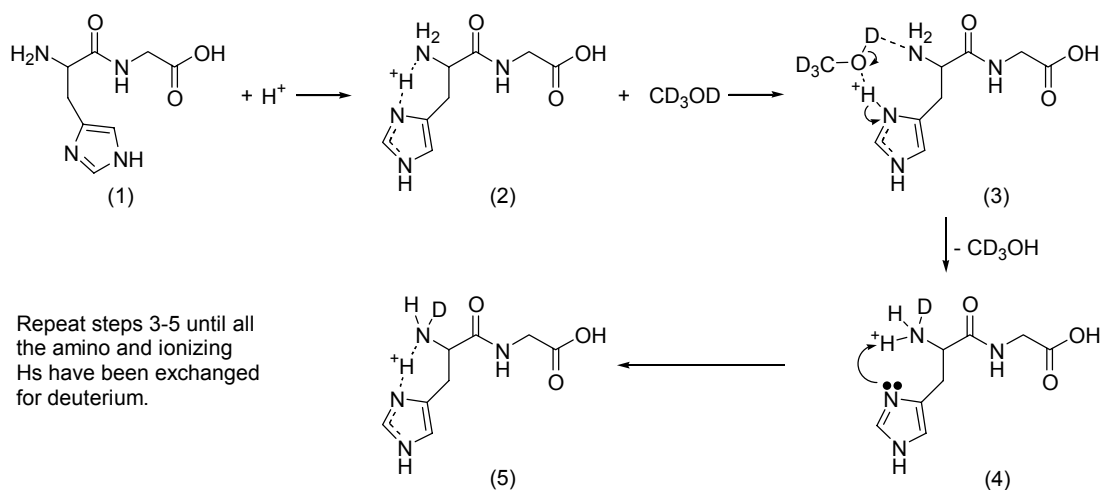
Initiated by formation of an ion-molecule complex, exchange of hydrogen for deuterium is suggested to proceed through the "relay mechanism" proposed by Beauchamp.[39] This model requires the charge site and a basic site, within the molecule, to be in close proximity for facile isotopic hydrogen exchange. The labile amide and carboxylic acid hydrogens are expected to be less efficient at exchange due to their charge remote

positions. Hence, the time dependent incorporation of deuterium, for reaction of HisGlyH$^+$ with methanol-d$_4$, can be rationalized by the proposed intramolecular interactions involved with charge solvation of the peptide ion.

Differences between the gas-phase H/D exchange temporal plots for HisGlyH$^+$ and GlyHisH$^+$, when reacted with methanol-d$_4$, can be rationalized by the likelihood of dissimilar intramolecular interactions. In comparison to HisGly, the imidazole ring of GlyHis is remote from the amino group. This spatial separation may hinder formation of bridging interactions proposed for HisGlyH$^+$, resulting in charge solvation by an alternative intramolecular interaction. Inductive stabilization of the charge site in GlyHisH$^+$ most likely involves a bridging interaction between the imidazole ring and the amide carbonyl. Proposed as a likely interaction due to the general proximity and similar GB of these groups, charge stabilization can be further aided by remote hydrogen bonding of the amide hydrogen with the amino group. Delocalization of the charge site through multiple intramolecular interactions increases the relative GB difference between GlyHisH$^+$ and the deuterium reagent, resulting in a comparative decrease in reaction rate efficiency for the first exchange (Table 1). A proposed mechanism for gas-phase H/D exchange of GlyHisH$^+$ with methanol-d$_4$ is illustrated in Scheme 2. Similar to HisGlyH$^+$, reaction of GlyHisH$^+$ with methanol-d$_4$ may involve a relay mechanism. Evoking this mechanistic model explains the four exchanges for GlyHisH$^+$ that occurring at comparable efficiencies. As described earlier, the lower exchange efficiency for GlyHisH$^+$, relative to HisGlyH$^+$, is rationalized by a comparative increase in GB due to multiple intramolecular interactions. Increasing charge delocalization

Scheme 2
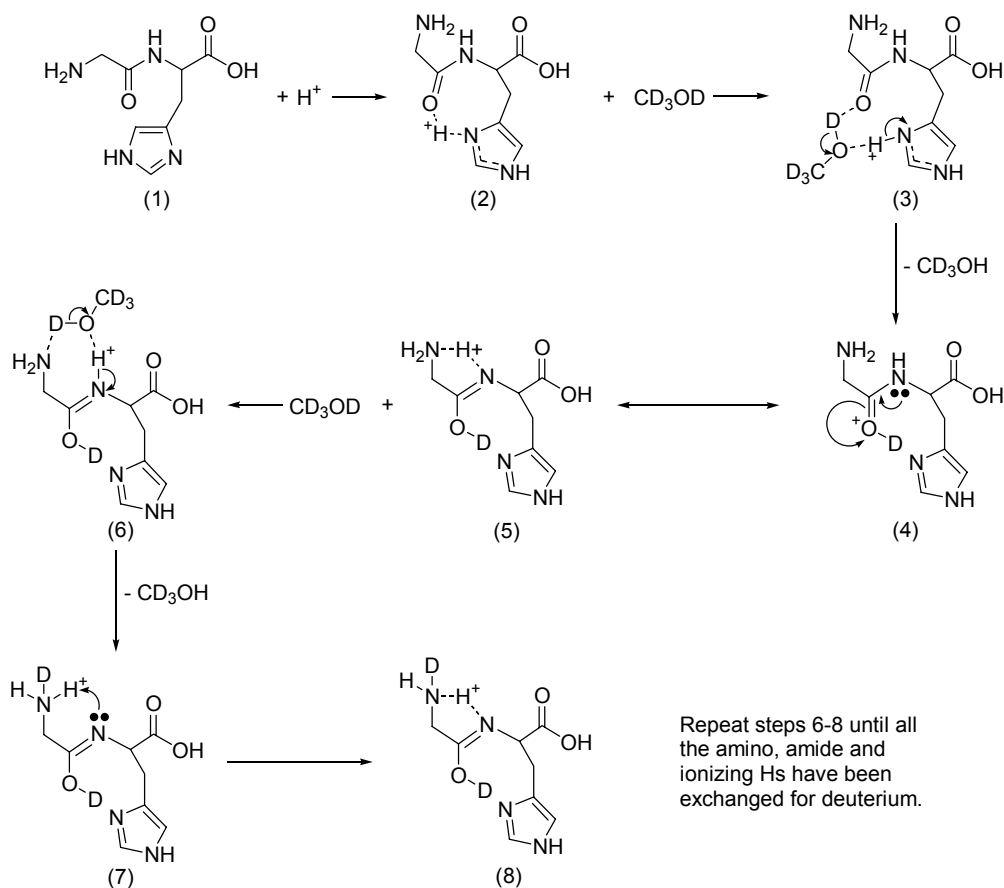
through multiple functional groups likely has a proportional effect on the number of facile exchanges in the peptide ion. Hence, the dissimilar gas-phase H/D temporal distributions for HisGlyH$^+$ and GlyHisH$^+$ when reacted with methanol-d$_4$ can be rationalized on the basis of conformational differences associated with charge solvation.

Gas-Phase H/D Exchange of the Tripeptides with Methanol-d$_4$

The tripeptides investigated in these gas-phase H/D exchange studies also demonstrate sequence specific temporal distributions for deuterium incorporation when reacted with methanol-d$_4$. Dissimilarities for the temporal plots between the tripeptide

ions are rationalized by differences in intramolecular interactions associated with inductive stabilization of the charge site. Although these tripeptide ions demonstrate unique H/D exchange temporal distributions, similarities observed between HisGlyH$^+$ and HisGlyGlyH$^+$ suggest the possibility of comparable peptide ion conformations. For example, both isomers contain an N-terminal histidine residue, and the proton bridging between the imidazole and amino terminus leads to three facile exchanges. A suggested mechanism for gas-phase H/D exchange of HisGlyGlyH$^+$ with methanol-d$_4$ is illustrated in Scheme 3. Note that the remaining labile carboxylic and amide hydrogens are predicted to be less efficiently exchanged due to their charge remote positions. Proposed conformational similarities for these N-terminal histidine containing peptide ions are further supported by comparable H/D exchange efficiencies (Table 1). Hence, the similar gas-phase H/D exchange temporal plots observed for HisGlyH$^+$ and HisGlyGlyH$^+$ are rationalized by the probability of common structural characteristics associated with charge solvation.

Unlike HisGlyGlyH$^+$, GlyHisGlyH$^+$ does not exhibit considerable reaction efficiency differences between the successive exchanges. Rather, the time dependent incorporation of deuterium for GlyHisGlyH$^+$ demonstrates a sequential temporal distribution, suggesting that labile hydrogens within the peptide ion lack reaction specificity for exchange with methanol-d$_4$. The temporal distribution of GlyHisGlyH$^+$ can be rationalized by proposed conformations for this peptide ion. Comparatively unique, GlyHisGly is the only oligopeptide ion investigated in these gas-phase H/D exchange studies that contains an internal histidine residue. The sequence position of

Scheme 3
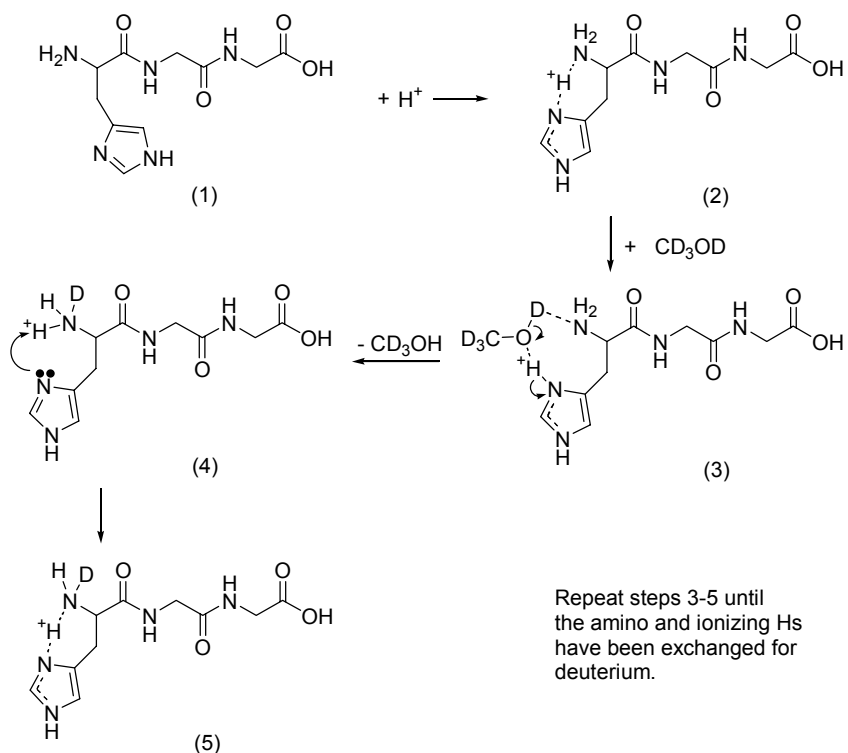
this amino acid allows the protonated imidazole ring to be charge solvated by either or both of the adjacent amide carbonyls. Multiple bridging interactions could efficiently delocalize the charge throughout the peptide, causing the labile hydrogens to be chemically similar. Alternatively, functional groups not involved in direct solvation of the ionizing proton could participate in remote hydrogen bonding, causing effective charge distribution throughout the molecule. A proposed mechanism, incorporating the latter of these suggested intramolecular interactions, for H/D exchange with methanol-d_4, is illustrated in Scheme 4. Multiple bridging interactions for this internal histidine containing peptide are further supported by a comparative decrease in exchange efficiency of GlyHisGlyH$^+$ relative to HisGlyGlyH$^+$ (Table 1).

Of the tripeptides investigated in this study, GlyGlyHisH$^+$ is the least efficient at deuterium incorporation with methanol-d$_4$ (Table 1). This comparative decrease in exchange efficiency may be attributed to spatial separation of the imidazole ring from the amine. As observed for the dipeptides, displacement of the imidazole from the *N*-terminus reduces the relative efficiency of the first exchange. This decrease in reaction efficiency is suggested to be influenced by an increase in the peptide ion's GB due to dissimilar intramolecular interactions. Conversely, reduction in reaction efficiency may be attributed to dissimilar GBs of groups involved with charge solvation. For example, bridging groups with similar GBs have been suggested to increased exchange efficiency despite unfavorable GB differences between the analyte ion and deuterium reagent.[39,45,46,107] This enhanced exchange efficiency is presumably attributed to energetics associated with formation of the ion-neutral complex between the bridging functional groups. Consistent with these observations, the reduced exchange efficiency of GlyGlyHisH$^+$, relative to its sequence isomers, could be caused by hindered interactions between the *N*-terminal amine and protonated imidazole. A proposed mechanism for gas-phase H/D exchange of GlyGlyHisH$^+$ with methanol-d$_4$ is shown in Scheme 5. GlyGlyHisH$^+$ incorporates five deuteriums at comparable rates, supporting the proposed intramolecular bridging interactions illustrated in Scheme 5. Hence, the relatively unique gas-phase H/D exchange temporal distributions and exchange efficiencies of these histidine containing tripeptides, for reaction with methanol-d$_4$, can be rationalized by dissimilar bridging interactions involved with inductive stabilization of the charge site.

Scheme 4
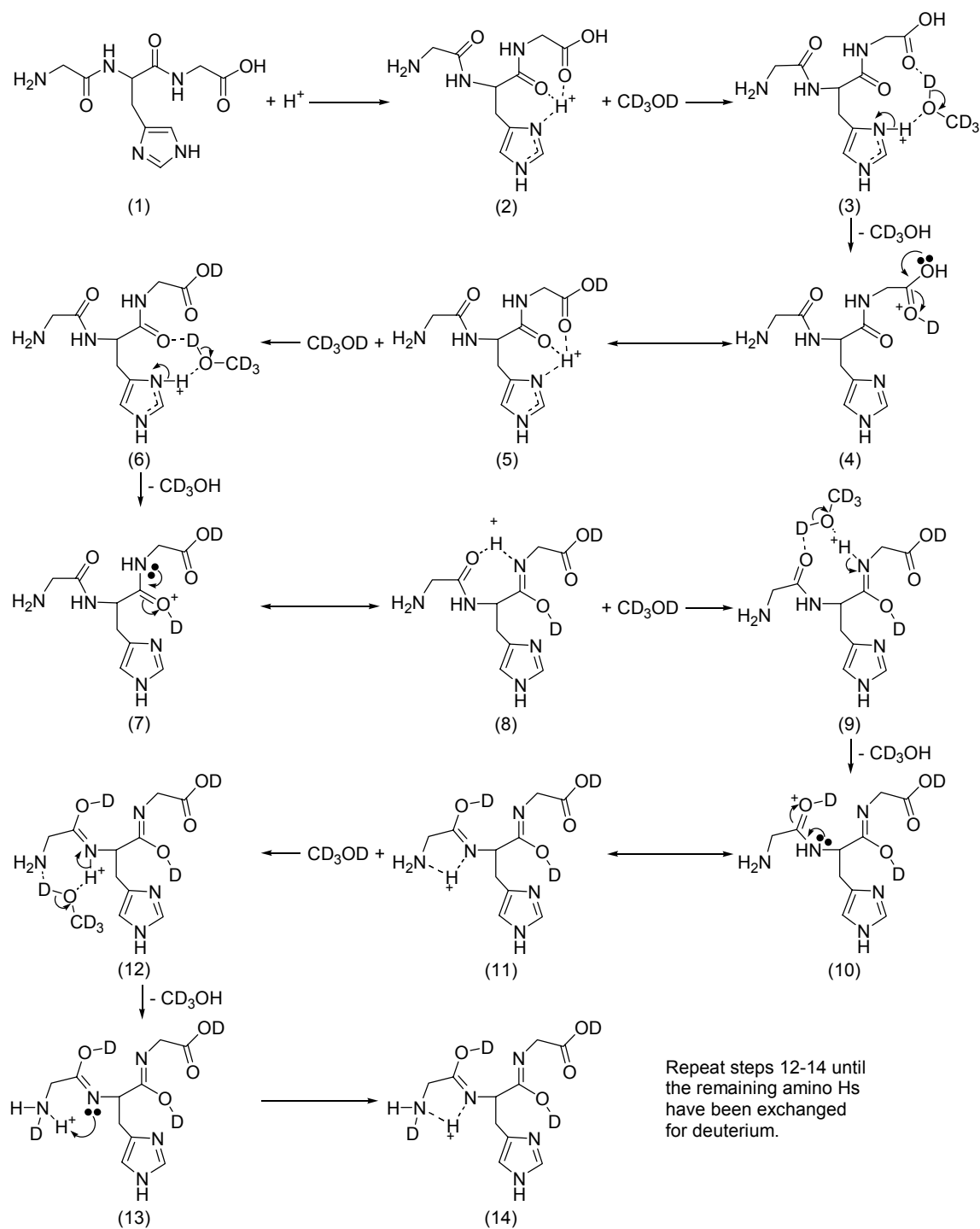
(1)

(2)

(3)

− CD$_3$OH

(6)

CD$_3$OD +

(5)

(4)

− CD$_3$OH

(7)

(8)

+ CD$_3$OD

(9)

− CD$_3$OH

(12)

CD$_3$OD +

(11)

(10)

− CD$_3$OH

(13)

(14)

Repeat steps 12-14 until
the remaining amino Hs
have been exchanged
for deuterium.

Scheme 5

(1)   + H⁺ →   (2)   + CD₃OD →   (3)

-CD₃OH

(6)   ← CD₃OD +   (5)   (4)

-CD₃OH

(7)   (8)

Repeat steps 6-8 until
the remaining amino Hs
have been exchanged
for deuterium.
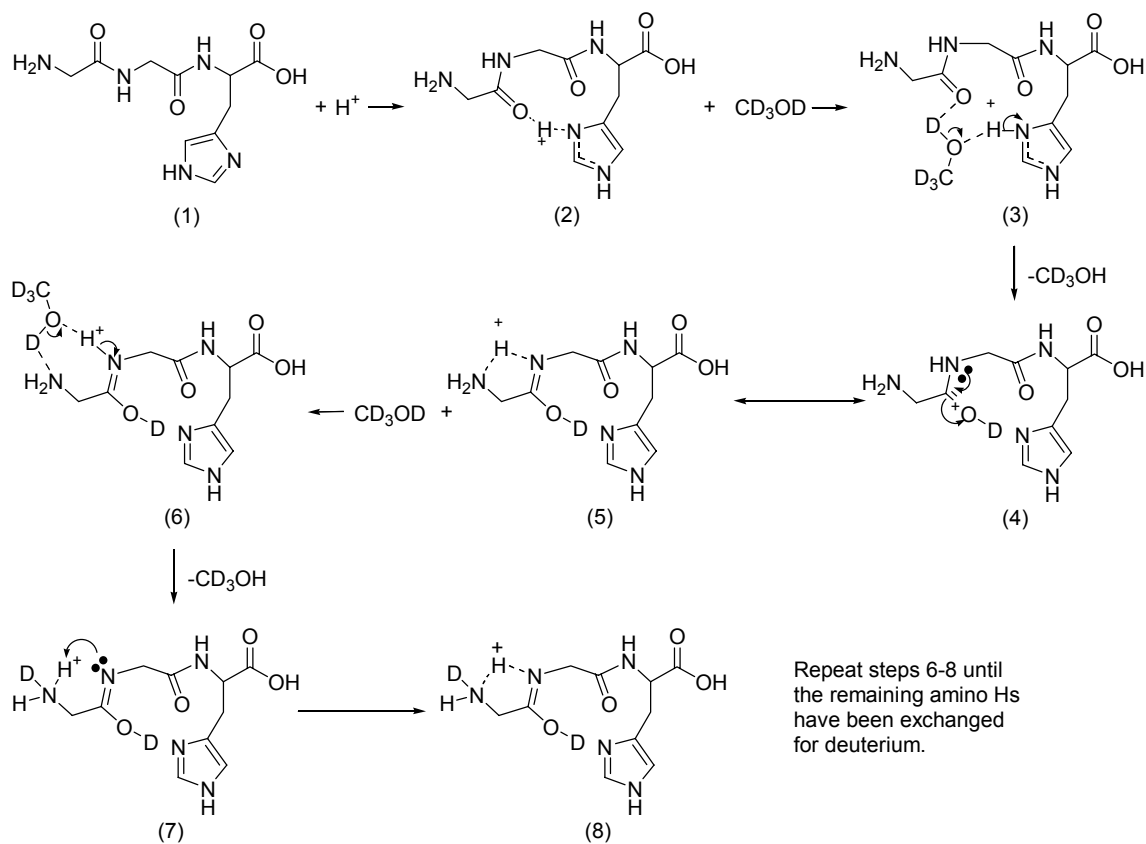
Gas-Phase H/D Exchange of the Dipeptides with Ammonia-d₃

Gas-phase H/D exchange reactions of histidine containing di- and tripeptides are more efficient with ammonia-d₃ than with methanol-d₄ (Table 1). The increased exchange efficiency can be attributed to a decrease in the relative GB differences between the oligopeptide ion and exchange reagent. In addition to reaction efficiency differences, gas-phase H/D exchange of oligopeptide ions with ammonia-d₃ exhibit different temporal plots for deuterium incorporation relative to reaction with methanol-d₄. Deviations in temporal distributions may be ascribed to mechanistic exchange

differences between the deuterium reagents.[39]   Unlike methanol-d_4, ammonia-d_3 is not

expected to exchange deuterium by a relay mechanism;[39] the anticipated mechanism for

H/D exchange with ammonia-d_3 involves proton transfer between the peptide ion and

deuterium reagent to form an ammonium ion, and the resultant ammonium ion is charge

solvated by the peptide, facilitating subsequent H/D exchange. Termed the "onium ion

mechanism"[39] exchange with amminia-d_3 does not require a basic site to be in close

proximity to the charge site as proposed for the relay mechanism. Hence, comparative

deviations in selectivity for reaction with these deuterium reagents may be attributed to

differences in their respective exchange mechanisms.   Proposed mechanistic

contributions to deviations in reaction selectivity may be complemented by relative

decreases in GB differences between peptides ions and the deuterium reagent. Reducing

the GB difference by changing the basicity of the deuterium reagent may alter reaction

selectivity, as comparatively inefficient exchanges, for reaction with methanol-d_4, are

rendered facile with ammonia-d_3 due to an increase in deuterium reagent basicity. These

mechanistic and basicity issues may explain the differences in H/D exchange temporal

plots for peptide ions with different exchange reagents.

Gas-phase H/D exchange of the histidine containing dipeptide ions display

similar temporal distributions for reaction with ammonia-d_3. As shown in Table 1, both

HisGlyH$^+$ and GlyHisH$^+$ incorporate the first deuterium at comparable reaction

efficiencies, suggesting common peptide ion conformations. Structural similarities have

also been proposed by Cassady to justify the identical GB values of these protonated

molecules, as measured by bracketing and kinetic methods.[50]   Molecular modeling

calculations performed on HisGlyH$^+$ and GlyHisH$^+$ point out structural features that are common to these sequence isomers. For example, Figure 30 shows optimized conformations for the protonated dipeptides. Both dipeptide ions incorporate the same functional groups for inductive stabilization of the charge site. These similar intramolecular interactions may contribute to the identical GB values reported for these protonated dipeptides and comparable H/D exchange temporal distributions (Figure 25 and 26) and reaction efficiencies (Table 1) observed for exchange with ammonia-d$_3$. Closer inspection of temporal plots for each dipeptide suggests that subsequent incorporation of deuterium is more efficient for HisGlyH$^+$ than GlyHisH$^+$. These differences may be attributed to dissimilar primary (*i.e.* groups involved in direct
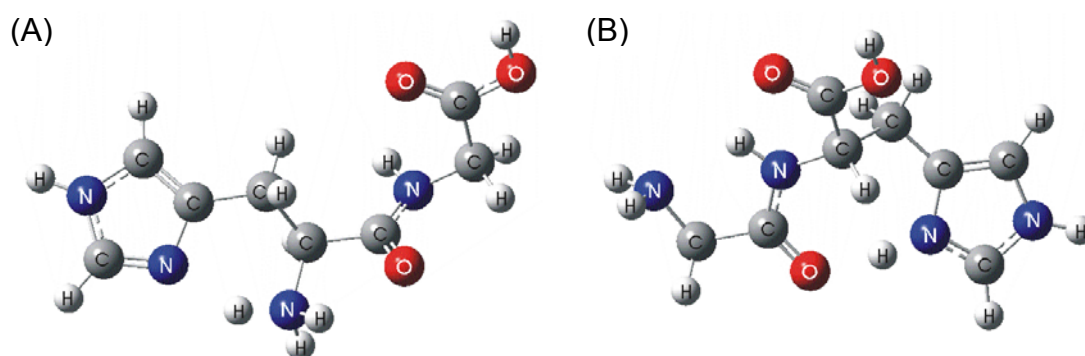
Figure 30. Optimized conformations for (A) HisGlyH$^+$ and (B) GlyHisH$^+$.

solvation of the ionizing proton) and secondary (*i.e.* groups participating in charge stabilization by remote hydrogen bonding) bridging interactions within the peptide ions. For HisGlyH$^+$ (Figure 30 A) the primary bridging interaction involves the protonated

imidazole ring and *N*-terminal amine, whereas, an *N*-terminal amine hydrogen and amide carbonyl comprise the secondary bridging interaction. Conversely, the primary bridging interaction for GlyHisH$^+$ (Figure 30 B) involves the protonated imidazole ring and glycyl amide carbonyl with a secondary interaction between the glycyl amide hydrogen and amino group. Amines are approximately 4 kcal/mol more basic[45] than amide carbonyls, thus a more efficient primary bridging interaction is possible for HisGlyH$^+$ than GlyHisH$^+$. Stronger bridging interactions have been attributed to efficient H/D exchange reaction rates despite considerable GB differences between the analyte ion and reagent[44,45,46,107], and may contribute to differences observed for the time dependent incorporation of deuterium. Temporal plots for these protonated dipeptides demonstrate exchange of five labile hydrogens at comparable reaction efficiencies with the sixth relatively hindered. According to proposed conformations of HisGlyH$^+$ and GlyHisH$^+$ groups involved with charge solvation contain five labile hydrogens and are presumably the facile exchanges for reaction with ammonia-d$_3$. Assignment of the carboxylic acid hydrogen as the inefficient exchanger is consistent with observations by Lebrilla for gas-phase H/D exchange of protonated histidine. Esterification of the histidine containing dipeptides prior to gas-phase H/D exchange may support this proposed assignment.

Gas-Phase H/D Exchange of the Tripeptides with Ammonia-d$_3$

The temporal plots for H/D exchange of the histidine containing tripeptides with ammonia-d$_3$ are very different from those obtained with methanol-d$_4$. As seen in Table 1, HisGlyGlyH$^+$ and GlyGlyHisH$^+$ incorporate the first deuterium at comparable

reaction efficiencies, suggesting similar intramolecular interactions. Common conformational features have also been proposed by Cassady to explain the identical GB values for these protonated peptides, as measured by bracketing methods.[50] Molecular modeling calculations for these sequence isomers suggest that HisGlyGlyH$^+$ and GlyGlyHisH$^+$ contain the same number of bridging interactions. For example, both peptide ions incorporate two bridging interactions for inductive stabilization of the charge site (see Figure 31). The intramolecular interactions may contribute to identical GB values reported for the tripeptide ions and comparable H/D exchange behavior observed for reaction with ammonia-d$_3$. Analogous to the dipeptides, subsequent incorporation of deuterium is more efficient for HisGlyGlyH$^+$ than GlyGlyHisH$^+$. These differences, seen in Figures 27 and 29, are attributed to dissimilar bridging interactions proposed for the peptide ions. Like HisGlyH$^+$, HisGlyGlyH$^+$ possesses a primary bridging interaction between the imidazole ring and *N*-terminal amine. Conversely, the primary bridging interaction for GlyGlyHisH$^+$ involves the protonated imidazole and the *N*-terminal glycyl amide carbonyl. The stronger primary bridging interaction afforded by HisGlyGlyH$^+$ may contribute to relative increases in H/D exchange efficiency for this *N*-terminal histidine containing tripeptide. In addition, temporal plots for HisGlyGlyH$^+$ and GlyGlyHisH$^+$ illustrate exchange of five labile hydrogens at comparable reaction efficiencies while remaining exchanges display relatively reduced efficiencies. Conformations for these protonated tripeptides suggest that groups involved with inductive stabilization of the charge site contain five labile hydrogens. As suggested for the dipeptides, these sites presumably account for the five facile exchanges observed

(A)   (B)
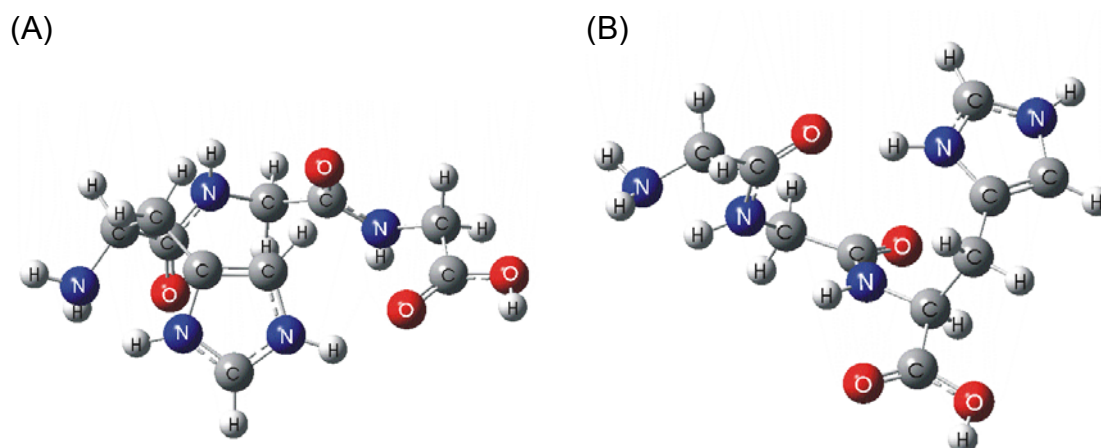
Figure 31. Optimized conformations for (A) HisGlyGlyH$^+$ and (B) GlyGlyHisH$^+$.

when reacted with ammonia-d$_3$.

Of the histidine containing tripeptides investigated, GlyHisGlyH$^+$ is the least efficient for incorporation of the first deuterium when reacted with ammonia-d$_3$. The decrease in H/D exchange efficiency is attributed to a comparative increase in the number of intramolecular interactions involved with charge solvation. The proposed conformations for GlyHisGlyH$^+$, generated by molecular modeling calculations, are shown in Figure 32. These two structural forms vary in energy by 0.32 kcal/mol, suggesting a high probability for interaction of the protonated imidazole with either amide carbonyl. Unlike its sequence isomers, conformations for GlyHisGlyH$^+$ imply that all functional groups within the peptide participate in proton bridging interactions. Increasing the number of intramolecular interactions has a proportional effect on peptide ion GB, causing reduction in relative H/D exchange reaction rate efficiency. In addition to efficiency observations, proposed conformations for GlyHisGlyH$^+$ may contribute to

(A)   (B)
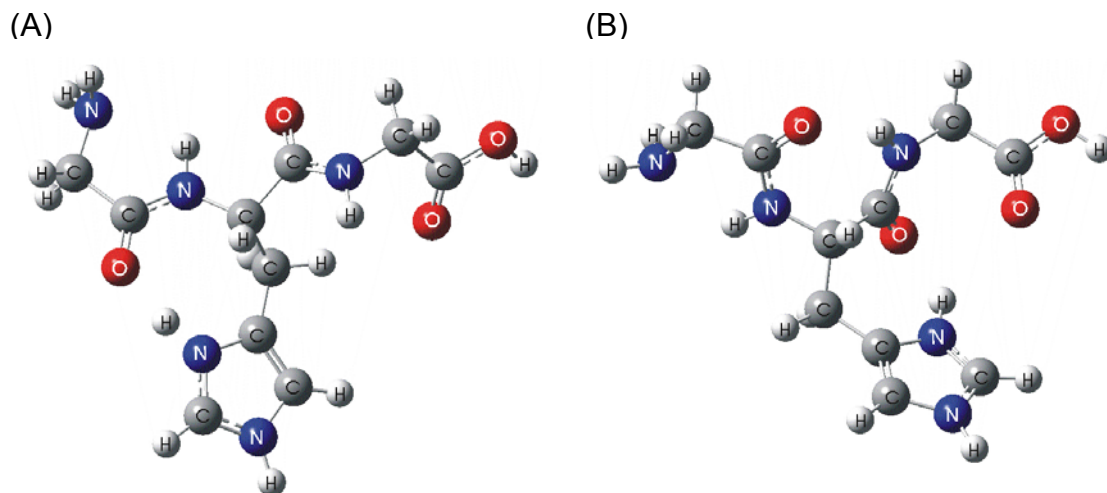
Figure 32. Optimized conformations for GlyHisGlyH$^+$

differences seen for the extent of deuterium incorporation. The temporal plot for reaction of GlyHisGlyH$^+$ with ammonia-d$_3$ (Figure 28) demonstrates exchange of all labile hydrogens at comparable reaction rates. Minimal reaction rate differences between successive exchanges suggest that the charge site is effectively delocalized throughout the peptide, supporting the proposed conformation for GlyHisGlyH$^+$.

Conclusion

Gas-Phase H/D exchange reactions have been performed on selected di- and tripeptides containing a histidine amino acid residue in a FT-ICR MS. The oligopeptide ions investigated in this study demonstrate sequence specific temporal distributions and reaction efficiencies with methanol-d$_4$ and ammonia-d$_3$. Differences in H/D exchange are likely attributed to the dissimilar intramolecular interactions involved in charge

solvation of the ionized peptide. Sequence position of the histidine residue influences both the H/D exchange reaction efficiency and the extent of deuterium incorporation for peptide ions. Specifically, protonated peptides containing a *N*-terminal histidine residue, exhibit the most efficient rate for incorporation of the first deuterium. The H/D exchange efficiency afforded to these peptide ions is ascribed to certain intramolecular interactions not present for peptides containing an internal or *C*-terminal histidine residue. Sequence specific differences in H/D exchange were complemented by the dissimilar temporal plots for these peptide ions when reacted with different reagents. These discrepancies are attributed to dissimilar exchange mechanism and GB of these deuterium reagents.

CHAPTER IV

THE GAS-PHASE HYDROGEN/DEUTERIUM EXCHANGE OF SELECTED DI-

AND TRIPEPTIDES CONTAINING A LYSINE AMINO ACID RESIDUE

Introduction

Investigating biomolecule conformations remains an active area of research in the life sciences. Emphasis placed on structural characterization is attributed to affects that peptide and protein conformations have on bioactivity and reactivity. The ability to infer structural information for these compounds has been aided by development of such techniques as ion-mobility and gas-phase ion-molecule reactions by mass spectrometry. These instruments allow for investigation of peptide secondary structure in the absence of solvent, revealing intrinsic intramolecular interactions as hydration effects are eliminated. A generally accepted method for probing ion conformations is by gas-phase H/D exchange. This isotopic labeling technique has been employed to determine the presence of multiple peptide ion conformations by mass spectrometry. Despite the utility of this technique, few experiments have been performed to elucidate factors influencing deuterium uptake. Specifically, gas-phase H/D exchange of peptides containing basic amino acid residues has received minimal attention. Since histidine, lysine and arginine amino acids are protonated on their respective side chains and H/D exchange is influenced by charge location, understanding the effects of basic residues on deuterium incorporation is important.

This study utilizes gas-phase H/D exchange to elucidate effects that sequence position (i.e. *N*-terminal, internal or *C*-terminal) of a basic amino acid residue has on deuterium uptake in peptides. Sequence isomers of selected di- and tripeptides, possessing a lysine and glycine residue(s), were employed for these experiments. Several semiempirical calculations and gas-phase ion-molecule studies of lysine containing peptides have suggested that the n-butyl amine is protonated with intramolecular charge solvation by neighboring functional groups. Consequently, position of lysine residues within peptides likely causes particular bridging interactions that are unique to that specific isomer. Intramolecular charge solvation by functional groups with similar GBs has been ascribed to efficient H/D exchange rates despite unfavorable GB between the analyte ion and deuterium reagent. Therefore, peptide sequence isomers displaying different exchange efficiencies may be attributed to dissimilar bridging interactions within the peptide, suggesting unique ion conformations.

Studies described herein utilize a Fourier transform ion cyclotron resonance mass spectrometer (FT-ICR MS) to investigate the gas-phase H/D exchange of peptide sequence isomers containing a lysine amino acid. Selected di- and tripeptides were protonated by matrix assisted laser desorption ionization (MALDI) and reacted with acetic acid-d_4 and ammonia-d_3. Results from these experiments suggest that sequence position of the lysine residue influences H/D exchange efficiency and the number of gas-phase conformations for an individual peptide. Dissimilarities in H/D exchange efficiencies and temporal distributions for these peptides are rationalized by the different intramolecular interactions proposed for inductive stabilization of the charge site.

Results

Gas-Phase H/D Exchange with Acetic Acid-d₄

The oligopeptides investigated in these gas-phase H/D exchange studies represent sequence isomers containing lysine and glycine amino acid residues. These oligopeptides (see Table 2) were selected to investigate effects of position (*i.e. N*-terminal, internal or *C*-terminal) of the lysine amino acid on rates and extent of deuterium incorporation. H/D exchange temporal distributions for the $[M+H]^+$ ions of

Table 2. Hydrogen/deuterium exchange efficiency (k_{exp}/k_{coll}) for incorporation of the first deuterium in lysine containing oligopeptide $[M+H]^+$ ions when reacted with acetic acid-d₄ or ammonia-d₃.

$[M+H]^+$	Acetic acid-d₄	Ammonia-d₃
LysGly	$0.39^†$; 0.014*	0.42
GlyLys	0.32	0.69
LysGlyGly	$0.40^†$; 0.0013*	0.46
GlyLysGly	0.21	0.76
GlyGlyLys	0.16	0.54

† H/D exchange reaction efficiency for the first portion of a double exponential decay fit.
* H/D exchange reaction efficiency for the second portion of a double exponential decay fit.

LysGly and GlyLys, reacted with acetic acid-d₄, are shown in Figures 33 and 34, respectively. As was observed for HisGly and GlyHis, LysGly and GlyLys illustrate dissimilar temporal plots for deuterium incorporation. For LysGlyH$^+$, the depletion of the $[M+H]^+$ ion appears to be a double exponential decay, whereas GlyLysH$^+$ is a single exponential decay. As seen in Table 2, incorporation of the first deuterium is slightly more efficient for LysGly than GlyLys. A series of partial mass spectra for these lysine containing dipeptide ions, reacted with acetic acid-d₄, is illustrated in Figures 35 and 36.

The gas-phase H/D exchange of tripeptides containing one lysine and two

Figure 33. Temporal plot for gas-phase H/D exchange of protonated LysGly with deuterated acetic acid at ~ 6.0 E-8 torr.

Figure 34. Temporal plot for gas-phase H/D exchange of protonated GlyLys with deuterated acetic acid at ~6.0 E-8 torr.
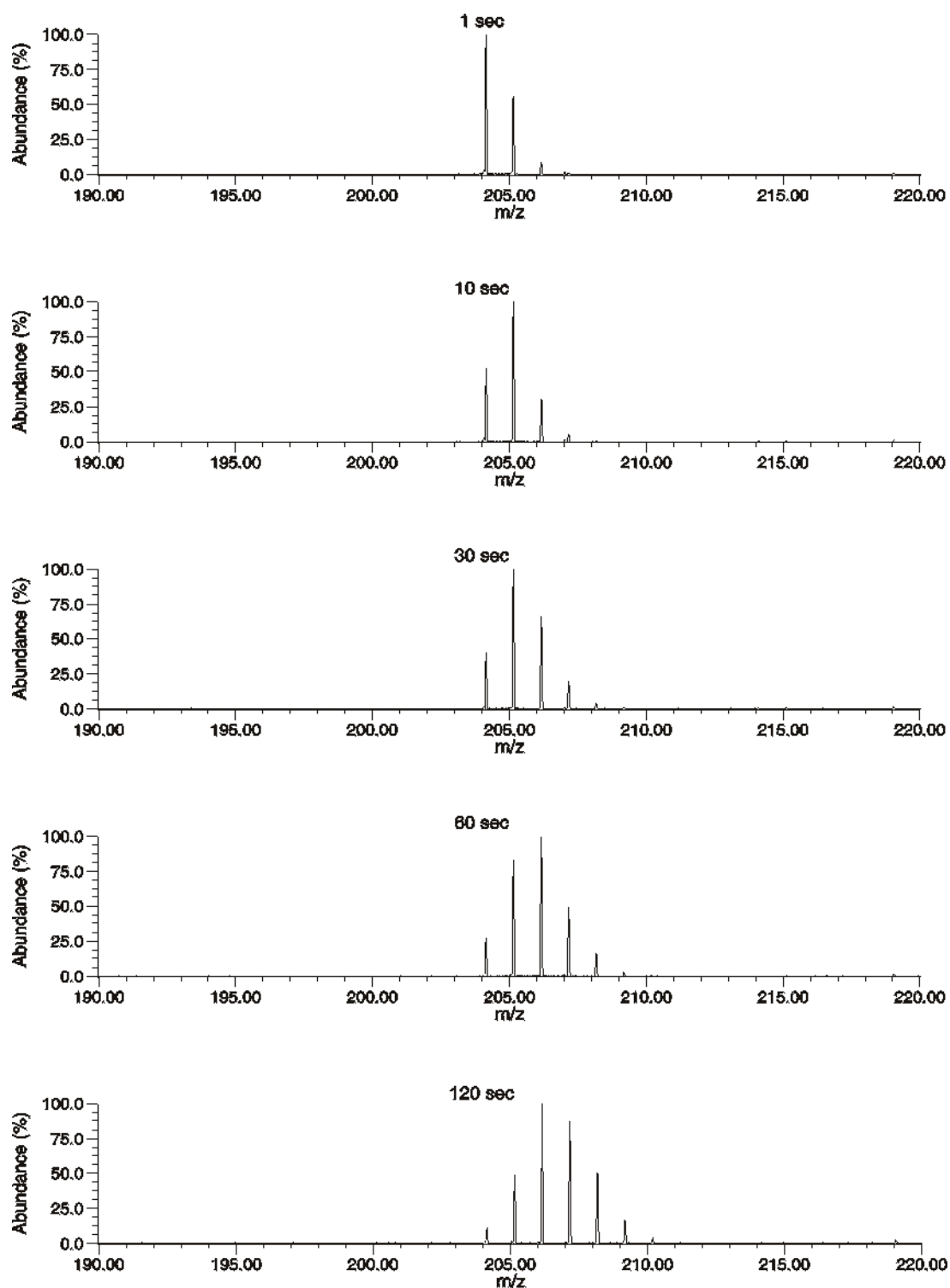
Figure 35. Partial mass spectra of protonated LysGly reacted with deuterated
acetic acid. Reaction times ranging from 1 - 120 seconds.
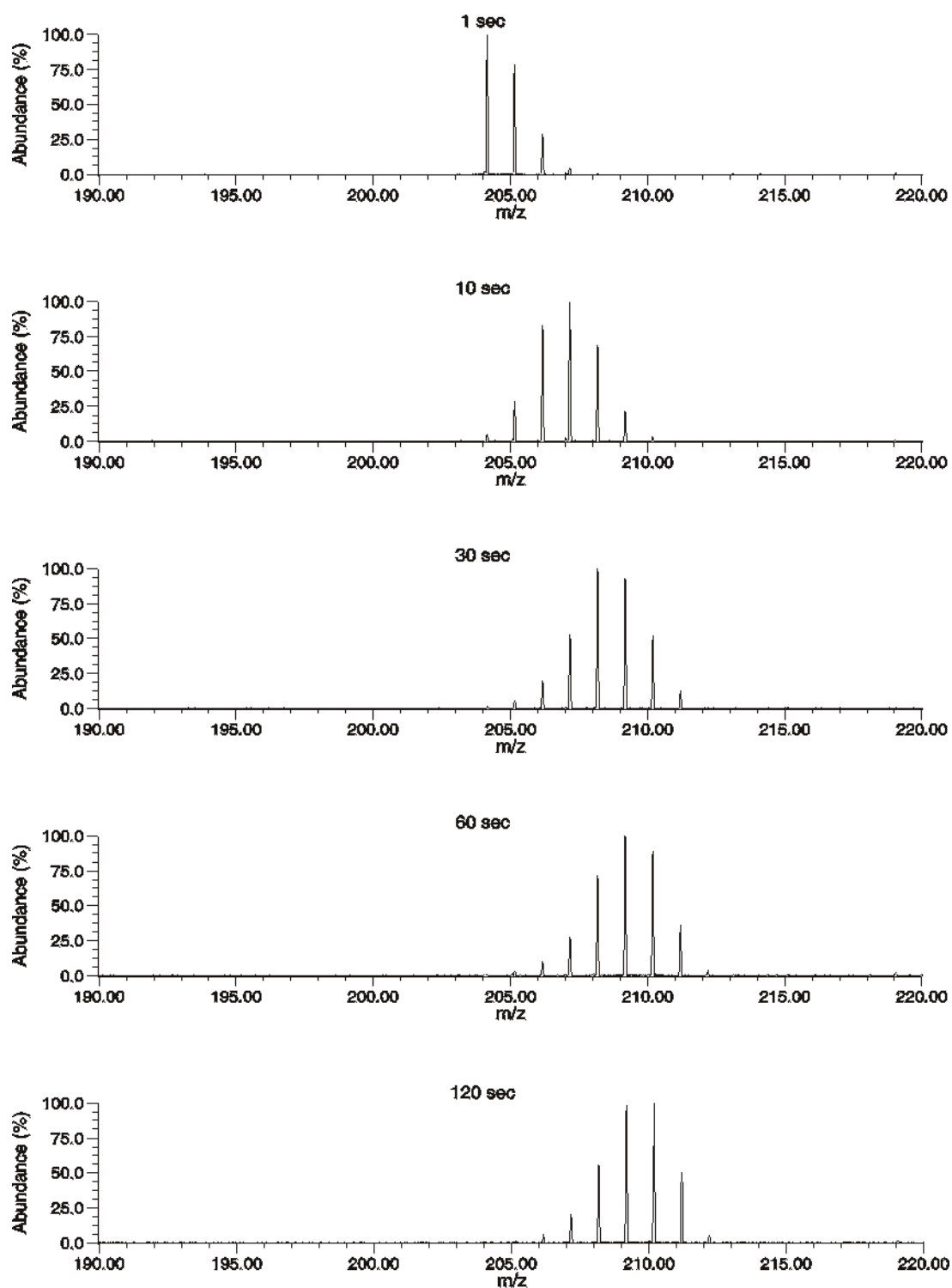
Figure 36. Partial mass spectra of protonated GlyLys reacted with deuterated
acetic acid. Reaction times ranging from 1 - 120 seconds.

glycine amino acid residues were also investigated. LysGlyGly, GlyLysGly, and GlyGlyLys [M+H]$^+$ ions also demonstrate sequence specific rates of deuterium incorporation for reaction with acetic acid-d$_4$, as illustrated in Figures 37, 38, and 39, respectively. Both LysGlyH$^+$ and LysGlyGlyH$^+$ decays appear to be a double exponential for incorporation of the first deuterium. These *N*-terminal lysine-containing peptides have nearly identical H/D exchange reaction efficiencies for the first portion of their respective decays (Table 2). The second segment of the double exponentials exhibit greater reaction efficiency for LysGlyH$^+$ than for LysGlyGlyH$^+$. Comparatively, gas-phase H/D exchange of GlyLysGlyH$^+$, performed under similar experimental conditions, is a single exponential decay at approximately half the reaction efficiency of LysGlyGlyH$^+$. Finally, the H/D exchange efficiency for GlyGlyLysH$^+$ is less efficient than both of its sequence isomers, exhibiting a single exponential temporal distribution.

Gas-Phase H/D Exchange with Ammonia-d$_3$

Studies of lysine-containing di- and tripeptide reactions with ammonia-d$_3$ were performed under similar conditions used for acetic acid-d$_4$. Decreasing the gas-phase basicity difference between the peptide ion and deuterium reagent, exchange is more efficient with ammonia-d$_3$ and demonstrates deviations in H/D exchange temporal distributions when compared to results obtained with acetic acid-d$_4$. As seen in Figures 40 and 41, LysGlyH$^+$ and GlyLysH$^+$ appear to have similar temporal plots for deuterium incorporation, with GlyLysH$^+$ showing greater reaction efficiency than LysGlyH$^+$ for the first exchange. Both lysine-containing dipeptides demonstrate a single exponential decay for incorporation of the first deuterium, exchanging seven of the eight labile

Figure 37. Temporal plot for gas-phase H/D exchange of protonated LysGlyGly with deuterated acetic acid at ~6.0 E-8 torr.

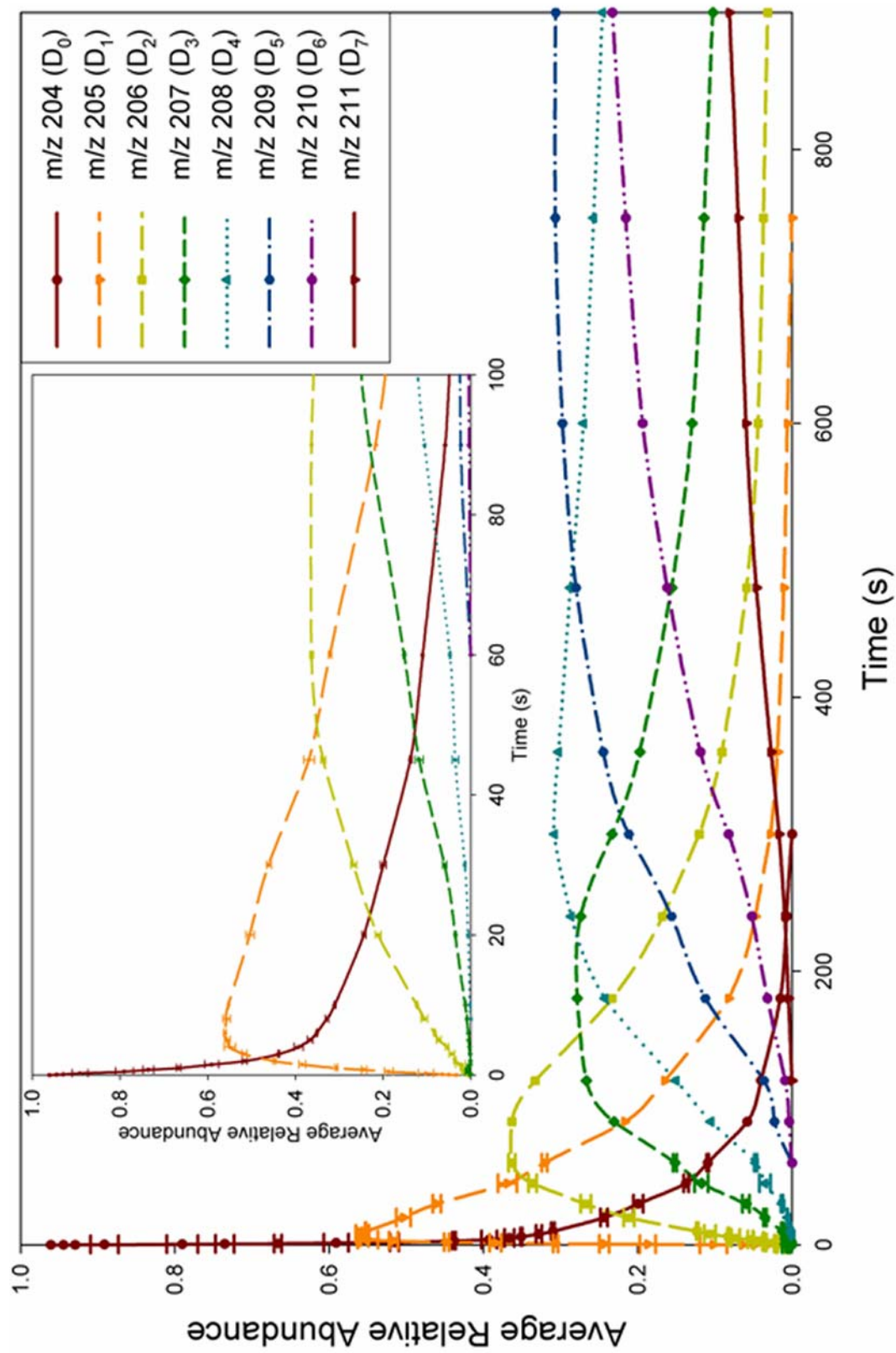Figure 38. Temporal plot for gas-phase H/D exchange of protonated GlyLysGly with deuterated ammonia at ~6.0 E-8 torr.
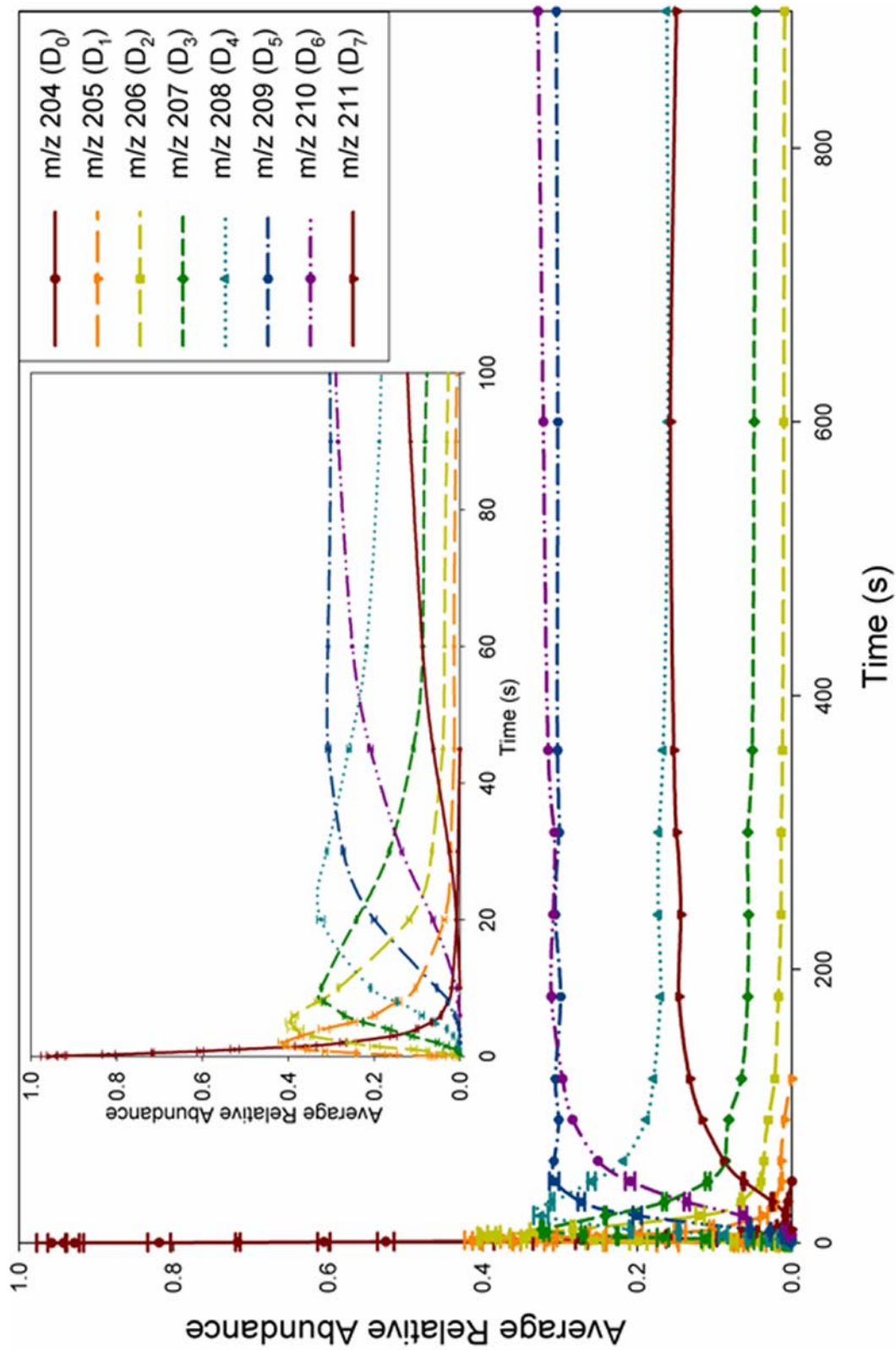
Figure 39. Temporal plot for gas-phase H/D exchange of protonated GlyGlyLys with deuterated acetic acid at ~6.0 E-8 torr.

Figure 40. Temporal plot for gas-phase H/D exchange of protonated LysGly with deuterated ammonia at ~6.6 E-8 torr.

Figure 41. Temporal plot for gas-phase H/D exchange of protonated GlyLys with deuterated ammonia at ~6.6 E-8 torr.

hydrogens.

Reactions of the [M+H]$^+$ ions of LysGlyGly, GlyLysGly, and GlyGlyLys with ammonia-d$_3$ also demonstrate differences in H/D exchange when compared to results obtained with acetic acid-d$_4$, as illustrated in Figures 42, 43 and 44, respectively. Gas-phase H/D exchange of LysGlyGlyH$^+$ is inefficient for incorporation of the first deuterium when reacted with ammonia-d$_3$. Exchanging seven of eight labile hydrogens during the time course of the experiment, LysGlyGlyH$^+$ demonstrates comparable reaction efficiency when compared to LysGlyH$^+$ (Table 2). Gas-phase H/D exchange of GlyLysGlyH$^+$ is the most efficient at incorporating the first deuterium when reacted with ammonia-d$_3$, exchanging all labile hydrogens. Finally, the H/D exchange of GlyGlyLysH$^+$ with ammonia-d$_3$ is 8% more efficient that LysGlyGlyH$^+$, incorporating six deuteriums during the time course of the experiment.

Discussion

Gas-phase H/D exchange studies of the [M+H]$^+$ ions of amino acids, oligopeptides and polyfunctional molecules by Lebrilla[44,46,107,112] and Nibbering[45,113] have shown that intramolecular interactions influence deuterium incorporation. The interaction of multiple functional groups for inductive stabilization of the charge site have been attributed to efficient H/D exchange rates despite considerable GB differences between the analyte ion and deuterium reagent. Typically, solvation of the ionizing proton by functional groups with similar GBs produces efficient reactions for deuterium incorporation. This enhanced exchange efficiency is presumably ascribed to energetics
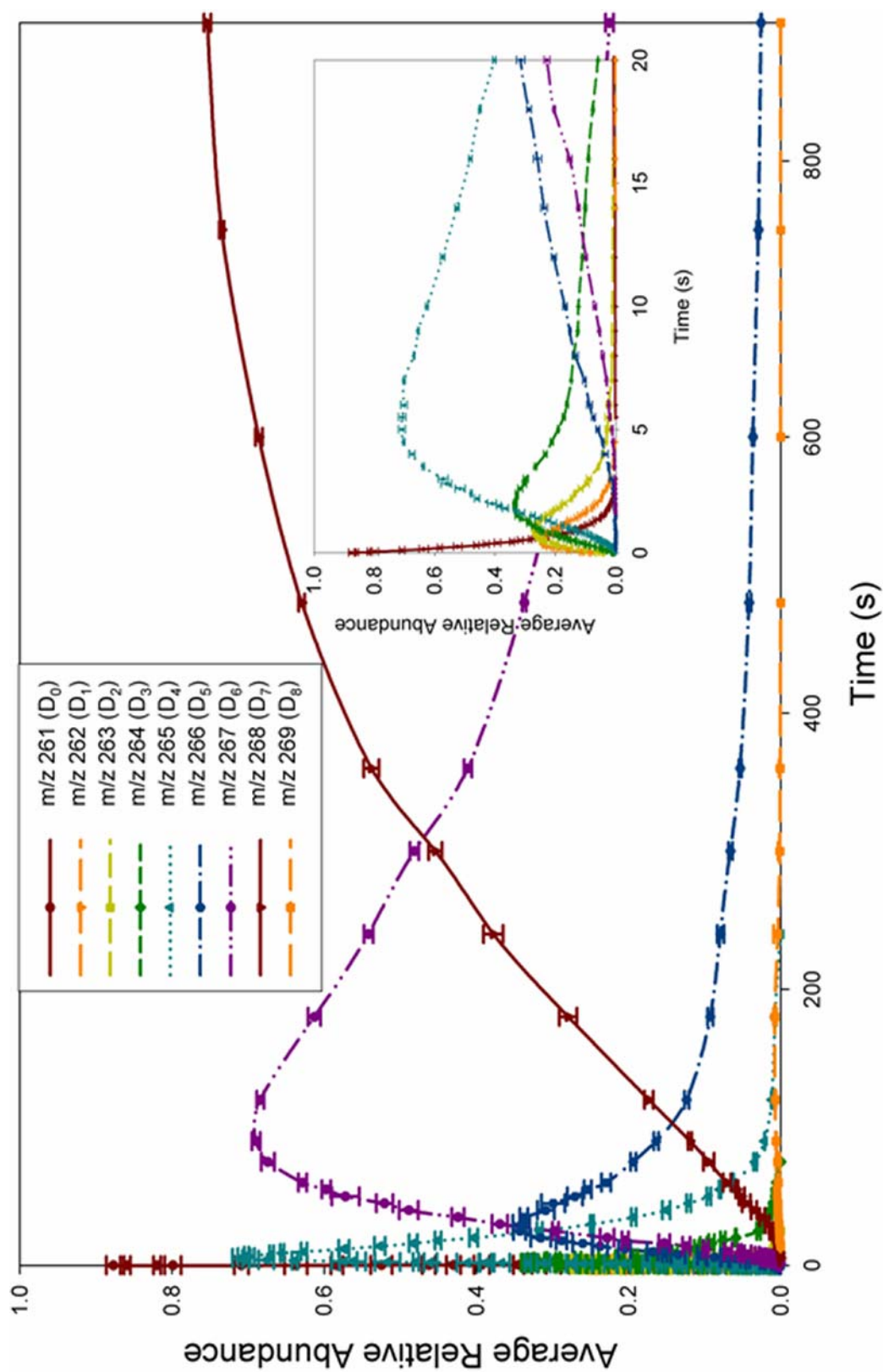
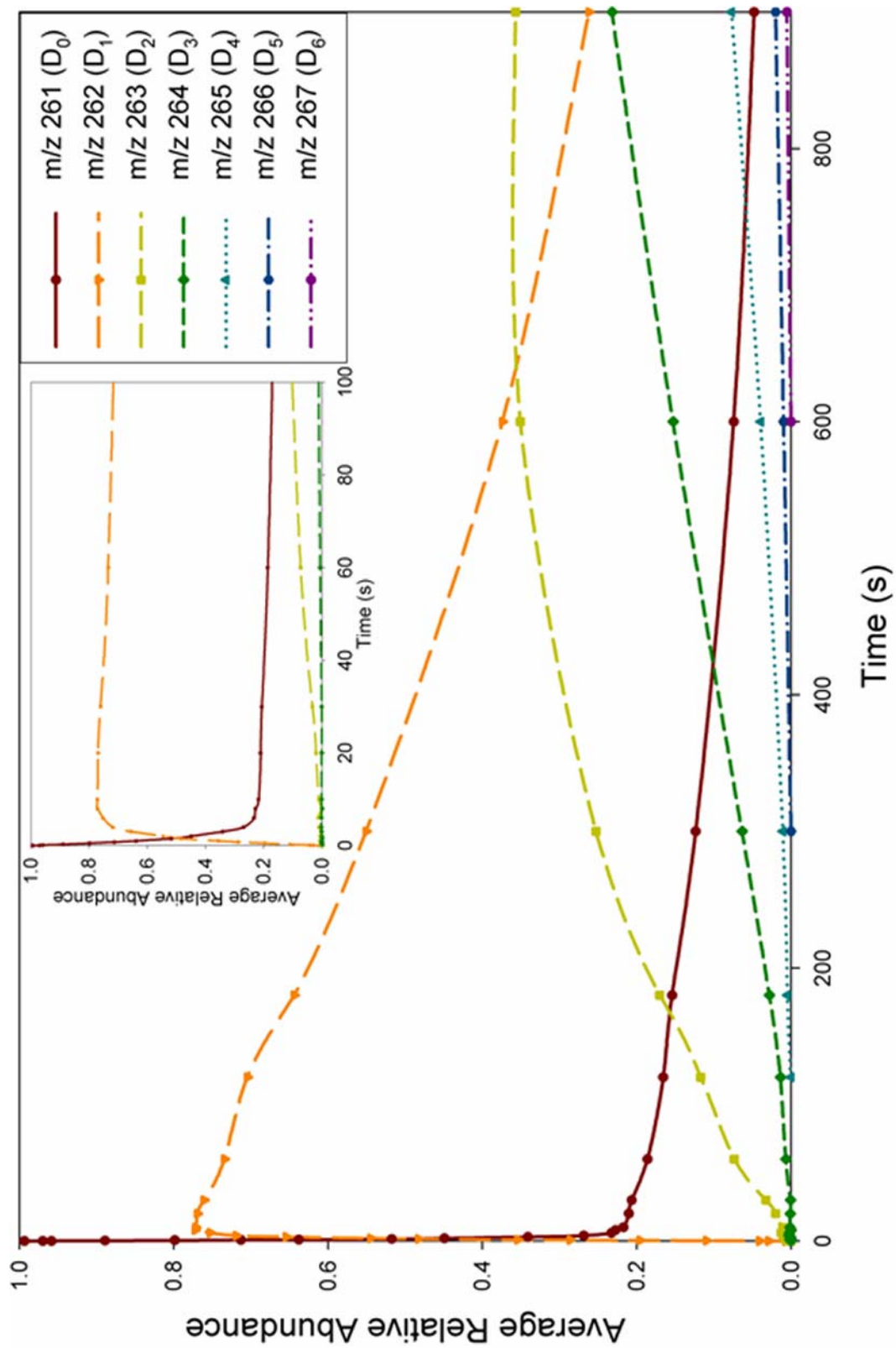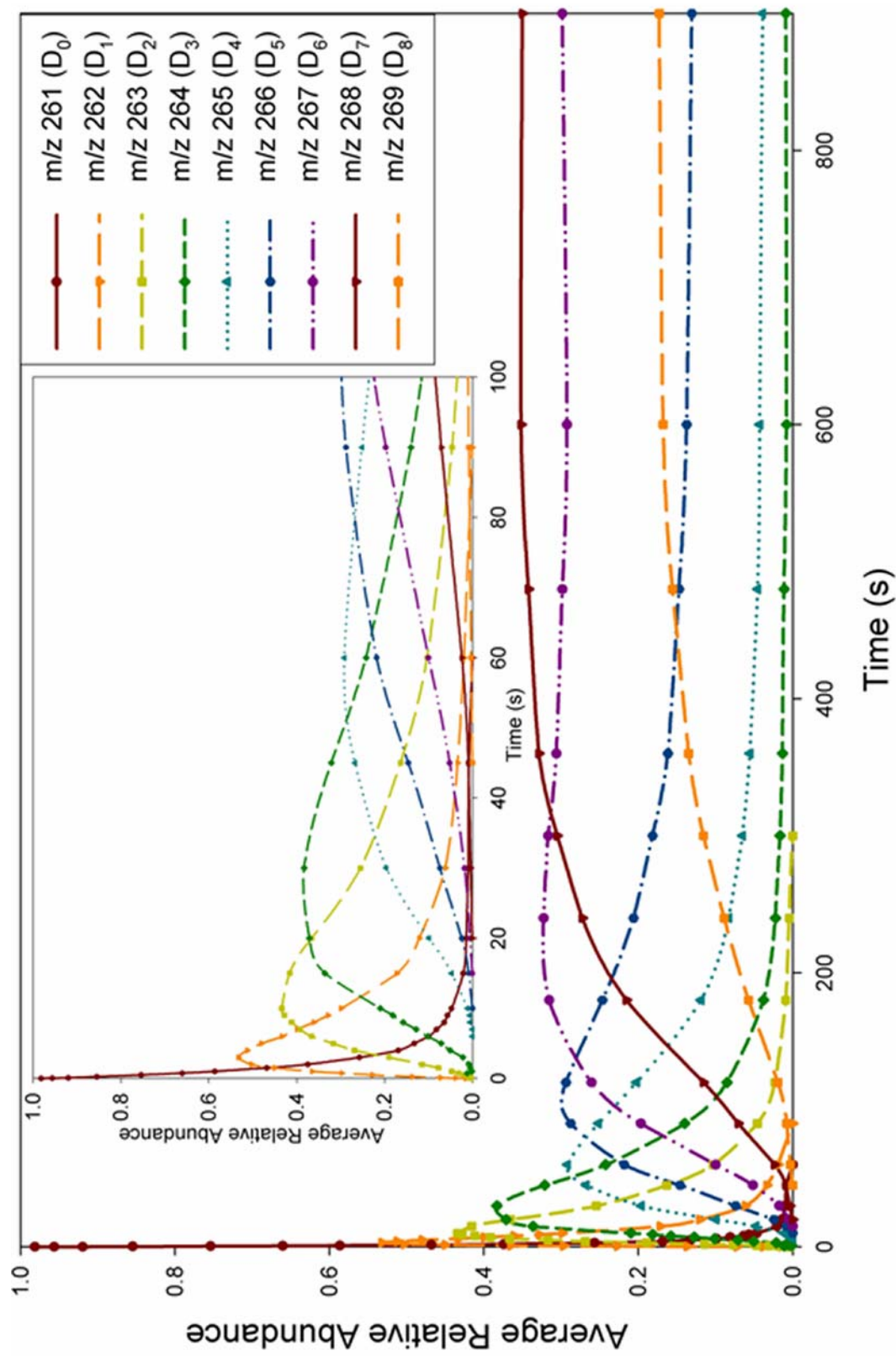Figure 42. Temporal plot for gas-phase H/D exchange of protonated LysGlyGly with deuterated ammonia at ~6.6 E-8 torr.
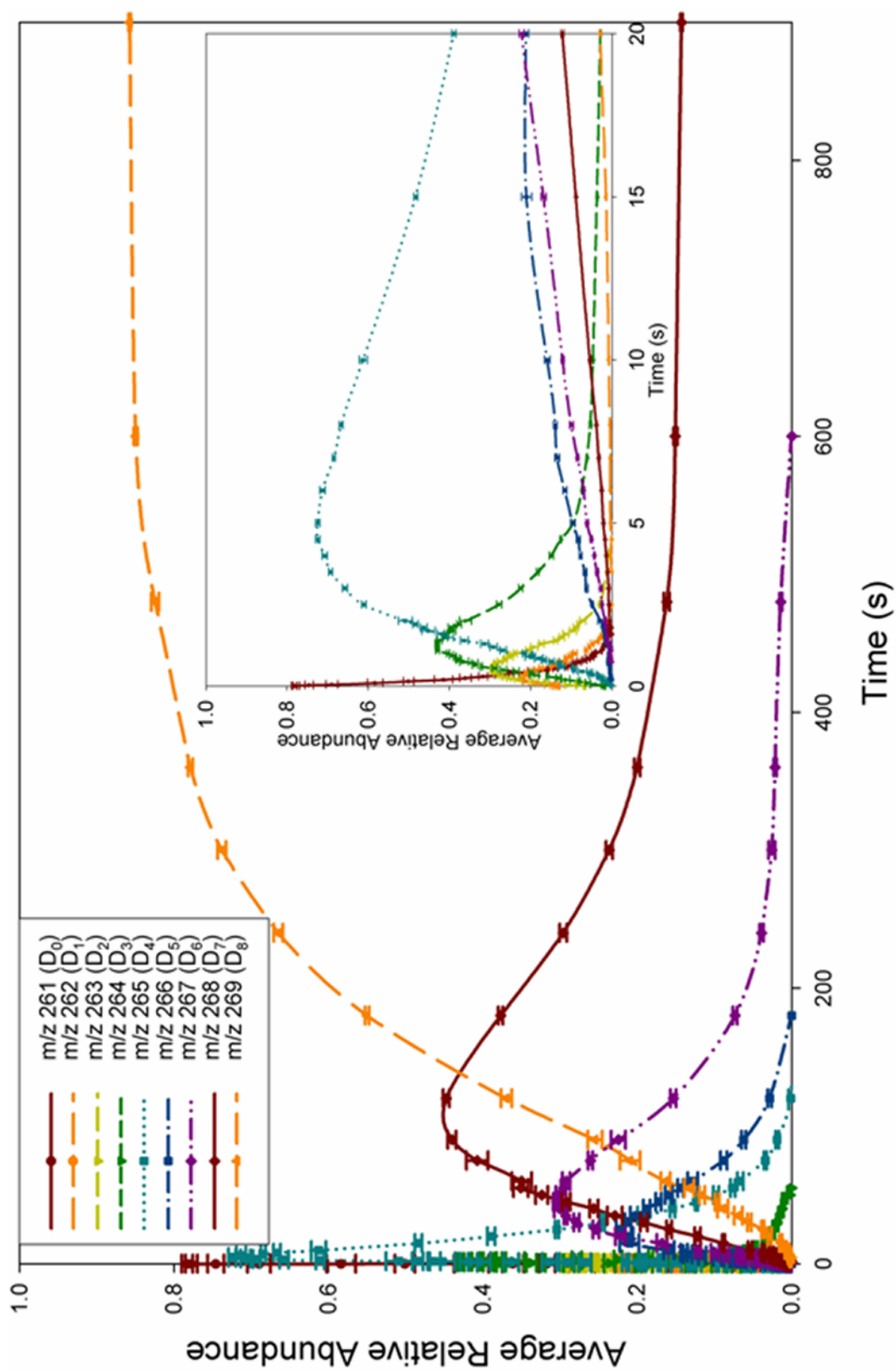
Figure 43. Temporal plot for gas-phase H/D exchange of protonated GlyLysGly with deuterated ammonia at ~6.6 E-8 torr.

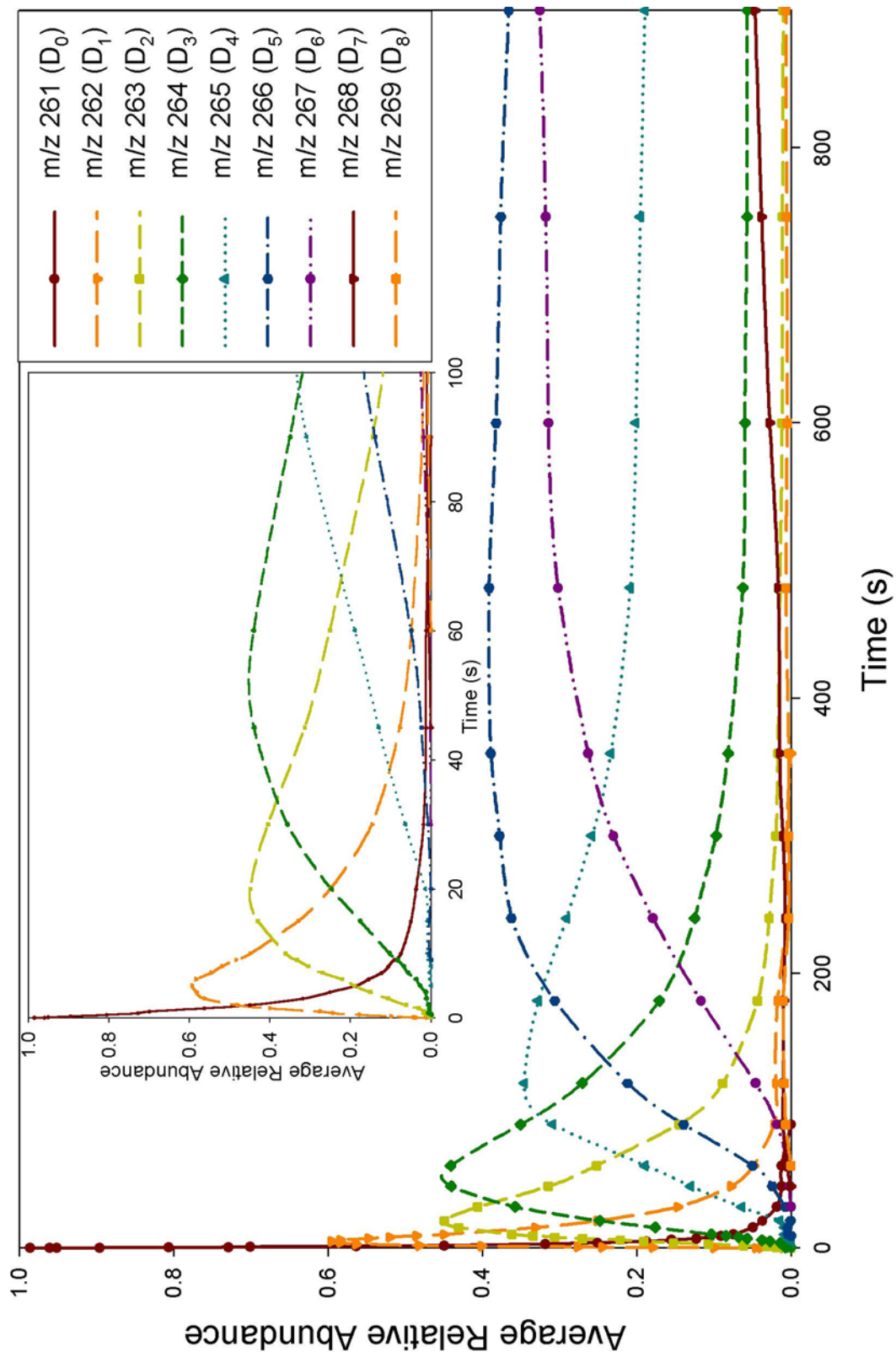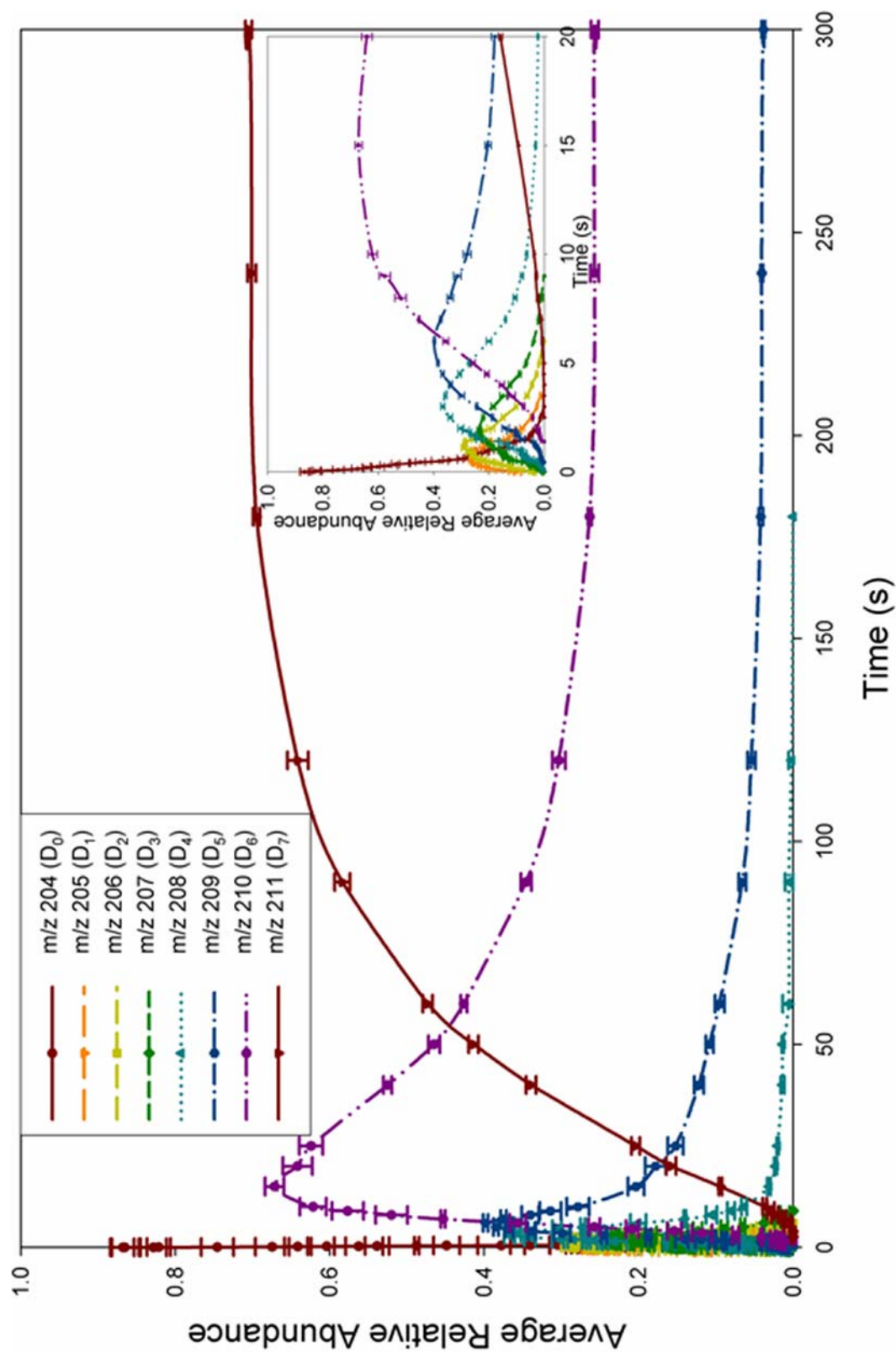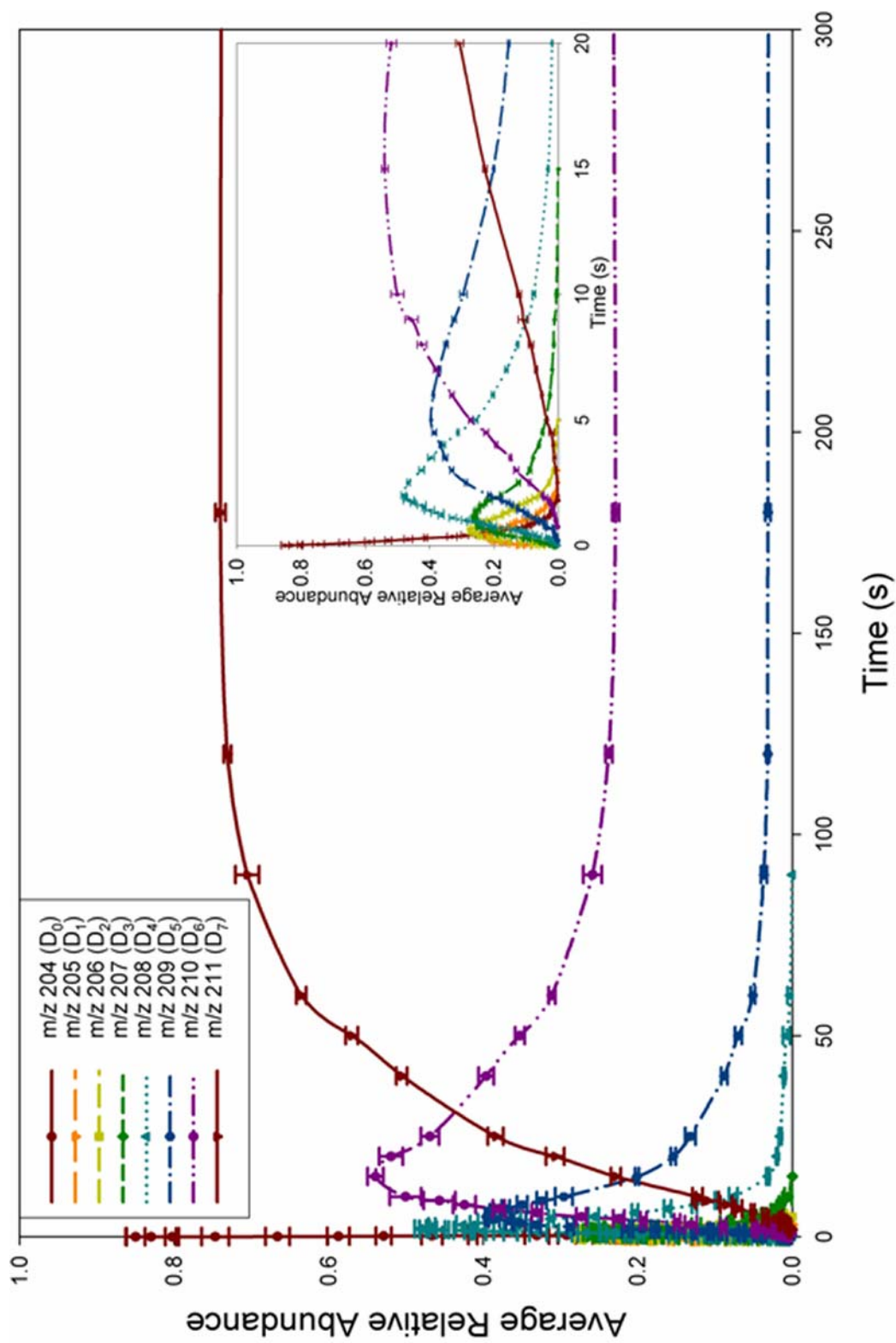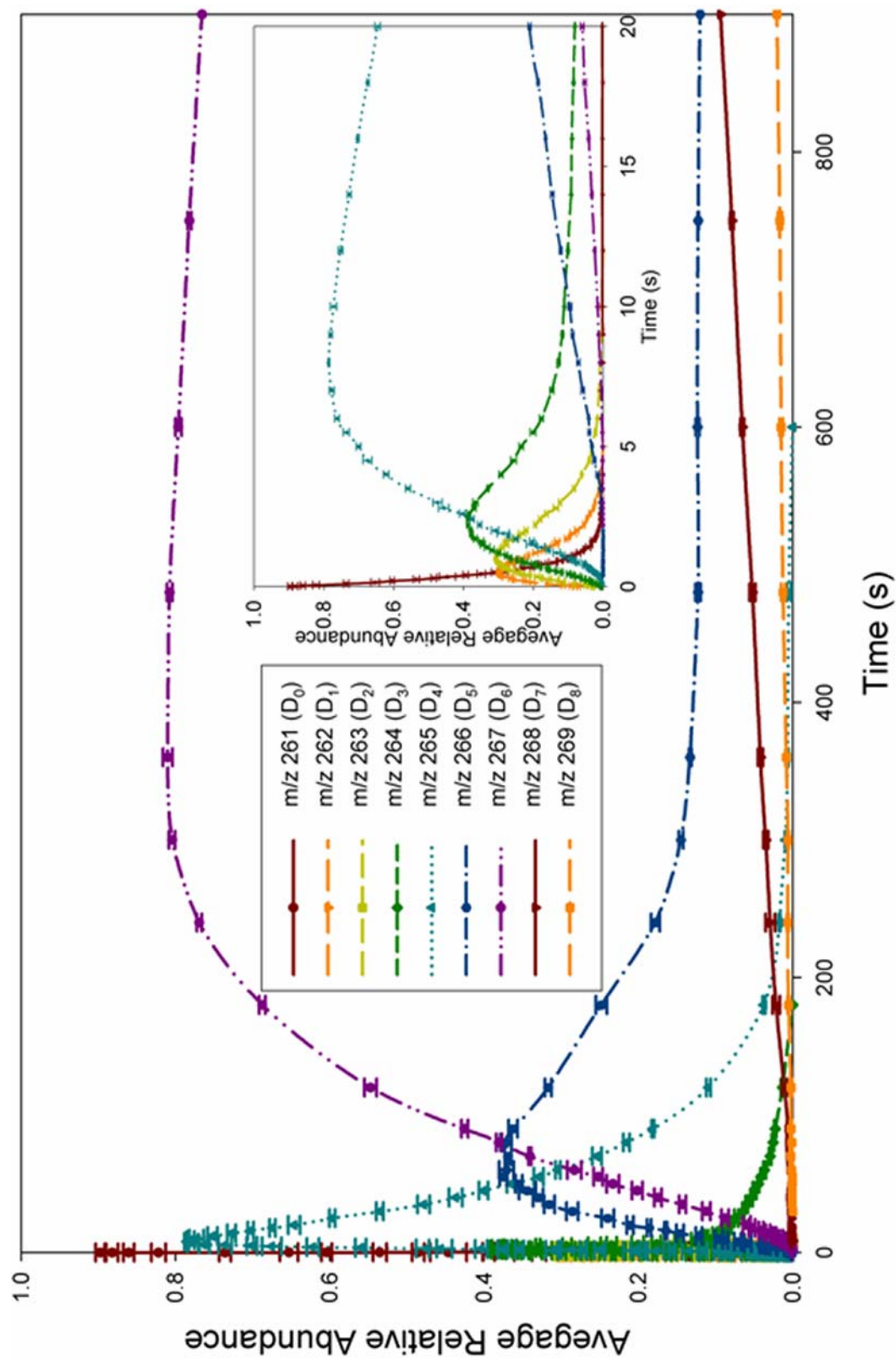Figure 44. Temporal plot for gas-phase H/D exchange of protonated GlyGlyLys with deuterated ammonia at ~ 6.6 E-8 torr.

associated with formation of the ion-neutral complex between the bridging functional groups. Therefore, observation of double exponential decays in gas-phase H/D exchange studies may be ascribed to dissimilar intramolecular bridging interactions for a peptide ion, suggesting the presence of multiple ion conformations.

Gas-Phase H/D Exchange of the Dipeptides with Acetic Acid-d₄

The [M+H]$^+$ ions of di- and tripeptide sequence isomers, containing a lysine amino acid residue, display different temporal distributions for deuterium incorporation when reacted with acetic acid-d₄. The dissimilar H/D exchange temporal distributions for oligopeptide ions containing the same amino acid residues but different sequences may be attributed to involvement of different functional groups for charge site stabilization. Dissimilar intramolecular interactions most likely produce unique GBs for the sequence isomers. Proposed as an influential factor in gas-phase H/D exchange, the GB difference between peptide ions and deuterium reagents has an inversely proportional effect on deuterium incorporation[39,45,46] possibly contributing to the dissimilar reaction rate efficiencies observed for LysGlyH$^+$ and GlyLysH$^+$.

Proposed gas-phase ion conformations for LysGly and GlyLys [M+H]$^+$ ions are based upon the relative GB differences between functional groups within the peptide and their general proximity to the charge site. Several independent studies and semiempirical calculations have suggested that lysine,[103] and related molecules,[50,107] are protonated on the n-butyl amino group with intramolecular charge solvation by the *N*-terminal amine. Bridging the ionizing proton between amino groups is a possible stabilizing interaction for *N*-terminal lysine containing peptides due to their general

proximity and identical GB. A suggested mechanism for gas-phase H/D exchange of LysGlyH$^+$ with acetic acid-d$_4$ is illustrated in Scheme 6. Initiated by formation of an ion-molecule complex, exchange of hydrogen for deuterium is suggested to proceed through Beauchamp's proposed, "relay mechanism."[39] Intramolecular interactions between the amino groups in LysGlyH$^+$ may also be complemented by an alternative gas-phase conformation involving the protonated n-butyl amino and amide carbonyl groups. Involvement of these functional groups, forming a bridging interaction in LysGlyH$^+$, is possible due to the proximity and similar GB of amine and amide carbonyls. Shown in Scheme 7 is a proposed mechanism for an alternative conformation of LysGlyH$^+$, reacted with acetic acid-d$_4$. Inductive stabilization of the charge site by different bridging interactions produces dissimilar peptide ion conformations for LysGlyH$^+$. These proposed structures most likely contribute to the double exponential decay, seen in Figure 45, for gas-phase H/D exchange of LysGlyH$^+$ with acetic acid-d$_4$.

Differences between the gas-phase H/D exchange temporal plots for LysGlyH$^+$ and GlyLysH$^+$, when reacted with acetic acid-d$_4$, can be rationalized by the likelihood of dissimilar intramolecular interactions. In comparison to LysGly, the n-butyl amino group of GlyLys is remote from the *N*-terminal amine. This spatial separation may hinder interactions between amino groups, as proposed for LysGlyH$^+$. Inductive stabilization of the charge site in GlyLysH$^+$ likely involves a bridging interaction between the n-butyl amino and the amide carbonyl. Proposed as a possible intramolecular interaction due to the proximity and similar GB of these functional groups, charge stabilization can further be aided by remote hydrogen bonding between

Scheme 6
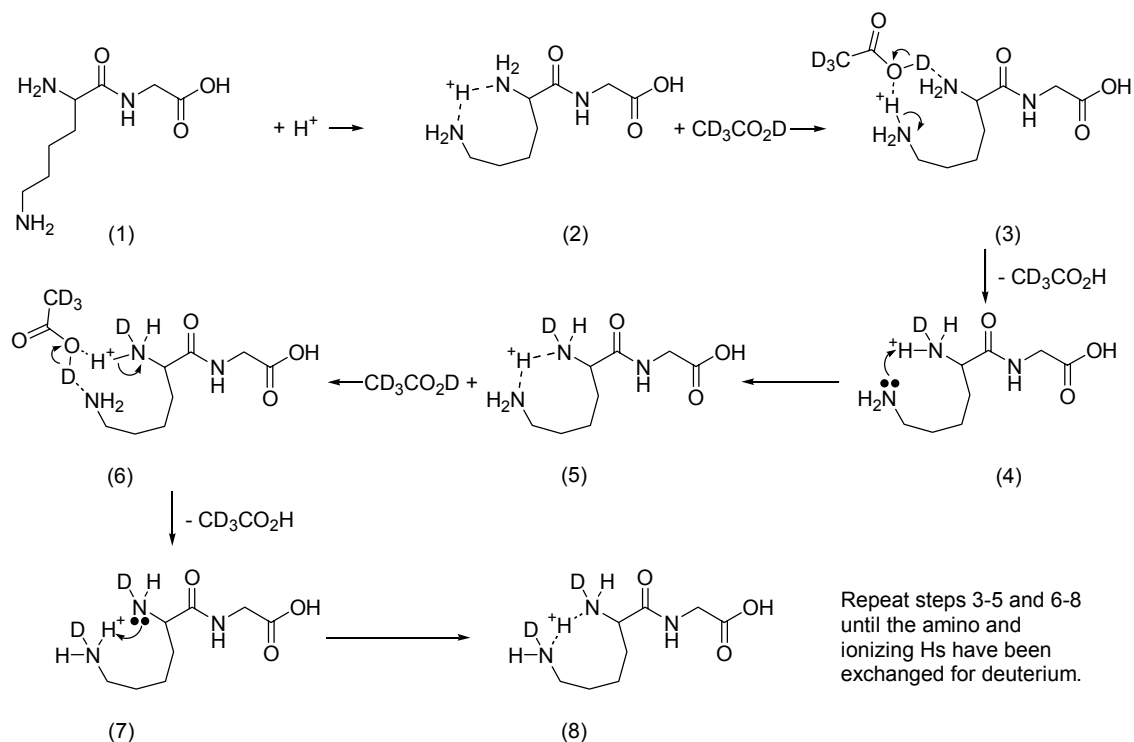
the amide hydrogen and *N*-terminal amine. Isotopic hydrogen exchange of GlyLysH$^+$ with acetic acid-d$_4$ is proposed to occur through the relay mechanism as illustrated in Scheme 8. Incorporation of the first deuterium is comparatively less efficient for GlyLysH$^+$ than LysGlyH$^+$ when reacted with acetic acid-d$_4$ (Table 2). Differences in exchange efficiency may be attributed to the dissimilar GB of functional groups involved with charge site solvation. As discussed earlier, gas-phase H/D exchange is typically most efficient when GB differences between the solvating functional groups are minimal. Participation of the relatively less basic amide carbonyl for inductive stabilization of the charge site in GlyLysH$^+$, rather than both amino groups, as suggested for LysGlyH$^+$, may contribute to the comparative decrease in exchange efficiency.

Scheme 7

Repeat steps 6-8 and 11-13
until all the amino, amide
and ionizing Hs have been
exchanged for deuterium.
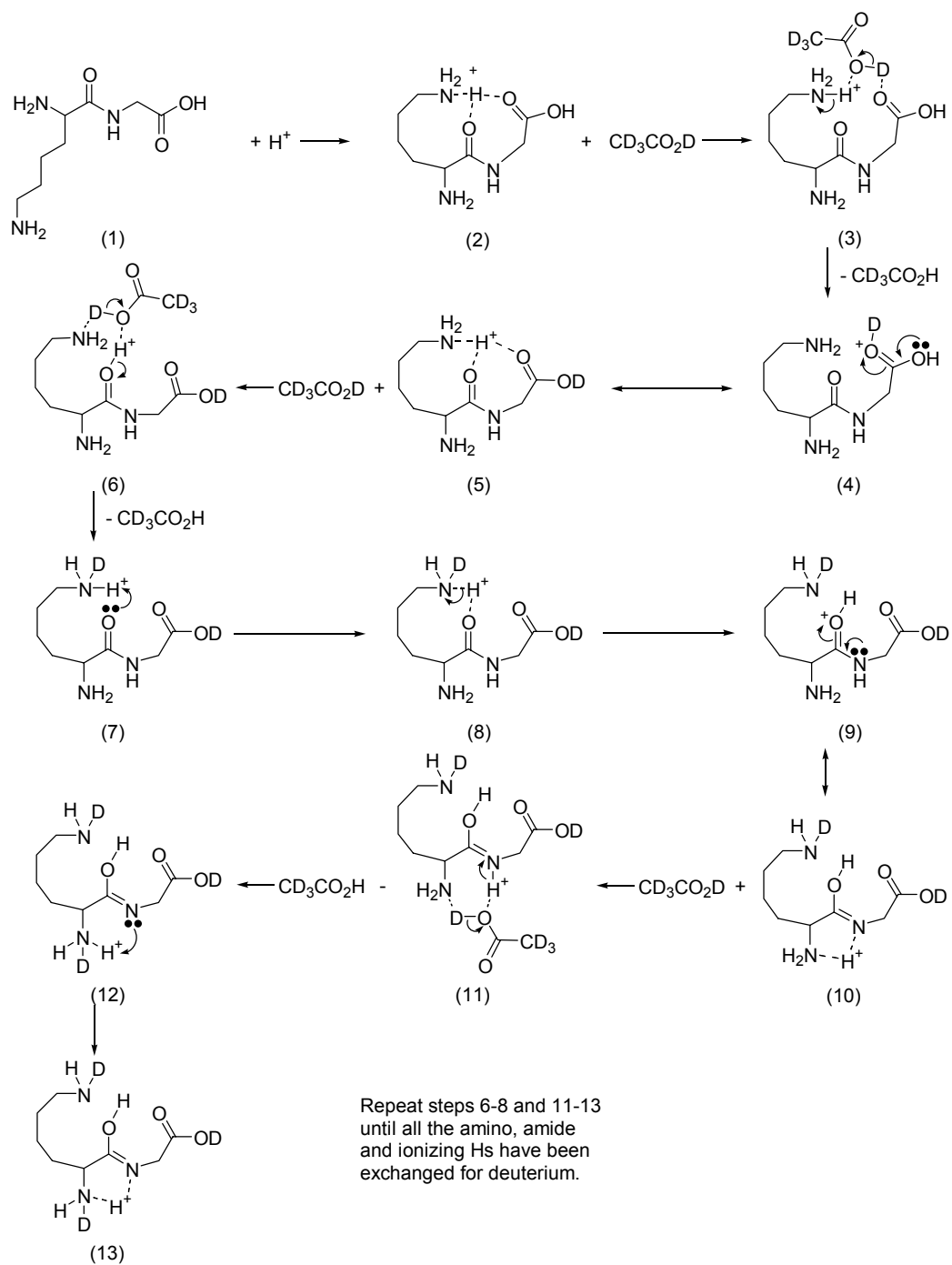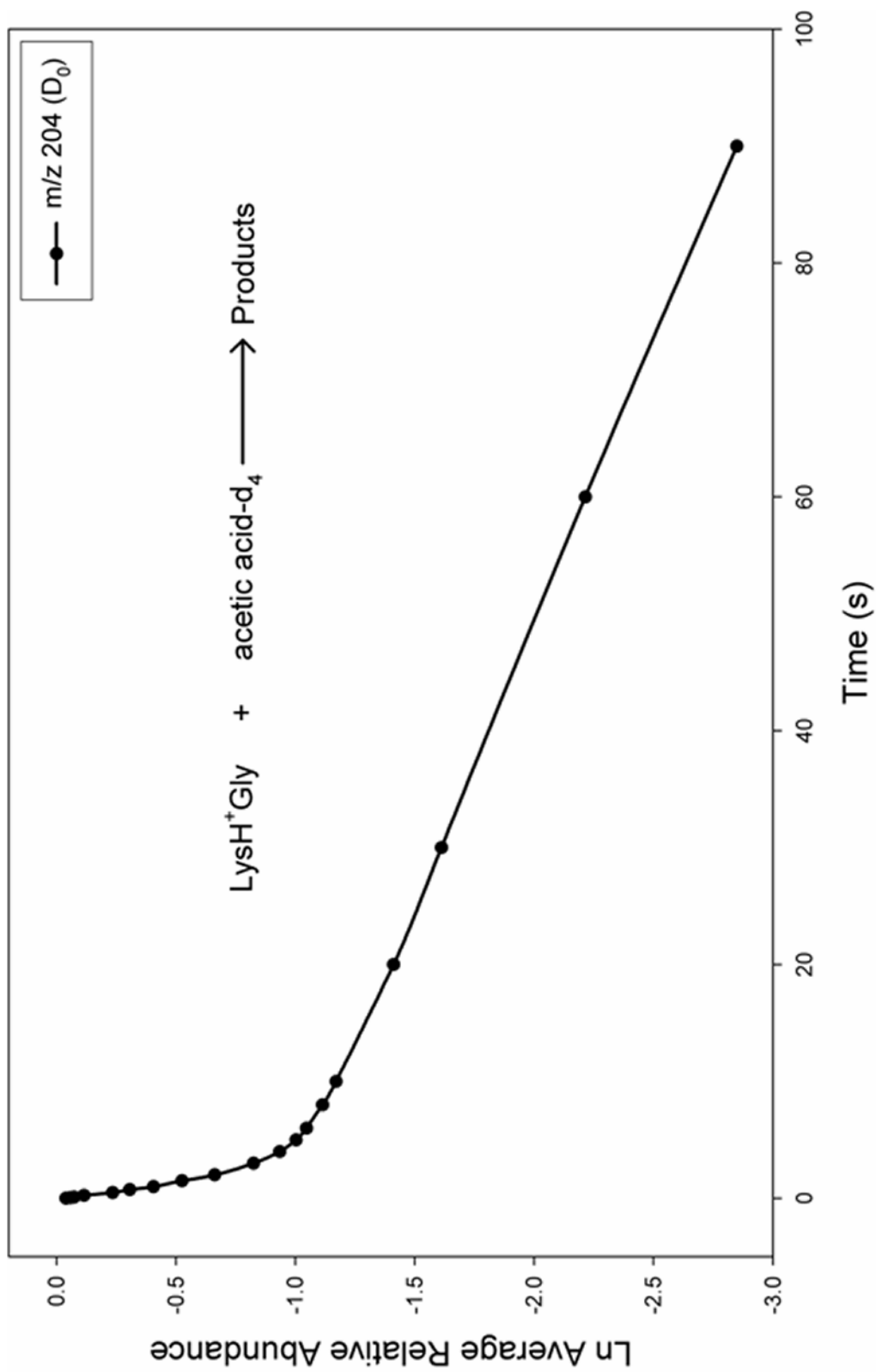
Figure 45. Plot of the natural log of the relative abundance of protonated LysGly as a function of time for reaction with deuterated acetic acid at ~6.0 E-8 torr.

Scheme 8

Repeat steps 6-8 and 11-13
until the remaining amino
and ionizing Hs have been
exchanged for deuterium.
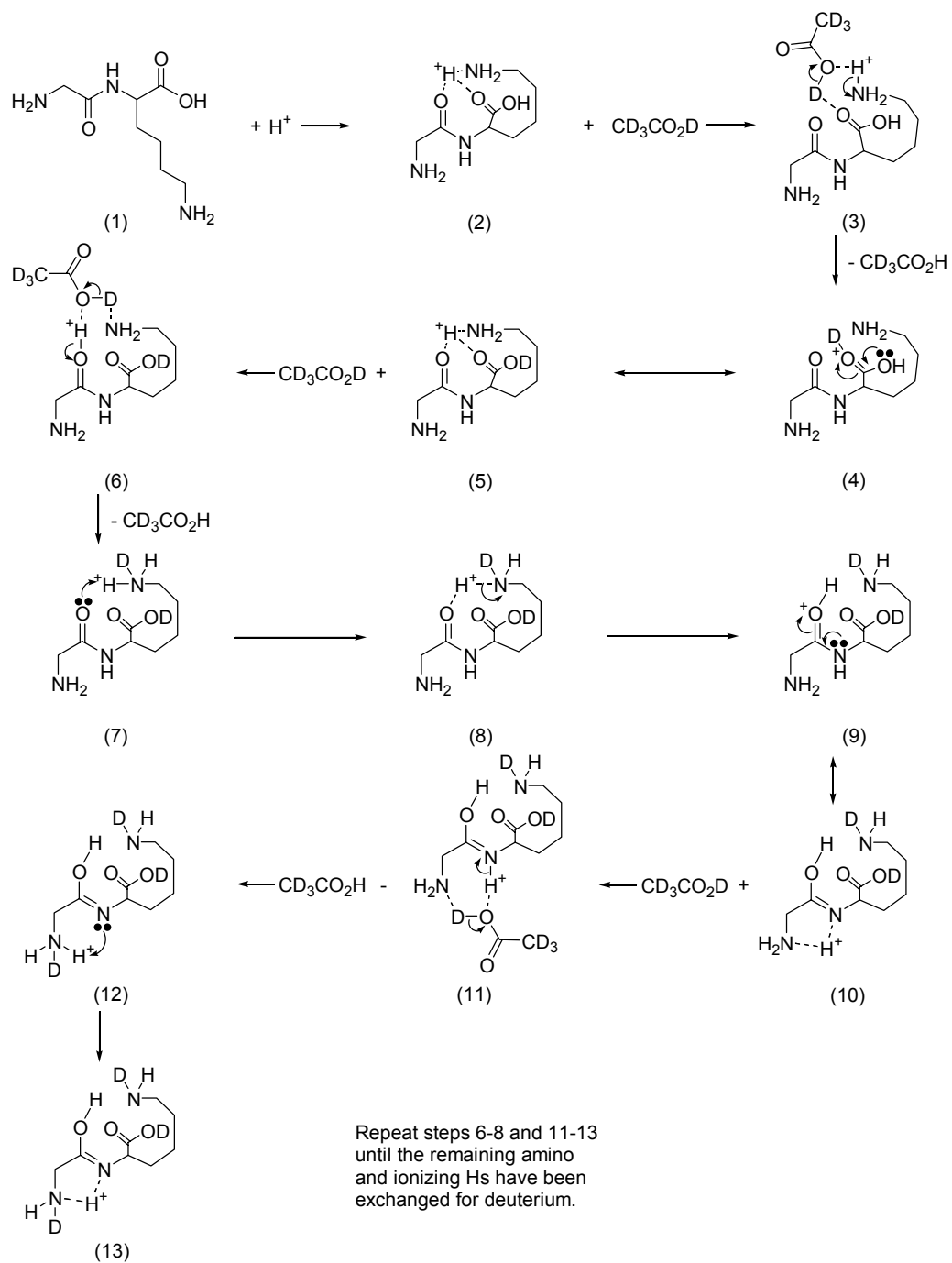
Hence, observation of dissimilar gas-phase H/D exchange temporal distributions and reaction efficiencies for exchange with acetic acid-d_4 can be rationalized by the proposed conformational differences associated with charge solvation.

Gas-Phase H/D Exchange of the Tripeptides with Acetic Acid-d_4

The tripeptides investigated in these gas-phase H/D exchange studies also demonstrate sequence specific temporal distributions for deuterium incorporation when reacted with acetic acid-d_4. Dissimilarities in the temporal plots for the tripeptide ions are rationalized by intramolecular interaction differences associated with charge solvation. Although the tripeptide ions demonstrate unique H/D exchange temporal distributions, similarities observed between LysGlyH$^+$ and LysGlyGlyH$^+$ suggest the possibility of comparable peptide ion conformations. Like LysGly, LysGlyGly contains an *N*-terminal lysine residue. Therefore, the n-butyl amino and *N*-terminal amine bridging interaction proposed for LysGlyH$^+$ may also be present in LysGlyGlyH$^+$. This structure may contribute to the double exponential decay, shown in Figure 46, for incorporation of the first deuterium. LysGlyGlyH$^+$ is suggested to undergo H/D exchange with acetic acid-d_4 *via* the relay mechanism, as illustrated in Scheme 9. Proposed conformational similarities for these *N*-terminal lysine containing peptide ions are further supported by comparable H/D exchange reaction efficiencies for the first portion of the double exponential decays (Table 2). Hence, the similar temporal plots observed for LysGlyH$^+$ and LysGlyGlyH$^+$ are rationalized by the probability of common structural characteristics associated with charge solvation. The second portion of the double exponential, for LysGlyGlyH$^+$, is likely attributed to an alternative gas-phase
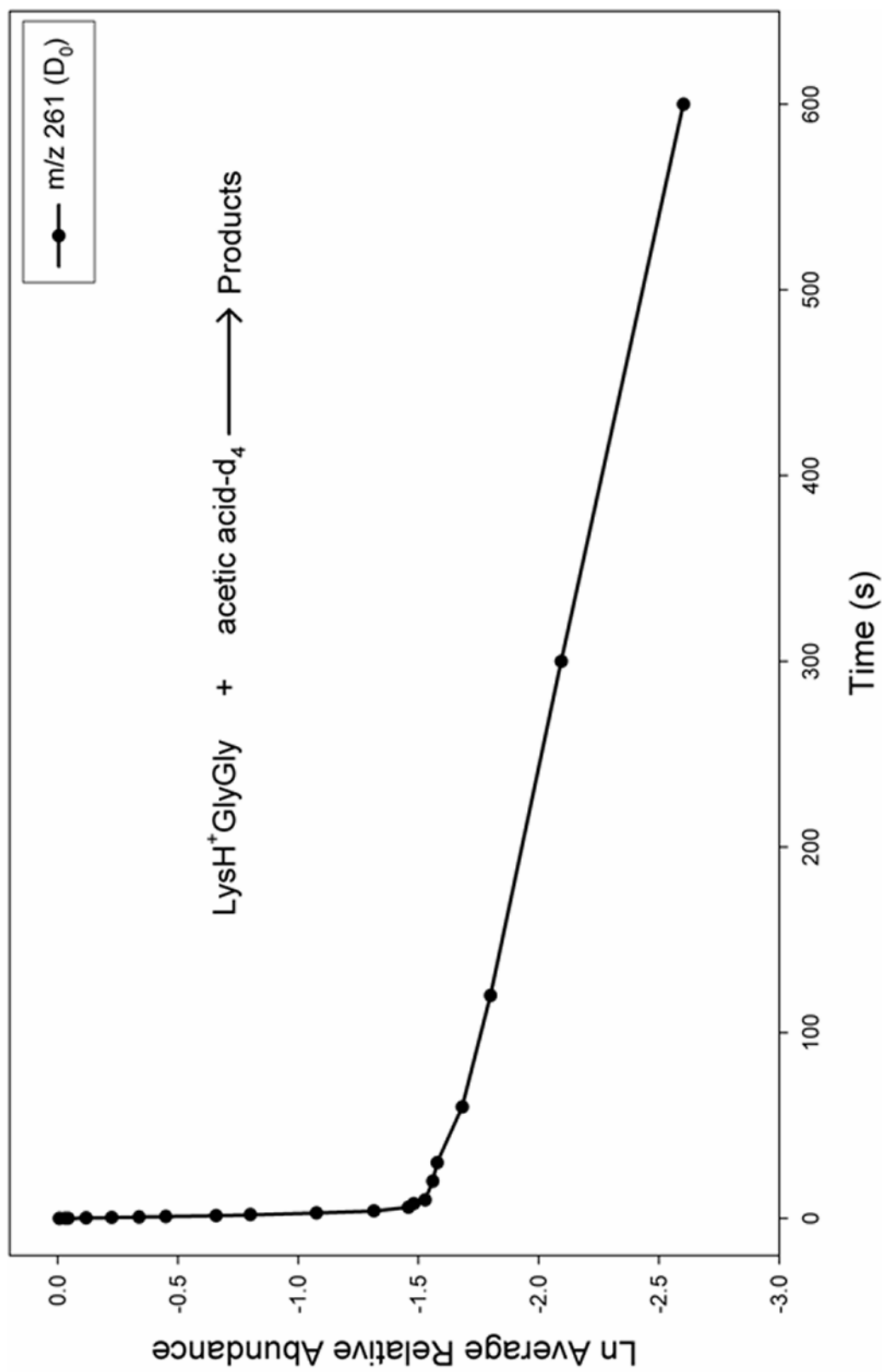
Figure 46. Plot of the natural log of the relative abundance of protonated LysGlyGly as a function of time for reaction with deuterated acetic acid at ~6.0 E-8 torr.

Scheme 9
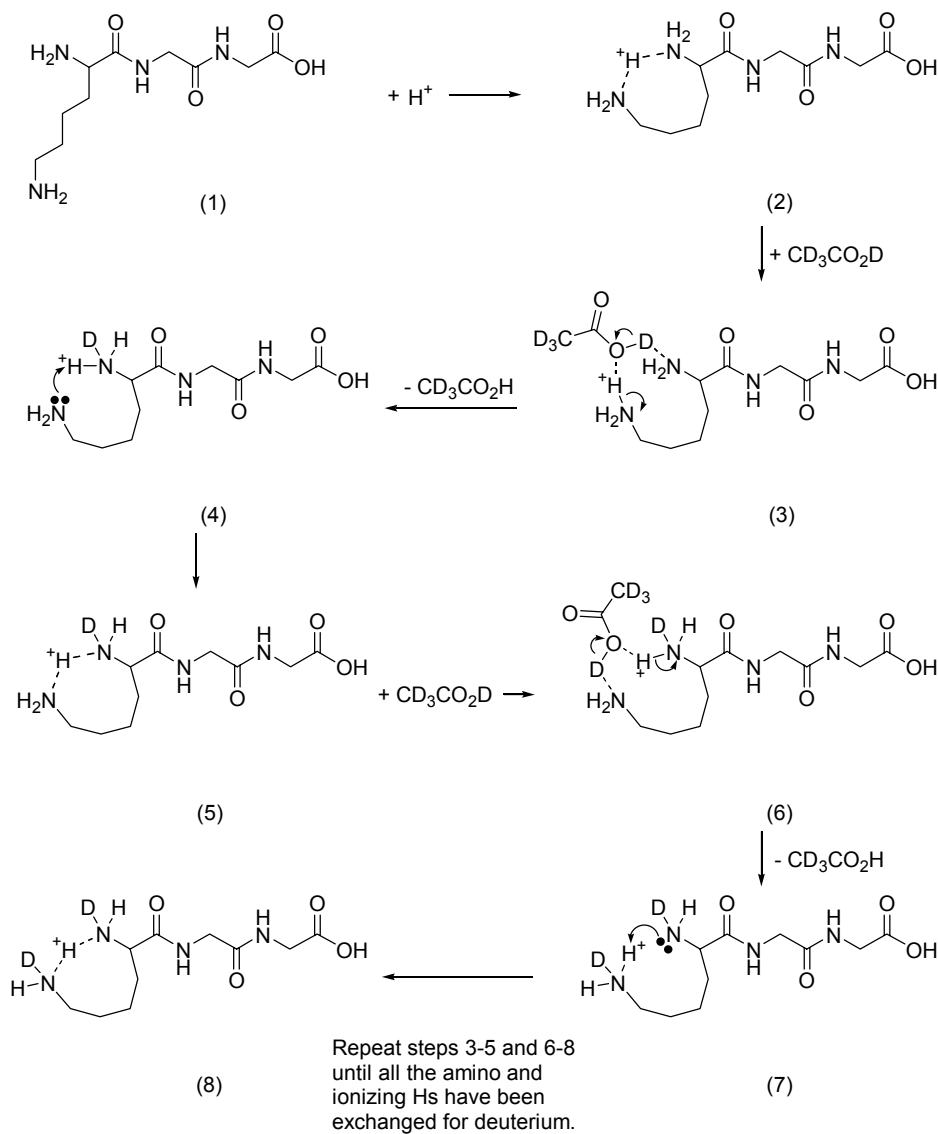
peptide ion conformation. As suggested for LysGlyH$^+$, the other structure of

LysGlyGlyH$^+$ may involve a bridging interaction between the protonated n-butyl amino

and both amide carbonyl groups. Shown in Scheme 10 is a proposed mechanism for an

alternative conformation of LysGlyGlyH$^+$ reacted with acetic acid-d$_4$. Comparatively,

Scheme 10

Repeat steps 6-8 and 12-14 until all the amino and ionizing Hs have been exchanged for deuterium.
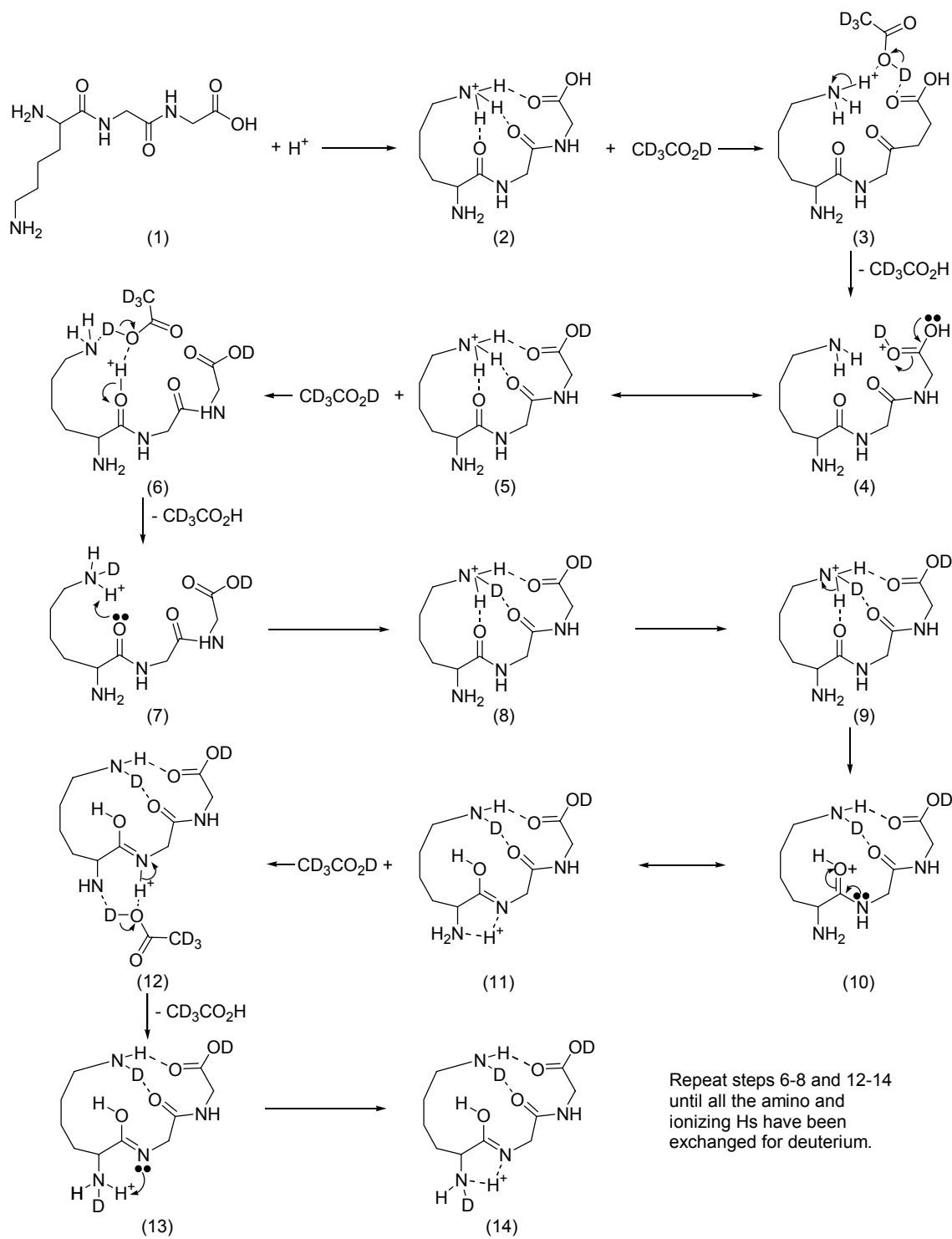
the second portion of the double exponential decay is approximately ten times less efficient at exchange for LysGlyGlyH$^+$ than LysGlyH$^+$ (Table 2). This relative decrease in reaction efficiency is consistent with the proposed conformation for LysGlyGlyH$^+$, as an additional amide carbonyl would likely increase the protonated peptide's GB.

Unlike LysGlyGlyH$^+$, GlyLysGlyH$^+$ does not exhibit a double exponential decay for incorporation of the first deuterium. Rather, gas-phase H/D exchange of GlyLysGlyH$^+$ demonstrates a single exponential decay, suggesting the presence of only one peptide ion conformation. Dissimilar temporal distributions for the lysine containing tripeptides may be attributed to sequence effects on gas-phase ion structure. Sequence position of the lysine residue in GlyLysGly, likely hinders formation of a bridging interaction between the amino groups as proposed for LysGlyGlyH$^+$. Thus, charge solvation of the protonated peptide may involve a single conformation consisting of intramolecular interactions between the n-butyl amine and adjacent amide carbonyls. A suggested mechanism for the gas-phase H/D exchange of GlyLysGlyH$^+$ with acetic acid-d$_4$ is shown in Scheme 11. The dissimilar temporal behavior of these lysine-containing tripeptides is complemented by differences in exchange efficiency. GlyLysGlyH$^+$ incorporates the first deuterium at approximately half the reaction rate efficiency of LysGlyGlyH$^+$ (Table 2), but exchanges all labile hydrogens during the time course of the experiment. This relative decrease in reaction rate efficiency is consistent with the proposed conformation of this internal lysine containing tripeptide ion, as functional groups involved with inductive stabilization of the charge site have a greater GB difference in GlyLysGlyH$^+$ than in LysGlyGlyH$^+$.

Scheme 11

Repeat steps 6-8 and 11-13 until the remaining amino and ionizing Hs have been exchanged for deuterium.
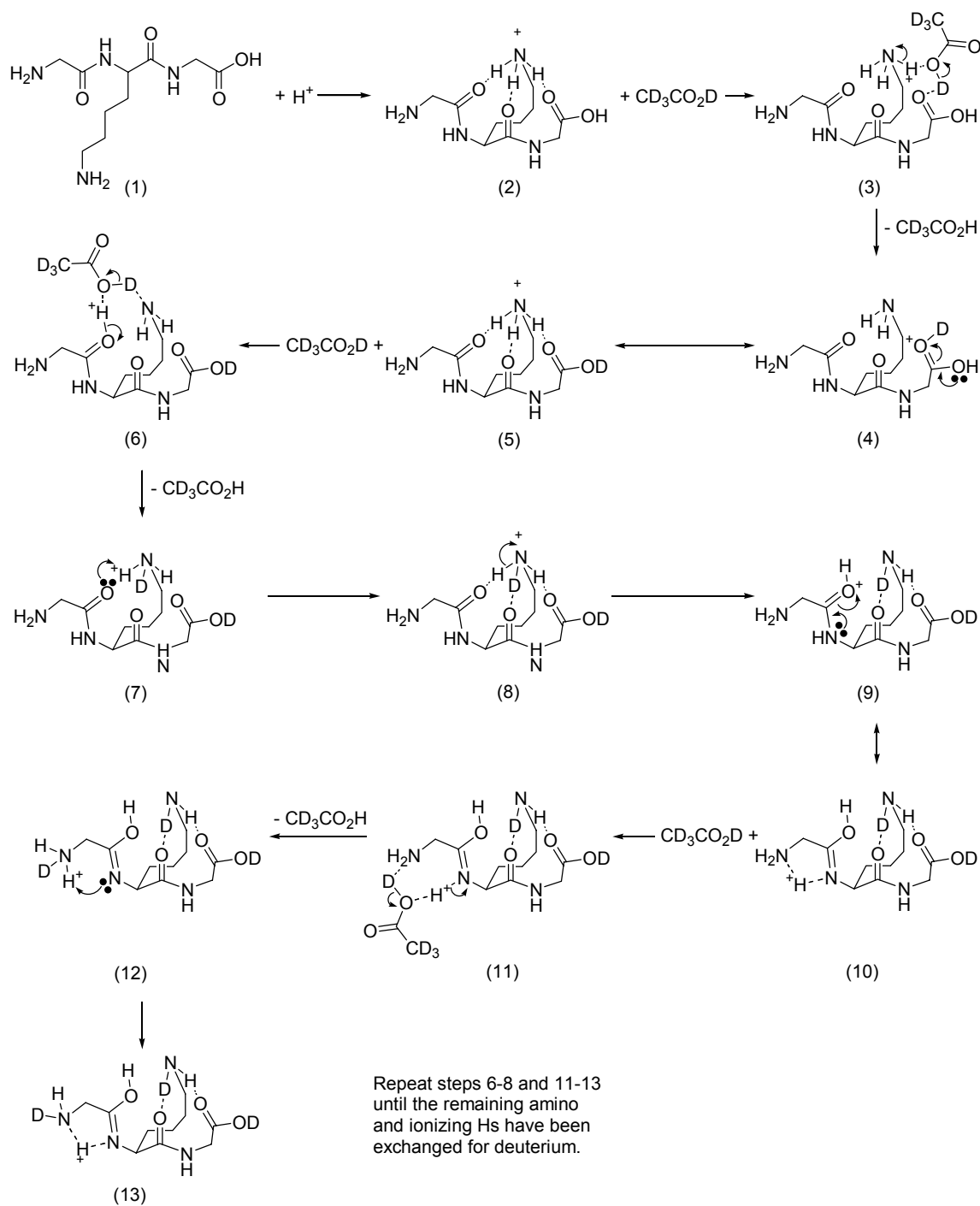
Of the tripeptides investigated in these gas-phase H/D exchange studies, GlyGlyLysH$^+$ is the least efficient at deuterium incorporation with acetic acid-d$_4$ (Table 2). This comparative decrease in reaction efficiency may be attributed to spatial separation of the n-butyl and *N*-terminal amines. As observed for the dipeptides, displacement of the lysine residue from the *N*-terminus reduces H/D exchange efficiency. This decrease in reaction efficiency is ascribed to different GBs between functional groups involved with charge solvation. Proposed as an influential factor in gas-phase H/D exchange, bridging groups with similar GBs have been suggested to increase reaction rate efficiency despite unfavorable GB differences between the analyte ion and deuterium reagent.[39,45,46,107] Consistent with these observations, the relatively inefficient H/D exchange of GlyGlyLysH$^+$ may be attributed to hindered interactions between the *N*-terminal amino and protonated n-butyl amine. A proposed mechanism for gas-phase H/D exchange of GlyGlyLysH$^+$ with acetic acid-d$_4$ is illustrated in Scheme 12. Like GlyLysGlyH$^+$, GlyGlyLysH$^+$ demonstrates a single exponential decay for incorporation of the first deuterium, suggesting the presence of one peptide ion conformation. The similar depletion of [M+H]$^+$ ions for these lysine containing tripeptide ions is complemented by comparable temporal distributions (Figures 38 and 39) and reaction efficiencies (Table 2), suggesting common intramolecular interactions for GlyLysGlyH$^+$ and GlyGlyLysH$^+$. Hence, the relatively unique gas-phase H/D exchange temporal distributions and reaction efficiencies of these lysine containing tripeptide ions, for reaction with acetic acid-d$_4$, may be rationalized by the dissimilar intramolecular interactions involved with inductive stabilization of the charge site.

Scheme 12

Repeat steps 3-5, 6-8 and 11-13 until all the amino, amide and ionizing Hs have been excanged for deuterium.
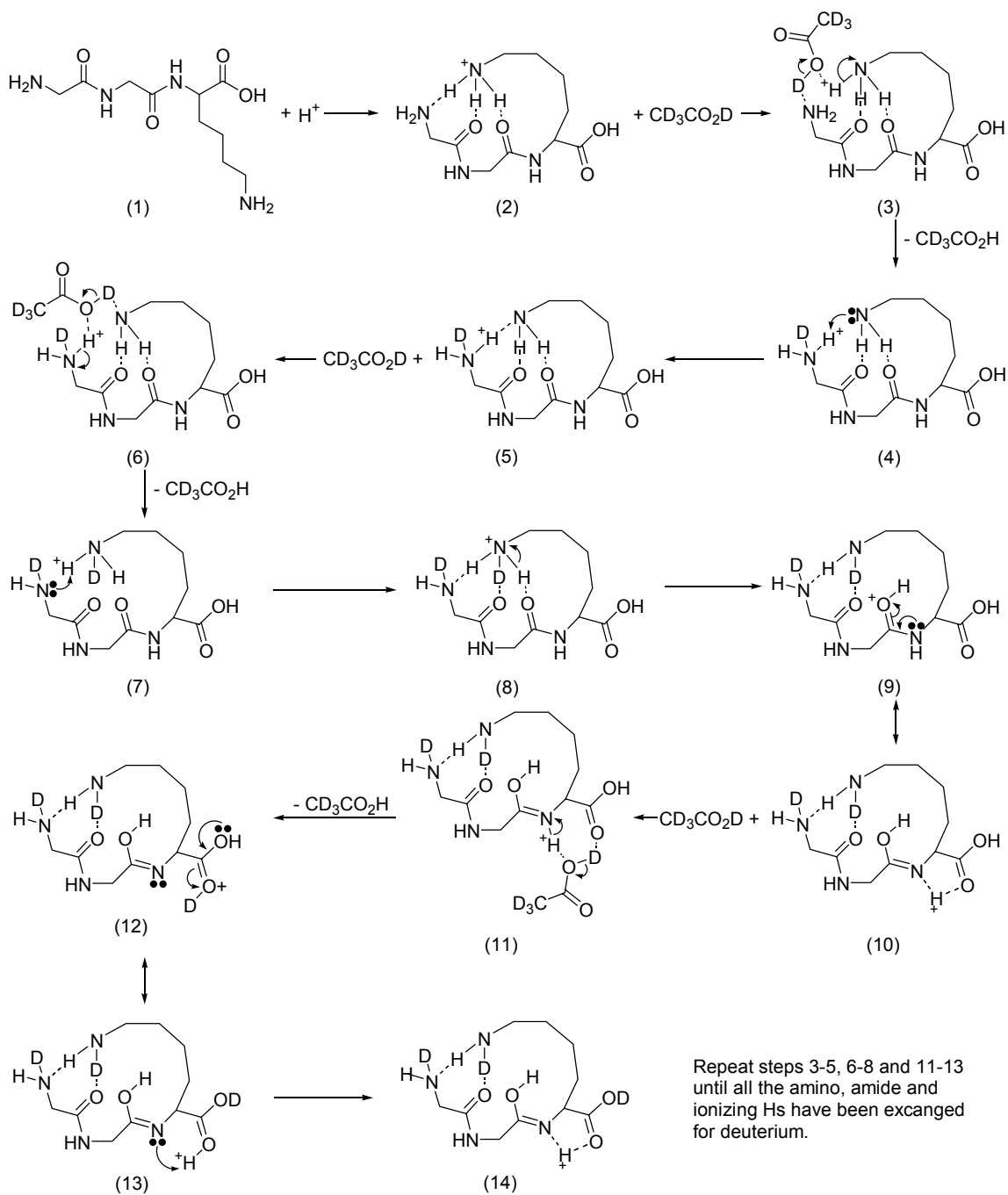
Gas-Phase H/D Exchange of the Dipeptides with Ammonia-d₃

Gas-phase H/D exchange reactions of lysine containing di- and tripeptides are more efficient with ammonia-d_3 than with acetic acid-d_4 (Table 2). This increased exchange efficiency is attributed to decreasing the relative GB difference between the protonated peptide and deuterium reagent. In addition to reaction efficiency differences, gas-phase H/D exchange of peptide ions with ammonia-d_3 exhibit different temporal plots for deuterium incorporation relative to reaction with acetic acid-d_4. Deviations in temporal distributions may be attributed to different exchange mechanisms for the deuterium reagents.[39] Unlike acetic acid-d_4, ammonia-d_3 is not anticipated to exchange deuterium *via* the proposed relay mechanism;[39] the expected exchange mechanism for H/D exchange with ammonia-d_3 involves proton transfer between the peptide ion and deuterium reagent to form an ammonium ion, and the resultant ammonium ion is charge solvated by the peptide, facilitating subsequent H/D exchange. Termed the "onium ion mechanism"[39] deuterium incorporation with ammonia-d_3 does not require a basic site to be in close proximity with the charge site for facile H/D exchange. Hence, differences observed in temporal distributions and reaction efficiencies for H/D exchange with these deuterium reagents may be ascribed to dissimilar exchange mechanisms. Mechanistic contributions to deviations in reaction selectivity may also be complemented by increases in deuterium reagent GB. Decreasing the GB difference between the peptide ion and deuterium reagent by employing ammonia-d_3 may render certain exchanges more facile. These mechanistic and basicity issues may explain the dissimilar H/D

temporal distributions and reaction efficiencies for peptide ions with different exchange reagents.

Gas-phase H/D exchange of the lysine containing dipeptide ions do not exhibit considerable differences in their respective temporal distributions for reaction with ammonia-d_3. Unlike acetic acid-d_4, exchange of both LysGlyH$^+$ and GlyLysH$^+$ with ammonia-d_3 display single exponential decays for incorporation of the first deuterium. The unique H/D temporal distributions of these peptides, for reaction with different deuterium reagents, are complemented by dissimilar trends in exchange efficiency. As shown in Table 2, incorporation of the first deuterium is approximately 27% more efficient for GlyLysH$^+$ than LysGlyH$^+$ when reacted with ammonia-d_3. These reaction efficiencies are consistent with bracketing experiments by Cassady, reporting GBs for GlyLysH$^+$ and LysGlyH$^+$ of 223.2 $\pm$ 3.3 kcal/mol and 227.4 $\pm$ 3.6 kcal/mol, respectively.[50] Dissimilar exchange efficiencies and GBs for the lysine containing dipeptides may be attributed to different peptide ion conformations. Molecular modeling calculations performed on LysGlyH$^+$ and GlyLysH$^+$ point out structural features that are unique to these sequence isomers. Shown in Figure 47 are optimized conformations for the lysine containing dipeptide [M+H]$^+$ ions. The proposed dipeptide structures suggest incorporation of different functional groups for inductive stabilization of the change site. LysGlyH$^+$ bridges the ionizing proton between the amino groups, whereas GlyLysH$^+$ employs the n-butyl amine and *N*-terminal glycyl amide carbonyl for charge stabilization. These different intramolecular interactions may contribute to the peptide ions' GB values and dissimilar H/D exchange efficiency for reaction with
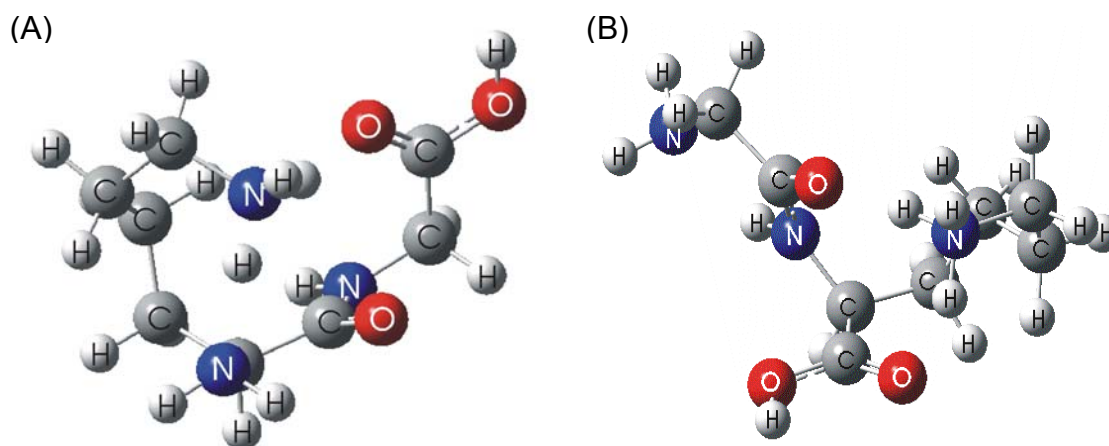
Figure 47. Optimized conformations for (A) LysGlyH$^+$ and (B) GlyLysH$^+$.

ammonia-d$_3$. The comparatively greater GB and inefficient exchange efficiency of LysGlyH$^+$ relative to GlyLysH$^+$ is consistent with the proposed conformations for these protonated dipeptides, as the amino groups have a larger combined GB than a n-butyl amine and amide carbonyl. Agreement between GB valves and H/D exchange reaction efficiencies may be attributed to similar mechanisms, involving proton transfer from peptide to reagent. Hence, reported GB values and H/D exchange results for LysGlyH$^+$ and GlyLysH$^+$ are consistent with intramolecular interactions proposed for these lysine containing dipeptide ions, suggesting dissimilar gas-phase conformations.

As discussed previously, gas-phase H/D exchange of the lysine containing dipeptides do not demonstrate the same trends in reaction efficiency or similar temporal distributions for exchange with different deuterium reagents. Specifically, the double exponential decay observed for H/D exchange of LysGlyH$^+$ with acetic acid-d$_4$, is absent when utilizing ammnonia-d$_3$. The dissimilar decay of the [M+H]$^+$ ion for this *N-*

terminal lysine containing dipeptide is ascribed to different deuterium reagent exchange mechanisms. Despite absence of a double exponential decay for H/D exchange with ammonia-d$_3$, reaction with acetic acid-d$_4$ suggests the presences of a second gas-phase ion conformation for LysGlyH$^+$. An alternative structure for LysGlyH$^+$, generated by molecular modeling calculations, is shown in Figure 48. This proposed conformation
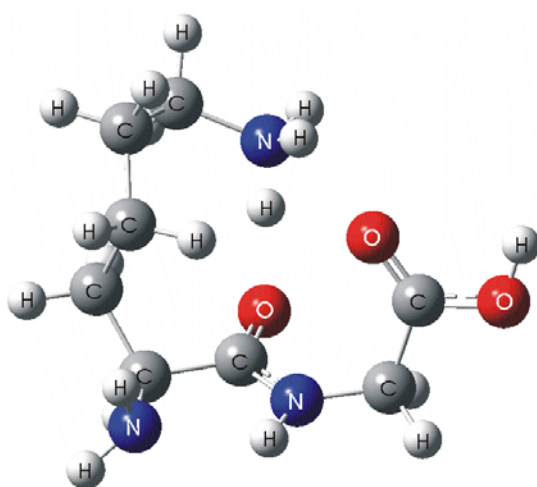
Figure 48. Alternative optimized conformation for LysGlyH$^+$.

suggests involvement of the n-butyl amine and amide carbonyl for inductive stabilization of the charge site. Calculated as approximately 0.21 kcal/mol less stable that a structure involving both amino groups for charge stabilization (Figure 47 A), this alternative conformation likely contributes to the double exponential decay observed when reacted with acetic acid-d$_4$.

Gas-Phase H/D Exchange of the Tripeptides with Ammonia-d$_3$

Gas-phase H/D exchange of the lysine containing tripeptide ions also displays

dissimilar trends in reaction efficiency for exchange with different deuterium reagents. Of the tripeptides investigated in this study, LysGlyGlyH$^+$ exhibits the least efficient H/D exchange efficiency with ammonia-d$_3$. The relatively inefficient exchange of this *N*-terminal lysine containing tripeptide may be attributed to unique intramolecular interactions, not present in other sequence isomers. Two proposed conformations for LysGlyGlyH$^+$, generated by molecular modeling calculations, are illustrated in Figure 49. These structures suggest involvement of different functional groups for charge site
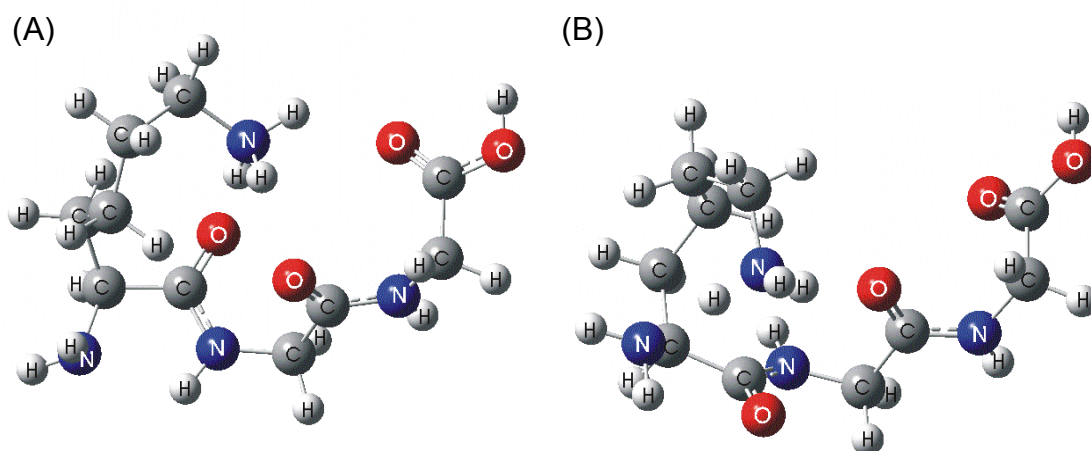
Figure 49. Optimized conformations for LysGlyGly$^+$.

solvation. As shown Figure 49, Conformation A (Conf. A) incorporates the protonated n-butyl amine and both amide carbonyls for inductive stabilization of the charge site, whereas Conformation B (Conf. B) utilizes a bridging interaction between the amino groups. Although Conf. B is calculated as approximately 4.7 kcal/mol less stable than Conf. A, the nearly identical exchange efficiencies of LysGlyH$^+$ and LysGlyGlyH$^+$, for

reaction with acetic acid-d_4, suggests common intramolecular interactions involving the amino groups. Therefore, both conformations of LysGlyGlyH$^+$ may contribute to the double exponential decay observed for reaction with acetic acid-d_4. Structural similarities between LysGlyH$^+$ and LysGlyGlyH$^+$ may also be supported by results from exchange with ammonia-d_3. Gas-phase H/D exchange of these *N*-terminal lysine containing peptide ions with ammonia-d_3 exhibit comparable reaction rates, demonstrating a 4% efficiency difference (Table 2). Hence, similarities in H/D exchange temporal distributions and reaction efficiencies for LysGlyH$^+$ and LysGlyGlyH$^+$ suggest common intramolecular interactions, supporting the proposed conformations for this *N*-terminal lysine containing tripeptide.

Relative to the other sequence isomers, gas-phase H/D exchange of GlyLysGlyH$^+$ with ammonia-d_3 is the most efficient for incorporation of the first deuterium. As seen in Table 2, the first exchange is approximately 30% more efficient for GlyLysGlyH$^+$ than LysGlyGlyH$^+$ when reacted with ammonia-d_3. These differences in reaction efficiency are consistent with bracketing experiments by Cassady, reporting GBs for LysGlyGlyH$^+$ and GlyLysGlyH$^+$ of 230.7 ± 2.8 kcal/mol and 225.3 ± 2.8 kcal/mol respectively.[50] The dissimilar exchange efficiencies and GBs of these lysine-containing tripeptides may be attributed to different intramolecular interactions. Shown in Figure 50 is a proposed conformation for GlyLysGlyH$^+$, generated by molecular modeling calculations. The structure of this internal lysine containing tripeptide ion suggests incorporation of the n-butyl amine and amide carbonyls for inductive stabilization of the charge site. Unlike LysGlyGlyH$^+$, the proposed conformation for
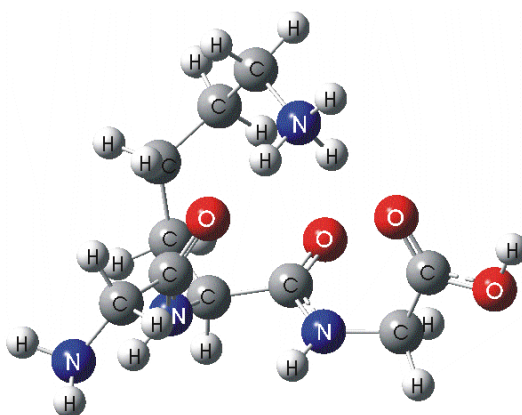
Figure 50. Optimized conformation for GlyLysGlyH$^+$.

GlyLysGlyH$^+$ does not utilize a bridging interaction between the amino groups for charge solvation. Absence of the *N*-terminal amine for intramolecular charge stabilization may result in a comparatively lower GB and greater H/D exchange efficiency of GlyLysGlyH$^+$ relative to LysGlyGlyH$^+$. As proposed for the dipeptides, agreement of GB values with H/D exchange reaction rate efficiencies is likely attributed to similar mechanisms, involving proton transfer from peptide to reagent. Thus, agreement between GB values and H/D exchange results for GlyLysGlyH$^+$ supports its proposed intramolecular interactions, suggesting a unique conformation for this internal lysine containing tripeptide ion.

Gas-phase H/D exchange of GlyGlyLysH$^+$ with ammonia-d$_3$ more closely resembles temporal distributions of LysGlyGlyH$^+$ than GlyLysGlyH$^+$. Temporal similarities between *N*- and *C*-terminal lysine containing tripeptide ions are complemented by comparable reaction efficiencies, displaying a 9% difference (Table 2). The efficiency of deuterium incorporation for GlyGlyLysH$^+$ and LysGlyGlyH$^+$ is

consistent with bracketing experiments by Cassady, reporting the same GB values of 230.7 ± 2.8 kcal/mol.[50] Similar H/D exchange and GB results may be attributed to common intramolecular interactions for these tripeptides. Shown in Figure 51 is a
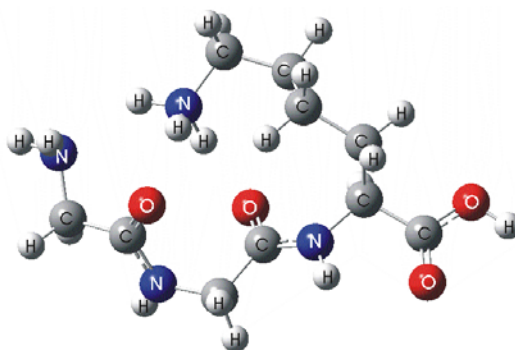
Figure 51. Optimized conformation for GlyGlyLysH$^+$.

proposed conformation of GlyGlyLysH$^+$, generated by molecular modeling calculations. The structure of this *C*-terminal lysine containing tripeptide suggests incorporation of the protonated n-butyl amino, amide carbonyls and *N*-terminal amine for inductive stabilization of the charge site. Utilizing the same functional groups as LysGlyGlyH$^+$ for charge solvation may explain comparable H/D exchange efficiencies and identical GBs of these tripeptides. The greater exchange efficiency of GlyGlyLysH$^+$ relative to LysGlyGlyH$^+$ may be attributed to spatial separation of the lysine residue from the *N*-terminus, causing hindered interactions between amino groups. Hence, GB and H/D exchange results for GlyGlyLysH$^+$ coincide with proposed intramolecular interactions for this *C*-terminal lysine containing tripeptide, supporting the proposed conformation.

Conclusion

Gas-phase H/D exchange reactions have been performed on sequence isomers of di- and tripeptides containing a lysine amino acid residue. The oligopeptide $[M+H]^+$ ions investigated in this study demonstrate different reaction efficiencies for H/D exchange, indicating a sequence effect on deuterium incorporation. These sequence specific reaction efficiencies may be attributed to dissimilar intramolecular interactions for inductive stabilization of the charge site. Differences in H/D exchange reaction efficiencies are complemented by unique temporal distributions for deuterium incorporation. Specifically, LysGlyH$^+$ and LysGlyGlyH$^+$ were the only oligopeptide ions that exhibit a double exponential decay for the first exchange when reacted with acetic acid-d$_4$. The H/D exchange chemistry of these *N*-terminal lysine containing peptides is ascribed to multiple intramolecular bridging interactions, suggesting the presence of more than one gas-phase ion conformation. Structural contributions to sequence specific differences in exchange efficiency were also influenced by the deuterium reagents. Deviations in reaction efficiency are attributed to dissimilar mechanisms of exchange for acetic acid-d$_4$ and ammonia-d$_3$. Results from these gas-phase H/D exchange studies are consistent with proposed intramolecular interactions for lysine containing peptide ions, suggesting that position of the n-butyl amino group influences ion conformation.

CHAPTER V

THE GAS-PHASE HYDROGEN/DEUTERIUM EXCHANGE OF SELECTED DI-
AND TRIPEPTIDES CONTAINING AN ARGININE AMINO ACID RESIDUE

Introduction

It is well accepted that amino acids, peptides, and proteins exist as zwitterions in aqueous solution. This ionic structure involves a protonated *N*-terminal amine and deprotonated *C*-terminal carboxylic acid to form a dipolar ion. The charge separated ion pair is stabilized by hydrogen bonding with water molecules. In the gas-phase, zwitterionic structures are not stabilized by a solvent. Therefore, amino acids, peptides and proteins that exist as zwitterions in solution are most likely non-zwitterionic in the gas-phase. Possible exceptions to this are arginine and arginine containing peptides. The high gas-phase basicity of the guanidino group of arginine may deprotonate the *C*-terminal carboxylic acid, thus forming an intramolecular salt bridge, ion-pair between the groups. Many independent studies and semiempirical calculations supported[114,115,116,117,118,119] and contradicted[120,121] zwitterionic structures for arginine and arginine containing peptides in the gas-phase. For example, infrared cavity ringdown laser absorption spectroscopy experiments by Saykally and coworkers[120] were interpreted as evidence that that arginine exists predominately in a non-zwitterionic configuration due to the absence of symmetric and asymmetric carboxylate stretches. Conversely, semiempirical calculation by Williams and coworkers[114] suggested that the

zwitterionic structure of arginine is approximately 0.3 – 1.0 kcal/mol more stable than the neutral form.

Gas-phase H/D exchange reactions of the $[M+H]^+$ ions of arginine, arginine containing di- and tripeptides, and their corresponding methyl ester derivatives were performed to determine if inductive stabilization of the charge site involves formation of gas-phase zwitterions. Oligopeptide sequence isomers containing arginine and glycine were selected to probe the effect of basic residue position (*i.e.* *N*-terminal, internal, or *C*-terminal) on the efficiency and extent of deuterium incorporation as well as the probability of zwitterion formation. Because intramolecular interactions have been shown to affect the rate of deuterium incorporation,[39,44,45,46] sequence isomers exhibiting dissimilar temporal distribution and reaction efficiencies may be the result of different bridging interactions, *i.e.* unique gas-phase ion conformations.

From the gas-phase H/D exchange results presented herein, we show that sequence position of the arginine residue dramatically influences the reaction efficiency and extent of deuterium incorporation. Temporal distributions of H/D exchange product ions and reaction efficiencies (*i.e.* the experimentally determined reaction rate vs. the theoretical reaction rate) are rationalized in terms of intramolecular interactions that stabilize the charge site.

Experimental

The methyl ester derivatives of each arginine and arginine containing di- and tripeptides were prepared according to a previously described method.[122] A 2M solution

of HCl in methanol was prepared at 25°C by the dropwise addition of 800 µL of acetyl chloride to 5 mL of anhydrous methanol while stirring. Following 5 min of agitation, a 1 mL aliquote of the reagent was added to 10 mg of the peptide. The reaction was allowed to proceed under agitation for approximately 2 hours at 25ºC and then dried by lyophilization.

Results

Gas-Phase H/D Exchange with Ammonia-d$_3$

The oligopeptides investigated in these gas-phase H/D exchange studies represent sequence isomers containing arginine and glycine amino acid residues. These oligopeptides (Table 3) were selected to investigate effects of position (*i.e. N*-terminal, internal or *C*-terminal) of the arginine amino acid on reaction efficiency and extent of deuterium incorporation. In addition, the methyl ester derivative of each arginine containing oligopeptide was also investigated by modifying the *C*-terminus through esterification. H/D exchange temporal distributions for the [M+H]$^+$ ions of ArgGlyGly, GlyArgGly and GlyGlyArg, reacted with ammonia-d$_3$, are shown in Figures 52, 53, and 54, respectively. The arginine containing tripeptides illustrate dissimilar temporal plots for incorporation of deuterium. For ArgGlyGlyH$^+$, depletion of the [M+H]$^+$ ion appears to be a double exponential, whereas GlyArgGlyH$^+$ and GlyGlyArgH$^+$ demonstrate single exponential decays. As seen in Table 3, incorporation of the first deuterium for ArgGlyGlyH$^+$ and GlyGlyArgH$^+$ display comparable H/D exchange efficiencies, whereas GlyArgGlyH$^+$ is approximately 22% less efficient than both of its sequence

Table 3. Hydrogen/deuterium exchange efficiency (k_{exp}/k_{coll}) for incorporation of the first deuterium arginine containing oligopeptide $[M+H]^+$ ions when reacted with ammonia-d_3 or acetic acid-d_4.

$[M+H]^+$	Ammonia-d_3	Acetic acid-d_4
Arg	0.24†; 0.015*	Not Performed
ArgGly	0.074	Not Performed
GlyArg	0.17	Not Performed
ArgGlyGly	0.27†; 0.0054*	0.12†; 0.00075*
GlyArgGly	0.059	0.071
GlyGlyArg	0.28	0.062
Arg-OMe	0.000099	Not Performed
ArgGly-OMe	0.00040	Not Performed
GlyArg-OMe	0.000050	Not Performed
ArgGlyGly-OMe	0.000025	Not Performed
GlyArgGly-OMe	0.00035	Not Performed
GlyGlyArg-OMe	0.00033	Not Performed

† H/D exchange reaction efficiency for the first portion of a double exponential decay fit.
* H/D exchange reaction efficiency for the second portion of a double exponential decay fit.

isomer counterparts when reacted with ammonia-d_3. A series of partial mass spectra for the arginine containing tripeptide ions are illustrated in Figures 55, 56, and 57.

Gas-phase H/D exchange of the methyl ester derivatives of each arginine containing tripeptide was also investigated. As seen in Table 3, modification of the *C*-terminus substantially reduces the H/D exchange efficiency for incorporation of the first deuterium when reacted with ammonia-d_3. H/D exchange temporal distributions for the $[M+H]^+$ ions of ArgGlyGly-OMe, GlyArgGly-OMe and GlyGlyArg-OMe, reacted with ammonia-d_3, are illustrated in Figures 58, 59, and 60, respectively.

Gas-phase H/D exchange of the $[M+H]^+$ ion of arginine and its corresponding methyl ester derivative were also investigated. Temporal distributions for the basic amino acid residue and its methyl ester for reaction with ammonia-d_3 are illustrated in Figures 61 and 62, respectively. Note that (Table 3) modification of the *C*-terminus

Figure 52. Temporal plot for gas-phase H/D exchange of protonated ArgGlyGly with deuterated ammonia at ~6.6 E-8 torr.

Figure 53. Temporal plot for gas-phase H/D exchange of protonated GlyArgGly with deuterated ammonia at ~6.6 E-8 torr.

Figure 54. Temporal plot for gas-phase H/D exchange of protonated GlyGlyArg with deuterated ammonia at ~6.6 E-8 torr.

Figure 55. Partial mass spectra of protonated ArgGlyGly reacted with deuterated ammonia. Reaction times ranging from 0.05 - 60 seconds.
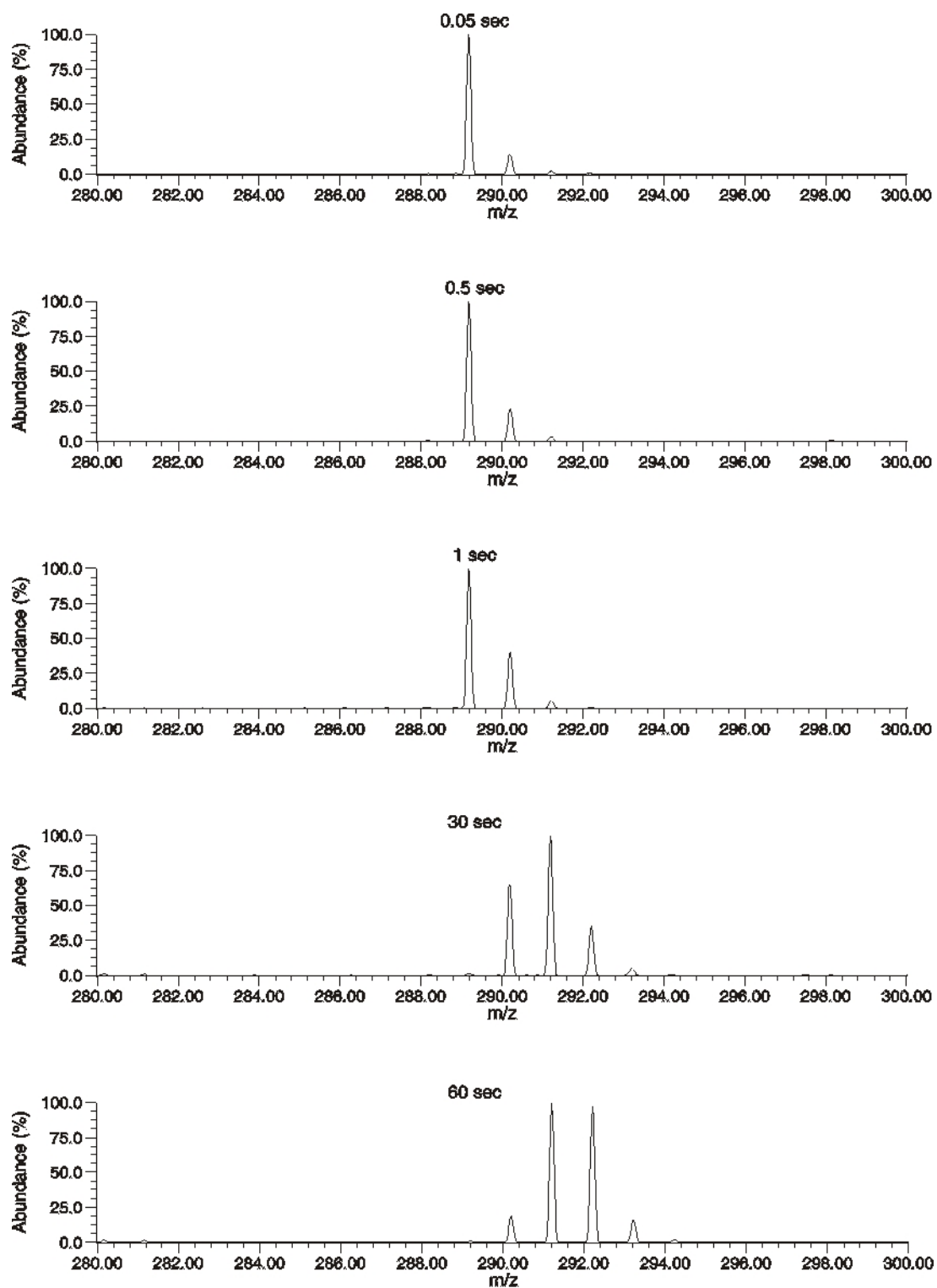
Figure 56. Partial mass spectra of protonated GlyArgGly reacted with deuterated ammonia. Reaction times ranging from 0.05 - 60 seconds.
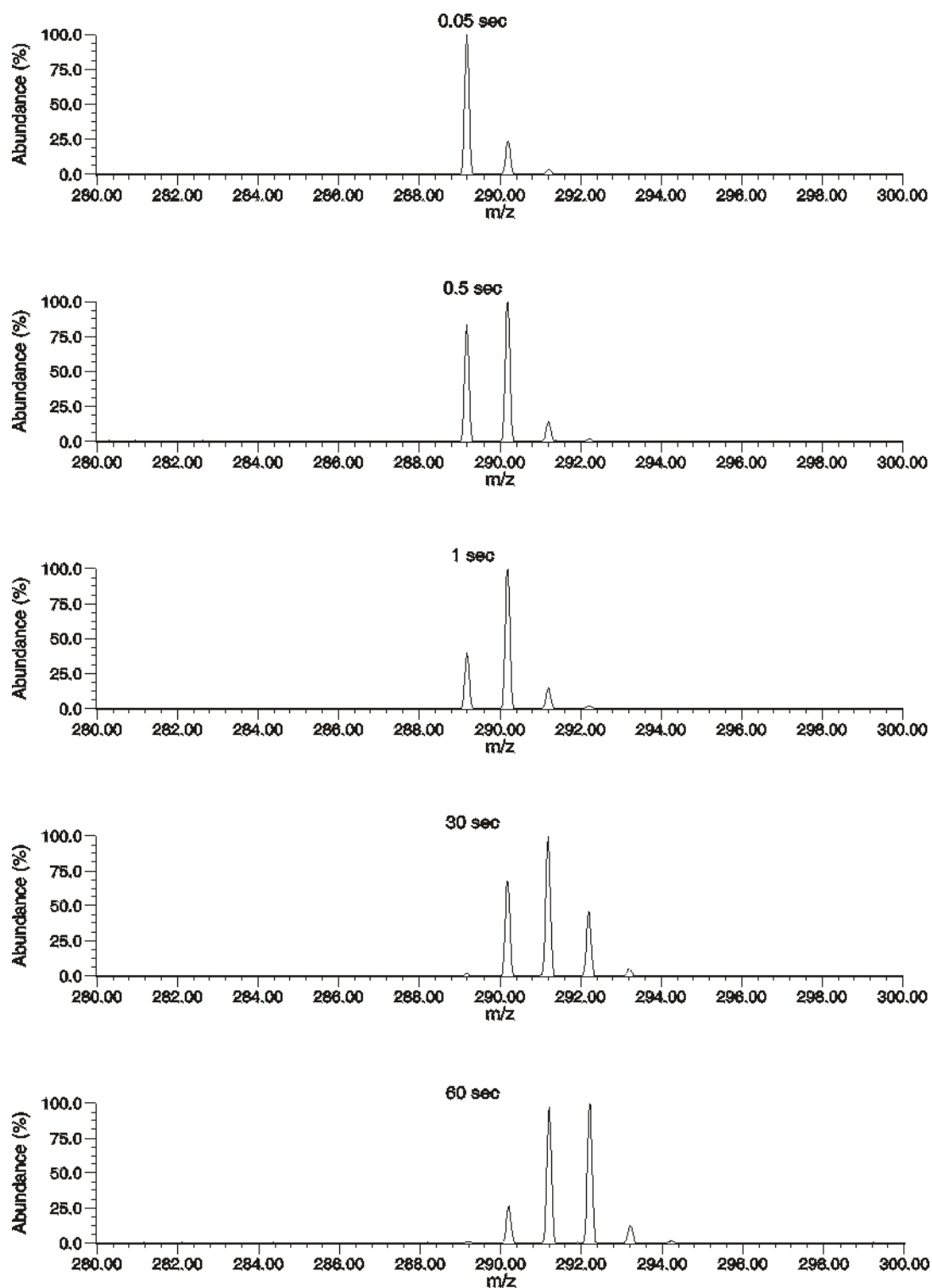
Figure 57. Partial mass spectra of protonated GlyGlyArg reacted with deuterated ammonia. Reaction times ranging from 0.05 - 60 seconds.

Figure 58. Temporal plot for gas-phase H/D exchange of the protonated methyl ester derivative of ArgGlyGly with deuterated ammonia at ~6.6 E-8 torr.

Figure 59. Temporal plot for gas-phase H/D exchange of the protonated methyl ester derivative of GlyArgGly with deuterated ammonia at ~6.6 E-8 torr.

Figure 60. Temporal plot for gas-phase H/D exchange of the protonated methyl ester derivative of GlyGlyArg with deuterated ammonia at ~6.6 E-8 torr.
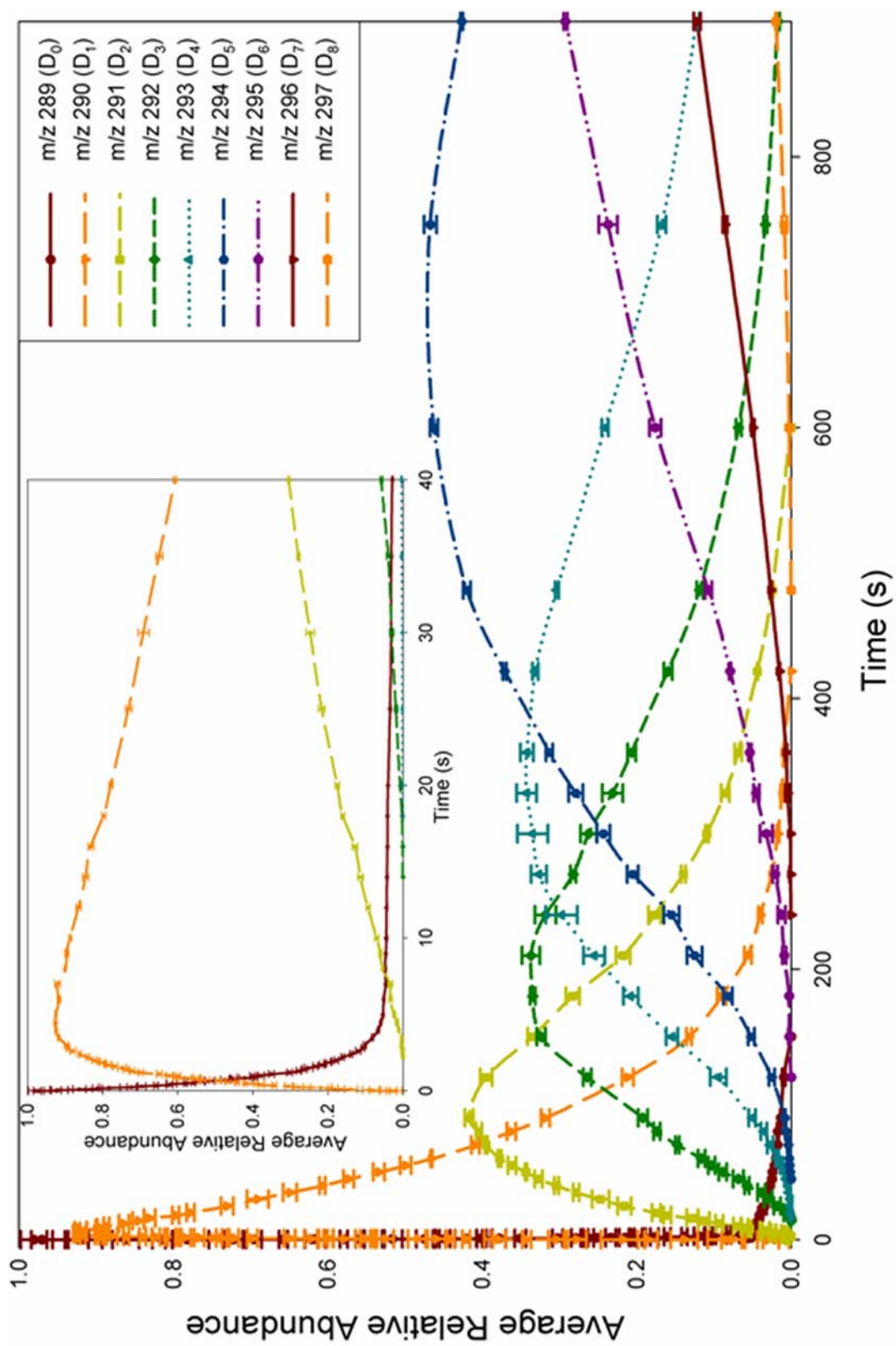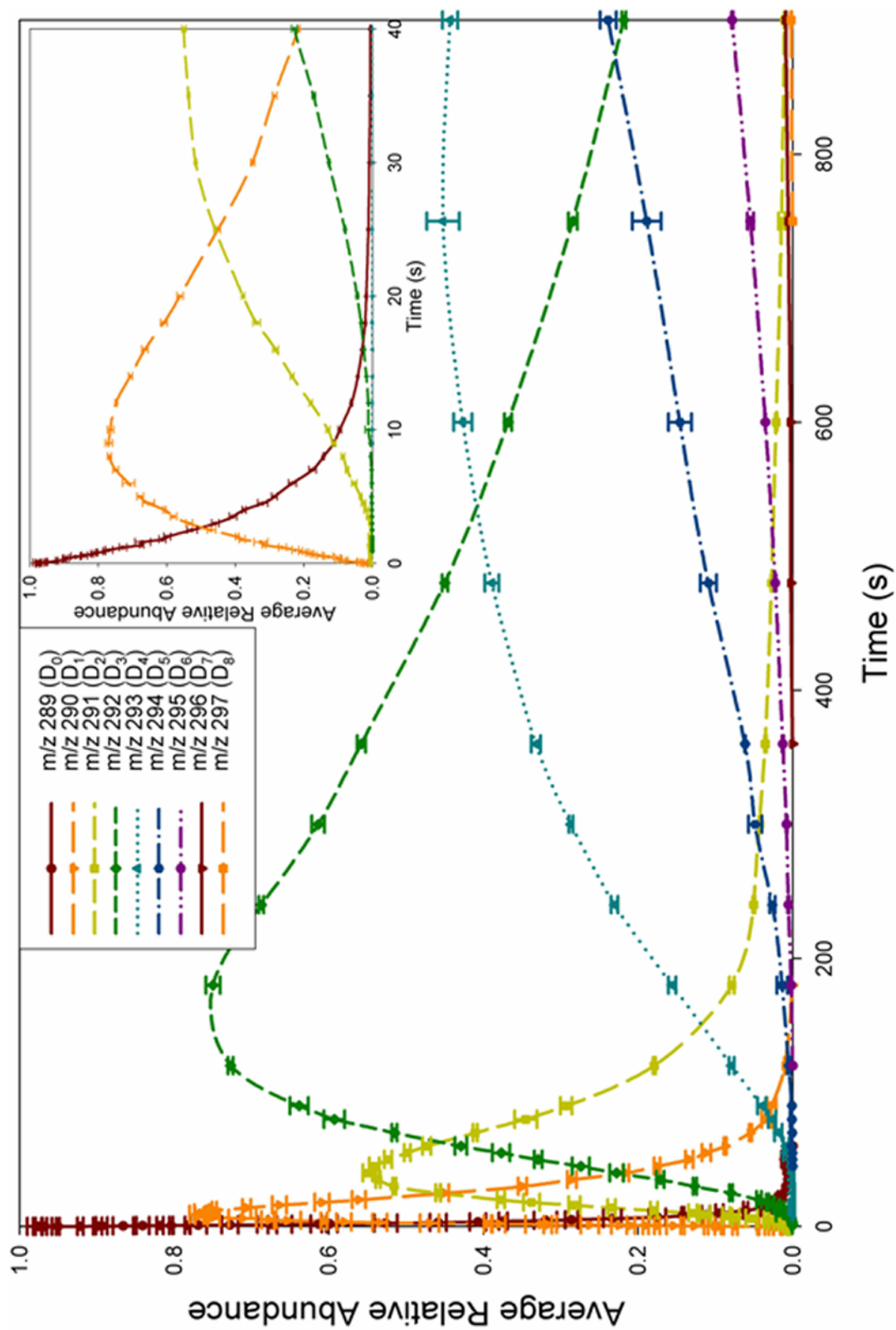
Figure 61. Temporal plot for gas-phase H/D exchange of protonated Arginine with deuterated ammonia at ~6.6 E-8 torr.

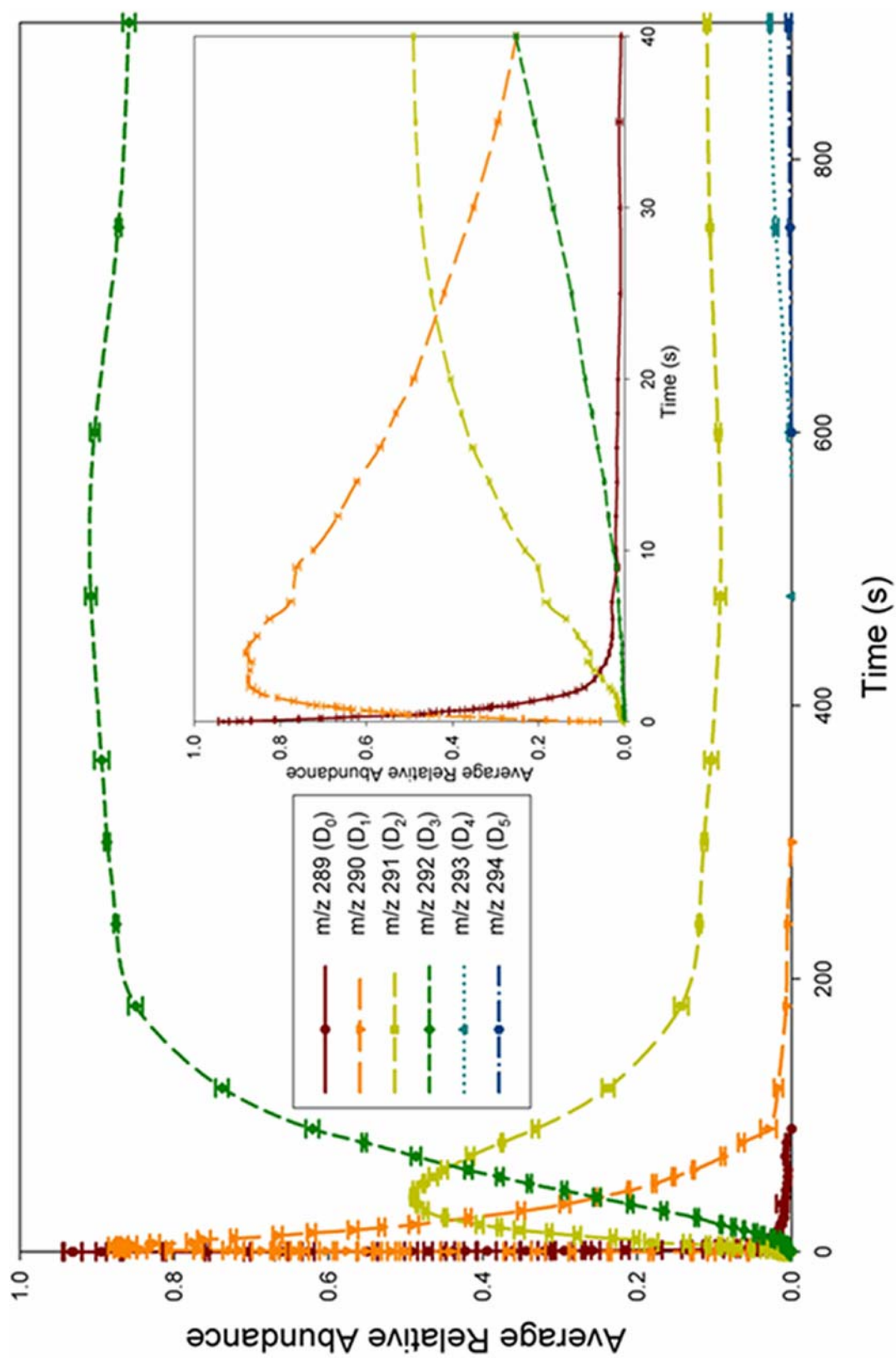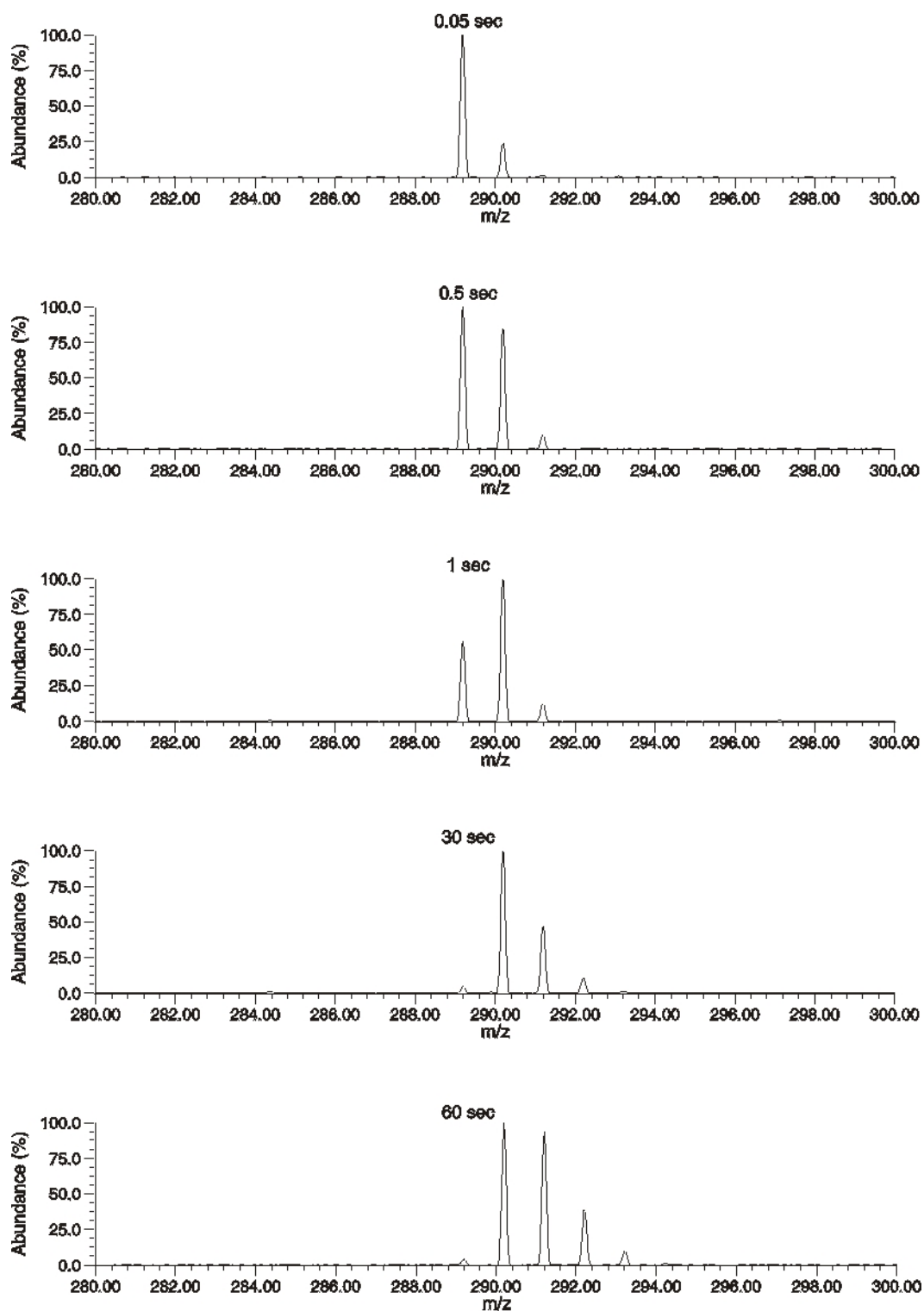Figure 62. Temporal plot for gas-phase H/D exchange of the protonated methyl ester derivative of Arginine with deuterated ammonia at ~6.6 E-8 torr.

reduces gas-phase H/D exchange efficiency for arginine [M+H]$^+$ ions.

The gas-phase H/D exchange of dipeptide ions containing arginine and glycine amino acid residues was also investigated. Temporal plots for H/D exchange of ArgGlyH$^+$ and GlyArgH$^+$ with ammonia-d$_3$ are shown in Figures 63 and 64, respectively. These plots illustrate nearly identical temporal distributions for deuterium incorporation. As seen in Table 3, the first exchange for ArgGlyH$^+$ is approximately 10% less efficient than GlyArgH$^+$. Temporal plots for gas-phase H/D exchange of the methyl ester derivatives of ArgGlyH$^+$ and GlyArgH$^+$ with ammonia-d$_3$ are illustrated in Figures 65 and 66. Note that (Table 3) modification of the *C*-terminus substantially reduces H/D exchange efficiency for the arginine containing dipeptide ions.

Gas-Phase H/D Exchange with Acetic Acid-d$_4$

Studies of arginine containing tripeptide ion reactions with acetic acid-d$_4$ were performed under similar conditions used for ammonia-d$_3$. Increasing the gas-phase basicity difference between the peptide ion and deuterium reagent reduces the efficiency with acetic acid-d$_4$. Temporal plots for reaction of the [M+H]$^+$ ions of ArgGlyGly, GlyArgGly, and GlyGlyArg with acetic acid-d$_4$ are illustrated in Figures 67, 68, and 69, respectively. Gas-phase H/D exchange of ArgGlyGly is the most efficient (Table 3) tripeptide ion for incorporation of the first deuterium when reacted with acetic acid-d$_4$. As was observed for reactions with ammonia-d$_3$, the decay curve for the [M+H]$^+$ ion of ArgGlyGly is a double exponential when reacted with acetic acid-d$_4$. Gas-phase H/D exchange of GlyArgGlyH$^+$ is approximately 5% less efficient (Table 3) than ArgGlyGlyH$^+$ for incorporation of the first deuterium when reacted with acetic acid-d$_4$.
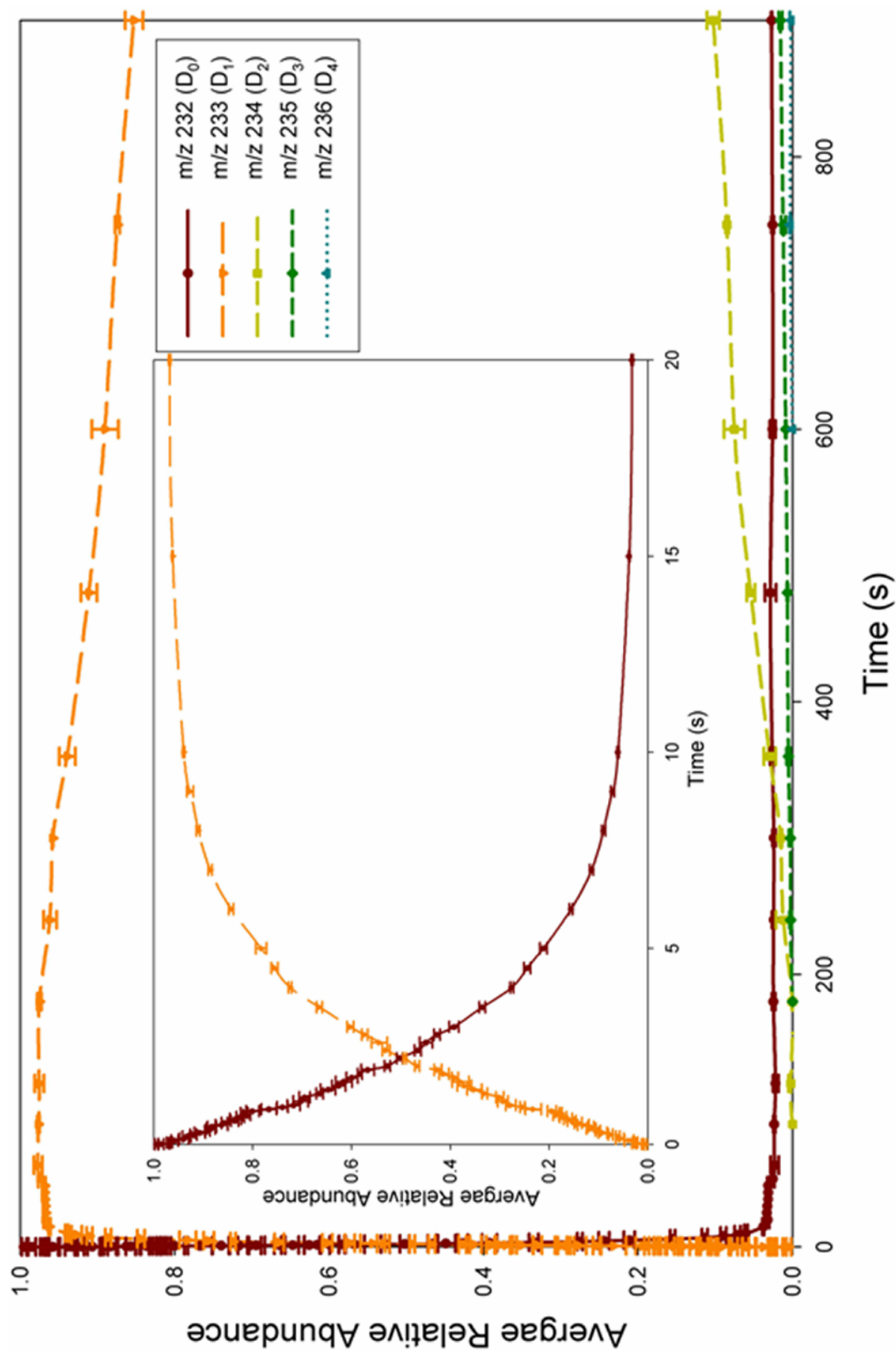
Figure 63. Temporal plot for gas-phase H/D exchange of protonated ArgGly with deuterated ammoinia at ~6.6 E-8 torr.
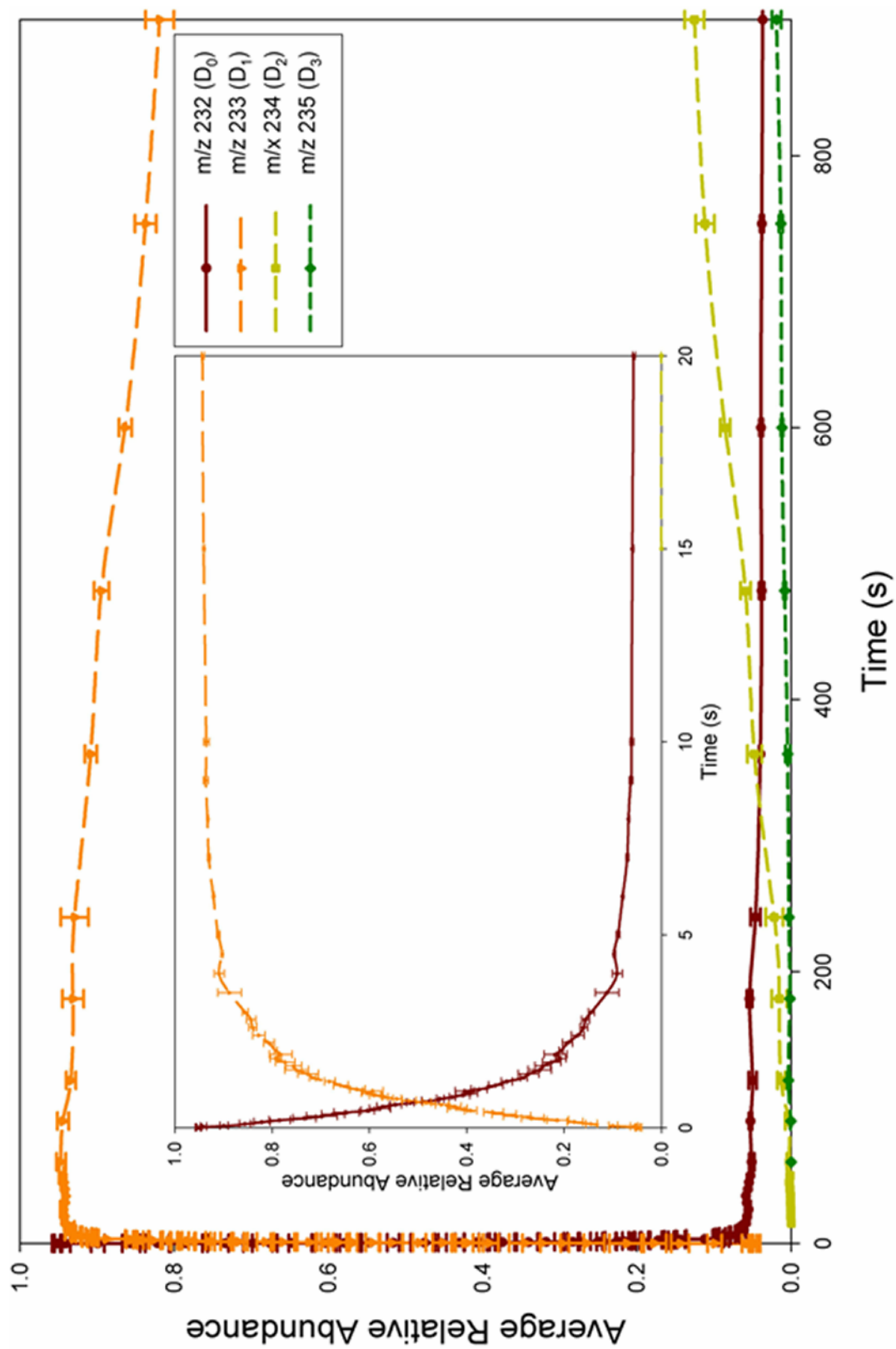
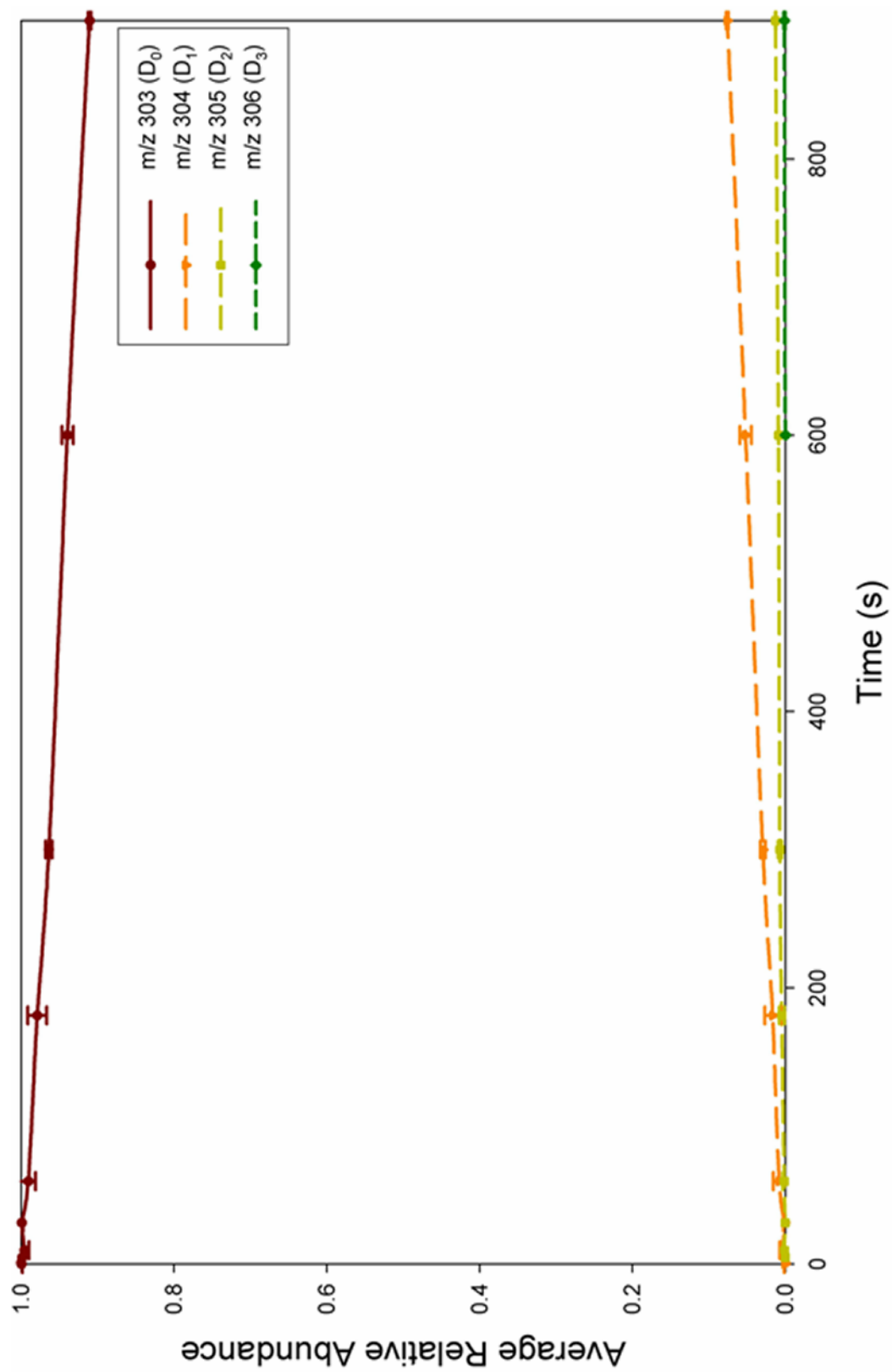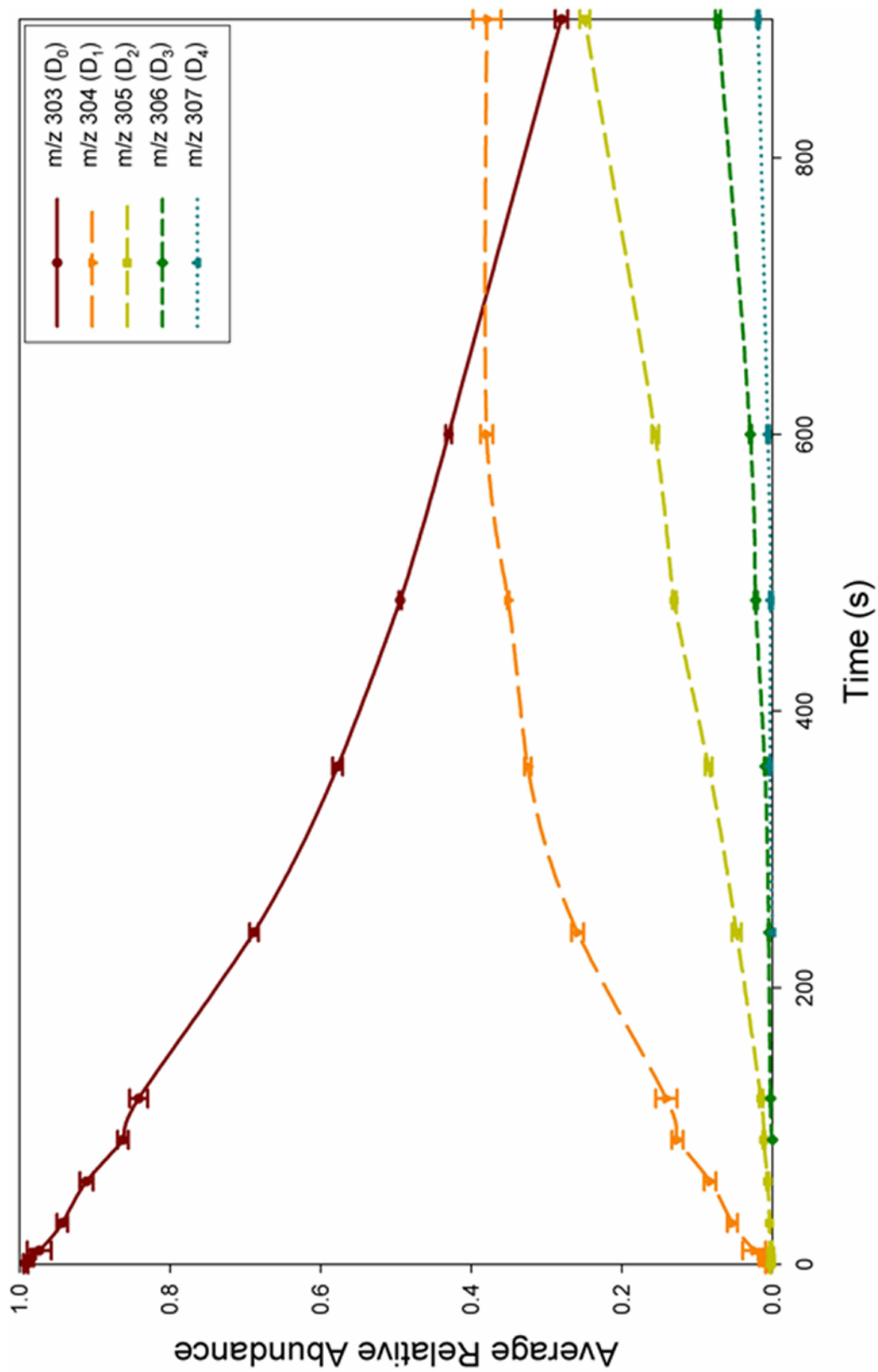Figure 64. Temporal plot for gas-phase H/D exchange of protonated GlyArg with deuterated ammoinia at ~6.6 E-8 torr.
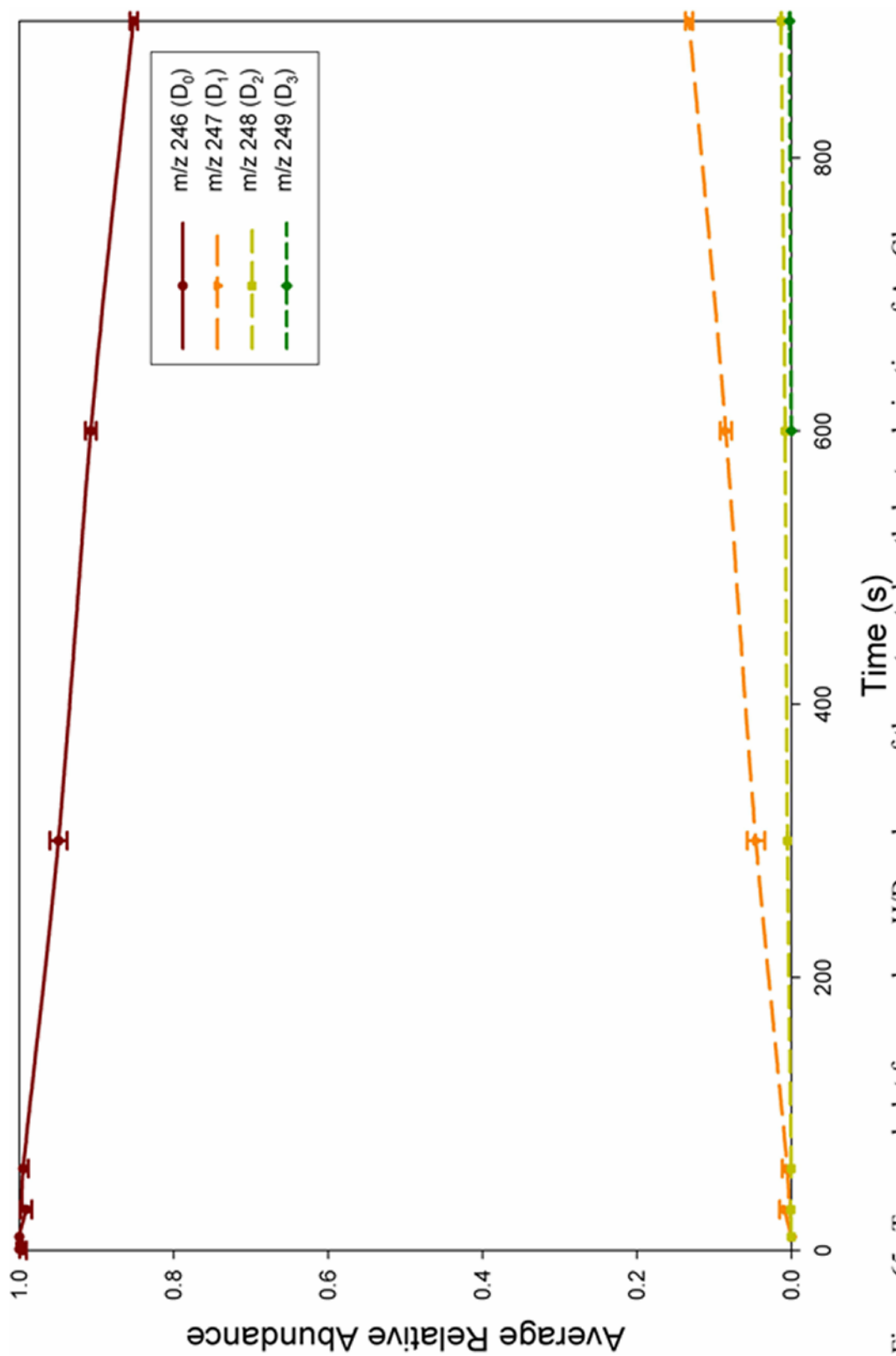
Figure 65. Temporal plot for gas-phase H/D exchange of the protonated methyl ester derivative of ArgGly with deuterated ammonia at ~6.6 E-8 torr.
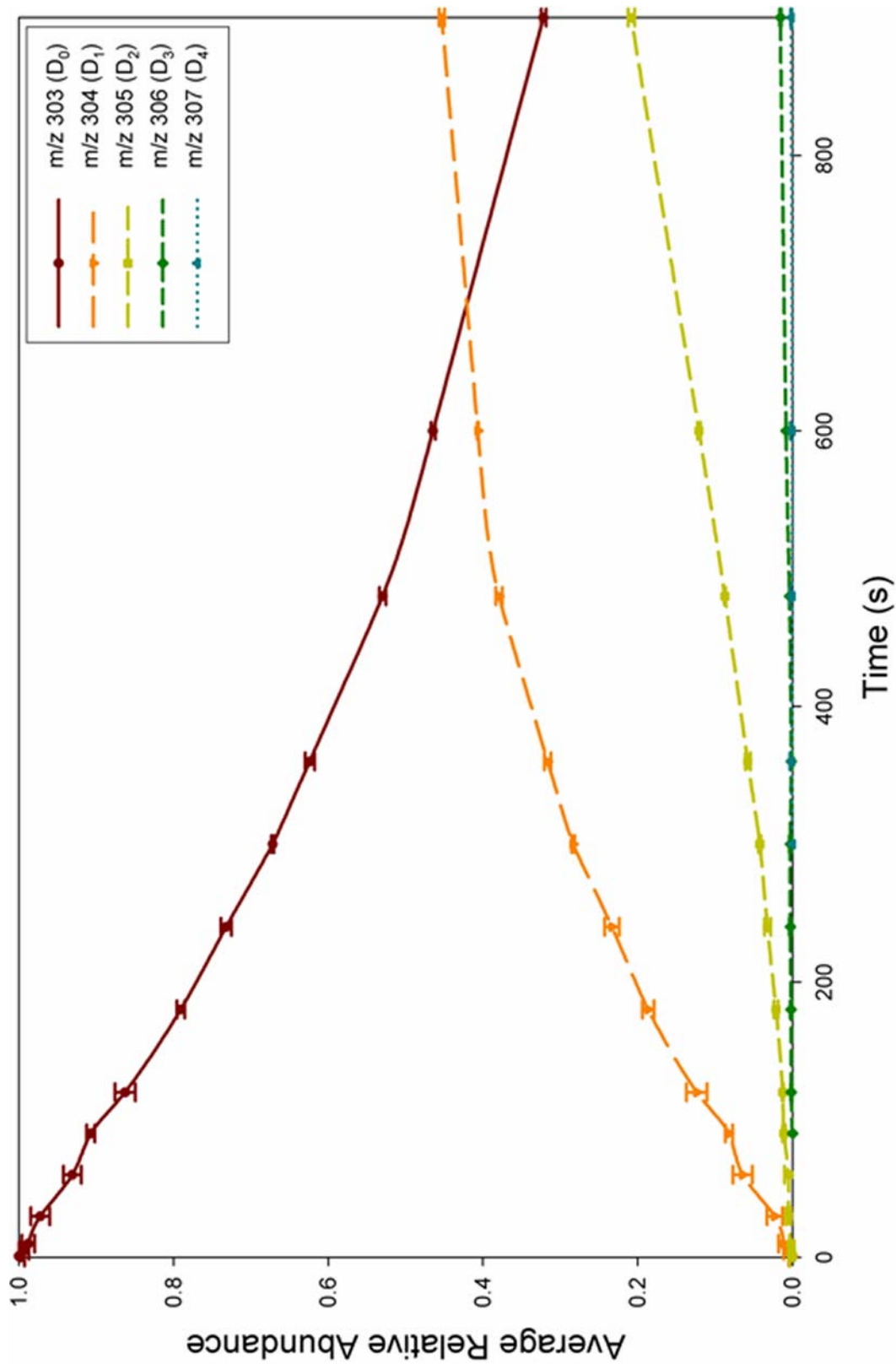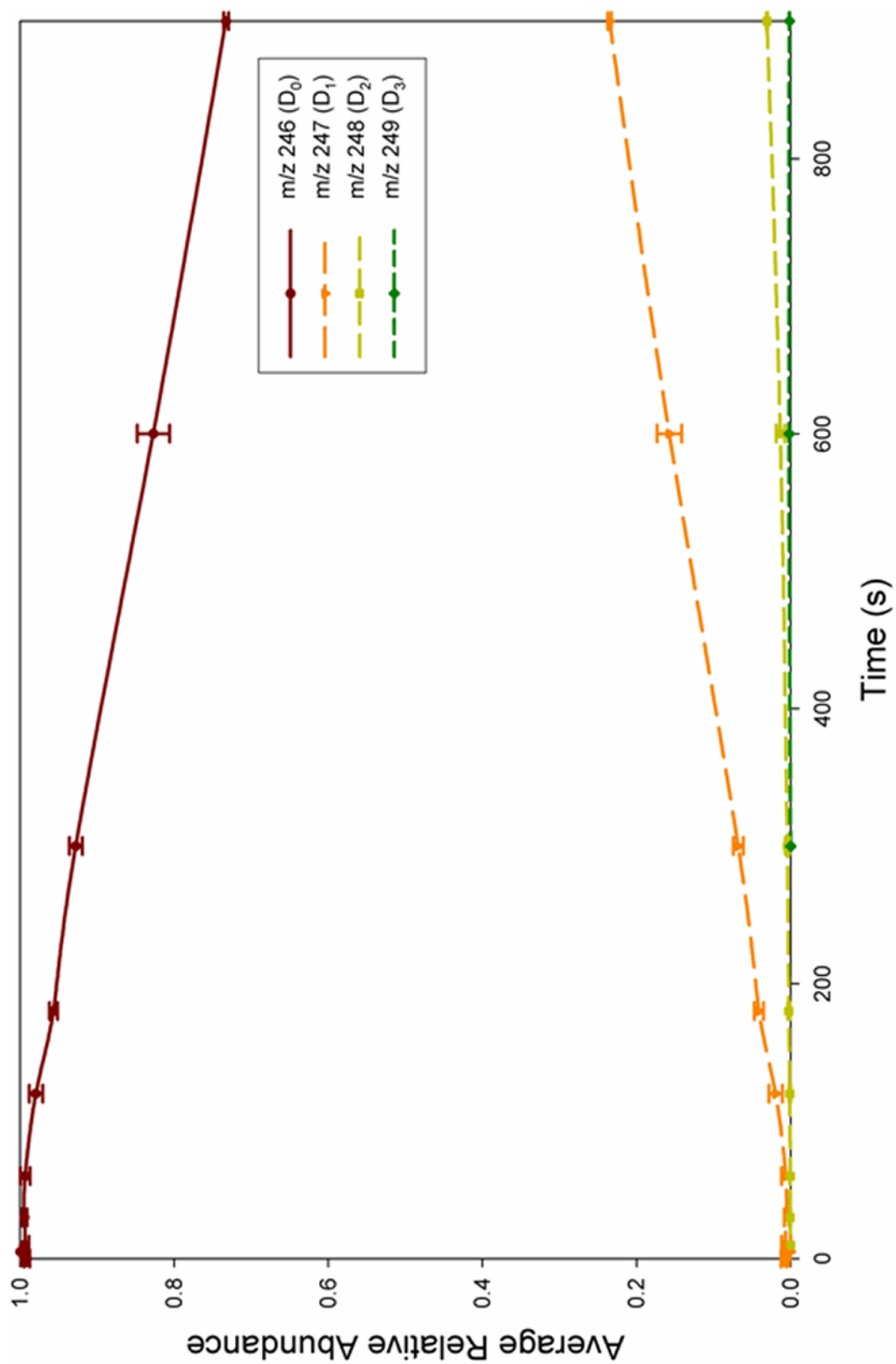
Figure 66. Temporal plot for gas-phase H/D exchange of the protonated methyl ester derivative of GlyArg with deuterated ammonia at ~6.6 E-8 torr.
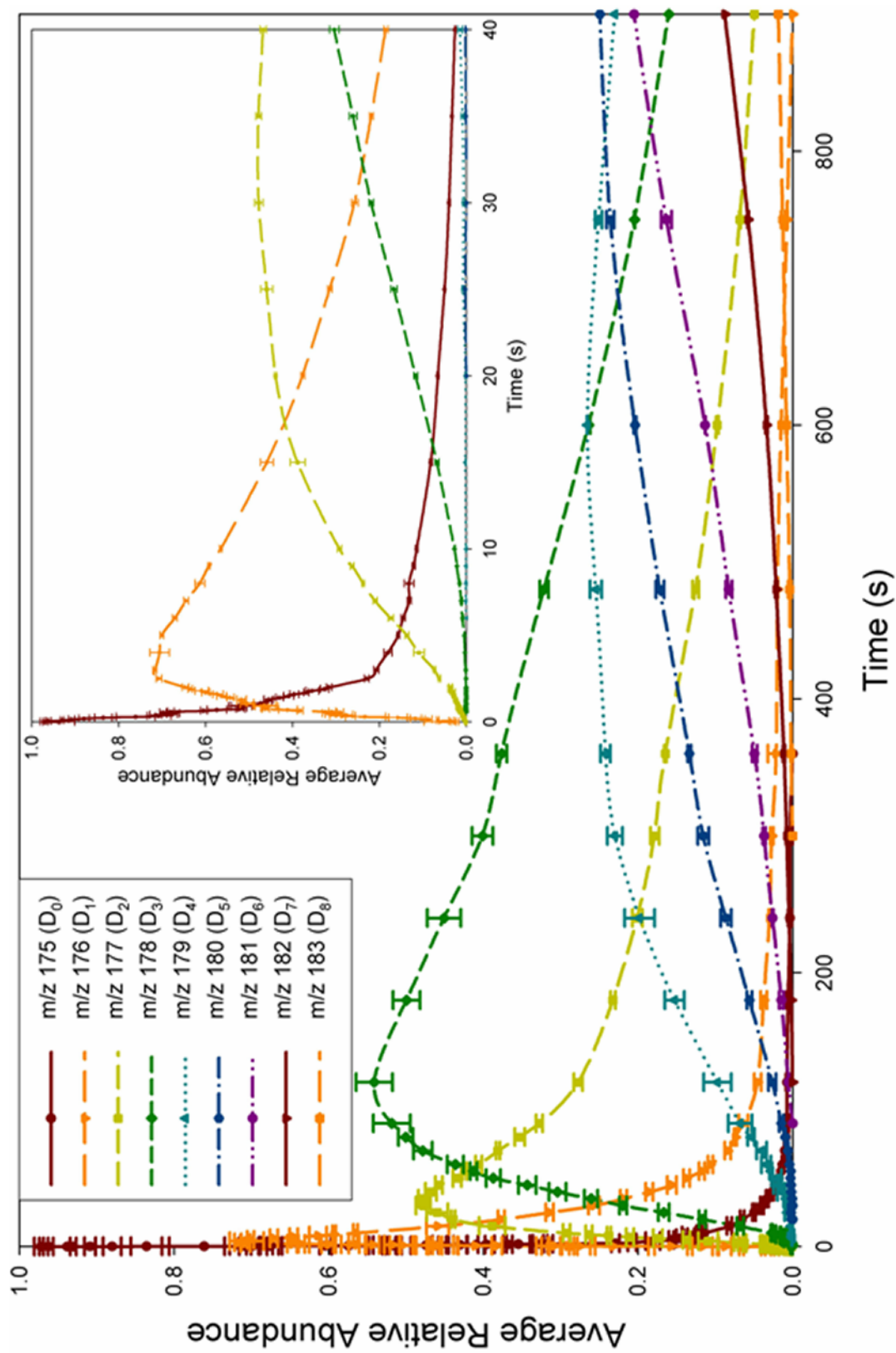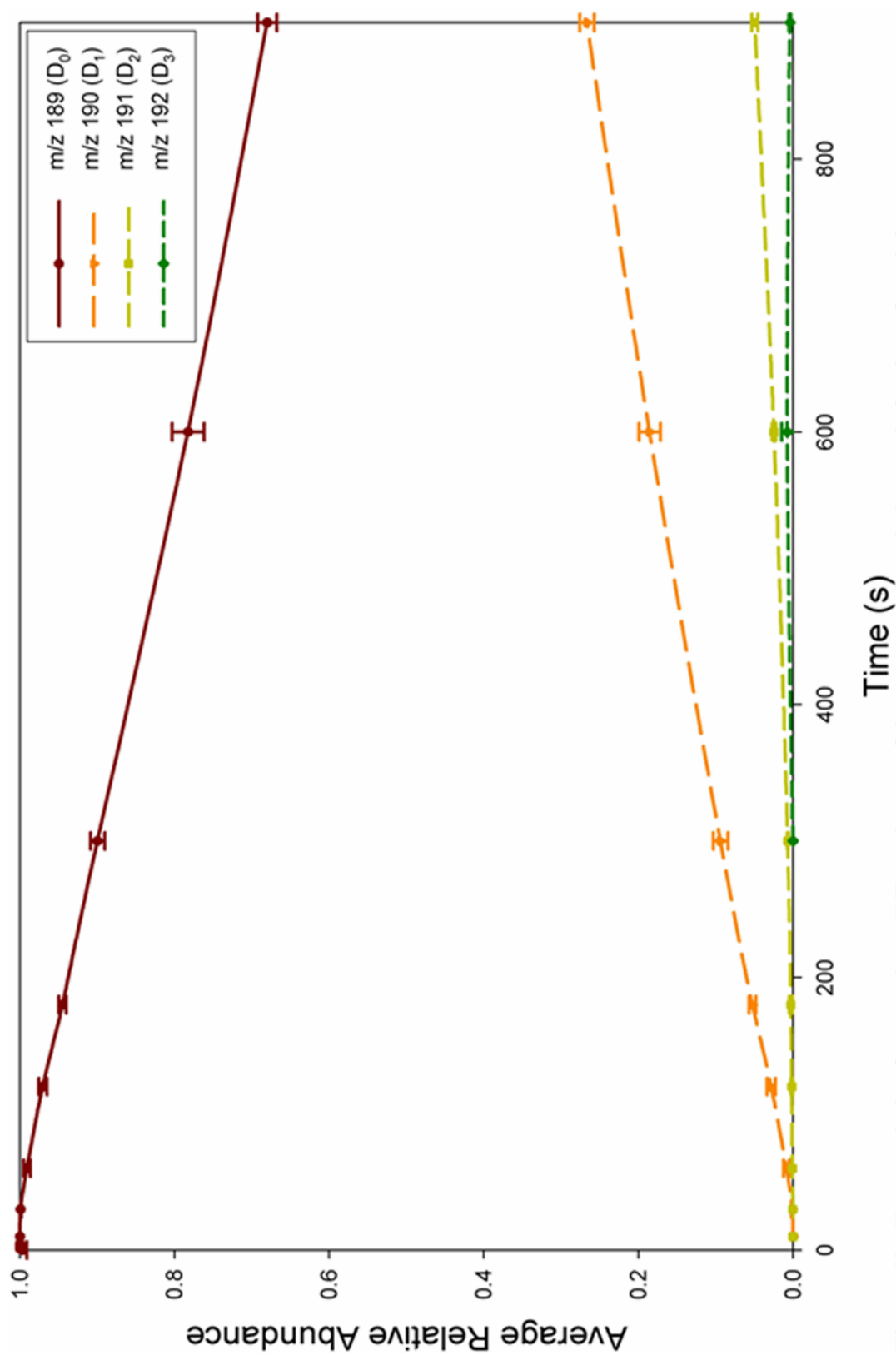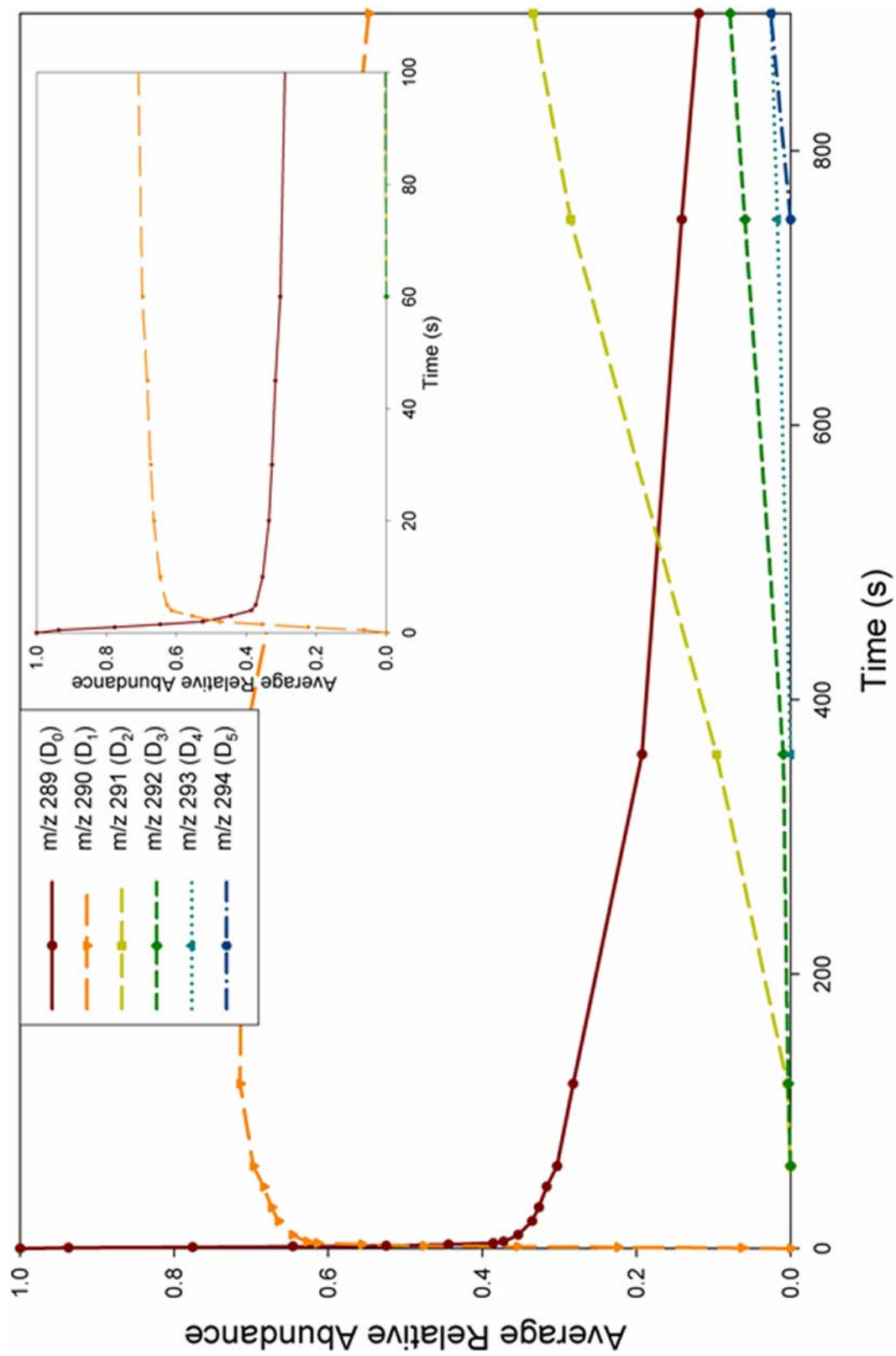
Figure 67. Temporal plot for gas-phase H/D exchange of protonated ArgGlyGly with deuterated acetic acid at ~6.0 E-8 torr.
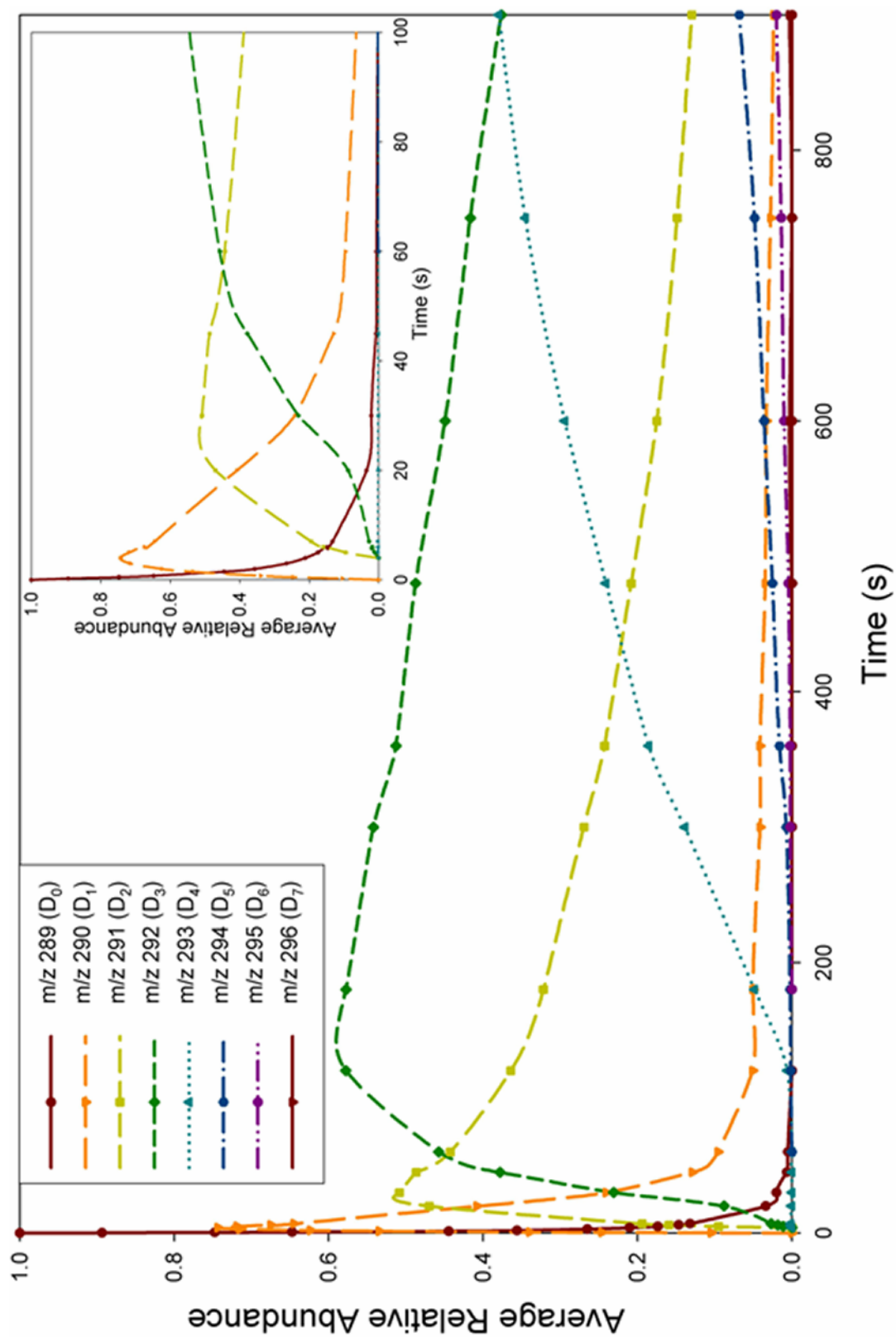
Figure 68. Temporal plot for gas-phase H/D exchange of protonated GlyArgGly with deuterated acetic acid at ~6.0 E-8 torr.
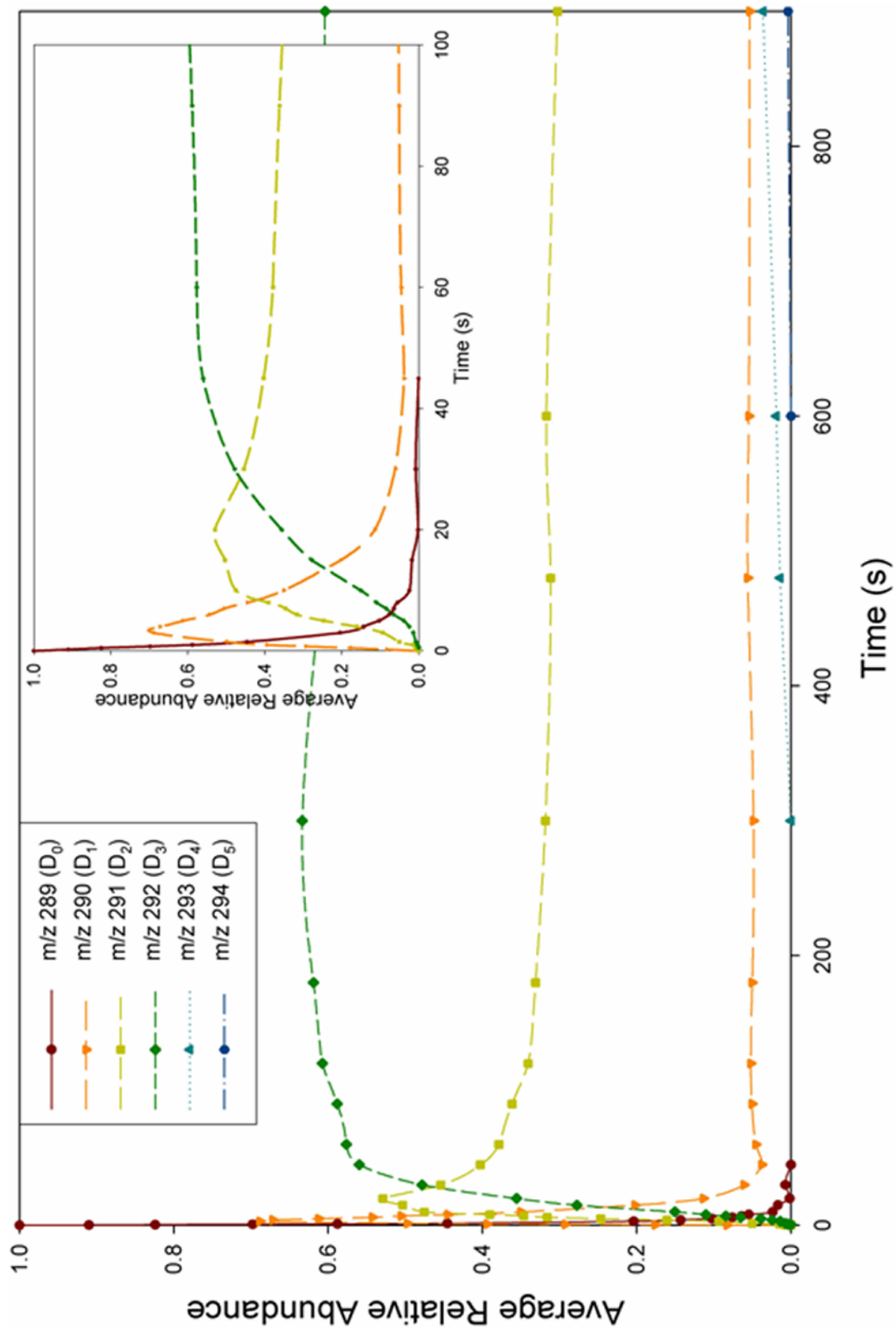
Figure 69. Temporal plot for gas-phase H/D exchange of protonated GlyGlyArg with deuterated acetic acid at ~6.0 E-8 torr.

Finally, the H/D exchange of GlyGlyArgH$^+$ with acetic acid-d$_4$ is approximately 6% less efficient (Table 3) than ArgGlyGlyH$^+$ for incorporation of the first deuterium when reacted with acetic acid-d$_4$.


Discussion

Gas-phase H/D exchange temporal distributions and reaction efficiencies of the [M+H]$^+$ ions of arginine and sequence isomers of arginine containing di- and tripeptides are very different. The dissimilarities are rationalized in terms of unique intramolecular interactions. Inductive stabilization of the charge site through intramolecular bridging interactions has been proposed to influence gas-phase H/D exchange,[39,44,45,46] but the affect of arginine residues on deuterium incorporation for peptide ions has not been fully explored. Examination of the gas-phase H/D exchange of arginine containing peptide sequence isomers can be used to probe how basic residues influence charge solvation, affecting deuterium incorporation and peptide ion structure.

Gas-Phase H/D Exchange of the Tripeptides with Ammonia-d₃

As discussed in the preceding section, the [M+H]$^+$ ions of ArgGlyGly, GlyArgGly and GlyGlyArg, exhibit very different temporal distributions for reaction with ammonia-d$_3$. Specifically, ArgGlyGlyH$^+$ is the only arginine containing tripeptide ion that exhibits two distinct reaction efficiencies (Figure 70) for depletion of the [M+H]$^+$ ion when reacted with ammonia-d$_3$. The unique gas-phase H/D exchange chemistry of this sequence isomer ion can be explained invoking different intramolecular bridging interactions. For example, two plausible conformations for ArgGlyGlyH$^+$,
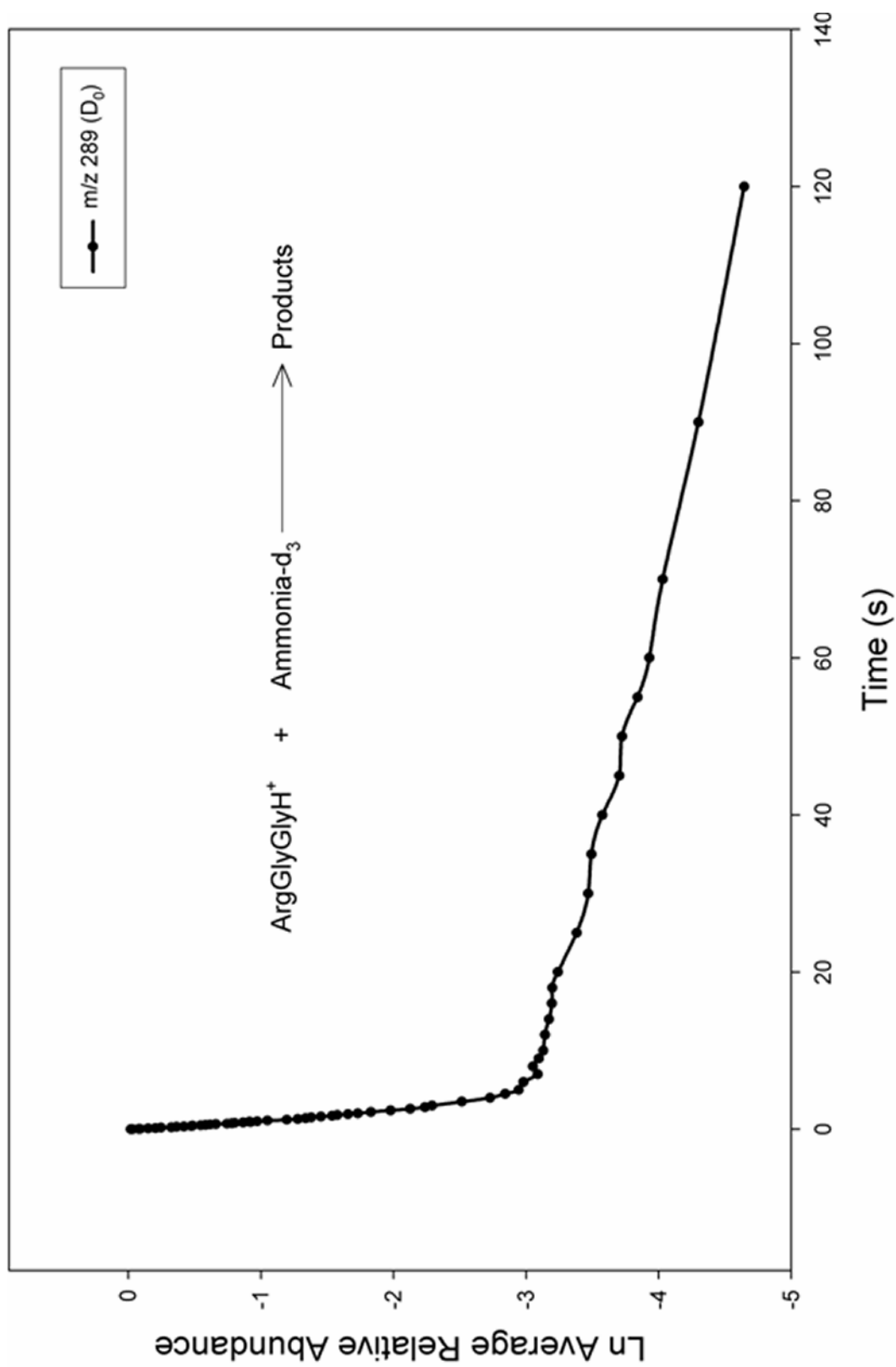
Figure 70. Plot of the natural log of the relative abundance of protonated ArgGlyGly as a function of time for reaction with deuterated ammonia at ~6.6 E-8 torr.

generated by molecular modeling calculations, are illustrated in Figure 71. Inductive
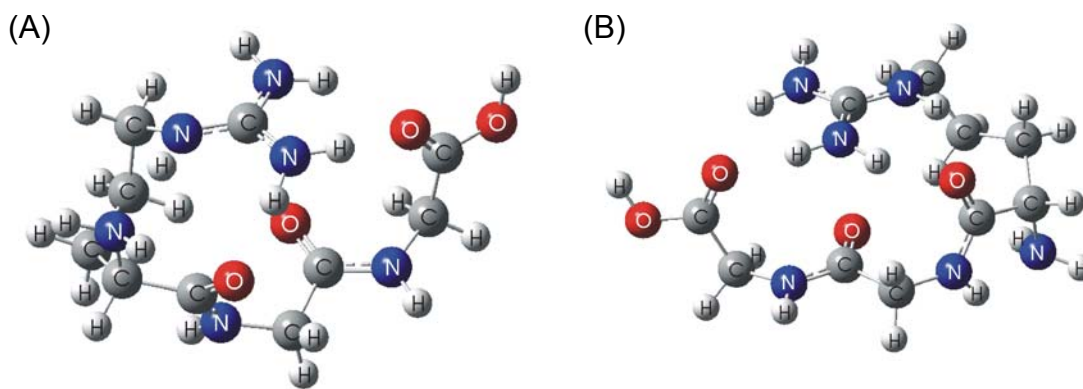
Figure 71. Optimized conformations for ArgGlyGlyH$^+$.

charge stabilization of Conformation A involves the protonated guanidino group, *N*-terminal amine, the arginine amide carbonyl, and *C*-terminal carboxylic acid. Conversely, charge stabilization of Conformation B only involves the protonated guanidino group, the arginine amide carbonyl, and *C*-terminal carboxylic acid for charge solvation. Conformations A and B are calculated to differ in energy by only 1.2 kcal/mol, therefore both conformations should be considered as possible gas-phase ion structures for this *N*-terminal arginine containing tripeptide ion. These conformations may contribute to the double exponential decay observed for gas-phase H/D exchange of ArgGlyGlyH$^+$ with ammonia-d$_3$ as both structures should have dissimilar GB and deuterium reagent accessibilities, affecting reaction efficiency. In addition to differences for depletion of the [M+H]$^+$ ion, the temporal plot for H/D exchange of the *N*-terminal arginine containing tripeptide ion displays dissimilar product ion

distributions for subsequent incorporation of deuterium. Exchanging eight of ten labile hydrogens during the time course of the experiment, the temporal plot for ArgGlyGlyH$^+$ exhibits comparable reaction efficiencies for incorporation of the second through fifth deuteriums. The similar H/D exchange of these labile hydrogens may be attributed to the proximity of the guanidino group with respect to the *C*-terminus. A detailed explanation of the temporal distribution of ArgGlyGlyH$^+$ with ammonia-d$_3$ will be provided in the following sections.

Compared to the other sequence isomers, gas-phase H/D exchange of GlyArgGlyH$^+$ with ammonia-d$_3$ is the least efficient for incorporation of the first deuterium. As seen in Table 3, the first exchange is approximately 21% less efficient for GlyArgGlyH$^+$ than AgrGlyGlyH$^+$ when reacted with ammonia-d$_3$. The decreased in reaction efficiency may be due to different intramolecular interactions. Figure 72 contains a possible conformation for GlyArgGlyH$^+$, generated by molecular modeling
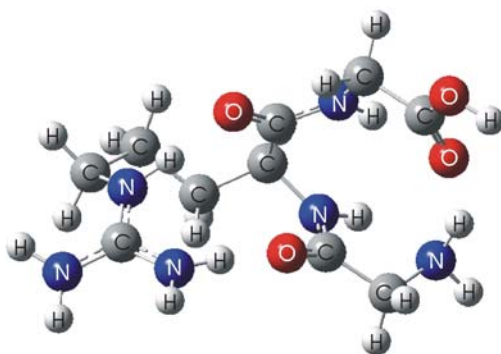
Figure 72. Optimized conformation for GlyArgGlyH$^+$.

calculations. In this conformation charge stabilization involves the protonated guanidine group, both amide carbonyls, the *N*-terminal amine, and *C*-terminal carboxylic acid group. Increasing the number of bridging interactions for inductive stabilization should have a proportional effect on the GB of the oligopeptide ion, decreasing reaction efficiency for incorporation of the first deuterium in GlyArgGlyH$^+$, as well as the overall temporal distributions for subsequent reaction products. For the internal arginine containing tripeptide ion, the first three exchanges proceeds relatively fast, whereas the remaining exchanges are more gradual. The temporal plot for H/D exchange GlyArgGlyH$^+$ with ammonia-d$_3$ may be attributed to the proximity of the *N*-terminal amine with respect to the *C*-terminal carboxylic acid. Interaction of these termini may explain the three facile exchanges for GlyArgGlyH$^+$, as described in the following sections.

Gas-phase H/D exchange of GlyGlyArgH$^+$ with ammonia-d$_3$ exhibits nearly identical reaction efficiency as ArgGlyGlyH$^+$ (Table 3). Figure 73 contains is a proposed conformation of GlyGlyArgH$^+$ generated by molecular modeling calculations.
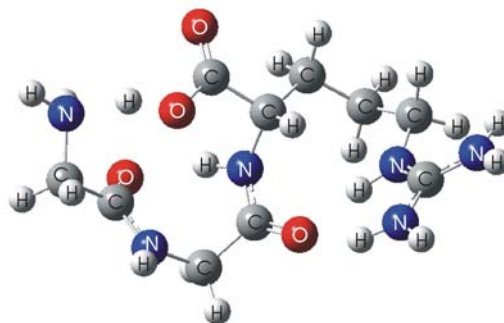
Figure 73. Optimized conformation for GlyGlyArgH$^+$.

Charge stabilization of this *C*-terminal arginine containing tripeptide ion involves the protonated guanidine group, the internal glycyl amide carbonyl, the *C*-terminal carboxylic acid and *N*-terminal amine. Thus, GlyGlyArgH$^+$ utilizes the same number of intramolecular bridging interactions as proposed for ArgGlyGlyH$^+$, which explains the similar exchange efficiency for incorporation of the first deuterium when reacted with ammonia-d$_3$. Despite the similar reaction efficiency of the *N*- and *C*-terminal arginine containing tripeptide ions, the temporal distribution for GlyGlyArgH$^+$ more closely resembles the temporal plot of GlyArgGlyH$^+$ for exchange with ammonia-d$_3$. Specifically, the first three exchanges for GlyGlyArgH$^+$ are relatively rapid, but the remaining exchanges occur much more slowly. This may be attributed to the proximity of the *C*-terminus with respect to the *N*-terminal amine. This issue will be discussed further in the following section.

Gas-Phase H/D Exchange of Modified Tripeptides with Ammonia-d$_3$

Many independent studies and semiempirical calculations have suggested that the [M+H]$^+$ ions of arginine and arginine containing peptides, exist as a zwitterions in the gas-phase[114,115,116,117,118,119]. Proposed structures for these ions involve salt bridge formation between the deprotonated *C*-terminal carboxylic acid and the arginine guanidino group as well as other basic sites of the molecule. Esterification of the *C*-terminal carboxylic acid, eliminates possible zwitterion involvement for the [M+H]$^+$ ions of arginine and arginine containing peptides, thus altering inductive stabilization of the charge site(s). The temporal distribution for H/D exchange product ions for arginine [M+H]$^+$ ions when reacted with ammonia-d$_3$ are contained in Figure 60. Note that

ArgH$^+$ exhibits a double exponential decay (Figure 74) for the first deuterium exchange, which is expected if the [M+H]$^+$ ion exists as two distinct ion conformations. Proposed structures for ArgH$^+$, generated by molecular modeling calculations, are illustrated in Figure 75. Each structure exhibits different intramolecular interactions for inductive stabilization of the charge site. Charge stabilization in Conformation A involves the protonated guanidino group, *N*-terminal amine, and the *C*-terminal carboxylic acid carbonyl. Conversely, charge solvation of Conformation B involves a zwitterionic form of ArgH$^+$ involving salt-bridge interactions between the protonated guanidino group and deprotonated carboxylic acid as well as the *C*-terminus and *N*-terminal amine. The zwitterionic form of ArgH$^+$ is calculated to be approximately 3.0 kcal/mol less stable than the non-zwitterionic form, thus the double exponential decay observed for H/D exchange with ammonia-d$_3$, may be an indication that both structural forms are present.

The gas-phase H/D exchange of the methyl ester of arginine [M+H]$^+$ ions exhibits a drastically different temporal distribution (Figure 62) and reaction efficiencies (Table 3) for exchange with ammonia-d$_3$. For example, the first exchange is approximately 2500 times less efficient than ArgH$^+$. The dissimilar reaction efficiencies for these ions indicates that the primary site for exchange of arginine [M+H]$^+$ ions is the *C*-terminal carboxylic acid. Subsequent exchanges presumably involve intramolecular randomization of the deuterium to regenerate the non-reiterated *C*-terminal carboxylic acid. Therefore, the proximity of the *C*-terminus to other labile hydrogens within the molecule may affect the efficiency at which subsequent deuterium incorporation is observed. For example, the temporal distribution observed for reaction of ArgH$^+$ with
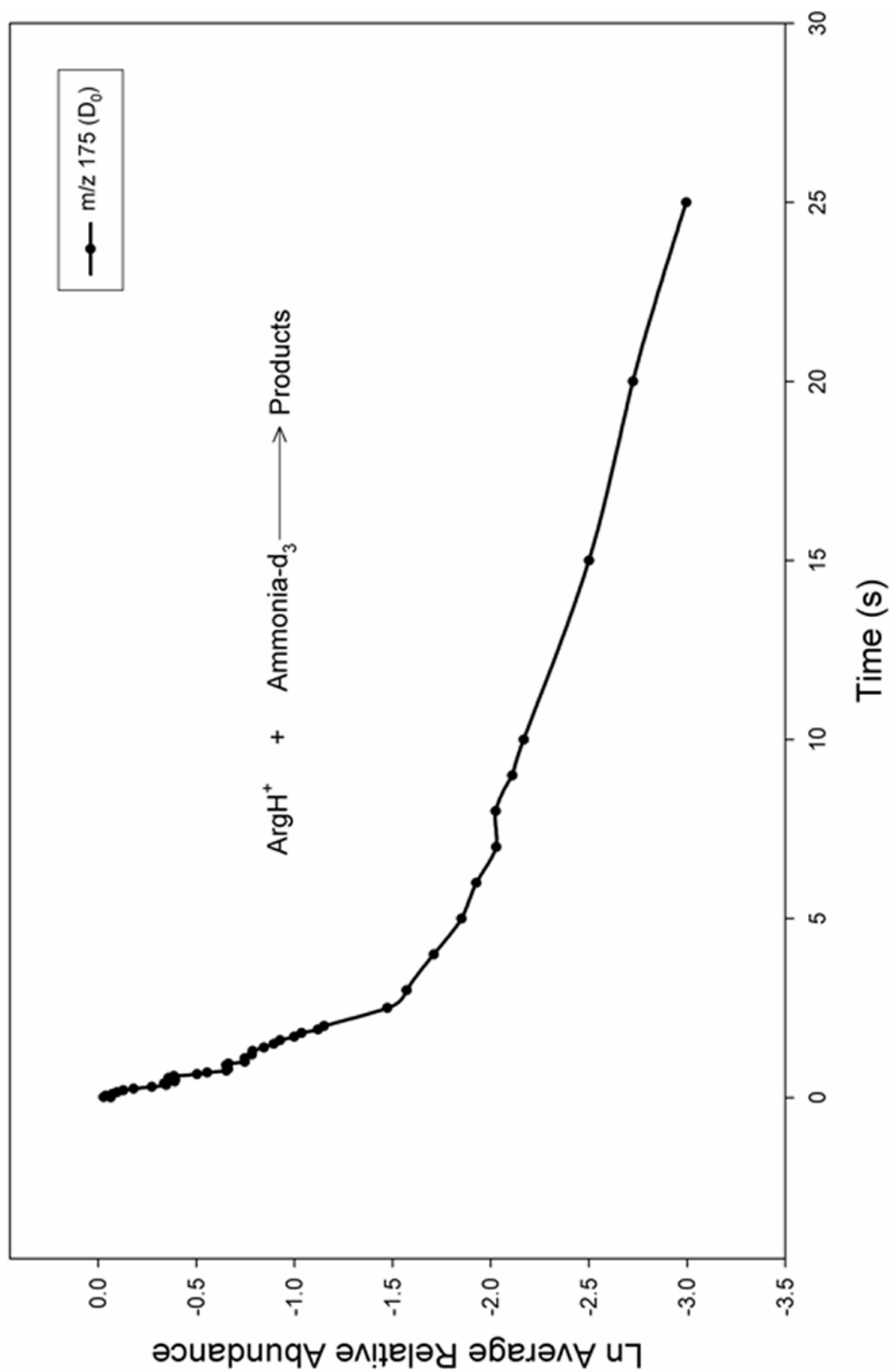
Figure 74. Plot of the natural log of the relative abundance of protonated Arginine as a function of time for reaction with deuterated ammonia at ~6.6 E-8 torr.
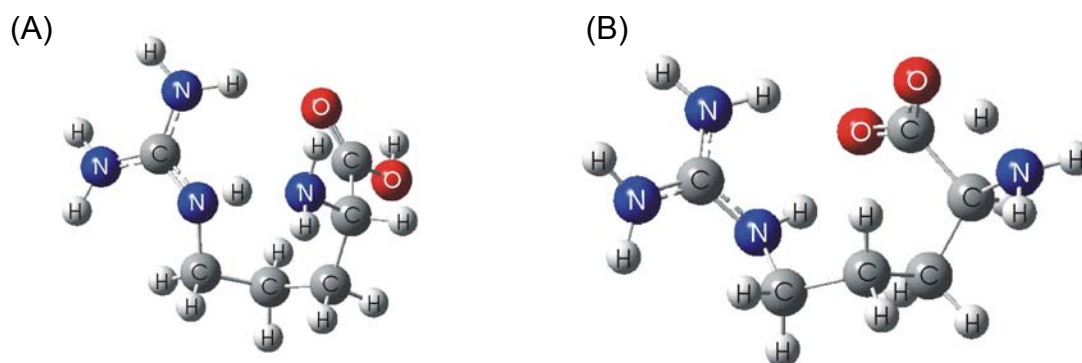
Figure 75. Optimized conformations for (A) non-zwitterionic and (B) zwitterionic forms of ArgH$^+$

amminia-d$_3$ (Figure 61) illustrates that the first three exchanges are relatively rapid whereas the remaining exchanges are more gradual. The temporal distribution is interpreted as evidence that the *C*-terminus is in close proximity to the *N*-terminal amine, presumably accounting for the three facile exchanges observed for reaction with ammonia-d$_3$. The five inefficient exchanges are most likely the labile hydrogens within the gunidino group.

Assignment of the *C*-terminal carboxylic acid as the primary site of exchange in arginine is supported by the gas-phase H/D exchange chemistry of methyl guanidine, creatine and the methyl ester derivative of creatine. Performed under similar conditions used for gas-phase H/D exchange of arginine and arginine containing oligopeptide ions, methyl guanidine does not exchange labile hydrogens during the time course of the experiment. This may be interpreted as evidence that charge solvation between the protonated guanidino group and other basic sites within polyfunctional molecules are necessary to facilitate deuterium incorporation. The effect of intramolecular bridging

interactions between protonated guanidino groups and *C*-terminal carboxylic acids was probed by investigating the gas-phase H/D exchange of creatine $[M+H]^+$ ions. Of the five labile hydrogens, the $[M+H]^+$ ion of creatine incorporates only one deuterium when reacted with ammonia-d_3. Conversely, esterification prevents deuterium incorporation for creatine $[M+H]^+$ ions, indicating that the primary site of exchange is most likely the carboxylic acid. Hence, gas-phase H/D exchange of arginine and arginine containing oligopeptide $[M+H]^+$ ions that exhibit substantially greater gas-phase H/D exchange reaction efficiency that their corresponding methyl esters, may indicate that the primary site for deuterium incorporation is the *C*-terminal carboxylic acid.

Gas-phase H/D exchange for methyl esters of the arginine containing tripeptide ions with ammonia-d_3 are also decreased in reaction efficiency (Table 3) relative to the non-modified ions. This comparative decrease in reaction efficiency indicates that the primary site of exchange for ArgGlyGlyH$^+$, GlyArgGlyH$^+$ and GlyGlyArgH$^+$ is the *C*-terminal carboxylic acid. As suggested for the $[M+H]^+$ ion of arginine, subsequent H/D exchange may involve intramolecular randomization of the deuterium to regenerate the non-deuterated *C*-terminal carboxylic acid. This proposed process for deuterium incorporation may contribute to the observed temporal distribution for H/D exchange of ArgGlyGlyH$^+$ with ammonia-d_3. As seen in Figure 52, the first exchange is relatively facile, and is presumably the labile *C*-terminal carboxylic acid hydrogen. The second through fifth exchanges undergo H/D exchange at comparable reaction efficiencies indicating that these hydrogens may be chemically similar. The primary amines within the guanidino group may constitute these four exchanges due to the general proximity of

the basic side chain with respect to the *C*-terminus. Hence, the H/D exchange model for deuterium incorporation of ArgGlyGlyH$^+$ may explain the temporal distribution for reaction with ammonia-d$_3$, thereby supporting the intramolecular interactions proposed for the *N*-terminal arginine containing tripeptide ion.

The proposed H/D exchange model for ArgH$^+$ and ArgGlyGlyH$^+$ may also be employed to rationalize temporal plots for the other arginine containing tripeptide ions. As seen in Figures 53 and 54, the first three exchanges for GlyArgGlyH$^+$ and GlyGlyArgH$^+$ are relatively rapid whereas remaining exchanges are more gradual. The three facile exchanges may be the labile sites on the *N*-terminal amine and *C*-terminal carboxylic acid. Assignment of these sites as the relatively rapid exchanges is consistent with the proposed exchange model due to the general proximity of *N*- and *C*-termini (Figures 72 and 73). Hence, the H/D exchange model for deuterium incorporation may explain the temporal distribution for reaction of GlyArgGlyH$^+$ and GlyGlyArgH$^+$ with ammonia-d$_3$, thereby supporting the intramolecular interactions proposed for the internal and *C*-terminal arginine containing tripeptide ions.

Gas-Phase H/D Exchange of Tripeptides with Acetic Acid-d$_4$

Gas-phase H/D exchange reactions of arginine containing tripeptide ions with ammonia-d$_3$ are less efficient with acetic acid-d$_4$ (Table 3). The decreased exchange efficiency can be attributed to an increase in the relative GB differences between the protonated peptide and exchange reagent. Despite dissimilar reaction efficiencies, comparable temporal distributions support proposed conformations for the arginine containing tripeptide ions. For example, gas-phase H/D exchange of ArgGlyGlyH$^+$ with

acetic acid-d_4 also exhibits a double exponential decay for incorporation of the first deuterium (Figure 76). Depletion of the $[M+H]^+$ ion for reaction of ArgGlyGlyH$^+$ with acetic acid-d_4 is consistent with multiple conformations proposed for the *N*-terminal arginine containing tripeptide ion. The internal and *C*-terminal arginine containing tripeptide ions also exhibit similar temporal distributions for reaction with acetic acid-d_4 when compared to results obtained with ammonia-d_3. Specifically, gas-phase H/D exchange of GlyArgGlyH$^+$ and GlyGlyArgH$^+$ with acetic acid-d_4 incorporates the first three deuteriums at comparable reaction efficiencies, supporting the proposed intramolecular interactions for these arginine containing tripeptide ions. Hence, gas-phase H/D exchange of the arginine containing tripeptide ions with acetic acid-d_4 coincide with results obtained with ammonia-d_3, confirming the proposed oligopeptide ion conformations.

Gas-Phase H/D Exchange of Dipeptides and Modified Dipeptides with Ammonia-d_3

The temporal plots for H/D exchange of the arginine containing dipeptide ions with ammonia-d_3 are very different from the arginine amino acid and the arginine containing tripeptide ions. Specifically, the first exchange for ArgGly and GlyArg $[M+H]^+$ ions are relatively efficient, whereas remaining exchanges are substantially hindered. Gas-phase H/D exchange of the methyl ester derivatives of each arginine containing dipeptide ion exhibit significant decreases in exchange efficiency for incorporation of the first deuterium (Table 3). This comparative decrease in exchange efficiency indicates that the primary site for deuterium incorporation of ArgGlyH$^+$ and GlyArgH$^+$ is the *C*-terminal carboxylic acid hydrogen. Agreement of the initial site for
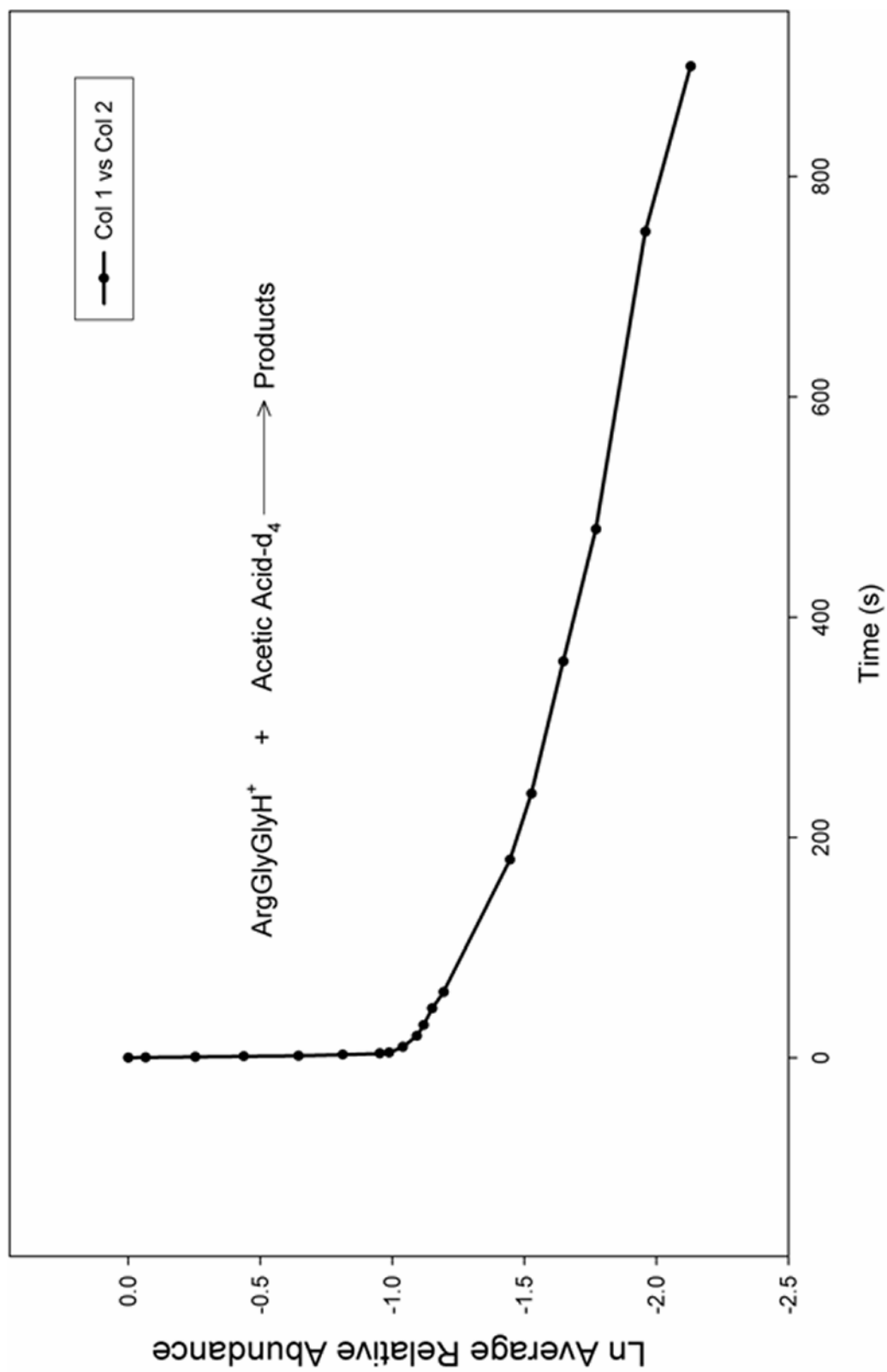
Figure 76. Plot of the natural log of the relative abundance of protonated ArgGlyGly as a function of time for reaction with deuterated acetic acid at ~6.0 E-8 torr.

exchange of arginine and arginine containing oligopeptide ions is complemented by similar intramolecular interactions for charge solvation. For example, the proposed conformation for ArgGlyH$^+$ (Figure 77), generated by molecular modeling calculations,
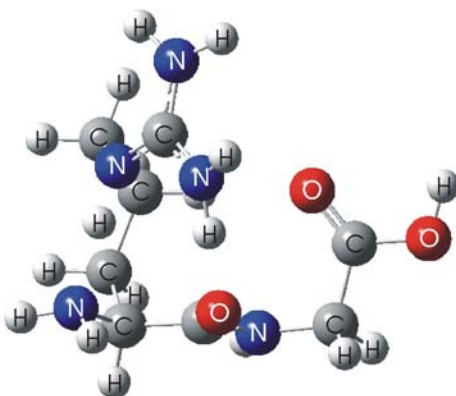
Figure 77. Optimized conformation for ArgGlyH$^+$

indicates a bridging interaction between the protonated guanidino group and *N*-terminal amine. A similar intramolecular interaction was proposed for ArgH$^+$ (Figure 75) and ArgGlyGlyH$^+$ (Figure 71), suggesting that sequence position of the arginine residue influences gas-phase ion conformation. Molecular modeling calculations also indicate common bridging interactions between GlyArgH$^+$, ArgH$^+$ and GlyGlyArgH$^+$. As seen in Figure 78, conformation B, the *C*-terminal arginine containing dipeptide ion utilizes a zwitterionic form of GlyArgH$^+$ for charge solvation. Approximately 1.4 kcal/mol less stable than conformation A, the zwitterionic form of GlyArgH$^+$ coincides with proposed zwitterionic structures for ArgH$^+$ and GlyGlyArgH$^+$, indicating that sequence position of the arginine residue affects gas-phase ion conformation. Despite common
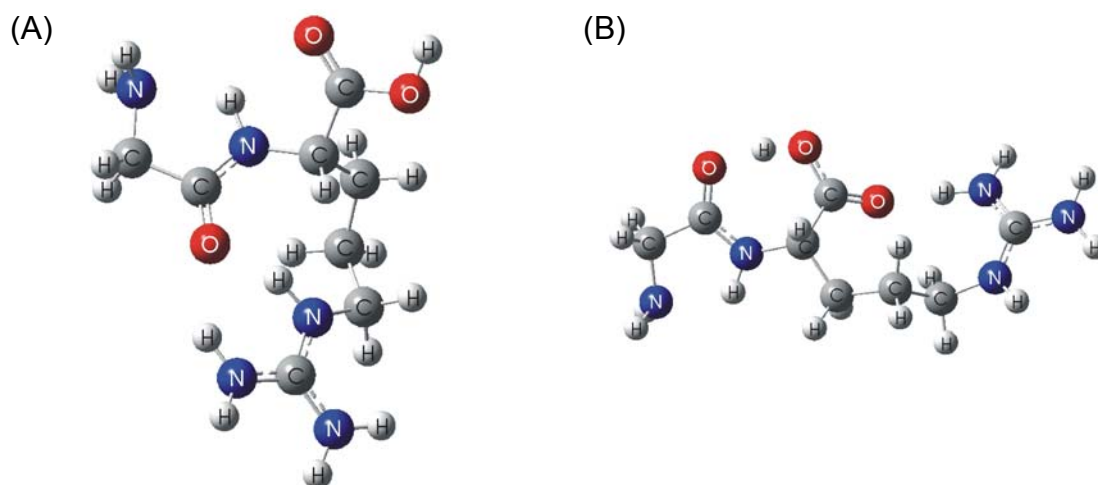
Figure 78. Optimized conformations for (A) non-zwitterionic and (B) zwitterionic forms of GlyGlyArgH$^+$

intramolecular interactions between arginine and the arginine containing oligopeptide ions, gas-phase H/D exchange temporal distributions for ArgGlyH$^+$ and GlyArgH$^+$ do not resemble the temporal plots for arginine and arginine containing tripeptide ions. These temporal anomalies can not currently be explained.

Conclusion

Gas-phase H/D exchange experiments have been performed on the [M+H]$^+$ ions of arginine and arginine containing di- and tripeptides. The oligopeptide sequence isomers investigated in this study demonstrate different reaction efficiencies and temporal distributions for deuterium incorporation, indicating that peptide ion amino acid sequence affects H/D exchange. Sequence specific reaction efficiencies may be attributed to dissimilar intramolecular interactions for inductive stabilization of the charge site. Differences in H/D exchange efficiencies are complemented by unique

temporal distributions for deuterium incorporation. Specifically, ArgH$^+$ and ArgGlyGlyH$^+$ were the only ions that exhibited a double exponential decay for incorporation of the first deuterium. The H/D exchange chemistry of these compounds is attributed to multiple intramolecular bridging interactions, indicating the presence of more than one gas-phase ion conformation. In addition, gas-phase H/D exchange of the methyl esters of arginine and arginine containing oligopeptide ions were also investigated. Studied to probe the probability of zwitterionic formation for inductive stabilization, the modified amino acid and oligopeptides demonstrate reduced reaction efficiency when compared to the non-esterified ions. The dissimilar H/D reaction efficiency of esterified and non-esterified arginine and arginine containing di- and tripeptides indicates that the primary site of exchange is the *C*-terminal carboxylic acid. Despite dissimilar H/D exchange efficiencies, assignment of zwitterionic contributions for charge stabilization was deemed inconclusive, as all biomolecules demonstrated a decrease in reaction efficiency upon esterification.

CHAPTER VI

CONCLUSIONS

The development of analytical instrumentation for the characterization of biomolecule structure remains an active area of research in the life sciences. Investigation of gas-phase peptide and protein secondary structure has been aided by ion-mobility mass spectrometry and ion-molecule reactions such as gas-phase hydrogen/deuterium (H/D) exchange. The later technique has been extensively used for the investigation of biomolecule conformations, but few experiments have been performed to determine the factors affecting deuterium incorporation. Therefore, goals of the research described herein were to develop a Fourier-transform ion cyclotron resonance (FT-ICR) mass spectrometer for gas-phase H/D exchange of peptide ions and to investigate the effect that specific amino acid residue have on conformation and deuterium incorporation of $[M+H]^+$ peptide ions.

The 3 Tesla (T) FT-ICR mass spectrometer employed for these gas-phase H/D exchange studies was modified from its original design to incorporate a solid state insertion probe for internal matrix assisted laser desorption ionization (MALDI) and a two-section cell for spatial separation of ion cooling and ion-molecule reaction events. The internal MALDI source provides a convenient and inexpensive means for ionizing non-volatile compounds for subsequent mass to charge analysis by FT-ICR mass spectrometry. Despite limitations associated with coupling an internal MALDI source

with a FT-ICR mass spectrometer, instrument modifications were deemed sufficient for studying the peptide ion systems investigated by gas-phase H/D exchange. Replacing the solid state insertion probe with a linear triple quadrupole assembly and an external MALDI or electrospray source may be necessary to investigate the gas-phase H/D exchange of larger molecular weight compounds.

Systems investigated these gas-phase H/D exchange studies were oligopeptide sequence isomers containing a basic amino acid residue. Position of the basic residue within di- and tripeptides (*i.e. N*-terminal, internal, or *C*-terminal) influenced deuterium incorporation for the $[M+H]^+$ ion, indicating a sequence effect on deuterium incorporation. Specifically, peptide sequence isomers exhibited dissimilar temporal distributions and reaction efficiencies based upon their primary structure. Peptides containing an *N*-terminal basic residue demonstrated distinct H/D exchange chemistry when compared to their internal and *C*-terminal counterparts. These differences were attributed to dissimilar intramolecular bridging interactions associated with inductive stabilization of the charge site.

Finally, gas-phase H/D exchange of the oligopeptide $[M+H]^+$ ions with different deuterium reagents also exhibited unique reaction efficiencies and temporal distributions for deuterium incorporation. The dissimilar reaction chemistry was attributed to changes in the relative gas-phase basicity between the peptide ion and deuterium reagent as well as proposed mechanistic exchange differences. These factors influenced deuterium incorporation for the di- and tripeptides investigated in this study.

RERENCES

1. (a) Yamashita, M.; Fenn, J. B. *J. Phys. Chem.* **1984,** *88,* 4451; (b) Yamashita, M.; Fenn, J. B. *J. Phys. Chem.* **1984,** *88*, 4671.

2. Aleksandrov, M. L.; Gall, L. N.; Krasnov, V. N.; Nikolaev, V. I.; Pavlenko, V. A.; Shkurov, V. A. *Dokl. Akad. Nauk SSSR* **1984,** *277*, 379.

3. Karas, M.; Bachmann, D.; Bahr U.; Hillenkamp, F. *Int. J. Mass Spectrom. Ion Processes* **1987**, *87*, 53.

4. Yates, J.R. *J. Mass Spectrom.* **1998,** *33*, 1.

5. Siuzdak, G. *P. Natl. Acad. Sci. USA* **1994,** *91*, 11290.

6. Zenobi, R.; Knochenmuss, R. *Mass Spectrom. Rev.* **1998,** *17*, 337.

7. Jarrold, M. F. *Annu. Rev Phys.* Chem. **2000,** *51*, 179.

8. Loo, J. A. *Mass Spectrom. Rev.* **1997,** *16*, 1.

9. Carr, S. A.; Hemling, M. E.; Bean, M. F.; Roberts, G. D. *Anal. Chem.* **1991,** *63*, 2802.

10. McLuckey, S. A. *J. Am. Soc. Mass Spectr.* **1992,** *3*, 599.

11. Clemmer, D. E.; Jarrold, M. F. *J. Mass Spectrom.* **1997,** *32*, 599.

12. Green, M. K.; Lebrilla, C. B. *Mass Spectrom. Rev.* **1997,** *16*, 53.

13. Cody, R. B.; Burnier, R. C.; Freiser, B. S. *Anal. Chem.* **1982,** *54*, 96.

14. Gauthier, J. W.; Trautman, T. R.; Jacobson, D. B. *Anal. Chim. Acta* **1991,** *246*, 211.

15. Ijames, C. F.; Wilkins, C. L. *Anal. Chem.* **1990,** *62*, 1295.

16. Williams, E. R.; Henry, K. D.; McLafferty, F. W.; Shabanowitz, J.; Hunt, D. F. *J. Am. Soc. Mass Spectr.* **1990,** *1*, 413.

17. Bowers, W. D.; Delbert, S. S.; Hunter, R. L.; McIver, R. T. *J. Am. Chem. Soc.* **1984,** *106,* 7288.

18. Woodin, R. L.; Bomse, D. S.; Beauchamp, J. L. *J. Am. Chem. Soc.* **1978,** *100*, 3248.

19. Dunbar, R. C.; McMahon, T. B. *Science* **1998,** *279*, 194.

20. Hudgins, R. R.; Mao, Y.; Ratner, M. A.; Jarrold, M. F. *Biophys. J.* **1999,** *76*, 1591.

21. Ruotolo, B. T.; Verbeck, G. F.; Thomson, L. M.; Gillig, K. J.; Russell, D. H. J. Am. Chem. Soc. **2002,** *124*, 4214.

22. Wu, C.; Siems, W. F.; Klasmeier, J.; Hill, H. H. *Anal. Chem.* **2000,** *72*, 391.

23. Shelimov, K. B.; Clemmer, D. E.; Hudgins, R. R.; Jarrold, M. F. *J. Am. Chem. Soc.* **1997,** *119*, 2240.

24. Brodbelt, J. S. *Mass Spectrom. Rev.* **1997,** *16*, 91.

25. Wyttenbach, T.; Bowers, M. T. *J Am. Soc. Mass Spectr.* **1999,** *10*, 9.

26. Dookeran, N. N.; Harrison, A. G. *J. Mass Spectrom.* **1995,** *30*, 666.

27. Schaaff, T. G., Stephenson, J. L,; McLuckey, S. A. *J. Am. Soc. Mass Spectr.* **2000,** *11*, 167.

28. Pastolic, L.; Huang, Y. L.; Guan, S. H.; Kim, H. S.; Marshall, A. G. *J. Mass Spectrom.* **1995,** *30*, 825.

29. Solouki, T.; PasaTolic, L.; Jackson, G. S.; Guan, S. G.; Marshall, A. G. *Anal. Chem.* **1996,** *68*, 3718.

30. Fellgett, P. B.; *J. Phys. Radium* **1958,** *19*, 187.

31. Marshall, A. G.; Verdun, F. R. *Fourier Transforms in NMR, Optical, and Mass Spectrometry.* Elsevier: New York 1990.

32. Marshall, A. G.; Schweikhard, L. *Int. J. Mass Spectrom.* **1992,** *118*, 37.

33. Marshall, A. G. *Int. J. Mass. Spectrom.* **2000,** *200*, 331.

34. Easterling, M. L.; Mize, T. H.; Amster, I. J. *Anal. Chem.* **1999,** *71*, 624.

35. Solouki, T.; Marto, J. A.; White, F. M.; Guan, S. H.; Marshall, A. G. *Anal. Chem.* **1995,** *67*, 4139.

36. Marshall, A. G.; Hendrickson, C. L. *Int. J. Mass Spectrom.* **2002,** *215*, 59.

37. Gillig, K. J.; Bluhm, B. K.; Russell, D. H. *Int. J. Mass Spectrom.* **1996,** *158*, 129.

38. Freitas, M. A.; Marshall, A. G. *Int. J. Mass. Spectrom.* **1999,** *183*, 221.

39. Campbell, S.; Rodgers, M. T.; Marzluff, E. M.; Beauchamp, J. L. *J. Am. Chem. Soc.* **1995,** *117*, 12840.

40. Solouki, T.; Fort, R. C.; Alomary, A.; Fattahi, A. *J. Am. Soc. Mass Spectr.* **2001,** *12*, 1272.

41. Suckau, D.; Shi, Y.; Beu, S. C.; Senko, M. W.; Quinn, J. P.; Wampler, F. M.; McLafferty, F. W. *Pro. Natl. Acad. Sci. USA* **1993,** *90*, 790.

42. Lee, S. W.; Lee, H. N.; Kim, H. S.; Beauchamp, J. L. *J Am. Chem. Soc.* **1998,** *120*, 5800.

43. Gard, E.; Willard, D.; Bregar, J.; Green, M. K.; Lebrilla, C. B. *Org. Mass Spectrom.* **1993,** *28*, 1632.

44. Gard, E.; Green, M. K.; Bregar, J.; Lebrilla, C. B. *J. Am. Soc. Mass Spectrom.* **1994,** *5*, 623.

45. Gur, E. H.; de Koning, L. J.; Nibbering, N. M. M. *J. Am. Soc. Mass Spectrom.* **1995,** *6,* 466.

46. Green, M. K.; Gard, E.; Bregar, J.; Lebrilla, C. B. *J. Mass Spectrom.* **1995,** *30*, 1103.

47. Wu, J. Y.; Lebrilla, C. B. *J. Am. Chem. Soc.* **1993,** *115*, 3270.

48. Gorman, G. S.; Speir, J. P.; Turner, C. A.; Amster, I. J. *J. Am. Chem. Soc.* **1992,** *114*, 3986.

49. Wu, Z. C.; Fenselau, C. *Rapid Commun. Mass Sp.* **1994,** *8*, 777.

50. Carr, S. R.; Cassady, C. J. *J. Am. Soc. Mass Spectr.* **1996,** *7*, 1203.

51. Comisaro, M. B.; Marshall, A. G. *Chem. Phys. Lett.* **1974,** *25*, 282.

52. Rodgers, R. P.; White, F. M.; Hendrickson, C. L.; Marshall, A. G. *Anal. Chem.* **1998,** *70*, 4743.

53. He, F.; Hendrickson, C. L. *Anal. Chem.* **2001,** *73*, 647.

54. Laskin, J.; Denisov, E.; Futrell, J. H. *Int. J. Mass. Spectrom.* **2002,** *219*, 189.

55. Mirgorodskaya, E.; O'Connor, P. B.; Costello, C. E. *J. Am. Soc. Mass Spectr.* **2002,** *13*, 318.

56. Gur, E. H.; de Koning L. J.; Nibbering, N. M. M. *Int. J. Mass. Spectrom.* **1997,** *167*, 135.

57. Zhang, X.; Ewing, N. P.; Cassady, C. J. *Int. J. Mass. Spectrom.* **1998,** *175*, 159.

58. Hunter, R. L.; Sherman, M. G.; McIver, R. T. *Int. J. Mass. Spectrom.* **1983,** *50*, 259.

59. Littlejohn, D. P.; Ghaderi, S. USA Patent No. 4,581,533, issued 8 April, 1986.

60. Beu, S. C.; Laude, D. A. *Int. J. Mass Spectrom.* **1992,** *112*, 215.

61. McIver, R. T. USA Patent No. 4,523,235, issued 13 August, 1985.

62. Senko, M. W.; Hendrickson, C. L.; Emmett, M. R.; Shi, S. D. –H.; Marshall, A. G. *J. Am. Soc. Mass Spectrom.* **1997,** *8*, 970.

63. Marshall, A. G.; Hendrickson, C. L.; Jackson, G. S. *Mass Spectrom. Rev.* **1998,** *17*, 1.

64. Comisarow, M. B. *Int. J. Mass Spectrom. Ion. Phys.* **1981,** *37*, 251.

65. Marshall, A. G.; Hendrickson C. L. *Int. J. Mass Spectrom.* **2002,** *215*, 59.

66. McIver, R. T. *Rev. Sci. Instrum.* **1970,** *41*, 555.

67. Comisarow, M. B.; Marshall, A. G. *Chem. Phys. Lett.* **1974,** *26*, 489.

68. Marshall, A. G.; Wang, T. C. L.; Ricca, T. L. *J. Am. Chem. Soc.* **1985,** *107*, 7893.

69. Guan, S.; Marshall, A. G. *Int. J. Mass Spectrom. Ion. Proc.* **1986,** *157/158*, 5.

70. Comisarow, M. B. *J. Chem. Phys.* **1978,** *69*, 4097.

71. Köster, C.; Castoro, J. A.; Wilkins, C. L. *J. Am. Chem. Soc.* **1992,** *114*, 7572.

72. Beavis, R. C.; Chait, B. T. *Chem. Phys. Lett.* **1991,** *181*, 479.

73. Solouki, T.; Russell, D. H. *Proc. Natl. Acad. Sci. USA* **1992,** *114*, 7501.

74. Yao, J.; Dey, M.; Pastor, S. J.; Wilkins, C. L. *Anal. Chem.* **1995,** *67,* 3638.

75. Solouki, T.; Russell, D. H. *Applied Spectrosopy* **1993**, *47*, 211.

76. Solouki, T.; Gillig, K. J.; Russell, D. H. *Rapid Commun. MASS Sp.* **1994,** *8*, 26.

77. Castoro, J. A.; Wilkins, C. L. *Anal. Chem.* **1993,** *65*, 2621.

78. Zhang, W.; Chait, B. T. *Int. J. Mass Spectrom.* **1997,** *160*, 259.

79. Savard, G.; Becker, S.; Bollen, G.; Kluge H. J.; Moore R. B.; Otto T.; Schweikhard, L.; Stolzenberg, H.; Wiess, U. *Phys. Lett. A* **1991,** *158*, 247.

80. Guan, S. H.; Kim, H. S.; Marshall, A. G.; Wahl, M. C.; Wood, T. D.; Xiang, X. Z. *Chem. Rev.* **1994,** *94*, 2161.

81. Schweikhard, L.; Guan, S.; Marshall. A. G. *Int. J. Mass Spectrom.* **1992,** *120*, 71.

82. Pitsenberg, C. C.; Amster, I. J. *Eur. Mass Spectrom.* **1997,** *3*, 1.

83. Mize, T. H.; Amster, I. J. *Anal. Chem.* **2000,** *72*, 5886.

84. Easterling, M. L.; Mize, T. H.; Amster, I. J. *Anal. Chem.* **1999,** *71*, 624.

85. Speir, J. P.; Gorman, G. S.; Pitsenberger, C. C.; Turner, C. A.; Wang, P. P.; Amster I. J. *Anal. Chem.* **1993,** *65*, 1746.

86. Pitsenberger, C. C.; Easterling, M. L.; Amster, I. J. *Anal. Chem.* **1996,** *68*, 3732.

87. Gillig, K. J.; Doctoral Dissertation, Texas A&M University 1997.

88. Pastor, S. J.; Castoro, J. A. Wilkins, C. L. *Anal. Chem.* **1995,** *67*, 379.

89. Kerley, E. L.; Russell, D. H. *Anal. Chem.* **1989,** *61*, 53.

90. Frankevich, V.; Zenobi, R. *Rapid Commun. Mass Sp.* **2001,** *15*, 2035.

91. Frankevich, V.; Zenobi, R. *Rapid Commun. Mass Sp.* **2001,** *15*, 979.

92. Bartmess, J. E.; Georgiadis, R. M. *Vacuum.* **1983,** *33*, 149.

93 . Rusconi, F.; Schmitter, J. M. *Analusis,* **1998,** *26*, M13.

94. Hettick, J. M.; McCurdy, D. L.; Barbacci, D. C.; Russell, D. H. *Anal. Chem.* **2001,** *73*, 5378.

95. Su, T.; Chesnavich, W. *J. Chem. Phys.* **1982**, *76*, 5183

96. Evans, S. E.; Lueck, N, L.; Marzluff, E. M. *Int. J. Mass Spectrom.* **2003,** *222*, 175.

97. Wang, F; Freitas, M. A.; Marshall, A. G.; Skyes, B. D. *Int. J. Mass Spectrom.* **1999,** *192*, 319.

98. Hunt, D. F.; McEwen, C. N.; Upham, R. A. *Anal. Chem.* **1972,** *44*, 1292.

99. Ranasinghe, A.; Cooks, R. G.; Sethi, S. K. *Org. Mass Spectrom.* **1992,** *27*, 77.

100. Wood, T. D.; Chorush, R. A.; Wampler, F. M.; Little, D. P; O'Connor, P. B.; McLafferty, F. W. *Proc. Natl. Acad. Sci. USA* **1995,** *92*, 2451.

101. Wu, J.; Lebrilla, C. B. *J. Am. Soc Mass Spectrom.* **1995,** *6*, 91.

102. Zhang, K.; Zimmerman, D. M.; Chung-Phillips, A.; Cassady, C. J. *J. Am. Chem. Soc.* **1993,** *115*, 10812.

103. Amster, I. J.; Gorman, G. S. *J. Am. Chem. Soc.* **1993,** *115*, 5729.

104. Ewing, N. P.; Zhang, X; Cassady, C. J. *J. Mass Spectrom.* **1996,** *31*, 1345.

105. Hernández-Laguna, A.; Abboud, J. L. M.; Notario, R.; Homan, H.; Smeyers, Y. G. *J. Am. Chem. Soc.* **1993,** *115*, 1450.

106. Maksić, Z. B.; Kovačević, B. *Chem. Phys. Lett.* **1999,** *307*, 497.

107. Green, M. K.; Lebrilla, C. B. *Int. J. Mass Spectrom.* **1998,** *175*, 15.

108. Olea-Azar, C. A.; Parra-Mouchet, J. E. *Bol. Soc. Chil. Quim.* **1998,** *43*, 189.

109. Campbell, S.; Rodgers, M. T.; Marzluff, E. M.; Beauchamp, J. L. *J. Am. Chem. Soc.* **1994,** *116*, 9765.

110. Wu, J.; Gard, E.; Bregar, J.; Green, M. K.; Lebrilla, C. B. *J. Am. Chem. Soc.* **1995,** *117*, 9900.

111. Bliznyuk, A. A.; Schaefer, H. F.; Amster, I. J. *J. Am. Chem. Soc.* **1993,** *115*, 5149.

112. Wu, J.; Gard E.; Bregar, J. Green, M. K. Lebrilla, C. B. *J. Am. Chem. Soc.* **1995,** *117*, 9900.

113. Sinnige, C. G.; de Koning, L. J.; Nibbering, N. M. M. *Int. J. Mass Spectrom.* **2000,** *195/196* 115.

114. Price, W. D.; Jackusch, R. A.; Williams, E. R. *J. Am. Chem. Soc.* **1997,** *119*, 11988.

115. Farrugia, J. M.; O'Hair, R. A. J. *Int. J. Mass. Spectrom.* **2003,** *222*, 229.

116. Freitas, M. A.; Marshall, A. G. *Int. J. Mass. Spectrom.* **1999,** *182/183*, 221.

117. Wyttenbach, T.; Witt, M. Bowers, M. Y. *Int. J. Mass. Spectrom.* **1999,** *182/183*, 243.

118. Schnier, P. D.; Price, W. D.; Jockusch, R. A.; Williams, E. R. *J. Am. Chem. Soc.* **1996,** *118*, 7178.

119. Strittmatter, E. F.; Williams, E, R. *J. Phys. Chem. A.* **2000,** *104*, 6069.

120. Chapo, C. J.; Paul, J. B.; Provencal, R. A.; Roth, K.; Saykally, R. J. *J. Am. Chem. Soc.* **1998,** *120*, 12956.

121. Skurski, P.; Gutowski, M.; Barrios, R.; Simons, J. *Chem. Phys. Lett.* **2001,** *337*, 143.

122. Reid, G. E.; Simpson, R. J.; O'Hair, R. A. J. *J. Am. Soc. Mass Spectrom.* **1998**, *9*, 945.
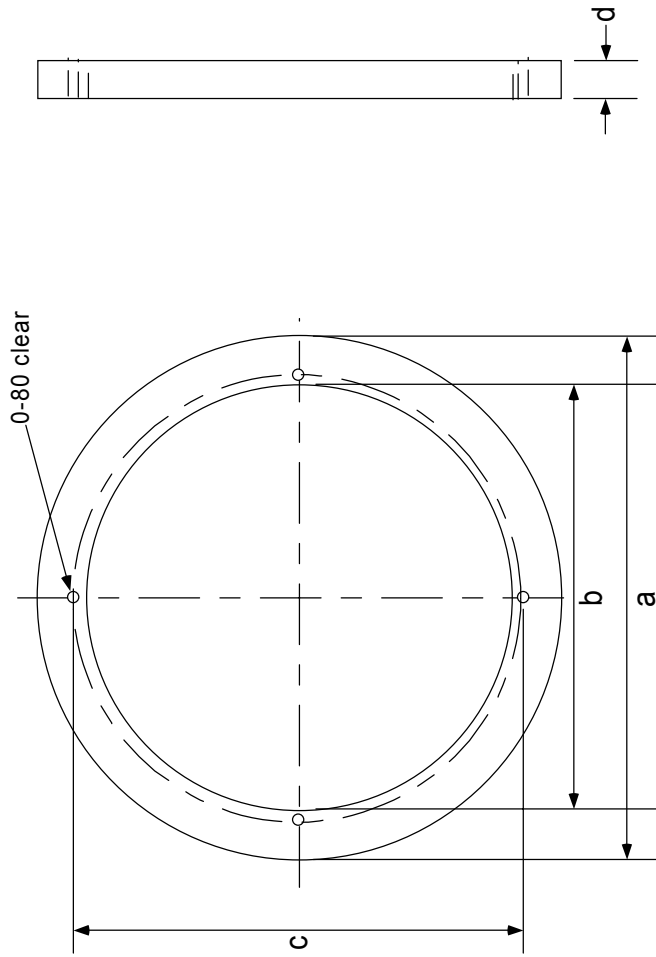
APPENDIX

Cell Base Ring

Material: Oxygen Free Copper
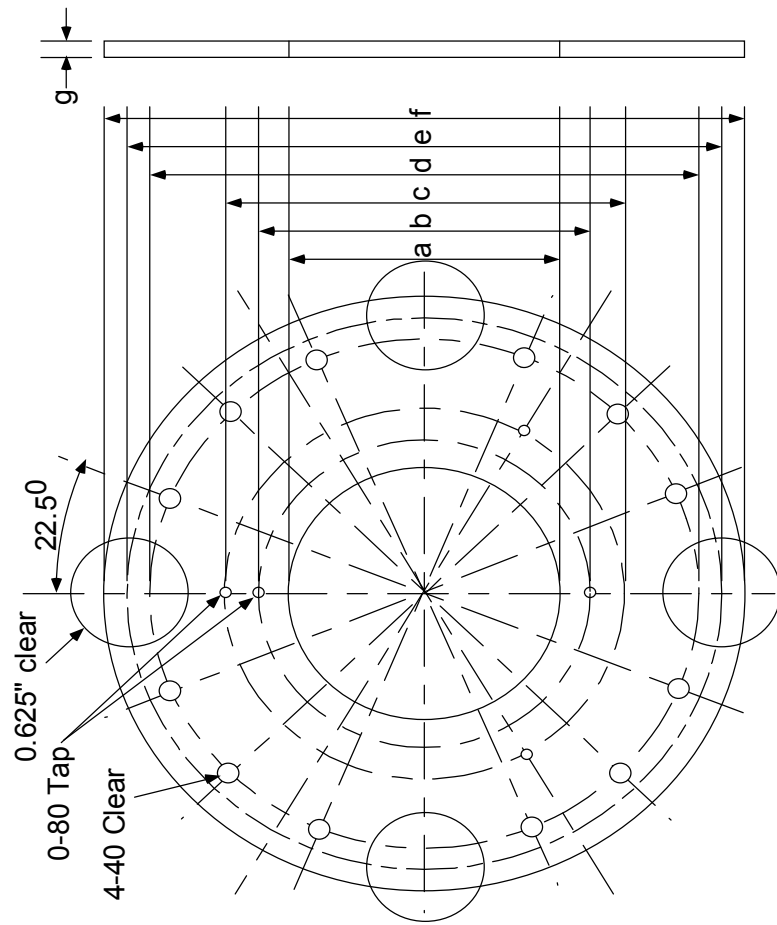
a = 1.500" +/- 0.020"
b = 1.835" +/- 0.010"
c = 2.207" +/-0.010"
d = 3.000" +/- 0.010"
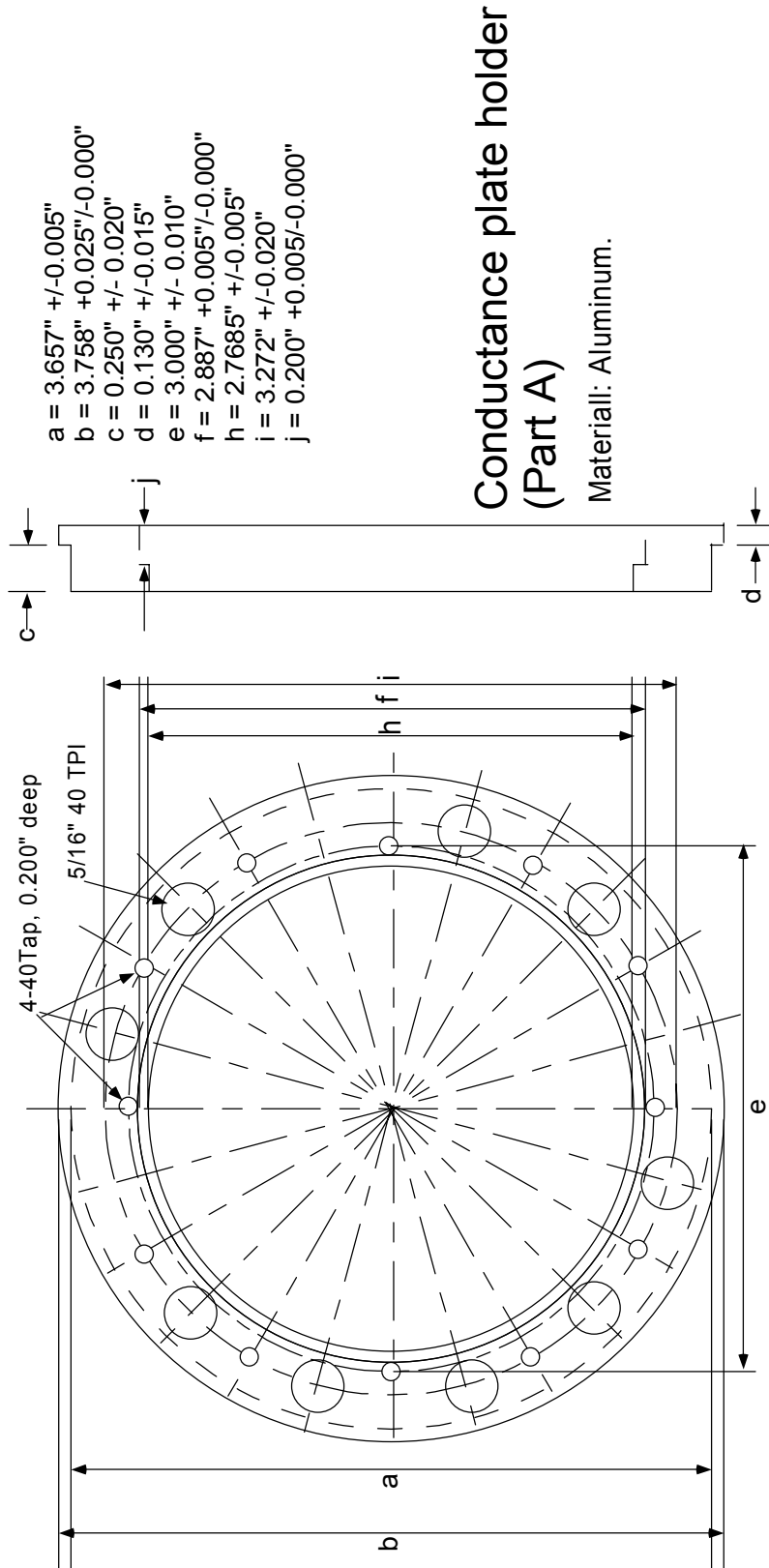e = 3.250" +/- 0.020"
f = 3.500" +/- 0.020"
g = 0.100" +/- 0.020"

22.5°

0.625" clear
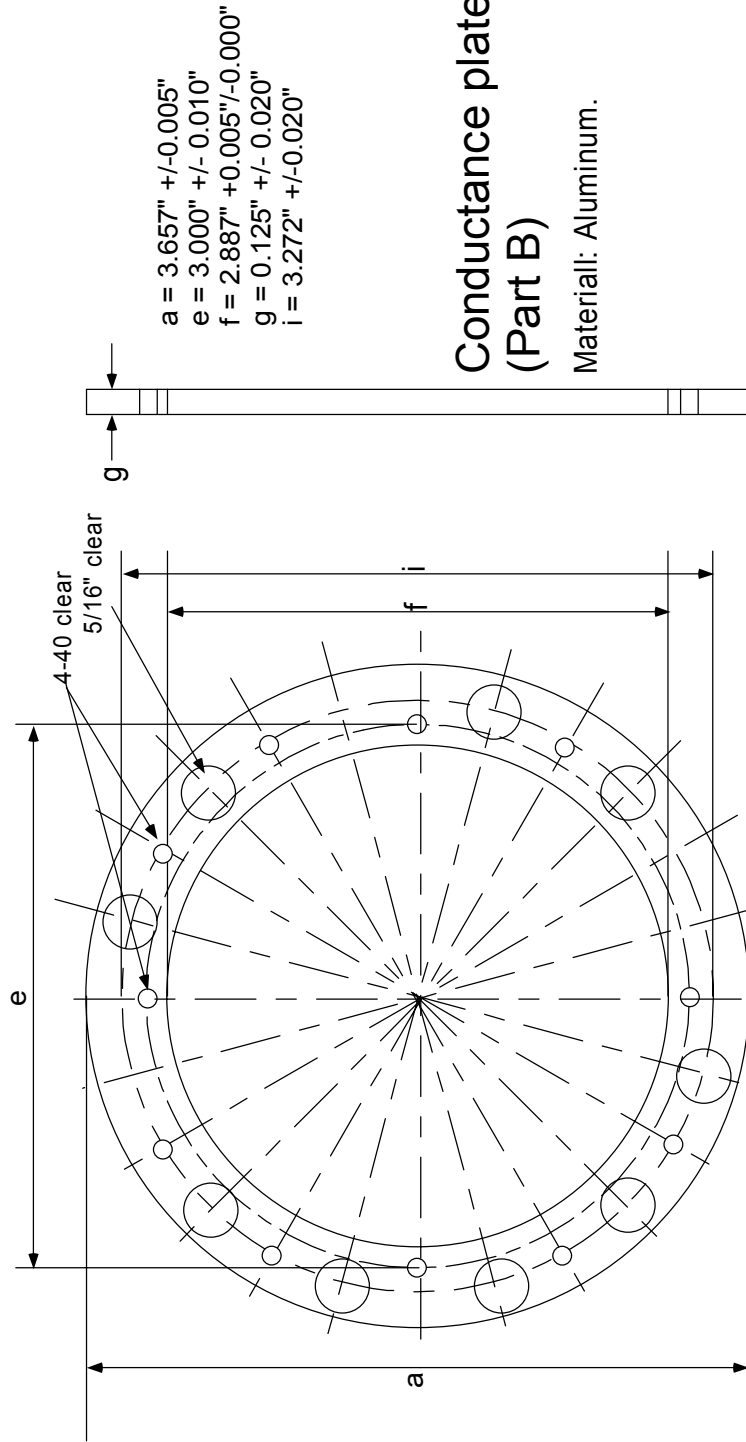
0-80 Tap

4-40 Clear

a b c d e f

g

0-80 clear

d

b

a

c

Conductance Limit Insolating Ring
Material: Macore

a = 2.887"+0.000"/-0.005"
b = 2.3285" +0.005"/-0.005"
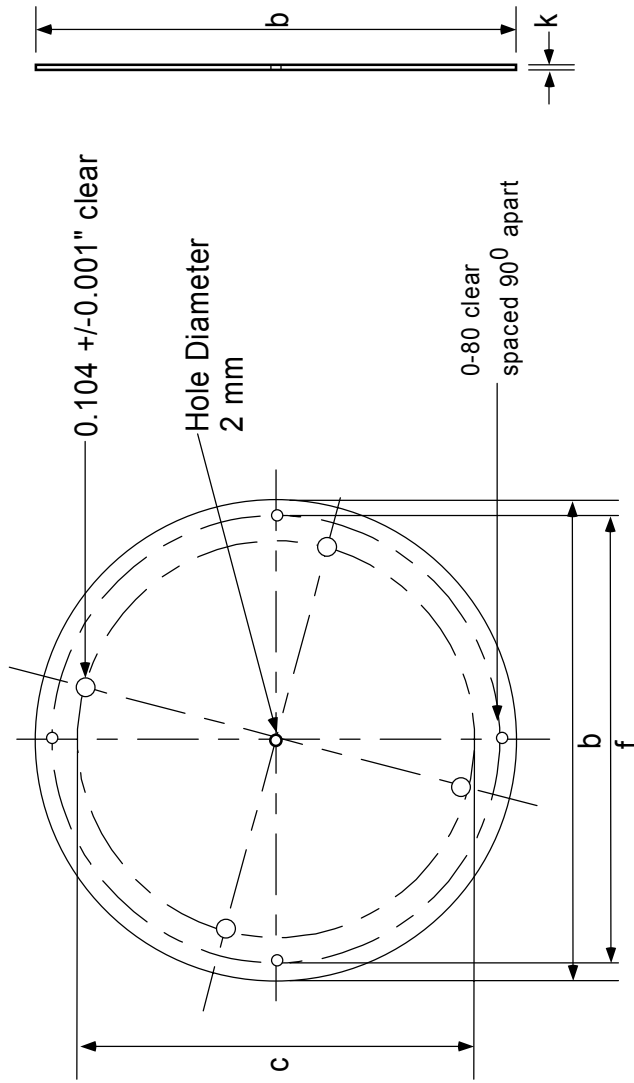c = 2.450" +/-0.002"
d = 0.200" +0.005"/-0.000"

a = 3.657" +/-0.005"
b = 3.758" +0.025"/-0.000"
c = 0.250" +/- 0.020"
d = 0.130" +/-0.015"
e = 3.000" +/- 0.010"
f = 2.887" +0.005"/-0.000"
h = 2.7685" +/-0.005"
i = 3.272" +/-0.020"
j = 0.200" +0.005/-0.000"

Conductance plate holder
(Part A)

Materiall: Aluminum.

4-40Tap, 0.200" deep

5/16" 40 TPI

a = 3.657" +/-0.005"
e = 3.000" +/- 0.010"
f = 2.887" +0.005"/-0.000"
g = 0.125" +/- 0.020"
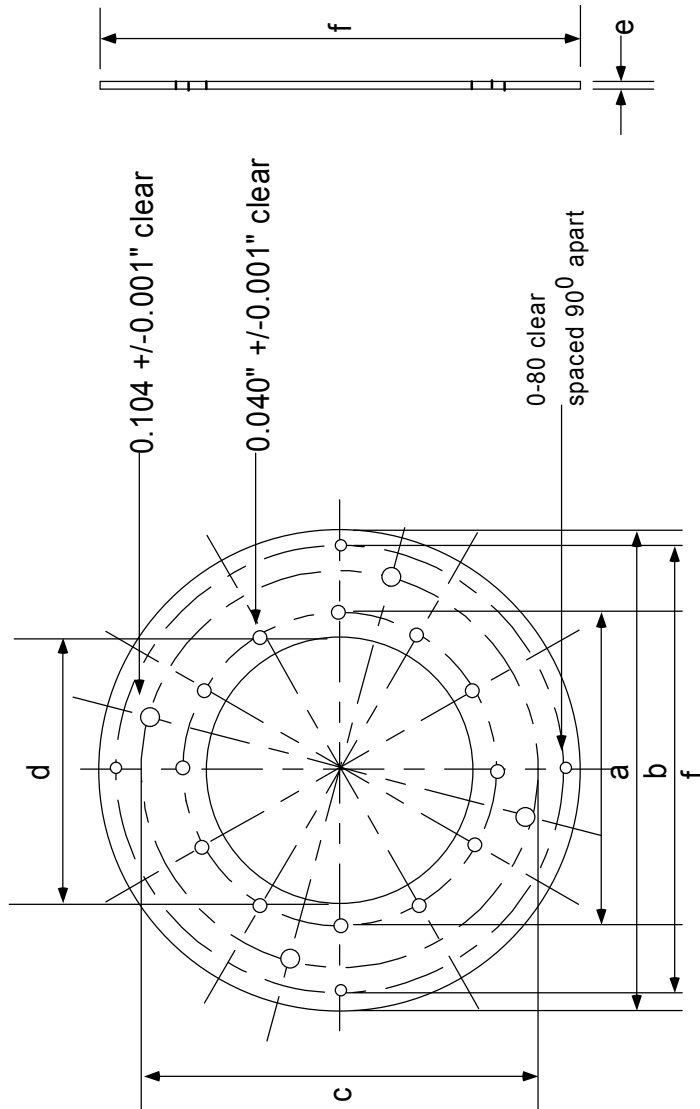i = 3.272" +/-0.020"

Conductance plate holder (Part B)

Materiall: Aluminum.

4-40 clear
5/16" clear

0.104 +/-0.001" clear

Hole Diameter
2 mm

0-80 clear
spaced 90^0 apart

b

c

b

f

k

Conductance Limit for 2 section cell
Material: Oxygen Free Copper

b = 2.600" +/-0.001"
c = 2.058" +/-0.001"
f = 2.450" +/-0.001"
k = 0.015" +/-0.001"

0.104 +/-0.001" clear

0.040" +/-0.001" clear

0-80 clear
spaced 90⁰ apart
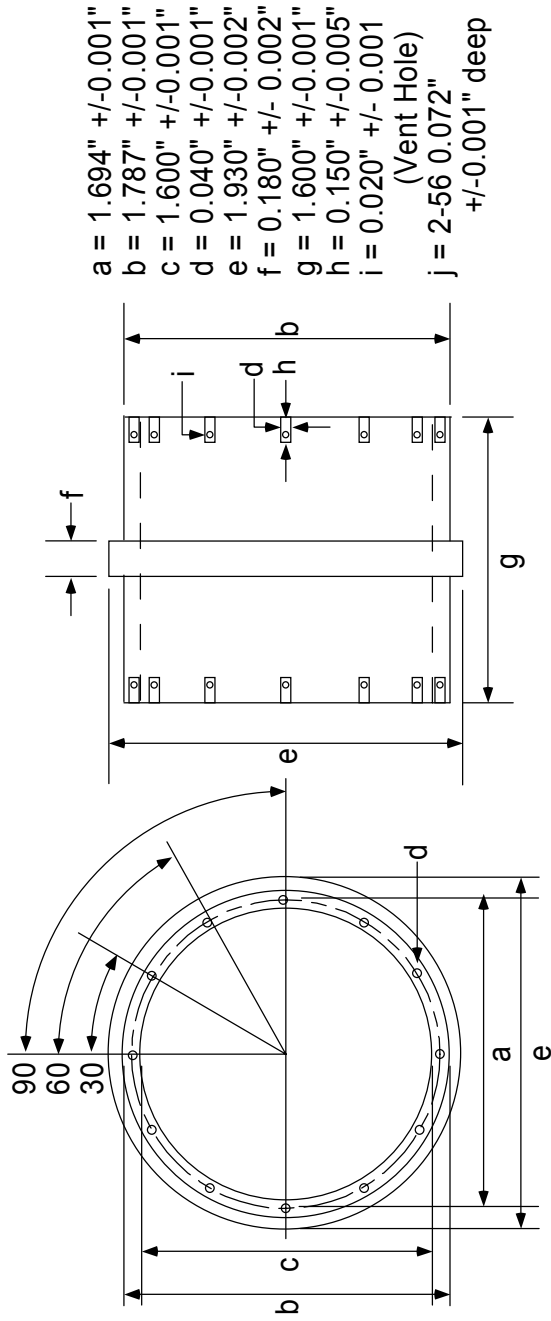
Conductance Limit Holder for 2 section cell
Material: Oxygen Free Copper

a = 1.694" +/-0.001"
b = 2.600" +/-0.001"
c = 2.058" +/-0.001"
d = 1.454"+/-0.001"
e = 0.0325" +/-0.001"
f = 2.450" +/-0.001"

Cylindrial Excite and Detect Plates
Material: Oxygen Free Copper
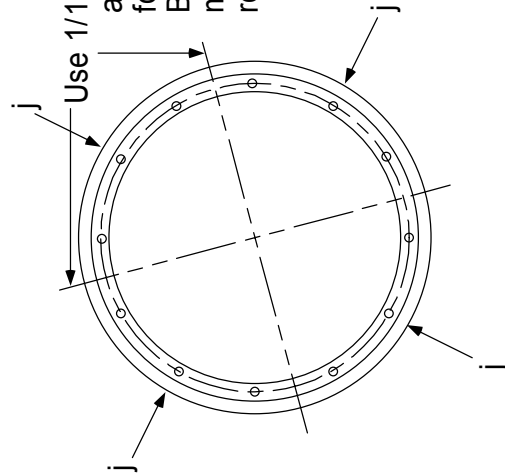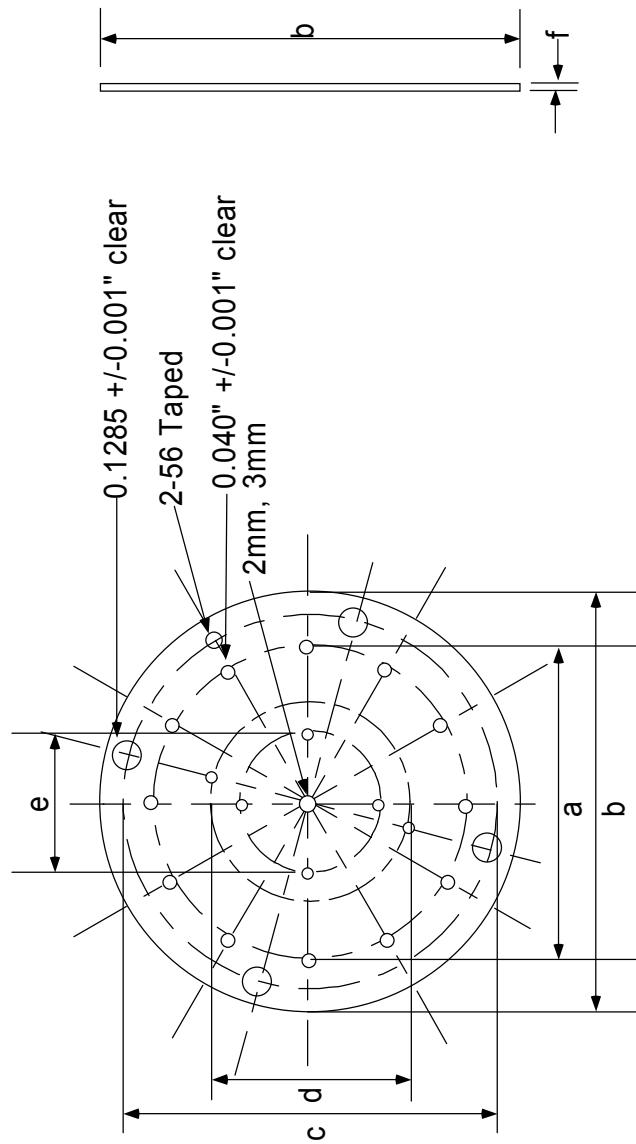
a = 1.694" +/-0.001"
b = 1.787" +/-0.001"
c = 1.600" +/-0.001"
d = 0.040" +/-0.001"
e = 1.930" +/-0.002"
f = 0.180" +/- 0.002"
g = 1.600" +/-0.001"
h = 0.150" +/-0.005"
i = 0.020" +/- 0.001
    (Vent Hole)
j = 2-56 0.072"
    +/-0.001" deep

Use 1/16" blade to cut accros indicated lines forming four plates. Before making 1/16" cut, make 3/16" grove in liped region.

EI/Lense Trap Plate

Material: Oxygen Free Copper
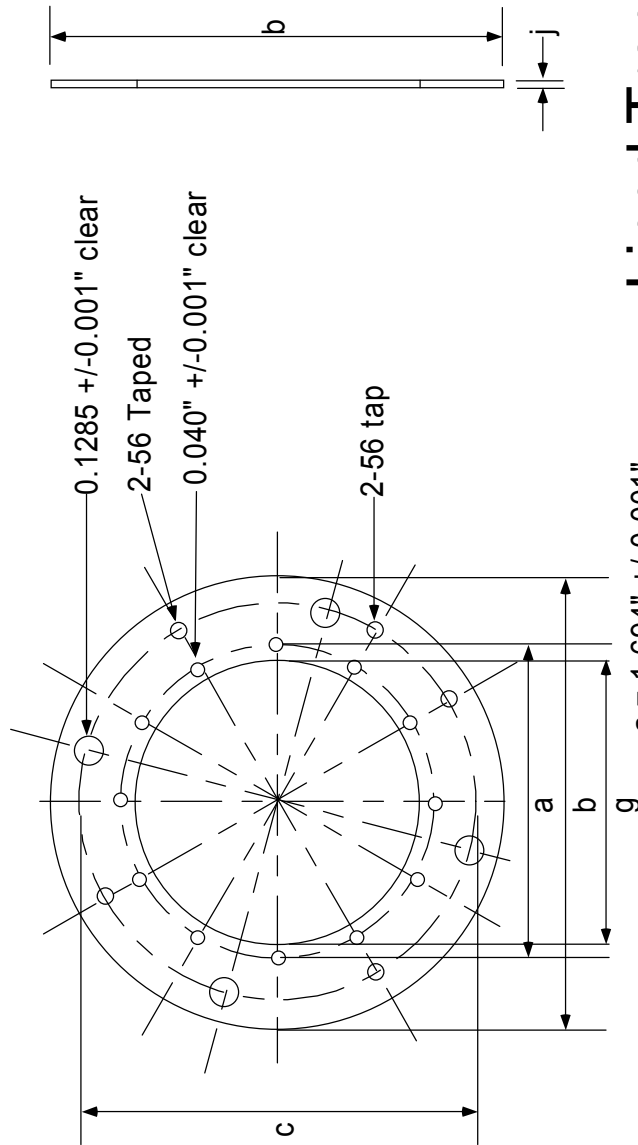
0.1285 +/-0.001" clear

2-56 Taped

0.040" +/-0.001" clear

2mm, 3mm

a = 1.694" +/-0.001"
b = 2.308" +/-0.005"
c = 2.058" +/-0.001"
d = 1.095" +/-0.001" (0-80 tap)
e = 0.784" +/-0.001" (0-80 tap)
f = 0.0625" +/-0.005"

a

b

c

d

e

f
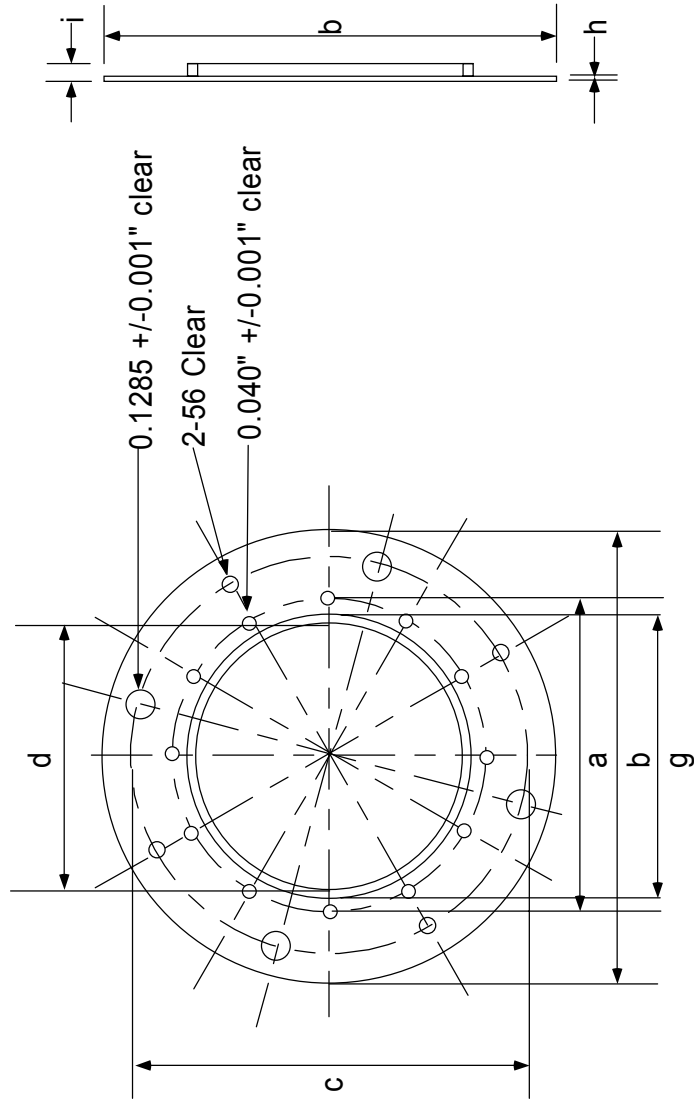
Liped Trap Plate
(Part A)

Material: Oxygen Free Copper

0.1285 +/-0.001" clear
2-56 Clear
0.040" +/-0.001" clear

a = 1.694" +/-0.001"
b = 2.500" +/-0.005"
c = 2.058" +/-0.001"
d = 1.454"+/-0.001"
g = 1.543" +0.000"/-0.002"
h = 0.040" +/-0.001"
i = 0.1025" +/-0.001

Liped Trap Plate (Part B)

Material: Oxygen Free Copper

0.1285 +/-0.001" clear

2-56 Taped

0.040" +/-0.001" clear

2-56 tap

a = 1.694" +/-0.001"
b = 2.500" +/-0.005"
c = 2.058" +/-0.001"
g = 1.543" +0.002"/-0.000"
j = 0.0625" +/-0.005"

Lense Holding Plate

Material: Oxygen Free Copper

2.308" +/-0.005"

0.0625" +/-0.005"

1.250" +/-0.005"

Ø06

2.308" +/-0.005"

2.058" +/-0.001"

1.250" +/-0.005"

0-80 clear
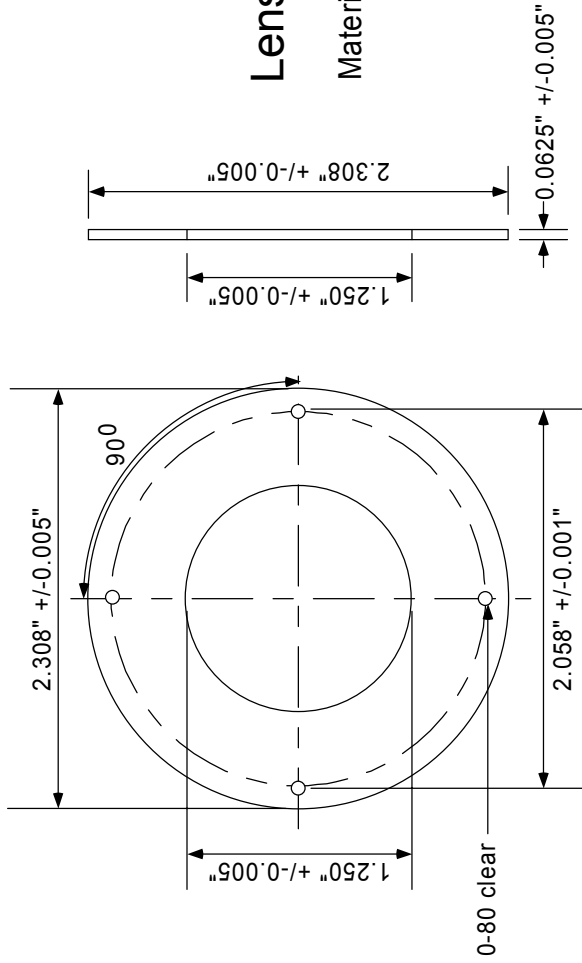
Lense Targeting Plate
Material: Oxygen Free Copper

2.308" +/-0.005"

0.0625" +/-0.005"

2.308" +/-0.005"

2.058" +/-0.001"

90°

2mm clear

0-80 clear
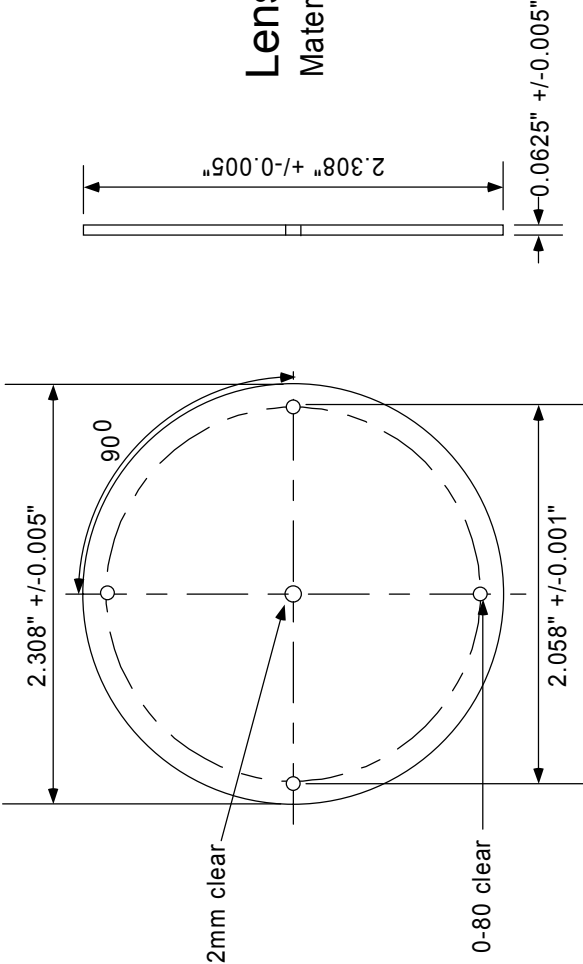
Holder - Base Plate Support Rods

Material: BeCu

0.250" +/-0.010"

0.300" +/-0.010"

0.263" +/-0.010"

0.250" +/-0.010"

1.918" +0.001"/-0.000"

4-40 Tap

Vent hole

4-40 Thread

a = 1.425" +/-0.015"
b = 1.835"+/- 0.010"
c = 2.000"+/- 0.020"
d = 0.185" +/- 0.020"
e = 2.058" +0.000"/-0.010"

Isolating Ring

Material: Teflon

0.175" clear

0.130" clear

0-80 clear, counter sink so head of screw is under teflon surface. (sugest 0,050" deep counter sink.)

0.175" +/- 0.002"
from edge to center line

0.440" +/- 0.005"

0.1125" +/- 0.002"
to center

0.350" +/- 0.005"

0.100" +/- 0.005"

0.525" +/- 0.005"

0.0625" +/- 0.005"

0.650" +/- 0.005"

Filament Holder
Material: Stainless Steel 304
Note: All holes taped for 0-80's

0.500" +/- 0.002"

0.1285" +/- 0.002
(# 30 drill)

0.390" +/- 0.002"

0.625" +/- 0.002"

0.750" +/- 0.002"

0.060" +/- 0.002

0-80 tap
0.250" +/- 0.002"
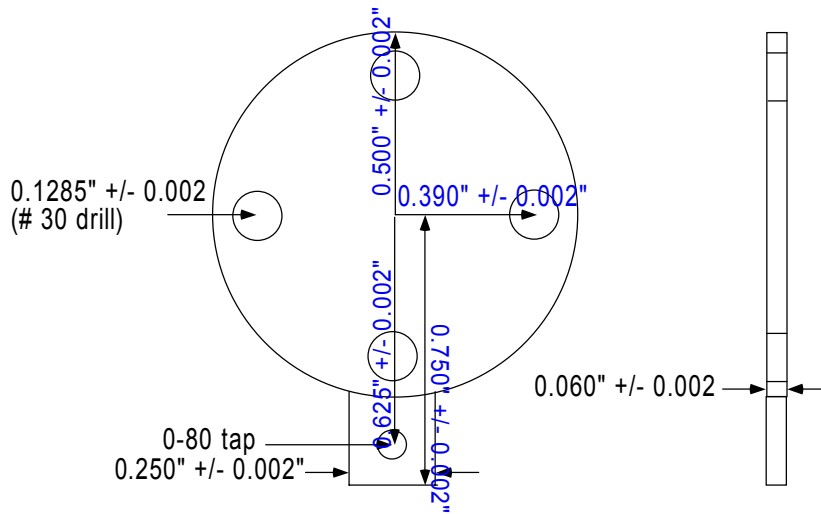
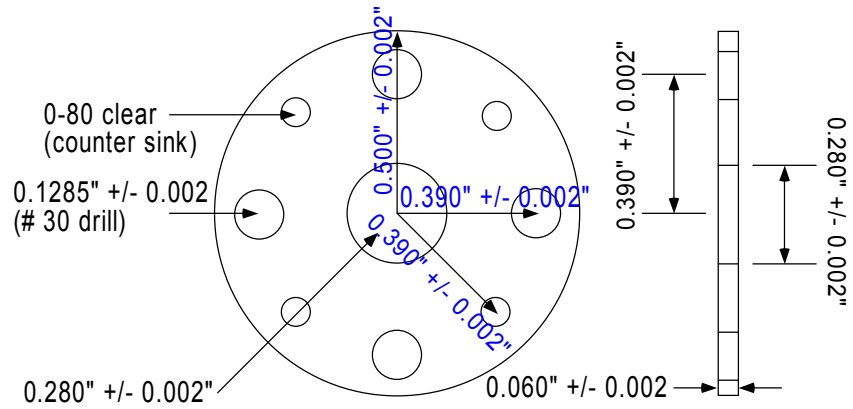## Filament Collector
Material: Stainless Steel 304
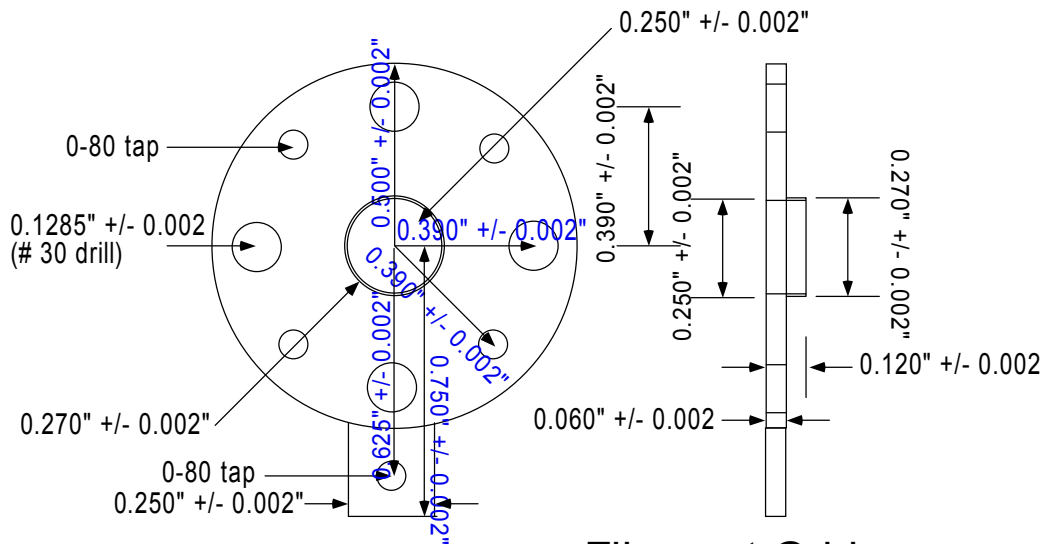Note: All hole sizes are given by diameter

Grid Overlayer
Material: Stainless Steel 304
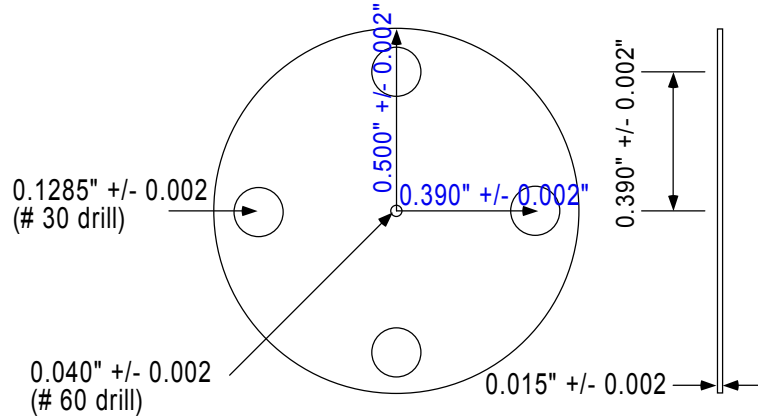Note: All hole sizes are given
by diameter

0-80 clear
(counter sink)

0.1285" +/- 0.002
(# 30 drill)

0.280" +/- 0.002"

0.060" +/- 0.002

0.390" +/- 0.002"

0.390" +/- 0.002"

0.500" +/- 0.002"

0.390" +/- 0.002"

0.280" +/- 0.002"

Filament Grid
Material: Stainless Steel 304
Note: All hole sizes are given
by diameter

0-80 tap

0.1285" +/- 0.002
(# 30 drill)

0.270" +/- 0.002"

0-80 tap
0.250" +/- 0.002"

0.250" +/- 0.002"

0.060" +/- 0.002

0.390" +/- 0.002"

0.390" +/- 0.002"

0.500" +/- 0.002"

0.390" +/- 0.002"

0.750" +/- 0.002"

0.625" +/- 0.002"

0.270" +/- 0.002"

0.250" +/- 0.002"

0.120" +/- 0.002

0.1285" +/- 0.002
(# 30 drill)

0.500" +/- 0.002"

0.390" +/- 0.002"

0.390" +/- 0.002"

0.040" +/- 0.002
(# 60 drill)

0.015" +/- 0.002

E-Beam Collimator
Material: Oxygen Free Copper
Note: All hole sizes are given
by diameter

0-80 clear
(? 0.0635" #52 drill)

0.225" +/- 0.002"
center to center

0.500" +/- 0.002"

0.390" +/- 0.002"

0.375" +/- 0.002"

0.390" +/- 0.002"
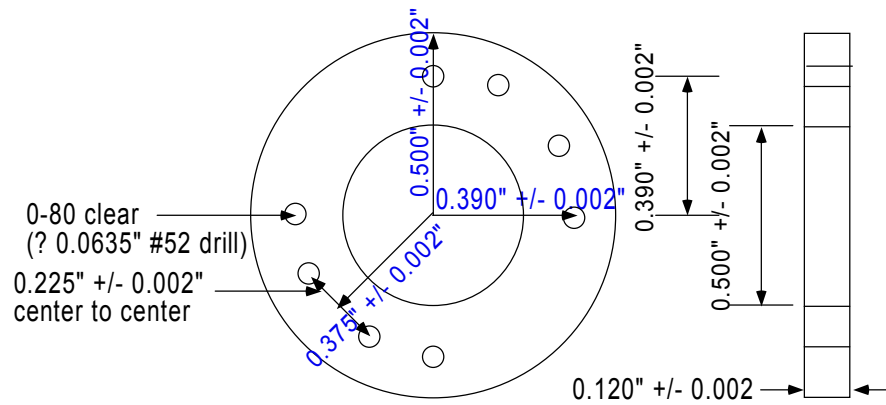
0.500" +/- 0.002"

0.120" +/- 0.002

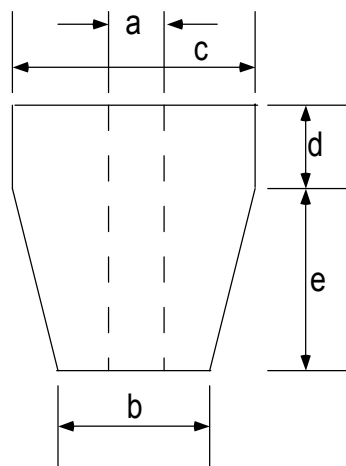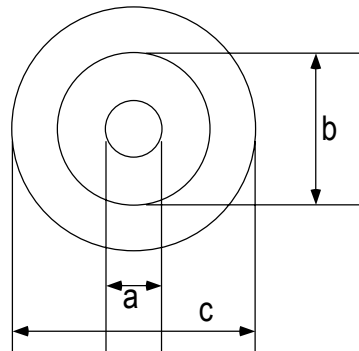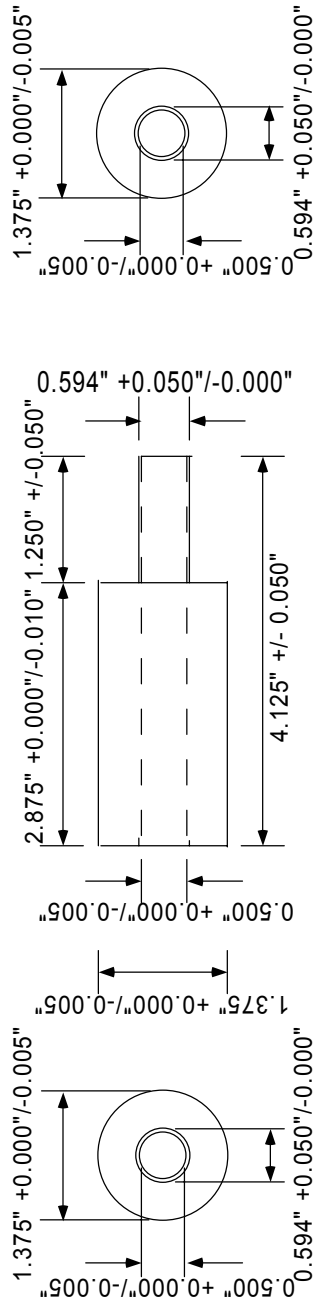# Filament Mount
Material: Macor
Note: All hole sizes are given
by diameter
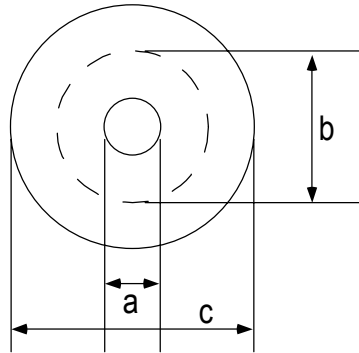
a = 0.032" size 67 drill
b = 0.086" +0.002/-0.000"
c = 0.130" +/-0.002"
d = 0.045" +/-0.002"
e = 0.100" +/-0.002"

Teflon Ferrules
Material: Teflon

High Vac Probe Seal
Material: Teflon

1.375" +0.000"/-0.005"
0.594" +0.050"/-0.000"
0.500" +0.000"/-0.005"

0.594" +0.050"/-0.000"
2.875" +0.000"/-0.010" 1.250" +/-0.050"
4.125" +/- 0.050"
0.500" +0.000"/-0.005"

1.375" +0.000"/-0.005"
0.500" +0.000"/-0.005"
1.375" +0.000"/-0.005"
0.594" +0.050"/-0.000"

Low Vac Probe Seal
Material: Teflon

1.000" +0.000"/-0.005"
0.500" +0.000"/-0.005"
0.625" +0.000"/-0.005"

0.625" +0.000"/-0.005"
0.500" +0.000"/-0.005"
0.969" +/-0.020"
0.125" +/-0.002"
1.000" +0.000"/-0.005"

1.000" +0.000"/-0.005"
0.500" +0.000"/-0.005"
0.625" +0.000"/-0.005"
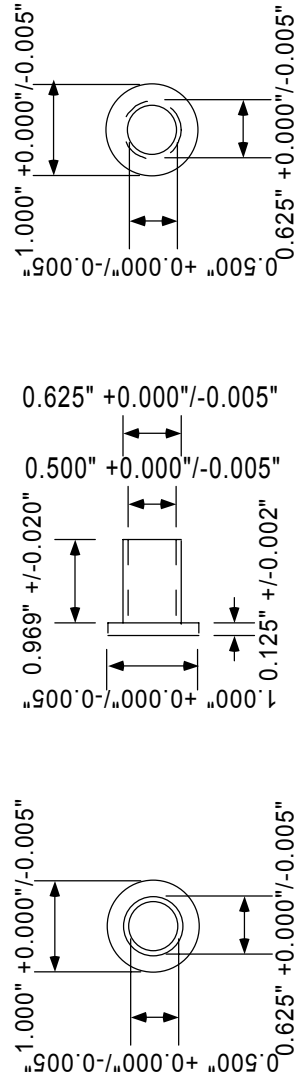
VITA

Joseph Thomas Marini

LOCAL ADDRESS   **PERMANENT ADDRESS**
3500 Finfeather Rd. Apt. 1204   705 Darley Circle
Bryan, TX 77801   New Hope, PA 18938
Home: (979) 779-7595   (215) 794-5022

EDUCATION

>**Ph.D. / Chemistry**
>Texas A&M University, College Station, TX, December 2003

>**B.A. / Chemistry/Biochemistry**
>La Salle University, Philadelphia, PA, 1997

SELECTED PRESENTATIONS

>16th International Mass Spectrometry Conference, August 31-September 5, 2003, Edinburgh, Scotland. "The Effect of Basic Amino Acid Residues on the Mechanism of Gas-Phase H/D Exchange: Determination of Gas-Phase Peptide Conformation."

>16th International Mass Spectrometry Conference, August 31-September 5, 2003, Edinburgh, Scotland. "Observation of Solution-Phase Memory Effects in Peptide Systems: Evidence from Ion Mobility and H/D Exchange Mass Spectrometry."

>17th Lost Pines Conference, October 25-27, 2002, Smithville, Texas. "The Investigation of Gas-Phase Structure by Ion Mobility-Mass Spectrometry and Gas-Phase Hydrogen/Deuterium Exchange."

>50th ASMS Conference on Mass Spectrometry, June 2-6, 2002, Orlando, Florida. "Probing the Secondary Structure of Peptide Ion Positional Isomers by Gas Phase H/D Exchange Utilizing a FT-ICR MS."

>50th ASMS Conference on Mass Spectrometry, June 2-6, 2002, Orlando, Florida. "Effect of Intra-Molecular Interactions on the Gas-Phase Conformation of Bradykinin as Probed by Ion-Mobility Mass Spectrometry."